

**Membrane module and process development  
for monopolar and bipolar membrane electro dialysis**

The research described in this thesis was supported by the Dutch Technology Foundation STW, applied science division of NWO.

Membrane module and process development for monopolar and bipolar membrane electrodialysis

J. Balster, PhD Thesis, University of Twente, The Netherlands

ISBN: 90-365-2452-0

Cover design by J. Balster

© J. Balster, Enschede, The Netherlands, 2006.

Printed by Wöhrmann Print Service, Zutphen, The Netherlands.

**MEMBRANE MODULE AND PROCESS DEVELOPMENT  
FOR MONOPOLAR AND BIPOLAR MEMBRANE ELECTRODIALYSIS**

**DISSERTATION**

to obtain  
the degree of doctor at the University of Twente,  
on the authority of the rector magnificus,  
prof. dr. W.H.M. Zijm,  
on account of the decision of the graduation committee  
to be public defended  
on Wednesday 13<sup>th</sup> of December 2006 at 13.15

by

**Jörg Henning Balster**

born 28<sup>th</sup> of July 1975  
in Nordhorn, Germany

This dissertation has been approved by the promotor Prof. Dr.-Ing M. Wessling and the assistant promotor Dr. D.F. Stamatialis.

## Preface

After more than 5 years in Twente, working on my Master and my PhD thesis in the Membrane Technology Group, it is time to look back and see how the story started. Until the start of the 12<sup>th</sup> grade in high school (Gymnasium), I always thought that I would study computer science or information technology. When I had to decide which topic I should choose for the main examination course a friend of mine, Jörg Hesselink, persuaded me to take chemistry, so that they had enough people to get the course started. So Jörg, I think I owe you something for that.

The next person I would like to acknowledge is Günther Briesemann from the EWABO Chemikalien GmbH. Günther ich danke Dir für deine Ratschläge und für die Möglichkeit, Erfahrung in der chemischen Industrie zu sammeln. Allen Mitarbeitern von EWABO danke ich für die tolle Atmosphäre während meiner Zeit dort.

During my studies in Steinfurt I met a lot of new friends with whom I still have contact. Holger, Anja, Ansgar, Uwe, Ralph, 2 mal Melanie, Helga, Sabine, Renny, Matthias...., die Zeit mit Euch war super. Holger, lernen mit Dir war immer sehr erfolgreich, auch wenn wir manchmal etwas von unserem Studium abgeschweift sind. Anja, ohne deine Unterlagen hätten ich mein Studium niemals geschafft ☺.

Für mich persönlich war auch der Masterstudiengang eine tolle Zeit. Steffi, Karin, Jürgen, es war toll mit Euch die Schulbank zu drücken.

I have to thank especially Prof. Volkmar Jordan, who supervised all my projects from the University of Applied Sciences Münster during my Diplom and my Master studies, and who also helped me to get into contact with Matthias, here in Twente. Volkmar ich danke Ihnen für Ihre Unterstützung und freue mich, dass Sie in meiner Prüfungskommission sind und der Verteidigung beiwohnen.

Finally arrived in Twente, I have first of all to thank Matthias for believing in my skills and giving me the opportunity to make my Master thesis and my PhD thesis in his group and also for giving me the possibility to work for the EMI.

During my Master thesis I was very impressed by my supervisor Jonathan. Jonathan your enthusiasm in science is affecting the people around you and made that time very special for me. You gave me a lot of inspiration. Some people will now say I really got inspired by you, because my desk looks even more chaotic than the one from you during your time here.

My supervisor during my time as PhD was Dimitris. We started both at the same time in our positions, you as Assistant Professor and me as your first PhD. I think we both did our jobs quite well, even when I started to make fun of you when some of my articles or abstracts were corrected for the sixth time and you started to correct your own corrections. In the end of my time I built up traps by giving you abstracts which were already printed to see if you start to correct again, but you recognised it. Dimitris I would like to thank you for all your input, discussions and also your corrections to improve this thesis. In parallel to the scientific part it was always nice to chat with you and I am very grateful that you were one of my wedding witnesses.

Especially in the beginning of my period in Twente, but also in between, there was a lot of paper work to be done. Greet, I think without your help nobody in this group would survive. Thank you very much for all your help with these things.

If you are working in the lab, a lot of things have to be arranged and prepared. Often people do not notice this help in the background, which is necessary for a working lab. John thank you for all your help. You were always there when I needed something.

During my work, I had a lot of help from different people. First of all I have to thank Ineke, who was working 3 years as a technician in my project. Ineke thank you very much for all your effort and the good work you did. Olga who worked as a Postdoc on this project, Hakan, Raghu, Sabeeth and Catarina who worked as students on parts of this thesis, thank you all for your effort. Your measurements gave a big contribution to this thesis, as can be seen in the author list of each chapter.

I also would like to thank the users of my project for their scientific input. Especially Hans Lammers from Akzo Nobel and Alber Verver from DMV International. Your ideas and help had a great impact on this work.

Two people more contributed to successful experimental work inside the lab. Friedrich, thank you for coming from your work at Audi to Twente to explain the program you developed during your PhD in this group. Most of the experiments carried out for this thesis were not possible without your help. Wilbert, thank you for all your help with Labview and Acrobat. Without you I could not have built and automatised the new setup and without your knowledge about Acrobat this thesis never would have been printed.

Another special person I would like to acknowledge is Rob. Rob, you joined our group after I started, and the beginning of our relation was under a big shadow ☹️. I had to change from the nice office downstairs (which was in Matthias eyes perfect for an Assistant Professor) into the so called chicken box. But you knew how to get light into the darkness immediately, by discussing motor races and soccer while drinking a few beers with me. Even if you were not one of my supervisors you gave a great input into this thesis. You prepared moulds, made Femlab simulations and had always a helping idea or advice. Thank you very much for everything.

During the last years I had a lot of room mates. Miriam (who joined me downstairs and also in the chicken box), Benoit, Maik (who was first sharing with me and Miriam the office downstairs and later on in the chicken box next door, so more or less also still my room mate), Joao (who was in the chicken box with Maik, so close enough to say room mate), Dana, Jorrit, Hylke, and Karina, thank you for the nice time.

Being for more than 5 years in the Membrane Technology Group means that you meet a lot of people, have a lot of activities and fun together. Thank you all for the nice time being here.

Next to my work I was also involved in the organisation of the group trip to Hamburg and of the 7<sup>th</sup> meeting of the Network Young Membrains in Enschede. I would like to thank everybody who helped me during this tasks, which made it much easier and most of the time also quite nice (Hamburg at least until an angry email appeared ☹️). Miriam and Harmen, I would like to thank you for being my paranims during my defence. It is nice to have friends at your side in such a situation.

Natürlich möchte ich mich am Ende bei meinen Eltern bedanken, welche mich immer unterstützt haben. Ich danke Euch dass Ihr immer für mich da wart, auch in schwierigen Zeiten. All meinen Freunden möchte ich für Ihre Unterstützung danken. Bastian, besonders Dir möchte ich danken für deine Unterstützung und Hilfe. Du bist immer da wenn ein Freund Hilfe braucht.

At the end I would like to say thank you to the two most important persons in my life. Dana and Julian I love you and I will always be there for you. Dana, te iubesc foarte mult. Vreau sa fiu tot timpul împreuna cu tine. Ești in adâncul inimii mele.

---

## Contents

<b>Introduction</b>	<b>11</b>
Scope of this thesis	11
General introduction	12
Structure of this thesis	15
References	17
<b>Chapter I: The development of bipolar membrane technology</b>	<b>19</b>
1. Introduction	20
2. Principle of a bipolar membrane	20
3. Principle of bipolar membrane electrodialysis	21
4. Preparation of bipolar membranes	22
5. Characterisation of bipolar membranes	24
6. Limitations of bipolar membrane electrodialysis	27
7. Bipolar membrane electrodialysis processes	28
8. List of symbols	29
9. References	30
<b>Chapter II: Tailoring the intermediate layer of the bipolar membrane</b>	<b>35</b>
1. Introduction	36
2. Experimental	40
2.1 Materials	40
2.2 Bipolar membrane preparation	41
2.3 Characterisation of the ion exchange layers	42
2.4 Characterisation of the bipolar membranes	42
3. Results and discussion	45
3.1 Influence of the amount of ionic groups at the interface layer	45
3.2 Influence of the composition of the anion exchange layer	46
3.3 Fe-based catalytic interface layer	48
3.4 Pyridine based catalytic interface layers	52
3.5 Comparison of prepared bipolar membranes with different catalytic layers	56
4. Conclusions	57
5. List of symbols	58
6. References	59
<b>Chapter III: Asymmetric bipolar membranes: A tool to improve product purity</b>	<b>63</b>
1. Introduction	64
2. Theoretical background	67
3. Experimental	71

3.1	Commercial membranes	71
3.2	Tailor made membranes	71
3.3	Characterisation of the ion exchange membrane layers	72
3.4	Characterisation of the bipolar membranes	72
4.	Results and discussion	76
4.1	Modification of the commercial BP-1 membrane	76
4.2	Tailor made asymmetric bipolar membranes	81
5.	Conclusions	84
6.	List of symbols	85
7.	References	87

**Chapter IV: Multi-layer spacer geometries with improved mass transport 89**

1.	Introduction	90
2.	Theory	93
2.1	Concentration polarization and limiting current density	93
2.2	Spacer – background	94
3.	Experimental	98
4.	Results and discussion	102
4.1	Single spacer	102
4.2	Multi-layer spacer	103
4.3	Down scale of the multi-layer spacers	106
4.4	Comparison of the optimal multi-layer spacers	107
5.	Conclusions	109
6.	Acknowledgement	110
7.	List of symbols	110
8.	References	111

**Chapter V: Morphology and micro-topology of cation exchange polymers and the origin of the overlimiting current 115**

1.	Introduction	116
1.1	Current transport by protons and hydroxyl ions	118
1.2	Current transport by salt ions	119
1.3	Aim of this chapter	124
2.	Experimental	124
2.1	Commercial membranes	124
2.2	Tailor made membranes	125
2.3	Membrane characterization	127
2.4	Current-voltage and chronopotentiometric curves	128
2.5	Simulation of the solution stream line distribution	131
3.	Results and discussion	131
3.1	Commercial membranes	131
3.2	Heterogeneous vs. homogeneous ion exchange membranes	134
3.3	Homogeneous blend membranes	137
3.4	Effect of geometrical heterogeneity	140
4.	Conclusions	148



---

5.	Acknowledgement	149
6.	List of symbols	149
7.	References	150
<b>Chapter VI: Preparation and characterisation of monovalent ion selective cation exchange membranes based on sulphonated poly(ether ether ketone)</b>		<b>157</b>
1.	Introduction	158
2.	Experimental	160
2.1	Commercial membranes	160
2.2	Tailor made membranes	160
2.3	Membrane characterisation	161
2.4	Ca <sup>2+</sup> flux measurements	163
3.	Results and discussion	166
3.1	Characterisation of the commercial and tailor made cation exchange membranes	166
3.2	Ca <sup>2+</sup> transport through the commercial cation exchange membranes	169
3.3	Ca <sup>2+</sup> transport through the tailor made cation exchange membranes	169
3.4	Comparison between commercial and tailor made cation exchange membranes	170
4.	Conclusions	174
5.	Acknowledgement	175
6.	List of symbols	175
7.	References	176
<b>Appendix chapter VI: Improvement of the monovalent ion selectivity of commercial membranes</b>		<b>181</b>
1.	Introduction	182
2.	Experimental	182
3.	Results and discussion	182
4.	Conclusions and outlook	183
5.	List of symbols	184
6.	References	184
<b>Chapter VII: Electrochemical acidification of milk by whey desalination</b>		<b>185</b>
1.	Introduction	186
2.	Experimental	189
2.1	Membranes	189
2.2	Membrane characterisation	189
2.3	Lab scale tests	189
2.4	Pilot scale tests	190
2.5	Ion analysis	190
3.	Results and discussion	191
3.1	Scaling and fouling of cation exchange membranes	191
3.2	Comparison of the desalination of whey and milk	195

3.3	Efficiencies and power consumption of different membrane configurations during pilot scale experiments	196
4.	Conclusions	199
5.	Acknowledgement	200
6.	List of symbols	200
7.	References	201
<b>Summary</b>		<b>203</b>
<b>Samenvatting</b>		<b>207</b>
<b>Curriculum vitae</b>		<b>211</b>
<b>List of publications</b>		<b>213</b>

## Scope of this thesis

In electro dialysis ion exchange membranes, membranes carrying fixed positive or negative charges are used to separate electrolyte solutions using an electrical potential gradient as driving force. A special kind of ion exchange membrane is a bipolar membrane, which consists of two ion exchange layers of opposite charge. A bipolar membrane allows the electro-dissociation of water into protons and hydroxyl ions and can be used for the production of acids and bases from their corresponding salts.

The feasibility of electro dialysis processes depends strongly on the selectivity of the used membranes. Undesired salt ion transport across the membranes occurs, leading to product impurities and increase of the energy requirements.

The operating currents in electro dialysis are restricted due to concentration polarisation, resulting in a limiting current density. This leads to the use of high membrane areas and therefore high investment costs to achieve the required separations.

This thesis aims on the development of more efficient monopolar and bipolar membrane electro dialysis processes. Three main topics are investigated:

1. Membrane selectivity
2. Concentration polarisation
3. Membrane scaling and fouling

Membranes with improved selectivities are developed. The investigation of the connection of specific membrane properties to the ion transport allows the development of membranes tailored to the specific needs of the corresponding process.

The reduction of concentration polarisation is possible in two different ways. In the first part the hydrodynamics inside the membrane module is enhanced to achieve higher mass transfer coefficients and therefore delay the appearance of concentration polarisation. Another approach is the earlier occurrence of the overlimiting conductance.

The application of bipolar membrane electro dialysis and problems which arise during operation such as scaling and fouling are investigated. In order to avoid

membrane scaling monovalent ion selective membranes are developed. In addition new possibilities of the use of electrodialysis are explored and investigated.

## General introduction

The membranes described in this thesis have positive or negative charged groups fixed to their polymeric matrix and are generally called ion exchange membranes. There are two different types of ion-exchange membranes: the cation-exchange membrane (CEM) which has negative charged groups fixed to its polymeric matrix and the anion-exchange membrane (AEM) which has positive charged groups fixed to its polymeric matrix. These membranes can be used for electrodialysis process to separate the ions from aqueous solutions under the influence of an electrical potential gradient. When placed in an electrolyte solution, the affinity of an ion exchange membrane for the ions in the solution is different, depending on their specific charge. Anions are repulsed by the electrical charge of CEMs which is identical to that of the fixed ions. The positively charged cations are attracted by the CEMs due to the negatively charged fixed groups in the membrane. This is presented schematically in Figure 1. The ions with opposite charge of the fixed groups of the membrane are denoted counter ions. The ions with the same charge of the fixed groups of the membrane are called co-ions. This type of exclusion of co-ions is usually called Donnan exclusion in honour of the pioneering work of F.G. Donnan [2].

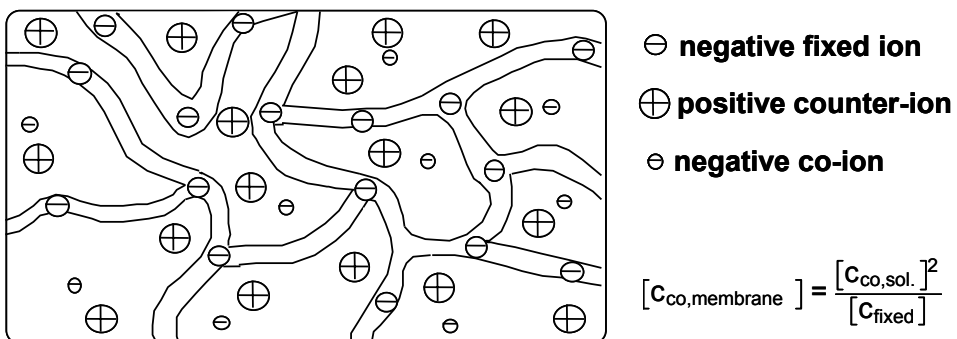


**Figure 1:** Schematic presentation of a cation-exchange membrane next to an electrolyte solution.

The principle of electrodialysis is shown in Figure 2. In the process, an aqueous salt solution is fed to an electrodialysis stack consisting of a series of cation and anion exchange membranes between two working electrodes. When an electric field is applied, the positively charged cations start migrating towards the cathode and the negatively charged anions towards the anode. The cations pass easily through the negatively charged CEMs, whereas the anions are excluded because of their electrical charge which is identical to that of the fixed ions. An alternating arrangement of CEMs and AEMs (see Figure 2) results in the separation of the feed solution into a solution enriched in ions (the concentrate) and a solution depleted of ions (the diluate).

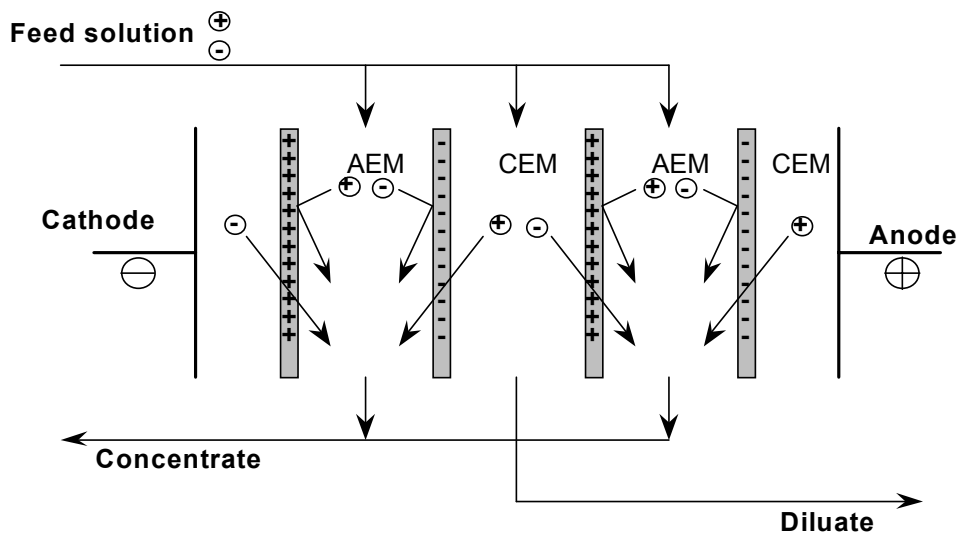


**Figure 2:** Principle of electrodialysis.

A bipolar membrane is a laminate of a cation and an anion exchange layer. It allows the electro-dissociation of water into hydroxide ions and protons without the generation of gases (Figure 3). Bipolar membranes are small chemical reactors with integrated separation, which allow the design of unique processes like the production and recovery of acids and bases, the variation of the pH of a process stream, and the separation of proteins [3].

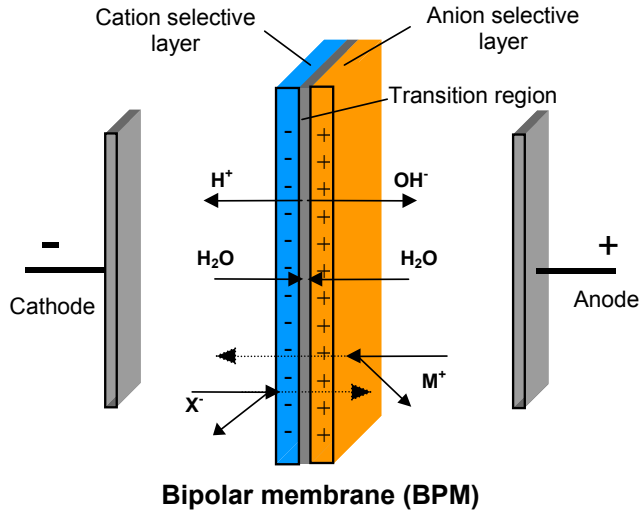


*Figure 3: Water splitting function of a bipolar membrane.*

A typical application of the bipolar membrane electro dialysis (ED-BPM), the production of acid and base from salt, is depicted in Figure 4. The working electrodes establish the electric field as a driving force, salt solution is fed to the central compartment, and the ions migrate out of this compartment into the neighbouring ones.

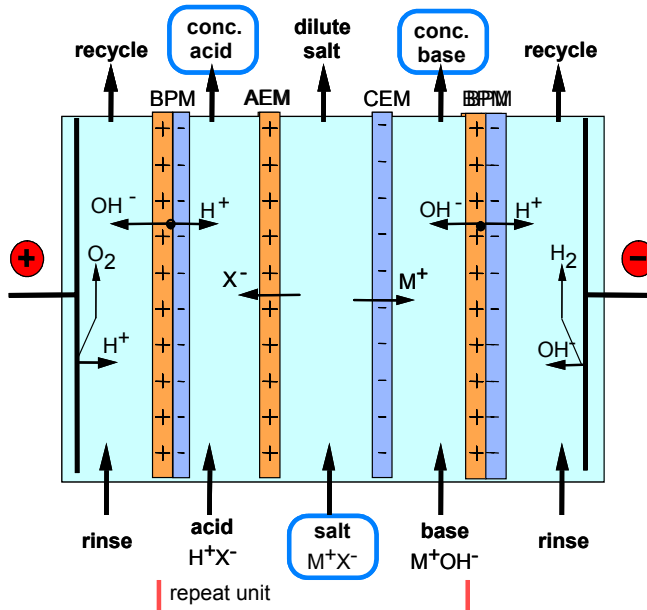


*Figure 4: Schematic of a ED-BPM membrane module for the production of acids and bases.*

Charge compensation because of electro-neutrality occurs due to the water splitting at the interface of the BPM. Other stack configurations (sequence of CEMs, AEMs and BPMs) are also possible as long as electro neutrality is obeyed and counter ions can go through the monopolar membranes to transport the current.

## Structure of this thesis

This thesis can be divided into three major parts. In the first part (Chapter I to III) the function and the use of bipolar membranes is reviewed and membranes are developed focussing on the water splitting activity and the co-ion leakage. The second part (Chapter IV and V) deals with one of the biggest problems in membrane processes and in electrodialysis in particular: concentration polarisation. In the third part (Chapter VI and VII) processes are investigated with high scaling and fouling potential.

In **Chapter I**, an overview is given about the development of bipolar membrane electrodialysis. It contains a literature review resembling the principles of a bipolar membrane and bipolar membrane electrodialysis. The preparation and characterisation methods as well as the limitations of bipolar membranes are given and possible applications are shown.

The influence of the intermediate layer of the bipolar membrane on the water splitting performance is described in **Chapter II**. Bipolar membranes are prepared and the influence of the amount of ionic groups, the composition of the anion exchange layer, the shape of the bipolar membrane junction and the influence of different catalysts are investigated. The results are used for the preparation of tailor made bipolar membranes.

In **Chapter III**, we use bipolar membrane asymmetry to improve selectivity and current efficiency. New asymmetric bipolar membranes with reduced salt leakages are prepared using the interface layer developed in chapter II. It is shown that the flux of salt ions is determined by the co-ion transport across the respective layer of the bipolar membrane. The layer thickness and charge density of the corresponding

ion exchange layer determine the co-ion flux and the asymmetry can be used to decrease these fluxes and obtain product of higher purity.

**Chapter IV** discusses the development and evaluation of optimal spacer configurations to decrease concentration polarisation in electrodialysis and improve the process performance. Standard non-woven net spacers are compared with multi-layer spacers in an electrodialysis desalination process and their performance is evaluated in the light of mass transfer enhancement and cross-flow power consumption.

In **Chapter V** the origin of the overlimiting current in electrodialysis is discussed. Different theories of the origin are evaluated leading to the suggestion that the overlimiting behaviour of the ion exchange membranes may be based on electro-convection. This is a convective mixing mechanism that develops spontaneously in the ion depleted diffusion layer at the advanced state of concentration polarisation. It is shown that under specific experimental conditions electro-convection is the origin of the overlimiting current.

The last two chapters focus on the application of bipolar membrane electrodialysis and problems which arise during operation such as scaling and fouling. In order to avoid membrane scaling monovalent ion selective membranes are developed.

**Chapter VI** analyses the separation properties of various commercial cation exchange membranes and tailor made membranes based on sulphonated poly(ether ether ketone) and poly(ether sulphone) for binary electrolyte solutions containing protons and calcium ions. All membranes are thoroughly characterised and relations between their electrochemical properties and ion selectivity are drawn. In the **Appendix** different coatings are applied to a commercial cation exchange membrane and the selectivity and coating stability are evaluated.

In **Chapter VII** an alternative process for the precipitation of casein proteins from milk is proposed and tested in lab and pilot scale. The scaling and fouling behaviour using various cation exchange membranes is evaluated and the efficiency of the new process is estimated.



**References**

- [1] M. Mulder, Basic Principles of Membrane Technology, 2<sup>nd</sup> Edition, Kluwer Academic Publishers, Dordrecht (1996).
- [2] F.G. Donnan, The theory of membrane equilibrium in presence of a non-dialyzable electrolyte, Z. Elektrochemistry 17 (1911) 573.
- [3] J. Balster, D.F. Stamatialis, M. Wessling, Electro-catalytic membrane reactors and the development of bipolar membrane technology, Chemical Engineering and Processing 43 (2004) 1115-1127.



## Chapter I

### The development of Bipolar Membrane Technology

J. Balster, D.F. Stamatialis, M. Wessling

#### **Abstract**

Membrane reactors are currently under extensive research and development. Hardly any concept however is realized yet in practice. Frequently, forgotten as membrane reactors are electro-catalytic membrane reactors where electrodes perform chemical conversions and membranes separate the locations of conversion.

In this chapter we extensively describe a technology where the membrane itself is catalytically effective, splitting water into protons and hydroxyl ions: bipolar ion-exchange membrane technology.

## 1. Introduction

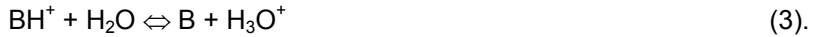
A bipolar membrane (BPM), a special type of polymeric layered ion exchange membrane, consists of a cation and an anion exchange layer joined together. BPMs allow the electro-dissociation of water into hydroxide ions and protons without generating gases. This membrane water splitting technology is a typical example for process intensification. Electrodialysis with BPMs combines reaction and separation in one unit and allows the design of unique processes like the production and recovery of acids and bases, the variation of the pH of a process stream, and the separation of proteins.

## 2. Principle of a BPM

If a CEM and an AEM are placed in an electric field and salt solution is fed in between the two membranes, the salt ions are removed from the enclosed compartment (Figure 1a). This desalination proceeds until all ions are depleted from the compartment. As a result, a significant increase of the electrical resistance due to the decreased ion conductivity is observed. After the salt ion depletion, current can only be transported by hydroxyl ions and protons generated by water dissociation (Figure 1b). To minimize the electrical resistance, the AEM and CEM have to be placed closely together. Laminating both on top of each other results in minimum resistance and a BPM is formed. Water diffuses into the BPM from the surrounding solutions and dissociates under the electric field, at the interface between the anion and the cation exchange membrane, to generate protons and hydroxyl ions (Figure 1c).



The  $\text{H}^+$  and  $\text{OH}^-$  ions further migrate out of the junction layer through the anion and cation exchange layers of the BPM. The thickness of the transition region, where the water dissociation takes place, is less than 10 nm [1]. Strathmann et al. [2] reported that the water dissociation in a BPM is accelerated up to 50 million times compared to the rate of water dissociation in aqueous solutions. This acceleration is influenced by the strong electric field across the transition region. The main driving force for the enhanced water dissociation seems to be the reversible protonation and deprotonation of the functional groups of the ion-exchange membranes, mainly of the tertiary amino groups B of the anion-exchange layer (see Equation 2 and 3) [1- 4].



The BPMs can be used not only for the dissociation of water, but also for the splitting of other self-dissociating liquids, like methanol [5].

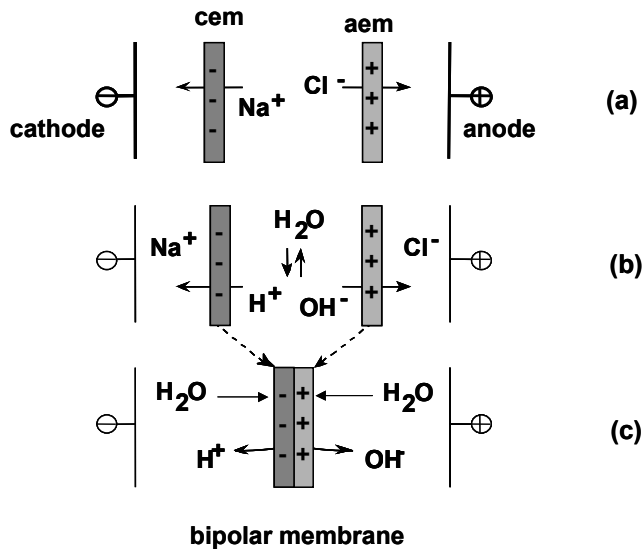


*Figure 1: Schematic drawing of the water splitting function of a BPM, taken from [3].*

### 3. Principle of Bipolar Membrane Electrodialysis

The BPM is stacked together with monopolar CEM and AEM into a membrane module. A typical application of the bipolar membrane electrodialysis (ED-BPM), the production of acid and base from salt, is depicted in Figure 2. The working electrodes establish the electric field as a driving force, salt solution is fed to the central compartment, and the ions migrate out of this compartment into the neighbouring ones. Charge compensation because of electro-neutrality occurs due to the water splitting at the interface of the BPM. Other stack configurations (sequence of CEMs, AEMs and BPMs) are also possible as long as electro neutrality is obeyed and counter ions can go through the monopolar membranes to

transport the current. The selectivity of the membranes strongly depends on the concentrations of salt, acid and base. According to Donnan equilibrium, more co-ions can migrate through the membranes at higher solution concentrations, which in fact reduces the purity of the produced acids and bases [6, 7]. These undesired ion migration fluxes are also visualised in Figure 2.

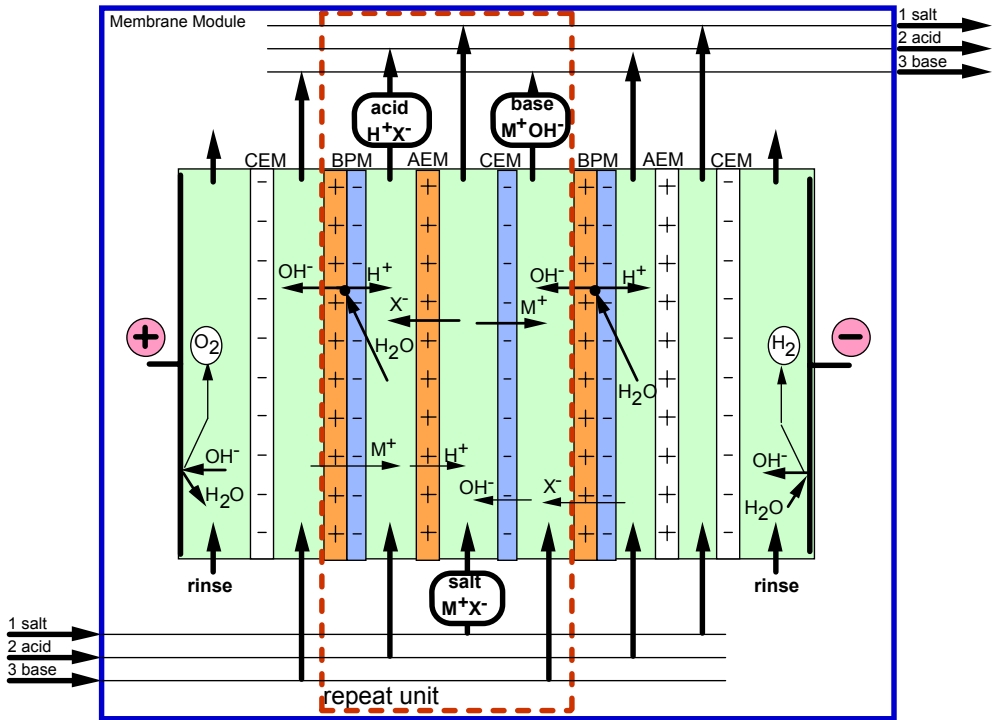


**Figure 2:** Schematic drawing of membrane stack with the indication of desired ion migrational fluxes (upper part) and undesired ion migrational fluxes (lower part), taken from [7].

#### 4. Preparation of BPMs

The performance of a BPM in electrodiagnosis processes depends on the BPM components. The selection of the membrane materials influences mainly the chemical and mechanical stability, the transport properties of the membrane layers and the strength and topology of the intermediate region. As a result the energy consumption, the product concentration, and quality (extent of salt impurities), the

long-term operation of such membranes and their economical feasibility is influenced as well.

The anion and cation permeable layers of the BPM consist of materials similar to standard anion and cation permeable membranes, which are stable in the environment encountered in acid/base electro dialysis. The two selective layers should allow the selective transport of the water splitting products. Furthermore the membrane layers should allow a sufficient water flux from the base and/or acid compartment into the membrane junction to replenish the water consumed by the water dissociation reaction (Figure 1c) otherwise irreversible degradation occurs [8]. In addition, the membrane layers should block co-ions from reaching the membrane junction and the opposite side of the membrane, because these co-ion fluxes are responsible for product contamination. Many BPMs are prepared by using commercial ion exchange membranes as a precursor for one or both bipolar membrane layers [9-14], but novel BPMs have been developed as well [6, 7].

The structure of the BPM junction is important for the electro catalytic water splitting function of the complete system. The water dissociation rate is accelerated, for a fixed electric potential across the contact region, when a catalyst is present. The catalyst reduces the activation energy of the water dissociation because it provides alternative reaction paths by forming reactive, activated complexes. As catalysts in the bipolar junction, immobile weak acids or bases with an equilibrium constant of the acid/base pair close to that of the water dissociation reaction ( $pK_a = 7$ ) could be used [9]. Alternatively, heavy metals ion complexes, like those of zirconium, chromium, iron or others could be applied [10-16]. The metal ions or complexes are immobilized by either including an insoluble salt of them in the interface layer [14] or by converting a soluble salt by a subsequent treatment. The most suitable multivalent metal ion hydroxides are immobilized due to their low solubility. The location of the water dissociation and the preferred location of the catalyst (to the anion or cation exchange layer) are still subject of investigation.

Besides the catalyst, the BPM junction should also have a certain surface roughness to increase the membrane contact area. Several BPMs have already been developed having smooth [11, 13, 15], corrugated [10, 16-18], or heterogeneous [14, 16, 19-21] membrane junctions.

The preparation of well-composed BPMs requires the establishment of efficient contact of the CEM and AEM. This can be established by either loosely laminating [11-13, 15], pressing [14, 21], gluing [22] of the two pre-formed membranes, or casting one membrane above the other [17-19, 23]. Other methods, however, like co-extruding [24] or modifying [20, 25] do not show well-defined interface structures due to the weak influence on these regions during the preparation processes. Recently, the gluing method has been used by Wilhelm et al [6] for the preparation of BPMs from commercially available AEMs (Neosepta AMX from Tokuyama Corp. and IonClad R4030 from Pall Gelman) and tailor-made cation-permeable layers [6]. The CEM was a sulphonated poly(ether ether ketone) (S-PEEK) / poly(ether sulphone) (PES) blend and the adhesive was S-PEEK / PES solution. The properties of the CEM could be adjusted through the S-PEEK content of the blend with PES. With increase of the SPEEK content, the ion exchange capacity and the water uptake increase, whereas the resistance and the density of the membrane decrease [6]. Hao et al. [23] have prepared BPMs by casting. Their membranes consisted of an AEM with cross-linked matrix (prepared by the reaction of chloromethylated polysulphone (Psf) with diamine), an interfacial layer (made from chloromethylated Psf solution containing cation exchange resin and amine), and a CEM (made from a cation resin powder dispersed in sulphonated Psf).

## **5. Characterization of BPMs**

The electrical energy consumption of a BPM process depends on the electrical resistances of the monopolar membranes included in the stack and the current-voltage characteristics of the BPM [26, 27]. Current-voltage curves can be obtained with the stack configuration, schematically drawn in Figure 3. The central BPM in the stack is the investigated one. The other membranes are auxiliary membranes preventing the transport of water dissociation products, formed at the two working electrodes, to the central compartments. During the experiment, the applied current density is increased stepwise and the system is allowed to reach a steady state. The voltage drop across the membrane is measured, followed by the next increase in current density.



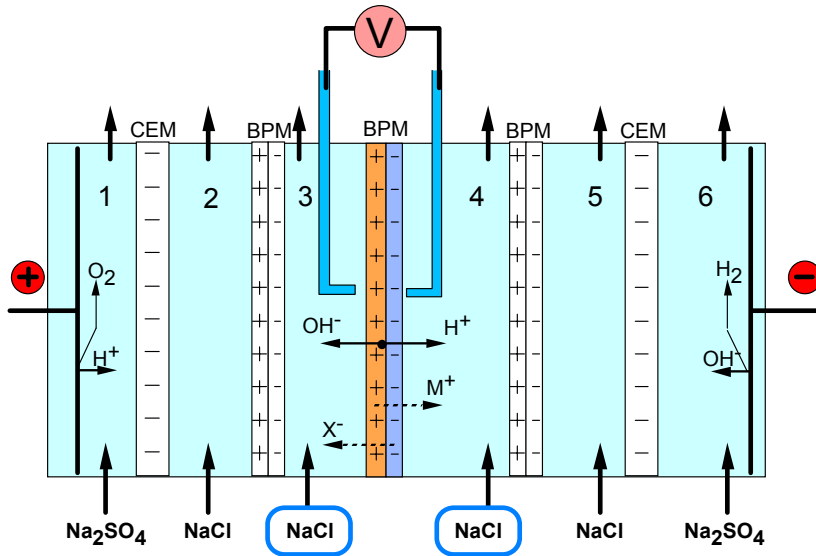


**Figure 3:** Schematic representation of a six-compartment measurement module for current-voltage curve and chronopotentiometric measurements, taken from [6].

The experimental current-voltage curve of a BPM recorded in a neutral salt solution ( $M^+X^-$ ) shows characteristic parts (see Figure 4) [9]. Below the lower limiting current density ( $i_{lim1}$ ) the current is only transported by salt ions.

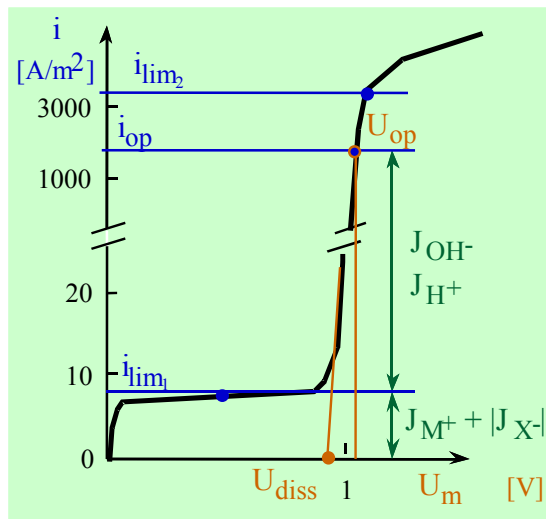


**Figure 4:** Schematic current-voltage curve of a BPM in a salt ( $M^+X^-$ ) solution [6].

At the limiting current density the electrical resistance is the highest since all salt ions are removed from the BPM junction. The magnitude of the lower limiting current is a measure for the selectivity of the BPM towards co-ion leakage (the reader is reminded that this lower limiting current density only exists to a membrane in its salt form). Above this current density, water splitting occurs ( $U_{\text{diss}}$ ) and the water splitting products ( $J_{\text{OH}^-}/J_{\text{H}^+}$ ) are also available to transport the current [28]. The operating current density ( $i_{\text{op}}$ ) is chosen as high as possible to reduce the relative salt ion transport and to have a high water splitting efficiency. According to Aritomi et al. [8] and Krol et al. [29], above the upper limiting current ( $i_{\text{lim}2}$ ) the water transport toward the BPM junction is not sufficient to replenish the water split at the corresponding rate.

Another technique commonly used for the characterization of the BPM is chronopotentiometry [30, 31]. Chronopotentiometry allows the determination of the actual water splitting voltage, the irreversible energy loss due to the resistance of the monolayers of the BPM and the salt ion transport behaviour through the BPM [27]. During the chronopotentiometric measurements a constant current density is applied and the voltage drop between electrode and reference electrode is measured as a function of time (Figure 5).

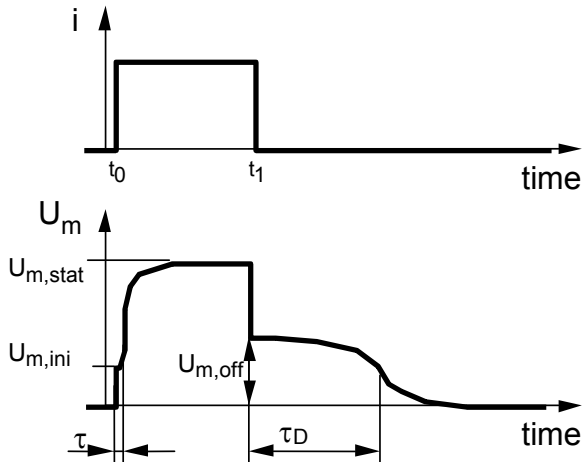


**Figure 5:** BPM chronopotentiometry principle, adapted from [31]. A current density  $i$  is imposed at time  $t_0$  and switched off at time  $t_1$  while the electric potential difference over the membrane  $U_m$  is recorded in time ( $U_{m,ini}$ = initial;  $U_{m,stat}$ = static;  $U_{m,off}$ = after switch off). The transition time  $\tau$  and the de-charging time  $\tau_D$  are obtained from the inflection points indicated.

Chronopotentiometry allows the direct comparison of the initial resistance of a BPM in equilibrium with the resistance in operation (water dissociation conditions) [27].

The current efficiency and the purity of the produced acids and bases of the electrodialysis process are directly related to the  $M^+/X^-$  leakages through the BPM. The co-ion leakage results in product contamination and reduces the efficiency of the  $H^+/OH^-$  electro generation. High water splitting capability and a low co-ion leakage are required at the same time. These properties as well as the maximal obtainable product concentrations are measured by acid/base titration [27].

## 6. Limitations of EDBPM

One of the main limiting phenomena of EDBPM is the water splitting performance [5, 32]. Water, which is consumed by the dissociation into protons and hydroxide ions, has to be replenished by diffusion of water from the outer solution of the two-monopolar layers into the BPM interphase. When the rate of the water dissociation is faster than the water transport into the BPM transition region, water transport is the limiting step and results in drying out of the BPM, which causes a drastic increase in the resistance [1, 33]. This performance is controlled by the permselectivities of the ion exchange layers of the BPM and by ion diffusive transport. An additional loss of process permselectivity is obtained by the leakage through the monopolar ion exchange membranes (Figure 2). Due to these leakages the current efficiency of the process is reduced and the purity of the products is limited [32].

Another major limitation is the concentration range in which the EDBPM processes can be used. At very low concentrations, the electric resistance of the electrolyte solution in the compartments between the membranes is very high, whereas at high concentrations the selectivity of the BPM and the ion exchange membranes is very low [34]. Additionally, the chemical stability of the BPM, especially against a concentrated base on the anion permeable side, is not always sufficient [7].

## 7. ED-BPM processes

ED-BPM processes can be performed with different stack configurations, depending on the desired application [5, 35-37]. For the treatment of concentrated salt solutions and the production of the corresponding acids and bases, a three-compartment cell system consisting of an AEM, a CEM and a BPM as repeat unit is used (Figure 2). In an industrial-type unit, up to 100 cell triplets could be installed in an electrodiolysis stack [8]. In applications where it is not possible to obtain high purity of both products (acid and base) or products with low conductivity are produced, a two-compartment cell is then recommended [5, 37]. This configuration can be used together with a CEM for acidification (see in Figure 6) or with an AEM for alkalization of a salt stream [5, 38]. If a high ratio of acid or base with respect to the product salt content is required, a configuration with two monopolar membranes of the same type can be applied. In this configuration the outlet of the middle loop is recycled again into the acidic or base loop next to the BPM for a more efficient exchange between protons and cations, or between hydroxyl ions and anions [35, 68].

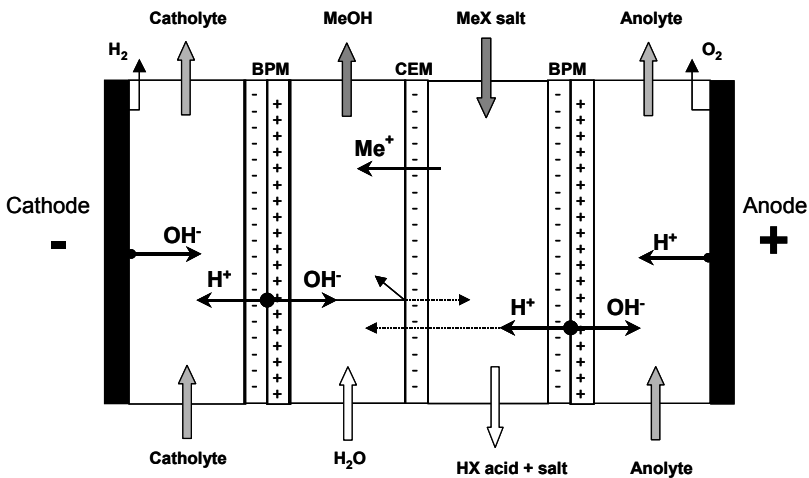


*Figure 6: Cell arrangement configuration for direct acidification.*

Several applications of EDBPM have already been investigated with promising results. Typical examples are the production of acid and base [36, 39], the acidification of product streams [40, 41] or special separations like the separation of amino acids and proteins on the basis of their isoelectric points [5, 6]. Economically,

the most interesting applications are those in the overlap of the areas schematically presented in Figure 7.

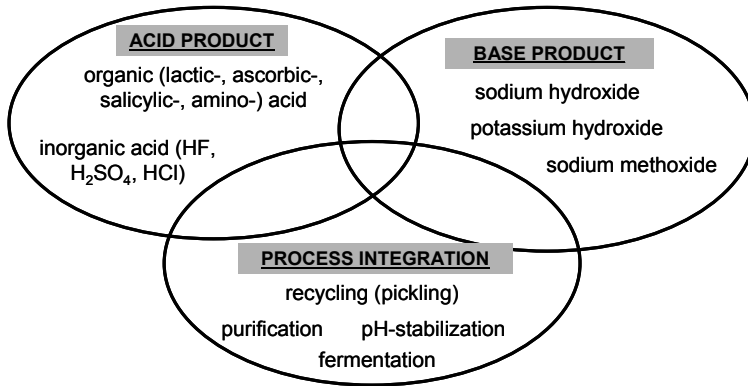


**Figure 7:** Possible areas of applications for ED-BPM, taken from [7].

Designing ED-BPM in the overlapping areas provides increasing prospects for its economic feasibility, but it also increases the complexity and the challenges that have to be met [7]. An example of a successful overlap is the conversion of sodium lactate from a fermentation step into lactic acid by ED-BPM with a use of the side product, sodium hydroxide, to control the fermentation reaction [4]. Further examples can be found in other reviews concerning ED-BPM applications [5, 35, 37].

## 8. List of symbols

$i$	Current density [ $A/m^2$ ]
$i_{lim}$	Limiting current density [ $A/m^2$ ]
$i_{op}$	Operation current density [ $A/m^2$ ]
$J$	Flux [ $mol/(m^2s)$ ]
$J_{H^+}$	Hydrogen ion flux [ $mol/(m^2s)$ ]
$J_{OH^-}$	Hydroxide ion flux [ $mol/(m^2s)$ ]
$J_{M^+}$	Cation flux [ $mol/(m^2s)$ ]
$J_{X^-}$	Anion flux [ $mol/(m^2s)$ ]

$M^+$	Salt or base cation
$t$	Time [s]
$t_0$	Starting time [s]
$t_1$	Ending time [s]
$U$	Potential difference [V]
$U_{\text{diss}}$	Dissociation potential difference [V]
$U_m$	Membrane potential difference [V]
$U_{m, \text{ini}}$	Initial membrane potential difference [V]
$U_{m, \text{stat}}$	Static membrane potential difference [V]
$U_{m, \text{off}}$	Membrane Potential difference after [V] switching off
$U_{\text{op}}$	Operation potential difference [V]
$X^-$	Salt or acid anion
$\tau$	Transition time [s]
$\tau_D$	Decharging time [s]
AEM	Anionic exchange membrane
BPM	Bipolar membrane
CEM	Cationic exchange membrane
ED-BPM	Bipolar membrane electrodialysis
PEEK	Poly(ether ether ketone)
PES	Poly(ether sulphone)
Psf	Polysulphone
S-PEEK	Sulphonated poly(ether ether ketone)

## 9. References

- [1] H.-J. Rapp, Elektrodialyse mit bipolaren Membranen – Theorie und Anwendungen, Ph.D. thesis, Universität Stuttgart, Institut für Chemische Verfahrenstechnik, Germany (1995).
- [2] H. Strathmann, J.J. Krol, H.-J. Rapp, and G. Eigenberger, Limiting current density and water dissociation in bipolar membranes, Journal of Membrane Science 125 (1997) 123-142.

- [3] J. J. Krol, Monopolar and bipolar ion exchange membranes – Mass transport limitations, Ph.D. thesis, University of Twente, Enschede, The Netherlands, (1997).
- [4] S. Mafe, P. Ramirez, A. Alcatraz, and V. Aquilella, Ion Transport and Water Splitting in Bipolar Membranes: Theoretical Background, in A.J.B. Kemperman (ed.), Bipolar membrane Handbook, Twente University Press, Enschede, The Netherlands, (2000) Chapter 3 pp. 47-78.
- [5] G. Pourcelly, Electrodialysis with Bipolar Membranes: Principles, Optimization, and Applications, Russian Journal of Electrochemistry 38 (2002) 919-926.
- [6] F.G. Wilhelm, I. Punt, N.F.A. van der Vegt, M. Wessling, and H. Strathmann, Optimization strategies for the preparation of bipolar membranes with reduced salt ion leakage in acid-base electrodialysis, Journal of Membrane Science, 182 (2001) 13-28.
- [7] F.G. Wilhelm, Bipolar Membrane Electrodialysis – Membrane Development and Transport Characteristics, PhD thesis, University of Twente, Enschede, The Netherlands (2001).
- [8] T. Aritomi, T. van der Boomgaard and H. Strathmann, Current voltage curve of a bipolar membrane at high current density, Desalination 104 (1996) 13-18.
- [9] F. G. Wilhelm, N. F. A. van der Vegt, M. Wessling, and H. Strathmann, Bipolar Membrane Preparation, in A.J.B. Kemperman (ed.), Bipolar membrane Handbook, Twente University Press, Enschede, The Netherlands (2000) Chapter 4, pp. 79-108.
- [10] F. Hanada, K. Hiraya, N. Ohmura, and S. Tanaka, Bipolar membrane and method for its production, Tokuyama Soda Ltd. (Japan), US Patent 5221455 (1993).
- [11] R. Simons, High Performance Bipolar Membranes, Unisearch Ltd. (Australia) WO Patent 89/01059 A1 (1989).
- [12] R. Simons, Preparation of a high performance bipolar membrane. Journal of Membrane Science, 78 (1993) 13-23.

- [13] F. Posar and M. Riccardi, Process for the manufacture of a bipolar membrane and process for the manufacture of an aqueous alkali metal hydroxide solution, Solvay S.A. (Belgium), US Patent 5380413 (1995).
- [14] K. Umemura, T. Naganuma, and H. Miyake, Bipolar membrane, Asahi Glass Company Ltd. (Japan), US Patent 5401408 (1995).
- [15] F. Posar, Method for making a bipolar membrane. Solvay S.A. (Belgium), US Patent 5849167 (1998).
- [16] F. P. Chlanda, L. T. C. Lee and K. J. Liu, Verfahren zur Herstellung bipolarer Membranen (Process for preparing bipolar membranes), Allied Chemical Corporation (U.S.A.), DE Patent 2737131 (1978).
- [17] R. B. Hodgdon and S. S. Alexander, Novel bipolar membranes and process of manufacture. Ionics, Inc. U.S.A.), US Patent 4851100 (1989).
- [18] B. Bauer, Bipolare Membran und Verfahren zu deren Herstellung (Bipolar membrane and process for its preparation), Fraunhofer-Gesellschaft zur Förderung der Angewandten Forschung e.V (FhG) (Germany), EP Patent 563851 (1993).
- [19] F. P. Chlanda and M. J. Lan, Bipolar membranes and methods of making same, Allied Chemical Corporation, WO Patent 87/07624 (1987).
- [20] K. J. Liu and H. L. Lee, Bipolar membranes. Union Resources and Technology Inc. (U.S.A.), EP Patent 0143582 A2 (1985).
- [21] G. J. Dege, F. P. Chlanda, L.T.C. Lee, and K.J. Liu, Method of making novel two component bipolar ion exchange membranes. Allied Chemical Corp. (U.S.A.), US Patent 4253900 (1981).
- [22] H. Müller and H. Pütter, Verfahren zur Herstellung bipolarer Membranen (Procedure for the preparation of bipolar membranes). BASF AG, Ludwigshafen, (Germany)
- [23] J. H. Hao, C. Chen, L. Li, L. Yu and W. Jiang, Preparation of bipolar membranes (I), *Journal of Applied Polymer Science*, 80 (2001) 1658-1663.
- [24] K. Richau, P. Klug, G. Malsch, R. Swoboda, J. Ziegler, Th. Weigel, St. Otto, U. Martens, K. Kneifel, and H.H. Schwarz, Membranes made from polyelectrolytes – preparation and electrochemical properties, *Proceedings of Euromembrane '97*, (Enschede - the Netherlands) p 234.



- [25] R. El Moussaoui and H. Hurwitz, Single-film membrane, process for obtaining it and use thereof, Université Libre de Bruxelles (Belgium), US Patent 5840192 (1998).
- [26] J.L. Gineste, G. Pourcelly, Y. Lorrain, F. Persin, and C. Gavach, Analysis of factors limiting the use of BPM: a simplified model to determine trends, *Journal of Membrane Science*, 112 (1996) 199-208.
- [27] K. Richau et al, Bipolar Membrane Characterization, in A.J.B. Kemperman (ed.), *Bipolar membrane Handbook*, Twente University Press, Enschede - The Netherlands, (2000) Chapter 5, pp. 109-153.
- [28] F.G. Wilhelm, I. Punt, N.F.A. van der Vegt, M. Wessling and H. Strathmann, Asymmetric Bipolar Membranes in Acid-Base Electrodialysis, *Industrial & Engineering Chemistry Research* 41 (2002) 579-586.
- [29] J.J. Krol, M. Jansink, M. Wessling and H. Strathmann, Behaviour of bipolar membranes at high current density: Water diffusion limitation, *Separation Purification Technology* 14 (1998) 41-52.
- [30] F.G. Wilhelm, N.F.A. van der Vegt, M. Wessling and H. Strathmann, Comparison of bipolar membranes by means of chronopotentiometry, *Journal of Membrane Science* 199 (2002) 177-190.
- [31] F.G. Wilhelm, N.F.A. van der Vegt, M. Wessling and H. Strathmann, Chronopotentiometry for the advanced current-voltage characterisation of bipolar membranes, *Journal of Electroanalytical Chemistry* 502 (2001) 152-166.
- [32] X. Tongwen, Electrodialysis processes with bipolar membranes (EDBM) in environmental protection--a review, *Resources, Conservation and Recycling*, 37 (2002) 1-22.
- [33] B. Bauer, F.J. Gerner and H. Strathmann, Development of bipolar membranes, *Desalination* 68 (1988) 279-292.
- [34] F.G. Wilhelm, N.F.A. van der Vegt and M. Wessling, Bipolar Membrane Electrodialysis for the Production of Acids and Bases, *npt-wetenschapskatern, npt processtechnologie* 1 (2002) 19-21.

- [35] V. Cauwenberg, J. Peels, S. Resbeut and G. Pourcelly, Application of electro dialysis within fine chemistry, *Separation and Purification Technology* 22-23 (2001) 115-121.
- [36] L. Bazinet, F. Lamarche and D. Ippersiel, Bipolar-membrane electro dialysis: Applications of electro dialysis in the food industry, *Trends in Food Science & Technology* 9 (1998) 107-113.
- [37] X. Tongwen and Y. Weihua, Effect of cell configurations on the performance of citric acid production by a bipolar membrane electro dialysis, *Journal of Membrane Science* 203 (2002) 145-153.
- [38] B. Bauer, H. Holdik and A. Velin, Cell Equipment and Plant Design in Bipolar Membrane Technology, in A.J.B. Kemperman (ed.), *Bipolar membrane Handbook*, Twente University Press, Enschede, The Netherlands, (2000) Chapter 6, pp. 155-189.
- [39] G. Pourcelly and C. Gavach, Electro dialysis Water Splitting – Applications of Electro dialysis with Bipolar Membranes, in A.J.B. Kemperman (ed.), *Bipolar membrane Handbook*, Twente University Press, Enschede - The Netherlands, 2000.
- [40] M. Bailly, Production of organic acids by bipolar electro dialysis: realizations and perspectives, *Desalination* 144 (2002) 157-162.
- [41] X. Tongwen and Y. Weihua, Citric acid production by electro dialysis with bipolar membranes, *Chemical Engineering and Processing* 41 (2002) 519-524.

## Chapter II

### Tailoring the interface layer of the bipolar membrane

J. Balster, S. Srinantharajah, R. Sumbharaju, I. Pünt,  
R.G.H. Lammertink, D.F. Stamatialis, and M. Wessling

#### **Abstract**

In this chapter, the effects of various parameters affecting the water splitting of a bipolar membrane are investigated. We show that the amount of functional groups and the water content of the interface layer have a big influence on the bipolar membrane resistance due to the higher water content of the layer and the higher water molecule polarisation between the anion and cation exchange layer. The use of anion exchange layers containing quaternary ammonium groups instead of bicyclic amines results in bipolar membranes with strongly reduced resistance. The influence of two different types of catalysts based on Fe and pyridine are tested, too. We show that the pyridine based interface layer is a good tool to prepare tailor made bipolar membranes containing anion exchange layers with high base stability without having water splitting catalytic functional groups.

## 1. Introduction

Bipolar membrane electro dialysis (ED-BPM) can be used to produce acids and bases from their corresponding salt solutions. A bipolar membrane (BPM) is a laminate of a cation and anion exchange layer and allows the dissociation of water into protons and hydroxyl ions under the influence of an electric field (Figure 1). The three layers of a BPM, the anion exchange layer, the cation exchange layer and the bipolar membrane junction (interface between anion and cation exchange layer), play an important role in its performance in an electro dialysis process. The overall water dissociation reaction into hydroxyl ion and proton (hydronium ion) is described by the water equilibrium [1].



The water dissociation rate in a BPM was found to be 50 million times faster than the ordinary water dissociation in aqueous solution [2].

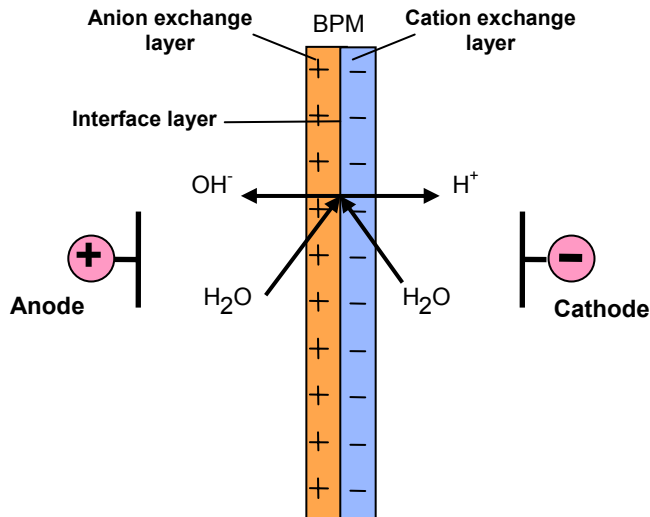


**Figure 1:** Schematic drawing of the water splitting function of a BPM.

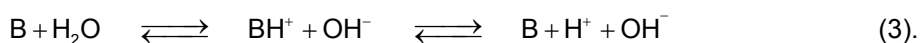
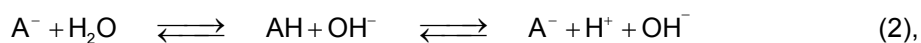
The conditions for water dissociation in a bipolar membrane junction are very different to the dissociation in free water. This is caused by the presence of a polymer matrix, the fixed ionogenic groups, counter ions and the presence of an

electrical charged layer between the cation and anionic membrane. Under operational conditions, this layer has low concentration of both counter and co-ions [3], but the current is carried by protons and hydroxyl ions which split in the BPM junction. The rate of water dissociation depends significantly on the characteristics of the interface layer [4-7].

Water splitting occurs already if a cation exchange and anion exchange membrane which are in loose contact with each other are placed in an electric field with the correct polarity and sufficient electric field strength [1]. The produced protons and hydroxyl ions are transported through the corresponding ion exchange layers, away from the interface (see Figure 1). The water splitting region can be part of the either anion or cation selective layer at the contact interface of the two layers.

Ramirez et al. [8] explained the water dissociation reaction using the Donnan effect and the Nernst-Planck equation. The water molecule dissociates at an increased rate in accordance with the second Wien effect [2, 8, 9], which suggests the degree of dissociation of weak electrolytes at high electric field to be accelerated. However, Strathmann et al. [4, 5] calculated that the increase in water splitting due to the second Wien effect is still at least three orders of magnitude smaller than the experimentally observed results.

Simons observed differences in the water dissociation behaviour between anion and cation exchange membranes and suggested that the water dissociation is caused by proton transfer between the fixed charged groups and water molecules existing in the interface [10, 11]. The water dissociation is a proton-transfer reaction that is catalysed by weak acids and bases. With an immobile weak neutral acid AH or the corresponding acid  $BH^+$  of a weak neutral base B as a catalyst, this reaction can be split into two consecutive reactions (simplified for the proton  $H^+$  instead of the hydronium ion  $H_3O^+$ ) [10]:



In an electric field, the charged mobile ions  $\text{OH}^-$  and  $\text{H}^+$  are removed from the reactive sites of the contact region. Their mobility is significantly accelerated due to the proton and hydroxide ion tunnelling similar to aqueous solutions [12].

As mentioned before, the ionic groups are extremely important in the water splitting mechanism. Investigation of membranes with sulphonic, carboxylic and phosphonic acid groups concludes that the decrease in the potential differences in the membrane is [3]:



This decrease can be explained by the activation energy which is necessary for the interaction of the ionic group with the water molecule. The pK increases namely in the same order. In terms of catalytic activity, the ionic groups of bipolar membranes can be arranged in order of increasing rate constants for the water dissociation (see Table 1).

**Table 1:** Catalytic activity of different ionic groups.

Ionic group	$-\text{N}(\text{CH}_3)_3$	$-\text{SO}_3\text{H}$	$-\text{PO}_3\text{H}^-$	$=\text{NH}, -\text{NH}_2$	$\equiv\text{N}$	$-\text{COO}^-$	$-\text{PO}_3^{2-}$
$k [\text{s}^{-1}]$	0	$3 \cdot 10^{-3}$	$3 \cdot 10^{-2}$	$10^{-1}$	1	10	$10^2$

The dependence of activation energy for the dissociation of water on the nature of ionogenic groups is important evidence to support the catalytic mechanism inside the bipolar membrane for water splitting. The activation energy for membranes with a weak catalytic effect is lower than the activation energy in pure water ( $56 \text{ kJ} \cdot \text{mol}^{-1}$ ). The phosphonic acid groups show the lowest value [3].

However, BPMs do not perform efficient water dissociation if they are prepared with anion and cation exchange layers only. To improve the performance of a BPM, a thin interface layer, containing a water dissociation catalyst, is generally introduced between the charged layers. Four parameters influence the water splitting performance of a BPM:

1. The amount of ionic groups at the interface layer [13-15],
2. the composition of the anion exchange layer [7],
3. the structure of the BPM junction [1, 16],
4. the water dissociation catalyst [17-23].

An increased amount of ionic groups present at the BPM function increase the polarity of the interface layer and enhances the water splitting reaction [13]. In addition the hydrophilicity of the BPM interface is enhanced, which accelerates the water-splitting reaction because the hydrophilic polymer layer increases the water activity by attracting water from the ion exchange layers to the space charge region [14, 15].

The composition of the anion exchange layer of a BPM plays an important role as well [7]. Anion exchange membranes show different water dissociation behaviour than cation exchange membranes due to the possible proton transfer between the fixed charged groups and the water molecules [10, 11]. If the anion exchange layer contains secondary or tertiary amines, the water splitting reaction is catalysed (equation 3). Nowadays most of the commercially available anion exchange membranes contain quaternary ammonium groups.

The structure of the BPM interface influences the resistance and the stability of the BPM. The electric resistance increases if a depleted film is developed between the two layers during operation. Therefore the interface of the BPM should be tailored to minimise electric resistance and to attain a firm bonding of the ion exchange layers. A firm bonding avoids the separation of the two layers (ballooning) if no sufficient current is applied [16].

Catalysts provide alternative reaction paths for the dissociation reaction by forming very reactive, activated complexes [10, 17]. The best catalytic activities have been found for sufficient amounts of weak acids (and the corresponding base) such as amino groups, pyridines, carboxylic acids, and phosphoric acid groups [1, 5, 18, 19]. Besides inorganic substances such as metal oxides and hydroxides [20] or heavy metal ion complexes (ruthenium trichloride, chromic nitrate, indium sulphate, and hydrated zirconium oxide) [13, 21, 23] are also good catalysts.

In theory the potential difference across a 100% permselective BPM for the generation of one molar acid and base at 25°C can be estimated to be 0.83V [24]. Higher potential drops across the BPM are resulting from the electrical resistance of the cation exchange, anion exchange and interface layer.

The objective of this chapter is to systematically investigate the influence of the interface layer on the water splitting performance of the BPM. We therefore address

the four parameters described above. Especially for the catalysts, different catalytic layers, based on iron and pyridine are introduced and their influence on the water splitting performance is investigated.

## 2. Experimental

### 2.1 Materials

The commercially available Neosepta CMX (from Tokuyama Soda Ltd.), or blends of sulphonated poly(ether ether ketone), S-PEEK, and poly(ether sulphone, PES, have been used as cation exchange layer of the BPMs. S-PEEK was prepared by sulphonation of poly(ether ether ketone) (PEEK) 450PF (Viktrex), as described in [25]. The S-PEEK/PES blends (indicated as S/P in the text) were prepared by adding 60% S-PEEK and 40% PES to the solvent N-methyl-2-pyrrolidinone, NMP, (in total 20 wt% polymer in solution), stirred for a minimum of 24 h and filtered over a 40  $\mu\text{m}$  metal filter.

As anion exchange layers, the Neosepta AM-3 (from Tokuyama Soda Ltd.), the IonClad R4030 (from Pall Gelman) or a tailor made membrane prepared from aminated polysulphone, Psf (FuMA-TECH GmbH, St. Ingbert, Germany, indicated as A-Psf in the text) in NMP (10 wt% polymer in solution) were used.

For the contact region of the BPM different materials have been used:

1. S-PEEK of various sulphonation degree (SD),
2.  $\text{Fe}(\text{OH})_3$  granular (0.2 - 2mm) from Merck,
3. poly(4-vinyl pyridine), P4VP, from Sigma-Aldrich ( $M_w=60000\text{g/mol}$ ),
4. poly(acrylic acid), PAA, from Sigma-Aldrich ( $M_w=100000\text{g/mol}$ ), and
5. poly(ferrocenyl dimethylsilane), PFS, an iron containing polymer prepared by the Materials Science and Technology of Polymers group of the University of Twente, Enschede (see Figure 2).



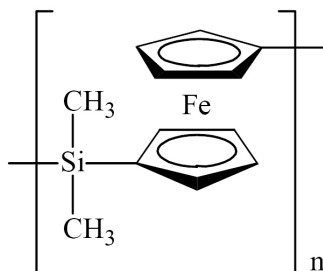


**Figure 2:** Repeat unit of poly(ferrocenyl dimethylsilane), PFS.

The PFS polymer was dissolved in chloroform while all the other materials were dissolved in NMP.

## 2.2 BPM preparation

Single ion exchange membranes as well as the BPMs were prepared by the evaporation technique [26]. In order to have a good contact between the different layers the casting method was used (Figure 3) [27]. The polymer layers were cast with the desired thickness and sequence onto a glass plate. After the solidification of one layer the next layer was cast on top of the former, which then was allowed to dry. This procedure was repeated until all desired layers (cation exchange layers, CELs, Interface layers, anion exchange layers, AELs) were cast onto each other. If one of the layers was a commercial membrane, the other layers were cast on top of it, as described above. When two commercial ion exchange membranes were used, the membranes were just pressed together.

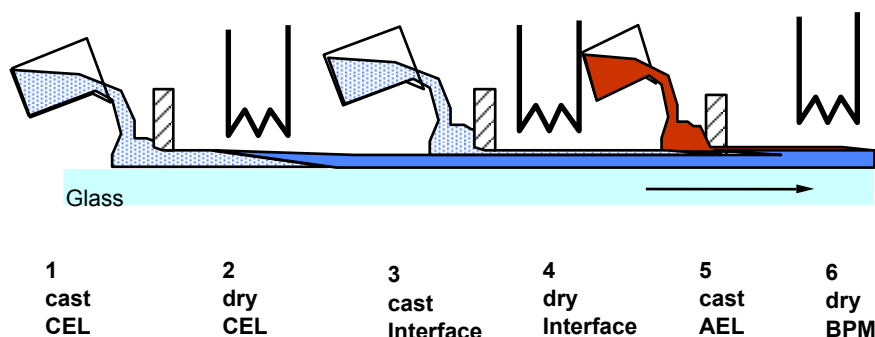


**Figure 3:** Schematic drawing of the BPM preparation by casting, adapted from [28].

The tailor made membranes were dried in  $N_2$  atmosphere at 40-80 °C for 1 week, then immersed in water and subsequently dried under vacuum at 30 °C for 1 week. The membranes were finally stored in a 2 M NaCl solution.

The  $Fe(OH)_3$  at the interface layer of the BPM junction was added by two different methods:

- The  $Fe(OH)_3$  granular was dispersed in a S-PEEK solution and casted, or
- Electrodeposition (as described by Kang et al. [21]), was performed using a two compartment cell (with a membrane area of 3.14 cm<sup>2</sup>, see Figure 4). The concentration of  $Fe(OH)_3$  immobilised at the junction was controlled over the applied current density and deposition time.

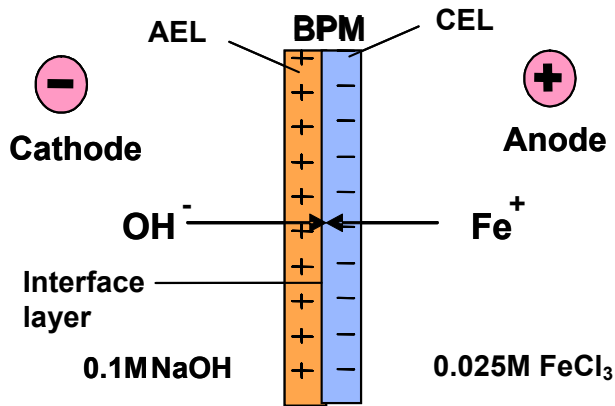


**Figure 4:** Schematic illustration of the electrodeposition of iron hydroxides at the BPM interface.

After the electrodeposition, the membrane was washed in a 2M NaCl solution for one day to remove excess of  $Fe^{3+}$  ions from the membrane.

### 2.3 Characterisation of the ion exchange membrane layers

The commercial AM-3 and CMX membranes and the tailor made ion exchange membrane layers were characterised by measurements of ion exchange capacity (IEC) and water uptake (w). These properties were used to calculate the sulphonation degree (SD) and the charge density ( $c_{char}$ ) of the membranes (more details in [25, 26]). The properties of all membranes are shown in Table 2.

**Table 2:** Properties of the commercial and tailor made ion exchange membranes used as ion exchange layers of the prepared BPMs.

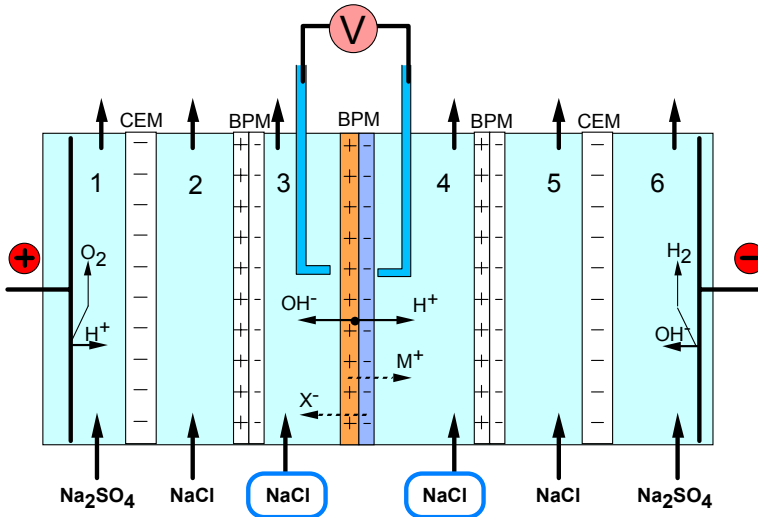
Membrane	Used as	Functional group	IEC [mol/kg <sub>dry</sub> ]	w [kg <sub>water</sub> /kg <sub>dry</sub> ]	C <sub>char</sub> [mol/L]
CMX	CEL	Sulphonic acid	1.65	0.26	6.4
S/P	CEL	Sulphonic acid	1.30	0.34	3.8
AM-3	AEL	quaternary ammonium	1.65	0.20	8.3
R4030	AEL	quaternary ammonium	0.81	0.19	4.3
A-Psf	AEL	bicyclic ammonium	1.84	0.36	5.1

## 2.4 Characterisation of the BPMs

Many properties of a BPM can be determined from steady state current density – voltage drop (*i-v*) measurements (see Figure 5) [28, 29]. The central BPM is the investigated membrane, whereas the other membranes are auxiliary membranes, necessary to maintain well defined, constant concentrations in the two central compartments. During the experiment the temperature was held constant at 25°C, the applied current density was increased stepwise and the system was allowed to reach steady state. The voltage drop across the membrane was measured with calomel electrodes at a fixed distance from the membrane surface by Haber-Luggin capillaries filled with concentrated KCl solution.

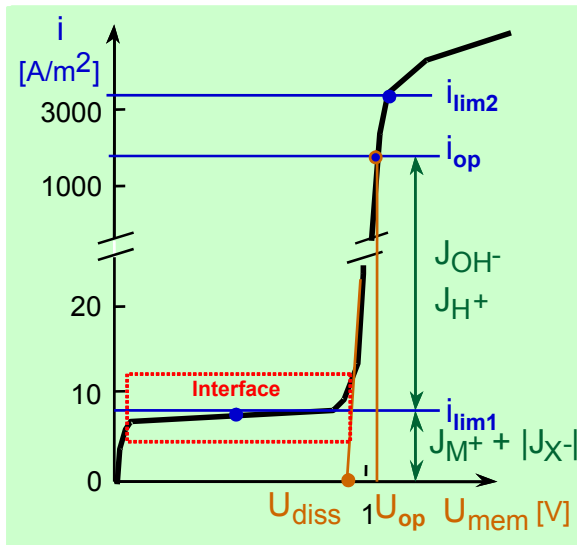
Generally, in such measurements, the solution resistance is subtracted. However, the solution resistance close to the BPMs decreases at higher current densities due to the generation of H<sup>+</sup> and OH<sup>-</sup> (the conductivity next to the membrane increases). Therefore the *i-v* curves were not corrected for the solution resistance.

Figure 6 presents a typical steady state current density – voltage drop (*i-v*) curve of a BPM for a neutral salt solution (M<sup>+</sup>X<sup>-</sup>) [28, 30]. Until the first limiting current density (*i<sub>lim1</sub>*) is reached, the current is only transported by salt ions.



**Figure 5:** Schematic drawing of a six compartment measurement module for  $i$ - $v$  curve measurements, taken from [28]

At  $i_{lim1}$ , the electrical resistance is the highest since all salt ions are removed from the BPM junction. The magnitude of  $i_{lim1}$  is a measure for the selectivity of the BPM. Above  $i_{lim1}$ , the water splitting potential ( $U_{diss}$ ) is reached leading to water dissociation. The water splitting products ( $J_{OH^-}/J_{H^+}$ ) are now also available for the current transport [30].



**Figure 6:** Schematic i-v curve of a BPM in a salt solution ( $M^+X^-$ ), adapted from [23, 27].

In order to reduce the relative salt ion transport and have high water splitting efficiency the operating current density ( $i_{op}$ ) should be as high as possible. Above the second limiting current ( $i_{lim2}$ ), water diffusion limitations occur because the water transport toward the BPM junction is not sufficient to replenish the water dissociated at the interface, leading to drying out of the membrane [31, 32].

$U_{diss}$  is strongly influenced by the thickness of the interface region and the catalytic activity of the groups present at the interface layer. The water splitting resistance ( $R_{diss}$ ), which can be calculated from the current density increase in the water splitting region, decreases with increasing catalytic activity. Both parameters,  $U_{diss}$  and  $R_{diss}$  determine the operational area resistance of the BPM ( $R_{op}$ ).

### 3. Results and discussion

#### 3.1 Influence of amount of ionic groups at the interface layer

In this section the influence of the amount of ionic groups at the BPM interface layer on the water splitting performance of the membrane is investigated. Three different BPMs were prepared using a S/P layer (80  $\mu\text{m}$ , IEC: 1.3 mol/kg<sub>dry</sub>) as cation exchange layer and an A-Psf layer (10  $\mu\text{m}$ , IEC: 1.8 mol/kg<sub>dry</sub>) as anion exchange layer. As interface layer (10  $\mu\text{m}$ ) two S-PEEKs with different SDs (IEC: 1.8 and 2.1 mol/kg<sub>dry</sub>, noted as S-PEEK 1.8 and S-PEEK 2.1 in the text) were used.

The introduction of the S-PEEK interface layer causes a decrease of the plateau length at  $i_{lim1}$  and therefore lowers the  $U_{diss}$ . In addition, a steeper increase of current density with increased voltage is achieved leading to a lower  $R_{diss}$ . This reduction in  $U_{diss}$  and  $R_{diss}$  leads to a strongly reduced  $R_{op}$  of the membrane (see Figure 7). The decrease of  $R_{op}$  is stronger for S-PEEK of higher IEC. As mentioned before,  $\text{SO}_3^-$  groups do not show catalytic water splitting activity, but the polarisation effect between cation and anion exchange layer is increased, when additional  $\text{SO}_3^-$  groups are introduced [13]. In addition the hydrophilicity of the interface layer is increased, leading to higher water content at the interface which shifts the water dissociation reaction to the right side (Equation 1) [14, 15].

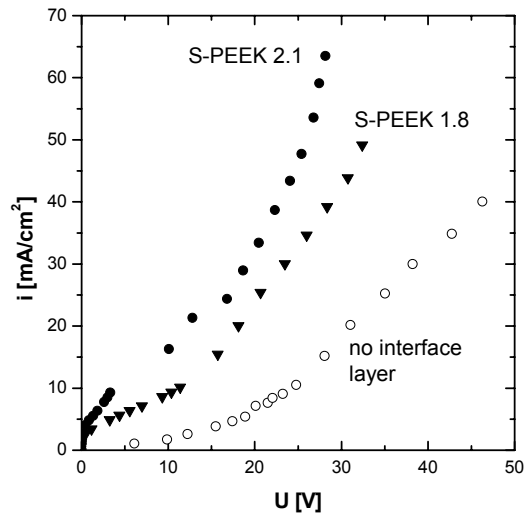


**Figure 7:** Effect of the S-PEEK interface layers with different SDs on the  $i$ - $v$  curve of tailor made BPMs measured in 2M NaCl.

Figure 7 shows a distinct limiting current density  $i_{lim1}$  for the BPMs having a modified interface. In contrast to the expected, the co-ion leakage for the BPM without interface layer is lower than of those membranes with S-PEEK interface layer. We think that this discrepancy might be due significant interpenetration of the anion exchange solution into the S-PEEK interface layer during casting. This seems to produce an anion exchange layer of lower thickness. Because the salt transport into the BPM depends on the layer thickness of the ion exchange layers [28, 30], the thinner anion exchange layer results in a higher co-ion leakage and therefore higher limiting current density. The influence of the compositions and thicknesses of the ion exchange layers to the co-ion leakage is thoroughly investigated in chapter 3.

In conclusion, our research suggest that a highly sulphonated layer at the BPM junction is preferable focussing on the water splitting activity.

### 3.2 Influence of the composition of the anion exchange layer

As we have seen earlier, the mechanism of water dissociation at the anion exchange layer of the BPM is different than at the cation exchange layer, due to the possible proton transfer between the fixed charged groups and the water molecules [10, 11]. Therefore the composition of the anion exchange layer of a BPM plays an

important role [7]. If the anion selective layer contains secondary or tertiary amines, the water splitting reaction is catalysed (equation 3). Nowadays most of the commercially available anion exchange membranes contain quaternary ammonium groups, which are generally not catalytically active. However, under the influence of a strong electric field in alkaline conditions, the groups degrade to tertiary and secondary amines, which are catalytically active [11].

Figure 8 shows the  $i$ - $U$  curves of BPMs prepared using the same S/P layer as cation exchange layer and S-PEEK 2.1 as interface layer, as described above. One was prepared by casting A-Psf (having bicyclic ammonium groups) onto the cation exchange layers, and the other by laminating the Pall Ionclad R4030 (having quaternary ammonium groups) anion exchange membrane onto the cation exchange layers.

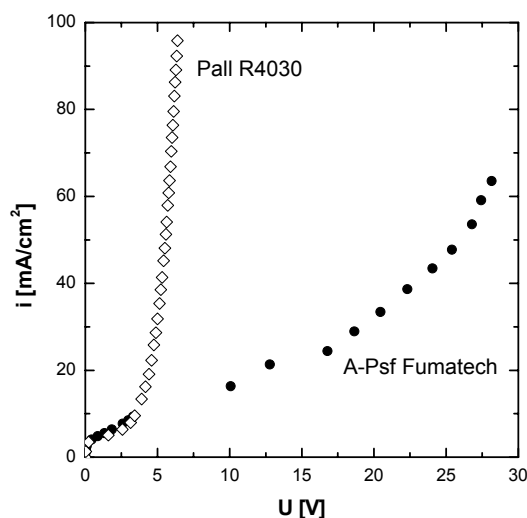


**Figure 8:** Effect of the anion exchange layer on the  $i$ - $v$  curve of the prepared BPMs containing a S/P cation exchange layer and a S-PEEK 2.1 interface layer, measured in 2M NaCl.

The BPM prepared with the Pall R4030 membrane has lower resistance ( $R_{\text{diss}}$ ,  $R_{\text{op}}$ ). The  $U_{\text{diss}}$  and therefore the activation energy necessary to achieve water splitting is nearly 5 times lower (see Table 3), due to the presence of ionic groups which become catalytically active under strong electric field. Neither the quaternary nor the bicyclic ammonium groups can undergo any protonation or deprotonation reactions,

which are necessary to catalyse the water dissociation reaction. However, as described before, the quaternary ammonium groups can degrade into tertiary and secondary amines [11].

**Table 3:** Influence of the anion exchange layer on the properties of the prepared BPMs.

CEL	Interface	AEL	$U_{\text{diss}}$ [V]	$R_{\text{diss}}$ [ $\Omega \text{ cm}^2$ ]	$R_{\text{op}}$ [ $\Omega \text{ cm}^2$ ]
S/P	S-PEEK 2.1	A-Psf	19.28	139.2	2822.7
S/P	S-PEEK 2.1	R4030	4.84	16.1	94.1

The BPM junction under water splitting conditions is completely desalinated and to avoid high resistance, it should be as thin as possible. The shape of the interface layer of the two prepared BPMs is probably different. The lamination of the S/P cation exchange layer and S-PEEK interface layer on the commercial R4030 membrane probably leads to a sharp BPM junction, because no penetration of the layers can occur (the polymer matrix of the R4030 membrane is perfluorinated and does not dissolve in NMP). Using A-Psf, penetration into the S-PEEK interface layer probably occurs due to casting. This leads to a firm bonding but less sharp BPM junction.

In the next section various catalysts will be investigated. For these tests we will prepare membranes with the non-catalytic A-Psf layers in order to compare purely the catalytic function of materials used to modify the interface.

### 3.3 Fe-based catalytic interface layer

Another approach to enhance the water splitting ability of a BPM is the introduction of Fe based catalyst [20-23]. Therefore we introduce Fe additionally to the highly sulphonated S-PEEK layer into the prepared BPM (S/P 80 $\mu\text{m}$  as cation exchange layer, S-PEEK 2.1, 10  $\mu\text{m}$  as interface layer, and A-Psf, 10  $\mu\text{m}$  as anion exchange layer). One BPM was prepared by dispersing  $\text{Fe}(\text{OH})_3$  into the S-PEEK solution prior casting of the interface layer.  $\text{Fe}(\text{OH})_3$  has a very low solubility constant and high catalytic water splitting capacity [1, 20, 21]. Next to  $\text{Fe}(\text{OH})_3$  a newly developed ionic Fe containing polymer (PFS, see Figure 2) is tested as catalytic material. A BPM (S/P 80 $\mu\text{m}$  as cation exchange layer, S-PEEK 2.1, 10  $\mu\text{m}$  as interface layer, and



A-Psf, 10  $\mu\text{m}$  as anion exchange layer) having 240 nm PFS layer as catalytic layer between the S-PEEK interface and the anion exchange layer was prepared. The thickness of the PFS layer was estimated from the height of the casting knife (12  $\mu\text{m}$ ) and the polymer content of the casting solution (2 wt%).

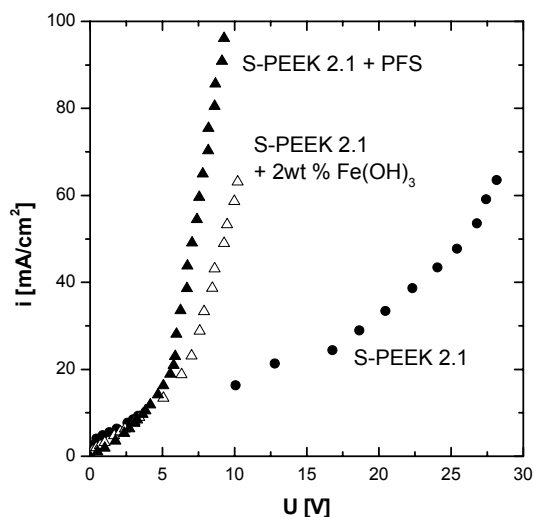


**Figure 9:** Effect of the Fe based catalytic interface layers on the  $i$ - $v$  curve of tailor made BPMs measured in 2M NaCl.

Figure 9 presents the effect of the prepared Fe based catalytic layers on the  $i$ - $v$  curves of the developed BPMs. The addition of  $\text{Fe}(\text{OH})_3$  leads to a strong decrease of  $U_{\text{diss}}$  and  $R_{\text{diss}}$ , compared to the BPM without catalytic layer (see Table 4 and Figure 9). Only by dispersion of 2wt%  $\text{Fe}(\text{OH})_3$  into the S-PEEK interface layer,  $U_{\text{diss}}$  decreases nearly 4 times. This shows that much lower activation energy is needed for the water dissociation reaction, because of the alternative paths for water dissociation created by the Fe catalyst. The rate of the water splitting is much higher than without catalyst ( $R_{\text{diss}}$  decreased nearly 50%). In total  $R_{\text{op}}$  decreased more than 2  $\text{k}\Omega\text{cm}^2$  by the introduction of a Fe catalyst.

The use of the PFS polymer in the intermediate layer leads also to a decrease of  $U_{\text{diss}}$  and  $R_{\text{diss}}$  and therefore  $R_{\text{op}}$  (see Table 4). In contrary to the BPM containing dispersed  $\text{Fe}(\text{OH})_3$  particles, the ionic Fe is present in every repeat unit of the PFS polymer and therefore homogenously distributed at the interface between cation and anion exchange layers. This is the first report demonstrating that a polymer

backbone containing Fe shows catalytic properties for the water dissociation reaction.

**Table 4:** Influence of the Fe based catalysts on the BPM performance.

CEL	AEL	Intermediate layer	Catalyst	$U_{\text{diss}}$ [V]	$R_{\text{diss}}$ [ $\Omega \text{ cm}^2$ ]	$R_{\text{op}}$ [ $\Omega \text{ cm}^2$ ]
S/P	A-Psf	S-PEEK 2.1	-	19.28	139.2	2822.7
S/P	A-Psf	S-PEEK 2.1	$\text{Fe}(\text{OH})_3$	5.74	71.6	482.0
S/P	A-Psf	S-PEEK 2.1 + PFS	$\text{Fe}^{2+}$	4.98	56.4	336.9

Both methods incorporating Fe as catalyst into the BPM junction have disadvantages. The dispersion method leads to an inhomogeneous catalyst distribution (clustering of the particles), whereas the introduction of the specific PFS polymer does not allow variation of the Fe content at the BPM junction. Such variation is desired because the Fe content has a strong influence on the water splitting efficiency [21].

In order to achieve a good Fe distribution at the BPM junction the electrodeposition method described by Kang et al. [21] was used. In the first experiments the commercial CMX (as cation exchange layer) and AM-3 (as anion exchange layer) membrane from Tokuyama Soda were pressed onto each other to form a BPM. The electrodeposition was performed as shown in Figure 4 at a current density of  $10 \text{ mA/cm}^2$ . The influence of the deposition time and therefore the amount of the iron hydroxides on the i-v curves of the prepared BPMs is shown in Figure 10. In comparison to the membrane without Fe, both BPMs prepared by electrodeposition show enhanced water splitting.  $R_{\text{diss}}$  is much lower after the introduction of iron hydroxides due to accelerated water dissociation. This leads to a strongly reduced  $R_{\text{op}}$  (more than  $2.5 \text{ k}\Omega\text{cm}^2$ ) compared to the initial membrane (Table 5).

Figure 10 shows that a longer electrodeposition time (15 min instead of 5 min) does not lead to a better water splitting performance. Longer electrodeposition time leads to a higher amount of iron hydroxides at the BPM junction, leading to a lower  $U_{\text{diss}}$ , but also to an increased  $R_{\text{diss}}$  of the prepared BPM (see Table 5).

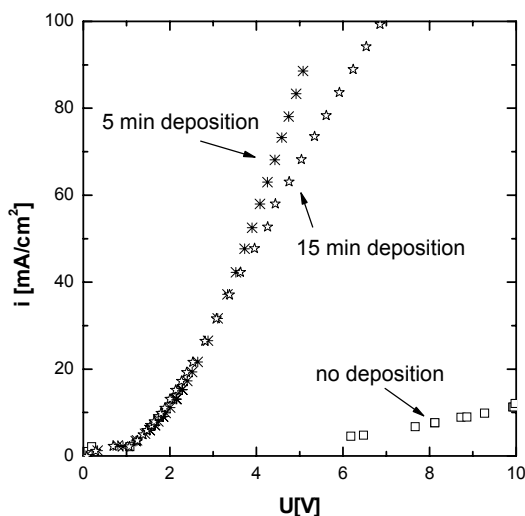


**Figure 10:** Effect of the electrodeposition time on the  $i$ - $v$  curve of prepared BPMs measured in 2M NaCl.

Kang et al. [21] found that between 2 and 3  $\text{mg}/\text{cm}^2$  of  $\text{Fe}(\text{OH})_3$  at the BPM junction leads to the lowest membrane  $R_{\text{op}}$  using electrodeposition with a current density of ca. 5  $\text{mA}/\text{cm}^2$  for 10 min. Because we used a current density of 10  $\text{mA}/\text{cm}^2$  for 5 min, the fluxes of  $\text{Fe}^{3+}$  and  $\text{OH}^-$  into the BPM should be comparable, suggesting that a similar amount of  $\text{Fe}(\text{OH})_3$  is deposited in our BPM. Electrodeposition longer than 5 min leads to an amount of  $\text{Fe}(\text{OH})_3$  at the BPM junction that is higher than 3  $\text{mg}/\text{cm}^2$ . Therefore the thickness of the uncharged layer and the distance between the anion and cation exchange layer is increased. This increase leads to a lower polarisation of the water molecules between the sulphonic acid groups of the cation exchange layer and the amine groups of the anion exchange layer [21] and therefore to higher  $R_{\text{diss}}$ .

**Table 5:** Effect of the electrodeposition time on the properties of the prepared BPMs.

CEL	AEL	Current density	Deposition Time	$U_{\text{diss}}$ [V]	$R_{\text{diss}}$ [ $\Omega \text{ cm}^2$ ]	$R_{\text{op}}$ [ $\Omega \text{ cm}^2$ ]
CMX	AM-3	-	-	4.27	505.0	2664.0
CMX	AM-3	10 $\text{mA}/\text{cm}^2$	5 min	2.17	32.9	104.4
CMX	AM-3	10 $\text{mA}/\text{cm}^2$	15 min	1.35	54.2	127.5

The use of electrodeposition to introduce  $\text{Fe}(\text{OH})_3$  into the interface of the tailor made BPMs (S/P as cation exchange layer, S-PEEK 2.1 as intermediate, and A-Psf as anion exchange layer) did not work. Instead of a sharp layer of  $\text{Fe}(\text{OH})_3$  between the S-PEEK interface layer and the anion exchange layer, the  $\text{Fe}(\text{OH})_3$  was precipitated in the S-PEEK intermediate layer and onto the S/P cation exchange layer.

The S/P layer used as cation exchange layer is monovalent ion selective as shown in [25], which hinders the transport of the  $\text{Fe}^{3+}$  ions to the BPM junction. This effect in addition with the higher  $\text{OH}^-$  leakage of the S-PEEK 2.1 interface layer leads to an immobilisation of the iron hydroxides on the surface of the cation exchange layer and in the S-PEEK 2.1 interface layer.

According to Kang et al. [21], the most effective catalytic water-splitting effects were found if the iron hydroxides are immobilised near the anion exchange layer. The electrodeposition technique therefore seems not suitable for the preparation of BPMs using S/P as cation exchange layer and S-PEEK 2.1 as interface layer and other techniques have to be used to improve the water splitting behaviour.

### **3.4 Pyridine based catalytic interface layers.**

Organic compounds containing weak ion exchange groups can be used as catalyst for the water splitting reaction [1]. Pyridine groups show the required dissociation constant ( $\text{p}K_a = 5.2$  [33]) and have been used as catalysts for the preparation of BPMs [4, 5, 19].

In order to produce a BPM with low  $R_{\text{op}}$  in a simple procedure, P4VP layers were introduced as catalyst at the interface of the BPM by casting. The BPMs have an 80  $\mu\text{m}$  S/P layer as cation exchange layer, 10  $\mu\text{m}$  S-PEEK 2.1 as interface layer and 10  $\mu\text{m}$  A-Psf layer as anion exchange layer. Figure 11 shows the comparison of the BPMs with and without P4VP between the S-PEEK 2.1 and A-Psf layers.

A thin layer of approximately 240 nm (estimated by the height of the casting knife, 12  $\mu\text{m}$ , and the polymer content of the casting solution, 2 wt%) of P4VP between the S-PEEK 2.1 and the A-Psf layer leads to a strong increase in water splitting activity. The  $U_{\text{diss}}$  and therefore the activation energy for the water splitting reaction decreases more than 5 times (see Table 6).

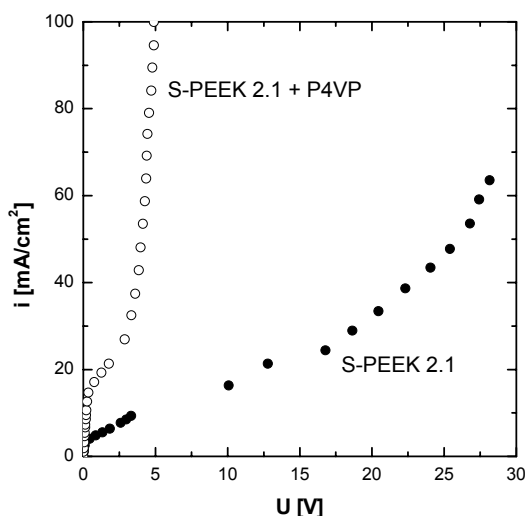


**Figure 11:** Influence of the P4VP layer on the *i-v* curve of the prepared BPM in comparison to a BPM without catalytic layer, measured in 2M NaCl.

The water splitting reaction is accelerated strongly by the presence of P4VP leading to 12 times lower  $R_{\text{diss}}$  compared to the BPM without P4VP layer. In total the P4VP decreases the  $R_{\text{op}}$  of the prepared BPM more than  $2.7 \text{ k}\Omega\text{cm}^2$ .

**Table 6:** Influence of P4VP on the BPM performance

CEL	AEL	Intermediate layer	$U_{\text{diss}}$ [V]	$R_{\text{diss}}$ [ $\Omega \text{ cm}^2$ ]	$R_{\text{op}}$ [ $\Omega \text{ cm}^2$ ]
S/P	A-Psf	S-PEEK 2.1	19.28	139.2	2822.7
S/P	A-Psf	S-PEEK 2.1 + P4VP	3.77	11.4	54.2

Besides the catalytic activity the functional groups of P4VP also form complexes with the  $\text{SO}_3^-$  groups of the S-PEEK 2.1 layer [34]. This results in a lower penetration and firm bonding of the interface layers, leading to a sharper interface and higher polarisation of the water molecules between the ionic groups of the anion and cation exchange layer.

However, the use of P4VP also leads to a strongly increased limiting current density. In order to use P4VP inside the BPM, the casting sequence had to be changed. No firm bonding of the anion exchange layer onto the P4VP layer was possible by casting because of the reaction described above. Therefore the  $10 \mu\text{m}$  anion

exchange layer is the first layer that is cast onto the glass plate, followed by the P4VP, the S-PEEK and the S/P layer. Due to this sequence, the P4VP solution penetrates into the thin anion exchange layer, reducing the effective anion exchange layer thickness. This leads to a higher co-ion leakage and higher limiting current density, as described already in section 3.1.

In order to investigate the influence of the amount of P4VP at the BPM interface, another BPM with a P4VP layer of 80 nm (estimated as described above) was prepared, too. Figure 12 and Table 7 show no differences in the performance of the BPMs with these two P4VP layers.

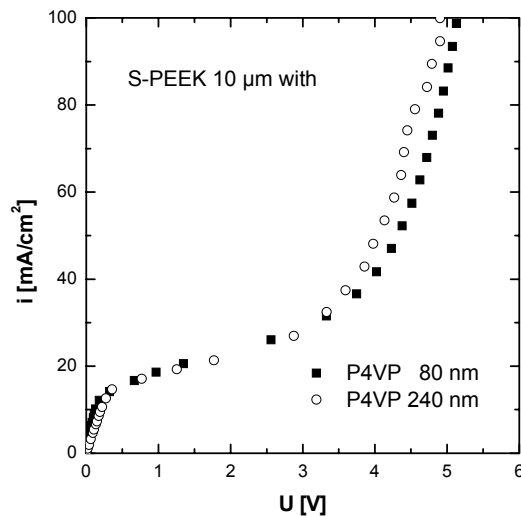


**Figure 12:** Influence of the P4VP layer thickness on the  $i$ - $v$  curve of the prepared BPMs, measured in 2M NaCl.

The  $i$ - $v$  curves are very similar showing that there is no difference in the water splitting performance using P4VP layers in the range of 80 to 240 nm. Because the 240 nm layer is easier to prepare we will continue our investigations with this layer thickness.

**Table 7:** Influence of the P4VP interface layer thickness on the BPM.

CEL	AEL	Intermediate layer	$U_{\text{diss}}$ [V]	$R_{\text{diss}}$ [ $\Omega \text{ cm}^2$ ]	$R_{\text{op}}$ [ $\Omega \text{ cm}^2$ ]
S/P	A-Psf	S-PEEK 2.1 + 80 nm P4VP	4.02	11.3	56.5
S/P	A-Psf	S-PEEK 2.1 + 240 nm P4VP	3.77	11.4	54.2

In order to investigate the influence of the S-PEEK 2.1 interface, one BPM was prepared without the 10  $\mu\text{m}$  S-PEEK layer, so that the P4VP layer was directly placed between the S/P cation exchange layer and the A-Psf anion exchange layer. In addition, a second BPM was prepared using a thin PAA layer (120 nm) instead of the S-PEEK layer. A combination of PAA and P4VP as BPM interface has been used by Strathmann et al. [4, 5], resulting in high performance BPMs.

Figure 13 shows a comparison of the  $i$ - $U$  curves of the prepared BPMs. Figure 13a compares to BPMs containing a 240 nm P4VP layer with and without the additional 10  $\mu\text{m}$  S-PEEK 2.1 layer. The  $U_{\text{diss}}$  of both membranes is comparable, only the  $R_{\text{diss}}$  of the BPM without S-PEEK 2.1 interface is 7.8  $\Omega\text{cm}^2$  higher (see Table 8). This difference shows once more the importance of the hydrophilicity of the S-PEEK 2.1 layer and of the amount of  $\text{SO}_3^-$  groups to the water splitting reaction. Because of the higher amount of  $\text{SO}_3^-$  groups (S-PEEK has an IEC of 2.1, the S/P cation exchange layer only of 1.3 mol/kg<sub>dry</sub>), the polarisation of the water molecules is higher, leading to lower  $R_{\text{diss}}$  and  $R_{\text{op}}$  for this membrane.

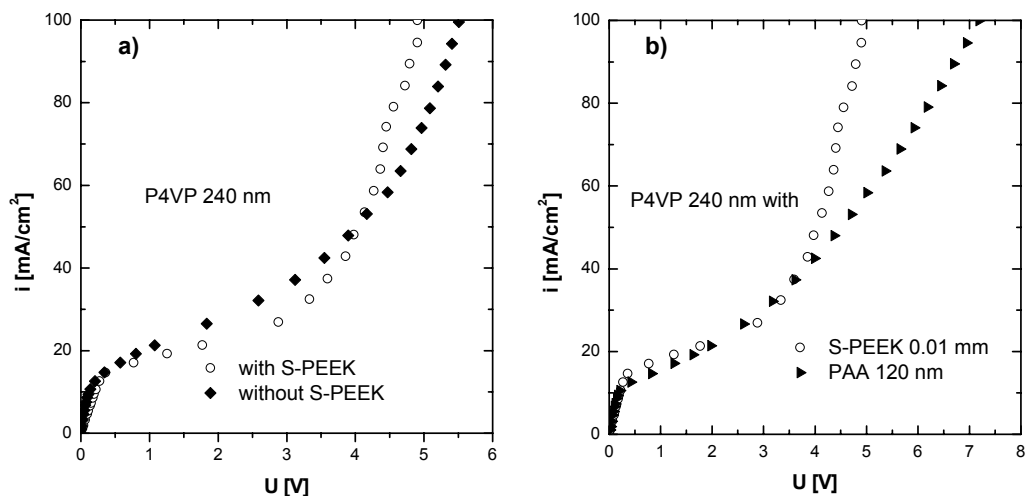


**Figure 13:** a) Influence of the S-PEEK 2.1 layer and b) comparison of the effect of a S-PEEK 2.1 and PAA layer at the interface on the  $i$ - $U$  curve of the prepared BPMs, measured in 2M NaCl.

The introduction of a thin PAA layer (120 nm) instead of the S-PEEK 2.1 layer leads to a BPM with higher  $R_{\text{op}}$  (Figure 13b). The  $U_{\text{diss}}$  using PAA is lower because of the

sharp interface between the ion exchange layers (see Table 8). When PAA comes into contact with P4VP an insoluble salt complex is formed directly, leading to a very sharp interface [1, 2]. Because of this reaction, however, a lower amount of pyridine groups are catalytically active. In addition, the polarisation of the water molecules between the cation and anion exchange layer is lower using the PAA instead of the S-PEEK layer. The amount of  $\text{SO}_3^-$  groups of the S/P cation exchange layer ( $\text{IEC} = 1.3 \text{ mol/kg}_{\text{dry}}$ ) is lower compared to the S-PEEK 2.1 layer. This leads to a BPM with higher  $R_{\text{diss}}$  and  $R_{\text{op}}$  using a thin PAA layer instead of the  $10 \mu\text{m}$  S-PEEK layer.

**Table 8:** Comparison of different P4VP based catalytic interface layers on the water splitting performance of the prepared BPMs.

CEL	AEL	Intermediate layer	$U_{\text{diss}}$ [V]	$R_{\text{diss}}$ [ $\Omega \text{ cm}^2$ ]	$R_{\text{op}}$ [ $\Omega \text{ cm}^2$ ]
S/P	A-Psf	240 nm P4VP	3.60	19.2	88.2
S/P	A-Psf	$10 \mu\text{m}$ S-PEEK 2.1 + 240 nm P4VP	3.77	11.4	54.2
S/P	A-Psf	120 nm PAA + 240 nm P4VP	2.49	47.0	163.8

In conclusion, our results suggest that the BPM containing the  $10 \mu\text{m}$  S-PEEK layer with the 240 nm P4VP layer shows the best water splitting performance.

### 3.5 Comparison of prepared BPMs with different catalytic groups

In this work various parameters affecting the performance of the BPM were investigated. Figure 14 shows a comparison of the best BPMs prepared in each case. The catalytic P4VP layer shows the best water splitting performance. The values of  $U_{\text{diss}}$ ,  $R_{\text{diss}}$  and  $R_{\text{op}}$  are the lowest from all prepared tailor made BPMs. Besides, the membrane was easy to prepare and no stability problems (ballooning) were observed. The thin P4VP catalytic layer combined with the highly sulphonated S-PEEK layer is therefore the most promising interface for the preparation of tailor made BPMs containing anion exchange layers without having functional groups that catalyse the water splitting reaction.



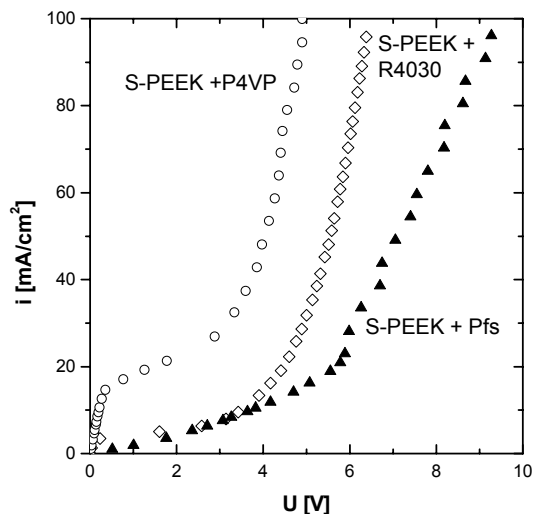


**Figure 14:** Comparison of the  $i$ - $v$  curves of the prepared BPMs with the best water splitting performances based on different catalytic groups, measured in 2M NaCl.

## 4. Conclusions

In this chapter, the effects of various parameters affecting the water splitting of a BPM were investigated.

It was shown that the amount of functional groups and the water content of the interface layer have a big influence on the BPM resistance. The addition of highly sulphonated S-PEEK (IEC 2.1) at the interface layer causes a decrease of the  $U_{\text{diss}}$  and  $R_{\text{diss}}$  of the prepared membranes, due to the higher water content of the layer and the higher water molecule polarisation between the anion and cation exchange layer.

The use of an anion exchange layer containing quaternary ammonium groups instead of bicyclic amines resulted in a better BPM. The  $R_{\text{op}}$  was strongly reduced due to the degradation of the quaternary amines into the catalytically active tertiary and secondary amines under the influence of a strong electric field in alkaline media. Using the bicyclic amine containing A-Psf as anion exchange layer no catalytic water splitting activity was observed.

Two different types of catalysts were tested, based on Fe and P4VP. Using the newly developed ionic Fe containing PFS polymer together with the S-PEEK 2.1 layer as interface resulted in a tailor made BPM with reduced  $U_{\text{diss}}$  and  $R_{\text{diss}}$  compared to the tailor made BPMs without catalytic layer. The combination of 240 nm P4VP as catalyst and 10  $\mu\text{m}$  S-PEEK 2.1 as interface layers resulted in the BPM with the lowest  $U_{\text{diss}}$ ,  $R_{\text{diss}}$  and  $R_{\text{op}}$ . BPMs with this interface were easy to prepare without stability problems (ballooning). The pyridine based interface layer was proven to be a good tool to prepare tailor made BPMs containing anion exchange layers with high base stability without having water splitting catalytic functional groups. Therefore this interface layer will be used in the following chapter for the development of asymmetric bipolar membranes with reduced co-ion leakage.

## 5. List of symbols

$C_{\text{char}}$	Charge density [mol/L]
$i$	Applied current density [ $\text{A}/\text{m}^2$ ]
IEC	Ion exchange capacity [mol/kg <sub>dry</sub> ]
$M^+$	Salt or base cation (also as subscript)
$M_w$	Molecular weight [g/mol]
$\text{pK}_a$	Acidity constant
$R$	Area resistance [ $\Omega \text{ cm}^2$ ]
SD	Sulphonation degree [%]
$U$	Potential difference [V]
$w$	Water uptake [ $\text{kg}_{\text{water}}/\text{kg}_{\text{dry}}$ ]
$X^-$	Salt or acid anion
AEL	Anion exchange layer
BPM	Bipolar membrane
CEL	Cation exchange layer
NMP	N-methyl-2-pyrrolidinone
PAA	Poly(acrylic acid)
PEEK	Poly(ether ether ketone)
PES	Poly(ether sulphone)

Psf	Polysulphone
PFS	Poly(ferrocenyl dimethylsilane)
P4VP	Poly-(4-vinyl pyridine)
S-PEEK	Sulphonated poly(ether ether ketone)
S/P	S-PEEK/PES blend, 60/40

### **Superscripts / Subscripts**

diss	Dissociation
lim	Limiting
op	Operational
n	Number of repeat units

## **6. References**

- [1] F. G. Wilhelm, N. F. A. van der Vegt, M. Wessling, and H. Strathmann, Bipolar Membrane Preparation, in A.J.B. Kemperman (ed.), Bipolar membrane Handbook, Twente University Press, Enschede, The Netherlands (2000) Chapter 4, pp. 79-108.
- [2] M. Wien, Über die Gültigkeit des Ohmschen Gesetzes für Elektrolyte bei Sehr hohen Feldstärken, Ann. Physik 73 (1924) 161-181.
- [3] Zabolotskii V.I., Shel'deshov N.V., Gnusin N.P., Dissociation of Water Molecules in Systems with Ion-exchange Membranes, Russian Chemical Reviews 57 (1988) 801-807.
- [4] H. Strathmann, H. J. Rapp, B. Bauer, and C. M. Bell, Theoretical and Practical Aspects of Preparing Bipolar Membranes, Desalination 90 (1993) 303-323.
- [5] H. Strathmann, B. Bauer, and H. J. Rapp, Better Bipolar Membranes, Chemtech 23 (1993) 17-24.
- [6] S. Mafe, P. Ramirez, A. Alcatraz, and V. Aquilella, Ion Transport and Water Splitting in Bipolar Membranes: Theoretical Background, in A.J.B. Kemperman (ed.), Bipolar membrane Handbook, Twente University Press, Enschede, The Netherlands, (2000) Chapter 3 pp. 47-78.

- [7] A. Tanioka, K. Shimizu, K. Miyasaka, H. J. Zimmer, and N. Minoura, Effect of polymer materials on membrane potential, rectification and water splitting in bipolar membranes, *Polymer* 37 (1996) 1883-1889.
- [8] P. Ramírez, J.A. Manzanares and S. Mafé, Water dissociation effects in ion transport through anion exchange membranes with thin cationic exchange surface films, *Ber. Bunsenges. Phys. Chem.* 95 (1991) 499-503.
- [9] M. Wien, Über eine Abweichung von Ohmsen Gesetze bei Elektrolyten, *Ann. Physik* 83 (1927) 327-361.
- [10] R. Simons, Water splitting in ion exchange membranes, *Electrochimica Acta* 30 (1985) 275-282.
- [11] R. Simons, Strong electric field effects on proton transfer between membrane bound amines and water, *Nature* 280 (1979) 824-826.
- [12] S. Mafé, P. Ramírez, A. Alcaraz, Electric field-assisted proton transfer and water dissociation at the junction of a fixed-charge bipolar membrane, *Chemical Physics Letters* 294 (1998) 406-412.
- [13] M.-S. Kang, Y.-J. Choi, S.-H. Kim, and S.-H. Moon, Enhancement of water splitting in bipolar membranes by optimized composite anion-exchange layer and alkali-treated polyacrylonitrile catalytic junction, *Journal of Membrane Science* 229 (2004) 137-146.
- [14] M. S. Kang, A. Tanioka, and S. H. Moon, Effects of interface hydrophilicity and metallic compounds on water-splitting efficiency in bipolar membranes, *Korean Journal of Chemical Engineering* 19 (2002) 99-106.
- [15] R. Q. Fu, T. W. Xu, G. Wang, W. H. Yang, and Z. X. Pan, PEG-catalytic water splitting in the interface of a bipolar membrane, *Journal of Colloid and Interface Science* 263 (2003) 386-390.
- [16] J. Pretz, E. Staude, Reverse electrodialysis (RED) with bipolar membranes, an energy storage system, *Ber. Bunsenges. Phys. Chem.*, 102 (1998), 676-685.
- [17] R. Simons, Preparation of a high performance bipolar membrane, *Journal of Membrane Science* 78 (1993) 13-23.

- [18] N.V. Sheldeshov, V.I. Zabolotskii, N.D. Pis'menskaya, N.P. Gnusin, Catalysis of water dissociation by the phosphoric-acid groups of an MB-3 bipolar membrane, translated from *Elektrokhimiya* 22 (1986) 791-795.
- [19] T. Jeevananda, K.-H. Yeon, and S.-H. Moon, Synthesis and characterization of bipolar membrane using pyridine functionalized anion exchange layer, *Journal of Membrane Science* 283 (2006) 201-208.
- [20] M.-S. Kang, Y.-J. Choi, H.-J. Lee, and S.-H. Moon, Effects of inorganic substances on water splitting in ion-exchange membranes: I. Electrochemical characteristics of ion-exchange membranes coated with iron hydroxide/oxide and silica sol, *Journal of Colloid and Interface Science* 273 (2004) 523-532.
- [21] M.-S. Kang, Y.-J. Choi, and S.-H. Moon, Effects of inorganic substances on water splitting in ion-exchange membranes: II. Optimal contents of inorganic substances in preparing bipolar membranes, *Journal of Colloid and Interface Science* 273 (2004) 533-539.
- [22] R. Simons, A novel method for preparing bipolar membranes, *Electrochimica Acta* 31 (1986) 1175-1176.
- [23] F. Hanada, K. Hiraya, N. Ohmura, and S. Tanaka, Bipolar membrane and method for its production, Tokuyama Soda Ltd. (Japan), US Patent 5221455 (1993).
- [24] K. Nagasubramanian, F. P. Chlanda, and K.-J. Liu, Use of bipolar membranes for generation of acid and base -- an engineering and economic analysis, *Journal of Membrane Science* 2 (1977) 109-124.
- [25] J. Balster, O. Krupenko, I. Pünt, D.F. Stamatialis, M. Wessling, Preparation and characterisation of monovalent ion selective cation exchange membranes based on sulphonated poly(ether ether ketone), *Journal of Membrane Science* 263 (2005) 137-145.
- [26] F. G. Wilhelm, I. G. M. Punt, N. F. A. van der Vegt, H. Strathmann, M. Wessling, Cation permeable membranes from blends of sulfonated poly(ether ether ketone) and poly(ether sulfone), *Journal of Membrane Science* 199 (2002) 167-176.

- [27] B. Bauer, Bipolare Mehrschichtmembranen (bipolar multilayer membranes), Fraunhofer-Gesellschaft zur Förderung der Angewandten Forschung e.V (FhG) (Germany), DE Patent 4026154 (1992).
- [28] F. G. Wilhelm, I. Punt, N. F. A. van der Vegt, M. Wessling, H. Strathmann, Optimisation strategies for the preparation of bipolar membranes with reduced salt ion leakage in acid-base electrodialysis, *Journal of Membrane Science* 182 (2001) 13-28.
- [29] J. J. Krol, M. Wessling, H. Strathmann, Concentration polarization with monopolar ion exchange membranes: current-voltage curves and water dissociation, *Journal of Membrane Science*, 162 (1999) 145-154.
- [30] F. G. Wilhelm, I. Punt, N. F. A. van der Vegt, M. Wessling, H. Strathmann, Asymmetric Bipolar Membranes in Acid-Base Electrodialysis, *Industrial & Engineering Chemistry Research* 41 (2002) 579-586.
- [31] T. Aritomi, T. van der Boomgaard and H. Strathmann, Current voltage curve of a bipolar membrane at high current density, *Desalination* 104 (1996) 13-18.
- [32] J.J. Krol, M. Jansink, M. Wessling and H. Strathmann, Behaviour of bipolar membranes at high current density: Water diffusion limitation, *Separation and Purification Technology*, 14 (1998) 41-52.
- [33] A. Streitwieser, C.H. Heathcock, E.M. Kosower, "Organische Chemie", 2<sup>nd</sup> edition, VCH, Weinheim, Germany, 1994.
- [34] M. Tiitu, M. Torkkeli, R. Serimaa, T. Makela, and O. T. Ikkala, Self-assembly and flow alignment of protonically conducting complexes of polystyrene-block-poly(4-vinylpyridine) diblock copolymer with phosphoric acid, *Solid State Ionics* 176 (2005) 1291-1299.

## Chapter III

### **Asymmetric Bipolar Membrane: A tool to improve product purity.**

J. Balster, R. Sumbharaju, S. Srikantharajah, I. Pünt,  
D.F. Stamatialis, V. Jordan, and M. Wessling

#### **Abstract**

Bipolar membranes (BPMs) are catalytic membranes for electro-membrane processes splitting water into protons and hydroxyl ions. To improve selectivity and current efficiency of BPMs, we prepare new asymmetric BPMs with reduced salt leakages. The flux of salt ions across a BPM is determined by the co-ion transport across the respective layer of the membrane. BPM asymmetry can be used to decrease the co-ion fluxes through the membrane and shows that the change of the layer thickness and charge density of the corresponding ion exchange layer determines the co-ion flux. The modification of a commercial BP -1 with a thin additional cation exchange layer on the cationic side results in a 47% lower salt leakage. Thicker layers result in water diffusion limitations. In order to avoid water diffusion limitations we prepared tailor made BPMs with thin anion exchange layers, to increase the water flux into the membrane. Therefore a BPM could be prepared with a thick cation exchange layer showing a 62% decreased salt ion leakage through the cationic side of the membrane.

## 1. Introduction

A bipolar membrane (BPM), a laminate of a cation (CEL) and an anion exchange layer (AEL), allows the electro-dissociation of water into hydroxide ions and protons without the generation of gases (Figure 1). BPMs are small chemical reactors with integrated separation, which allow the design of unique processes like the production and recovery of acids and bases, the variation of the pH of a process stream, and the separation of proteins [1].

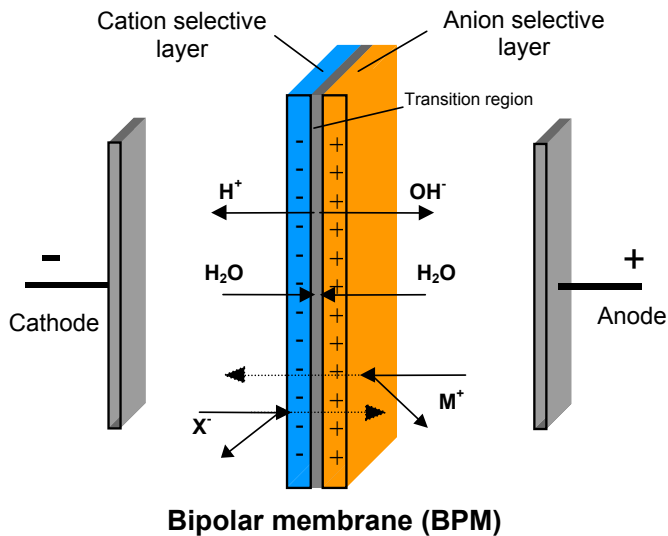


*Figure 1: Water splitting function of a BPM.*

The anion and cation selective layers of a BPM should allow the selective transport of the protons and hydroxyl ions out of the contact region into the acid and base chamber and block co-ions from reaching the contact region and the opposite side of the membrane (Figure 1). In addition, the layers should allow sufficient water flux into the BPM to replenish the water consumed by the water dissociation reaction [2]. In bipolar membrane electrodialysis (ED-BPM), the produced acid and base are in contact with the cation and anion permeable layer of the BPM (Figure 2). BPMs are not only permeable to the water splitting products, but to acid anions and base cations, as well. These ions are transported across the bipolar membrane junction to the other ion permeable layer, where they are transported as counter-ions



(co-ion leakage) (Figure 1) resulting in salt impurities of the products of ED-BPM processes (Figure 2) [3].

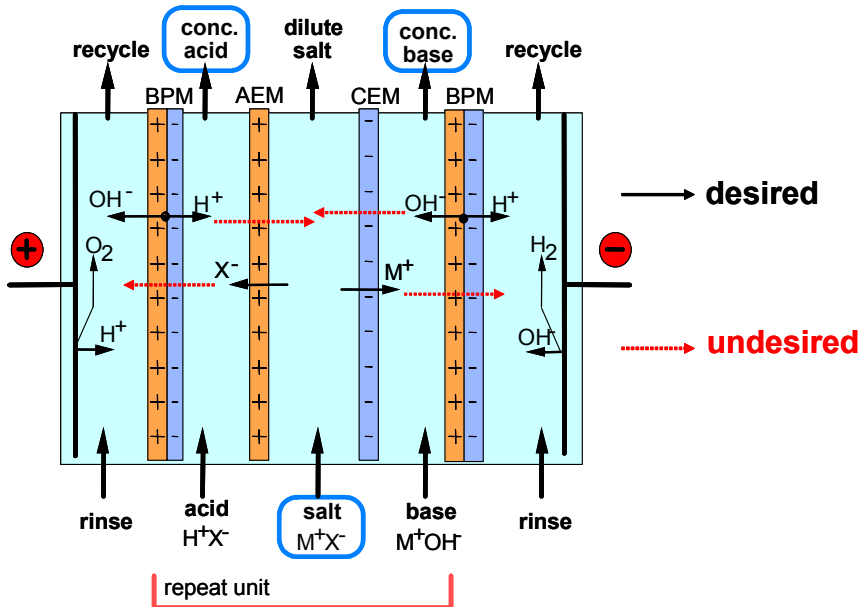


**Figure 2:** Schematic drawing of a membrane module for the production of acids and bases, indicating the ion and the co-ion transport.

Figure 3 presents a typical steady state current density – voltage drop (*i-v*) curves of a BPM for a neutral salt solution ( $M^+X^-$ ) starting out of the salt form of the BPM [4, 5]. Below the first limiting current density ( $i_{lim1}$ ) the current is only transported by salt ions.

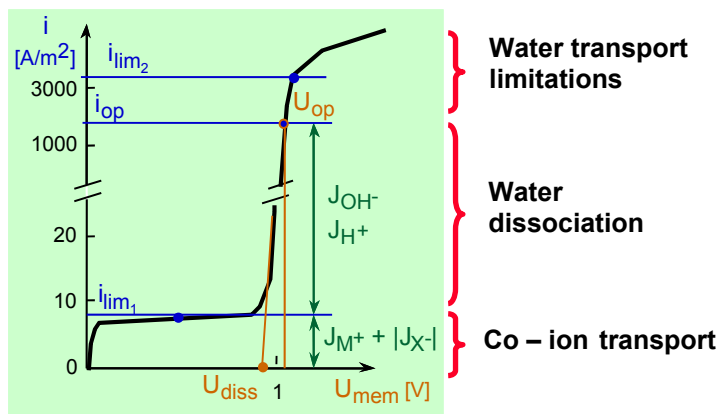


**Figure 3:** Schematic *i-v* curve of a BPM in a salt solution ( $M^+X^-$ ), adapted from [4, 5].

At  $i_{lim1}$ , the electrical resistance increases significantly since all salt ions are removed from the BPM junction. The magnitude of  $i_{lim1}$  is a measure for the selectivity of the BPM towards co-ion leakage [4]. The salt ion fluxes measured in acid-base electro dialysis are closely related to the salt ion fluxes during measurements in salt solutions [4]. Therefore the  $i_{lim1}$  of different membranes can be used to predict and compare their co-ion leakage.

Above  $U_{diss}$ , water splitting occurs and the products ( $J_{OH^-}/J_{H^+}$ ) are also available for the current transport resulting in a steep increase in  $i$  above  $i_{lim1}$  [5]. The operating current density ( $i_{op}$ ) should be as high as possible to reduce the relative salt ion transport and to have a high water splitting efficiency. Above the second limiting current ( $i_{lim2}$ ) the water transport toward the BPM junction is not sufficient to replenish the water dissociated at the interface, leading to water diffusion limitations and therefore to a dry out of the membrane [6, 7].

The total salt ion transport across commercial BPMs is generally over 0.01 mol<sub>salt</sub>/mol<sub>H<sup>+</sup>/OH<sup>-</sup></sub> when the concentration of the produced acids and/or base is above 4 mol/L [8, 9]. Therefore concentrated acids and bases with purity higher than 99 mol% (of dissolved ions) cannot be produced. ED-BPM can only become competitive for many industrial applications, if the salt impurity in the product is reduced drastically [4]. In general, the salt ion leakage into the produced acids and bases is not the same in both directions [8, 10, 11]. Hence, BPMs show an asymmetric salt ion transport behaviour depending on the transport properties of the ion exchange layers [11]. In fact, the flux of salt ions across the BPM is determined by the co-ion transport across the respective membrane layer [4].

Wilhelm et al [4, 5] have already shown that an improvement of the composition of one of the two layers [4] and an increase of layer thickness [5] can lead to an enhanced selectivity and therefore to a reduced salt ion leakage. However, if the properties of the second ion exchange layer (IEL) are not optimised, water transport limitations occur. Such a thickness dependence of the membrane selectivity has not been reported for standard ion exchange membranes [4].

In this work, we prepare new asymmetric BPMs by optimising the properties and / or increasing the thickness of one of the two charged layers until nearly no water transport occurs through this side of the membrane. In order to avoid water transport

limitation to the interface layer as well, the thickness of the other ion exchange layer is reduced. Our experimental study expands into two different directions:

1. Modification of the commercial BP-1 membrane (Tokuyama Soda). In fact the thickness of the anion or cation exchange layer is increased by lamination of either:
  - commercial anion (AMX) and cation (CMX) membranes (Tokuyama Soda) or
  - tailor made cation exchange membranes of polymer blends of sulphonated poly(ether ether ketone) (S-PEEK) and poly(ether sulphone) (PES).
2. Preparation of tailor made asymmetric BPMs using polymer blends of S-PEEK / PES as cation exchange material and functionalised poly(sulphone) (Psf) as anion exchange material. In this case, the properties of both ion exchange layers can be modified in order to avoid water diffusion limitations.

## 2. Theoretical background

The flux of salt ions ( $J_i$ ) across the BPM can be described with the actual transport number ( $t_i$ ) and the operational current density ( $i_{op}$ ) [4]:

$$J_i = t_i \frac{i_{op}}{z_i F} \quad (1),$$

where  $F$  is the Faraday constant and  $z_i$  is the electrochemical valence of the ion. If boundary layer effects in the salt solutions next to the membrane are neglected, the co-ion concentration in the membrane will remain constant at the solution interface, even with increased ion fluxes. Assuming no influence of the water splitting in the bipolar membrane interface on the salt ion transport across the BPM, the salt ion fluxes at the  $i_{op}$  and at  $i_{lim1}$  are the same [4].

$$J_i = J_i^{lim1} = t_i^{lim1} \frac{i_{lim1}}{z_i F} \quad (2).$$

The  $i_{lim1}$  of a BPM can also be written as

$$i_{lim1} = F(z_{M^+} J_{M^+} + z_{X^-} J_{X^-}) \quad (3),$$

where  $M^+$  is the salt cation and  $X^-$  is the salt anion (see Figure 2).

The salt ion flux  $J_i$  in a BPM with equal salt concentrations at the anionic and cationic membrane sides can be described by the extended Nernst Plack equations. These equations are phenomenological descriptions of the ion transport by diffusion due to a concentration gradient and migration due to an electrical field. Neglecting convective transport and bulk movement of the solution the ion flux can be described as [4]:

$$J_i = J_i^{Diffusion} + J_i^{Migration} = -D_i \frac{dc_i}{dx} - D_i \frac{c_i z_i F}{RT} \frac{dU}{dx} \quad (4),$$

where  $D_i$  is the ionic diffusion coefficient,  $c_i$  the ion concentration,  $R$  is the gas constant,  $T$  the actual temperature,  $U$  the electric potential and  $x$  is the location normal to the membrane. Assuming linear concentration profiles at steady state conditions at low current densities and constant electric field strength across the membrane layer, the use of an average concentration is required in the migrational term to describe the transport at steady state. Therefore the average concentration in the membrane layer at the solution interface and the inner membrane interface is used [4]. The co-ion leakage through the AEL can be written as

$$J_{M^+} = -D_{M^+,AEL}^m \frac{\Delta c_{M^+}^m}{d_{wet,AEL}} - D_{M^+,AEL}^m \frac{c_{M^+}^{m,av} F}{RT} \frac{\Delta U_{AEL}}{d_{wet,AEL}} \quad (5),$$

and

$$J_{X^-} = -D_{X^-,CEL}^m \frac{\Delta c_{X^-}^m}{d_{wet,CEL}} - D_{X^-,CEL}^m \frac{c_{X^-}^{m,av} F}{RT} \frac{\Delta U_{CEL}}{d_{wet,CEL}} \quad (6),$$

for the CEL, with  $d_{\text{wet}}$  as the wet thickness of the membrane layer. The superscripts  $m$  and  $av$  denote the membrane phase and average value across this phase, respectively.

At  $i_{\text{lim}1}$  the co-ion concentration at the inner interface is zero and the co-ion concentration difference across a layer is equal to the co-ion concentration next to the solution. This difference equals the concentration difference of the counter ions due to electroneutrality requirement. At  $i_{\text{lim}1}$  the arithmetic averages of the co- and counter-ion concentrations in the IELs become [4]:

$$c_{M^+}^{m,av} = 0.5c_{M^+,AEL}^s, \quad \text{in the AEL and} \quad (7),$$

$$c_{X^-}^{m,av} = 0.5c_{X^-,CEL}^s, \quad \text{in the CEL} \quad (8),$$

where the superscript  $s$  denotes the layer next to the solution. Taking the electroneutrality in the membrane into account, the arithmetic average of the counter ion concentration in the IELs are:

$$c_{X^-}^{m,av} = c_{M^+}^{m,av} + c_{\text{char},AEL} = 0.5c_{M^+,AEL}^s + c_{\text{char},AEL}, \quad \text{in the AEL and} \quad (9),$$

$$c_{M^+}^{m,av} = c_{X^-}^{m,av} + c_{\text{char},CEL} = 0.5c_{X^-,CEL}^s + c_{\text{char},CEL}, \quad \text{in the CEL} \quad (10),$$

where  $c_{\text{char}}$  is the charge density of the corresponding IEL [4].

By introducing the averages and differences into the Nernst-Planck equations and eliminating the potential drop across the IELs (it is the same for anion and cation flux equation) the Nernst-Planck equations for the ion fluxes at  $i_{\text{lim}1}$  ( $J_i^{\text{lim}}$ ) can be simplified [4]. Because the ion fluxes in steady state have to be the same in both layers of the BPM the ion fluxes can be described by the following equations:

$$J_{M^+}^{\text{lim}} = \frac{D_{M^+,AEL}}{d_{\text{wet},AEL} c_{\text{char},AEL}} (c_{M^+,AEL}^s + c_{\text{char},AEL}) c_{M^+,AEL}^s \quad (11),$$

$$J_{C^+}^{\text{lim}} = \frac{D_{X^-,CEL}}{d_{\text{wet},CEL} c_{\text{char},CEL}} (c_{X^-,CEL}^s + c_{\text{char},CEL}) c_{X^-,CEL}^s \quad (12).$$

To relate the content of co- and counter ions in the membrane to the concentration in the electrolyte solution the Donnan equilibrium is used leading to a further simplification of the ion transport equations [4]:

$$j_{M^+}^{\text{lim}} = \frac{D_{M^+,AEL} (c^s)^2}{d_{AEL} c_{\text{char},AEL}} \quad (13),$$

$$j_{X^-}^{\text{lim}} = \frac{D_{X^-,CEL} (c^s)^2}{d_{\text{wet},CEL} c_{\text{char},CEL}} \quad (14).$$

By inserting equation (13) and equation (14) into equation (3) the first limiting current density can be expressed as:

$$i_{\text{lim}1} = F \left( \frac{D_{M^+,AEL} (c^s)^2}{d_{\text{wet},AEL} c_{\text{char},AEL}} + \frac{D_{X^-,CEL} (c^s)^2}{d_{\text{wet},CEL} c_{\text{char},CEL}} \right) \quad (15).$$

The  $i_{\text{lim}1}$  and the salt transport across a BPM are directly dependent on the square of the solution concentration, the diffusion coefficients in the membrane layers, the fixed charge density and thickness of the IELs of the BPM.

Wilhelm et al [4, 5] developed models to simulate ion fluxes through BPMs and to relate them to  $i_{\text{lim}1}$  using either a symmetrical (assuming that the transport in both layers is the same) or an asymmetrical (assuming different transport in the two layers) approach. The measurements and simulations showed [4, 5], that both the anionic and the cationic co-ion leakage change, if one of the two layers of the BPM is changed.

In this study, we assume asymmetrical ion transport through the layers of the BPM, assuming that a change of one layer of the BPM reduces the ion flux through both layers symmetrically, i.e. when the  $\text{Cl}^-$  flux through the BPM is reduced about 30% because of a change of the CEL layer, we assume that also the  $\text{Na}^+$  flux is reduced about 30%. With this method we can use the ratio of the measured  $i_{\text{lim}1}$  of the BPMs to estimate the co-ion fluxes.

### 3. Experimental

#### 3.1 Commercial membranes

The commercial BPM Neosepta BP-1 from Tokuyama Soda Ltd. (Tokyo, Japan) was used in this study. In order to increase the asymmetry, commercially available Neosepta CMX (cation exchange) and AMX (anion exchange) membranes (also from Tokuyama Soda Ltd.), or tailor made S-PEEK/PES membranes have been laminated to the BP-1 by a frame (see Figure 4).

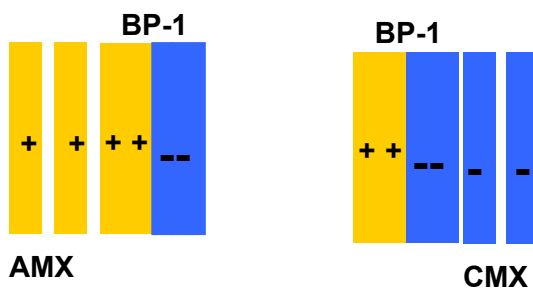


**Figure 4:** Addition of the ion exchange membranes to the corresponding side of the BP-1 membrane.

#### 3.2 Tailor made membranes

S-PEEK was prepared by sulphonation of poly(ether ether ketone) (PEEK) 450PF from Victrex as described in [12]. The S-PEEK and S-PEEK/PES blends (indicated as S/P in the text) were prepared by adding the desired amount of polymers to the solvent (NMP, 10 or 20 wt% polymer in solution), stirred for a minimum of 24 h and filtered over a 40  $\mu\text{m}$  metal filter. For the contact region of the BPM, a pure S-PEEK layer with a sulphonation degree (SD) of 80% on the cationic side and a poly(4-vinyl pyridine) (P4VP) layer were used. The AEL was prepared from aminated Psf in NMP (10 wt% polymer in solution) obtained from FuMA-TECH GmbH (St. Ingbert, Germany).

Single ion exchange films as well as the BPMs were prepared by the evaporation technique [13]. In order to have a good contact between the different layers the casting method was used (see Figure 5) [14].

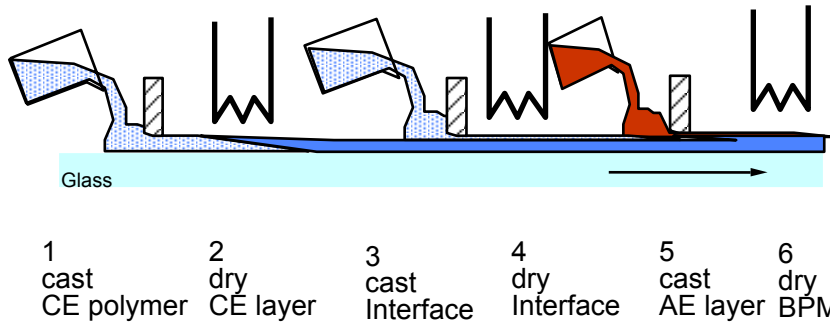


**Figure 5:** Schematic drawing of the BPM preparation by casting, adapted from [6].

The polymer layers were cast with the desired thickness and sequence onto a glass plate. After the solidification of one layer the next layer was cast on top of the former, which then was allowed to dry. This procedure was repeated until all desired layers (CEL, 2 Intermediate layers, AEL) were cast onto each other. Because all polymer solutions were prepared in the same solvent, the contact at the interface layers was firm. The prepared membranes were dried in  $N_2$  atmosphere at 40-80 °C for 1 week, then immersed in water and subsequently dried under vacuum at 30 °C for 1 week. The membranes were finally stored in a 2 M NaCl solution.

### 3.3 Characterisation of the ion exchange membrane layers

The commercial AMX and CMX membranes and the tailor made ion exchange membrane layers were characterised by measurements of the ion exchange capacity (IEC), water uptake ( $w$ ), permselectivity ( $P$ ) and electrical resistance ( $R$ ). These properties were used to calculate the SD, the specific membrane conductivity (Cond), and the  $c_{char}$  of the membranes (more details in [12, 13]).

### 3.4 Characterisation of the BPMs

The i-v curve measurements were performed in a six compartment membrane stack as shown schematically in Figure 6 (see more details about the procedure in [4] and the experimental setup in [15]).



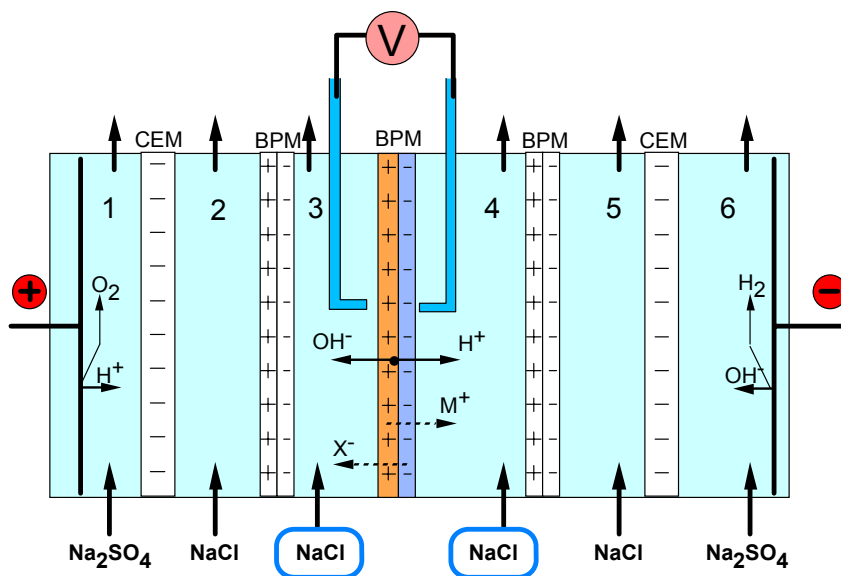


**Figure 6:** Schematic drawing of a six compartment measurement module for *i-v* curve measurements, taken from [5].

The central BPM was the one under investigation. The other membranes were auxiliary membranes which were necessary to maintain well defined, constant concentrations in the two central compartments. During the experiment, the applied current density was increased stepwise and the system was allowed to reach steady state. The voltage drop across the membrane was measured with calomel electrodes at a fixed distance from the membrane surface by Haber-Luggin capillaries filled with concentrated KCl solution, followed by the next increase in current density. The temperature was held constant at 25°C.

Generally, in such measurements, the solution resistance is subtracted. However, because the limiting current density is not affected by the solution resistance [4] and the solution resistance close to the BPMs decreases at higher current densities because of the generation of  $H^+$  and  $OH^-$  (the conductivity next to the membrane changes), the *i-v* curves in this article were not corrected for the solution resistance. The current efficiency and the purity of the produced acids and bases are directly related to the  $M^+/X^-$  leakages through the BPM. The co-ion leakage results in product contamination and reduces the efficiency of the  $H^+/OH^-$  generation. The

current efficiency of the BPMs was measured with the arrangement shown in Figure 7.

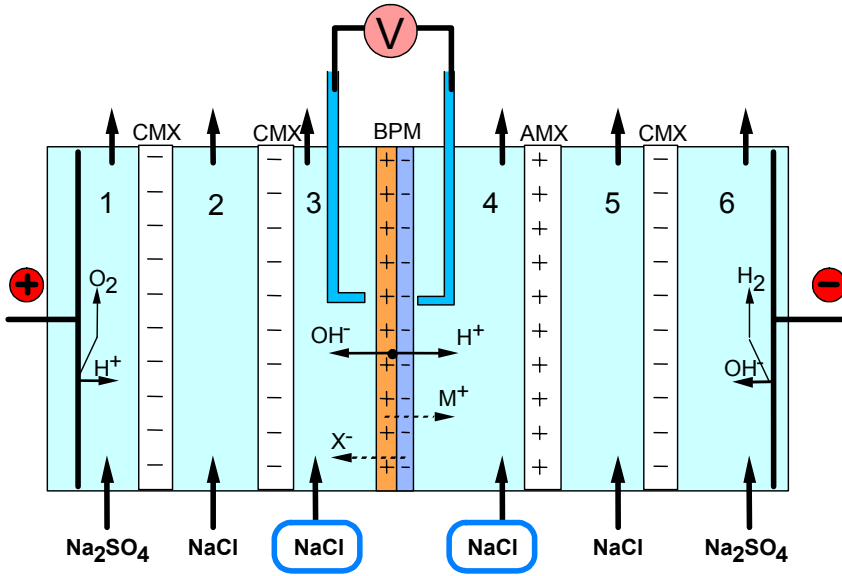


**Figure 7:** Schematic drawing of a six compartment measurement module for the efficiency measurements, adapted from [5].

The experiments were performed in batch mode measuring the base concentration in compartment 3 over time. The current efficiency was calculated [16]:

$$\eta = \frac{(c_0 - c_t) * V * F}{I * t} \quad (16),$$

where  $c_0$  and  $c_t$  are the equivalent concentration of the produced base at time 0 and  $t$  respectively,  $V$  is the circulated volume of solution per compartment, and  $I$  the applied current.

The salt ion leakage measurements were performed in a 4 compartment cell configuration (Figure 8). A 0.5M NaSO<sub>4</sub> solution was used as electrode solution, a 2M NaCl solution was fed to the acid compartment and a 0.1M NaOH solution to the base compartment. The experiments were performed in batch mode with a constant current density of 100 mA/cm<sup>2</sup> and the Cl<sup>-</sup> concentration in the base compartment was measured by titration.

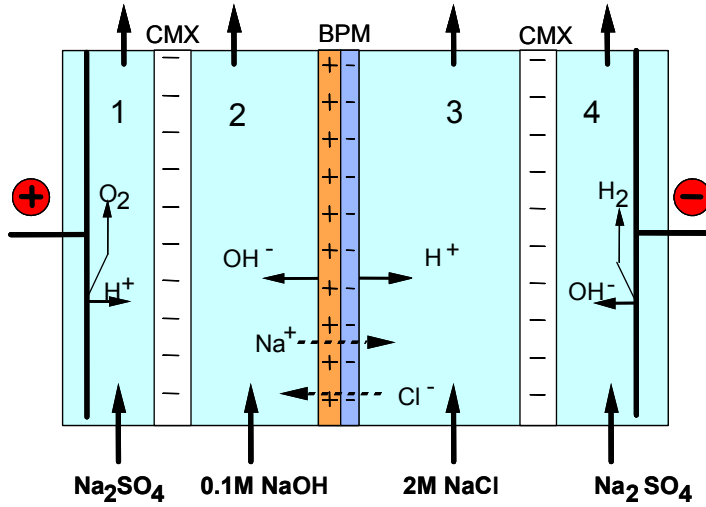


**Figure 8:** Schematic drawing of a 4 compartment measurement module for the salt leakage determination.

The corresponding  $\text{Cl}^-$  flux ( $J_{\text{Cl}^-}$ ) through the membrane was calculated from the

change of  $\text{Cl}^-$  concentration in time  $\left(\frac{dc_{\text{Cl}^-}}{dt}\right)$  in the base compartment (2):

$$J_{\text{Cl}^-} = \frac{V * \frac{dc_{\text{Cl}^-}}{dt}}{A} \quad (17),$$

where  $A$  is the membrane area. Transport numbers of  $\text{Cl}^-$  ( $t_{\text{Cl}^-}$ ) were calculated from the corresponding  $\text{Cl}^-$  fluxes:

$$t_{\text{Cl}^-} = \frac{J_{\text{Cl}^-} * F}{i} \quad (18),$$

where  $i$  is the applied current density.

## 4. Results and discussion

### 4.1 Modification of the commercial BP-1 membrane

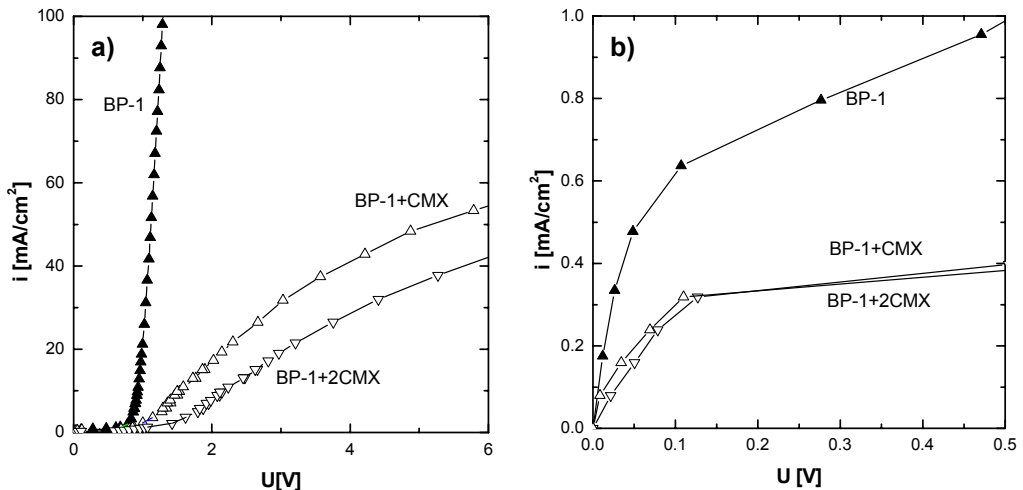
#### Lamination of commercial anion (AMX) and cation (CMX) exchange layers

Table 1 presents the properties of the commercial CMX and AMX membranes laminated on the BP-1 membrane.

**Table 1:** Properties of the commercial ion exchange membranes.

Membrane	$d_{\text{wet}}$ [ $\mu\text{m}$ ]	Cond [mS/cm]	IEC [mol/kg <sub>dry</sub> ]	w [kg <sub>water</sub> /kg <sub>dry</sub> ]	$C_{\text{char}}$ [mol/L]	P [%]
CMX	163	4.8	1.65	0.26	6.4	97
AMX	146	5.4	1.42	0.26	5.5	96

Figure 9 shows the effect of the lamination of CMX membranes to the cationic side of the BP-1 membrane and Table 2 presents the properties of the new BPMs. Figure 9a presents the entire  $i$ - $U$  curves and Figure 9b focuses at the low current density region.



**Figure 9:**  $i$ - $v$  curves of a BP-1 and BP-1 + CMX laminates, measured in 2M NaCl.

(a) Full curves, (b) focusing at low current density.

The addition of one CMX membrane leads to a significant decrease of the  $i_{\text{lim}1}$  of about 50% (from 0.61 to 0.31 mA/cm<sup>2</sup>) corresponding to lower salt leakage through the cationic side of the membrane. The  $R_{\text{op}}$  however, increases more than 15 times

from 8.1 to 125.4  $\Omega\text{cm}^2$  (Table 2). In addition, the water transport through this membrane side is reduced and the  $i_{\text{lim}2}$  decreases sharply (see Table 2 and Figure 6a). The addition of a second CMX layer on the cationic side of the BP-1 does not result in further decrease of  $i_{\text{lim}1}$  (Figure 6a), it only causes further decrease of  $i_{\text{lim}2}$  and further increase in  $R_{\text{op}}$  (Table 2).

**Table 2:** Characteristics of the different BPM arrangements.

Membrane	$i_{\text{lim}1}$ [mA/cm <sup>2</sup> ]	$i_{\text{lim}2}$ [mA/cm <sup>2</sup> ]	$U_{\text{diss}}$ [V]	$R_{\text{diss}}$ [ $\Omega\text{cm}^2$ ]	$R_{\text{op}}$ [ $\Omega\text{cm}^2$ ]
BP-1	0.61	298	0.9	4.3	8.1
BP-1+ CMX	0.31	43	0.9	67.3	125.4
BP-1+2CMX	0.31	30	1.3	86.5	201.3
BP-1+ AMX	0.46	193	1.1	5.1	10.7
BP-1+2AMX	0.43	182	1.3	6.5	14.9

Figure 10 presents the  $i$ - $v$  curves of the BP-1 membrane when AMX membranes are laminated to the anionic side. In comparison to the single BP-1, the  $i_{\text{lim}1}$  decreases about 25% by the addition of one AMX membrane and 30% by the addition of two AMX membranes (see Table 2).

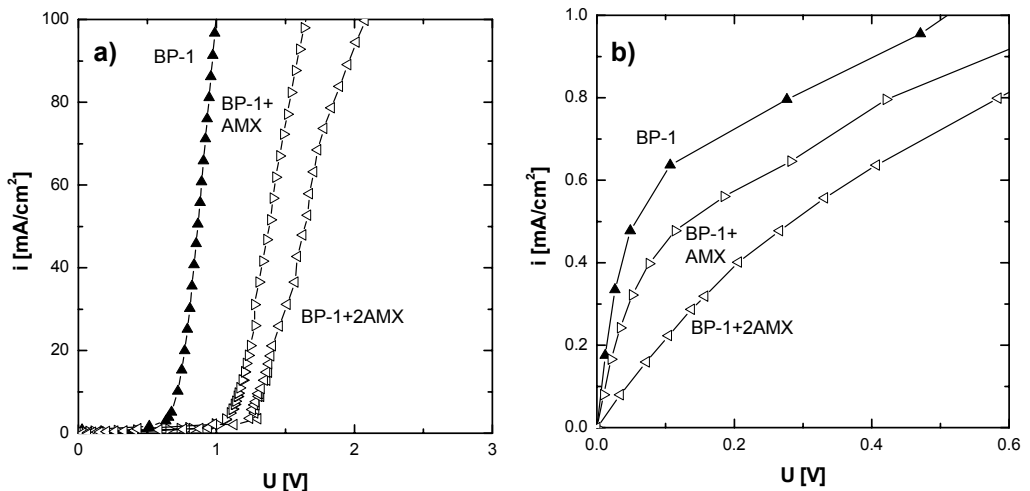


**Figure 10:**  $i$ - $v$  curves of a BP-1 and BP-1 + AMX laminates, measured in 2M NaCl.  
(a) Full curves, (b) focusing at low current density.

The  $R_{op}$  of the new membrane increases about 32% (from 4.3 to 5.1  $\Omega\text{cm}^2$ ) and 84% (from 4.3 to 6.5  $\Omega\text{cm}^2$ ) by the addition of one or two AMX membranes, respectively. The  $i_{lim2}$  of the new membranes decreases too (35% for the lamination of one and 37% for the lamination of two AMX membranes, see Table 2).

The results of Figures 9 and 10 indicate that the cationic side of the BP-1 membrane contains more water and co-ions than the anionic side. Therefore the  $i_{lim1}$  and the water transport into the BP-1 can be significantly reduced by adding extra CMX membranes, leading to lower co-ion leakage, but also to water diffusion limitations. The reduction of the co-ion leakage through the anionic side of the BP-1 membrane can be achieved by the lamination of AMX membranes. In this case, the new laminates have acceptable resistances.

### Laminates of S-PEEK / PES blend membranes

In this section, we laminate 60wt% S-PEEK / 40wt% PES blends (indicated as S/P) on the cationic side the BP-1 membrane. Table 3 presents the properties of the blends. For the preparation of the blends, we used two S-PEEK polymers with SDs of 80% and 62%. Therefore we prepared blends of two different charge densities, 3.8 and 6.4 mol/L (indicated as S/P-3.8 and S/P-6.4, Table 3).

**Table 3:** Properties of the prepared CELs.

Membrane	Blend composition	SD S-PEEK	$d_{wet}$ [ $\mu\text{m}$ ]	Cond [mS/cm]	IEC [mol/kg <sub>dry</sub> ]	w [kg <sub>water</sub> /kg <sub>dry</sub> ]	$C_{char}$ [mol/L]	P [%]
S/P-3.8	60% S-PEEK 40% PES	80%	80	1.9	1.3	0.34	3.8	96
S/P-6.4	60% S-PEEK 40% PES	62%	65	0.1	0.9	0.14	6.4	97

Figure 11 shows the effect of the lamination of S/P-3.8 membranes of different thickness to the cationic side of the BP-1. Figure 11a shows the complete  $i$ - $v$  curve and Figure 11b focuses on the lower current density region. The addition of the 80  $\mu\text{m}$  S/P-3.8 leads to a reduction of  $i_{lim1}$  of 33% (from 0.61 to 0.41  $\text{mA}/\text{cm}^2$ ), an increase of  $R_{op}$  of only 7% (from 8.1 to 8.7  $\Omega\text{cm}^2$ ) and a decrease of  $i_{lim2}$  of 27% (from 298 to 217  $\text{mA}/\text{cm}^2$ ) in comparison to the BP-1 membrane (see Table 4). The addition of a 150  $\mu\text{m}$  S/P-3.8 results in water diffusion limitations (see Figure 11a).

The operable current density is reduced drastically (97%, from 298 to 9 mA/cm<sup>2</sup> compared to the initial BP-1 membrane and 96% compared to the thinner BP-1 S/P 3.8 laminate), whereas  $i_{lim1}$  is only reduced to 0.39 mA/cm<sup>2</sup>.

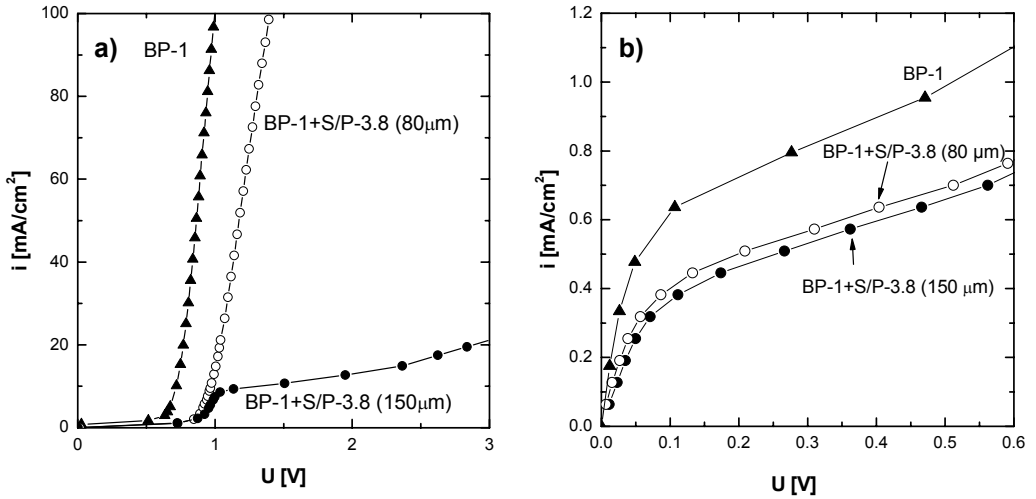


**Figure 11:** *i-v* curves of a BP-1 and BP-1 + S/P laminates, measured in 2M NaCl. Influence of the layer thickness. (a) Full curves, (b) focusing at low current density.

Figure 12 and Table 4 show the effect of the addition of S/P membranes with different charge density to the cationic side of the BP-1. Figure 12a shows the complete *i-v* curve and Figure 12b focuses at the lower current density region.

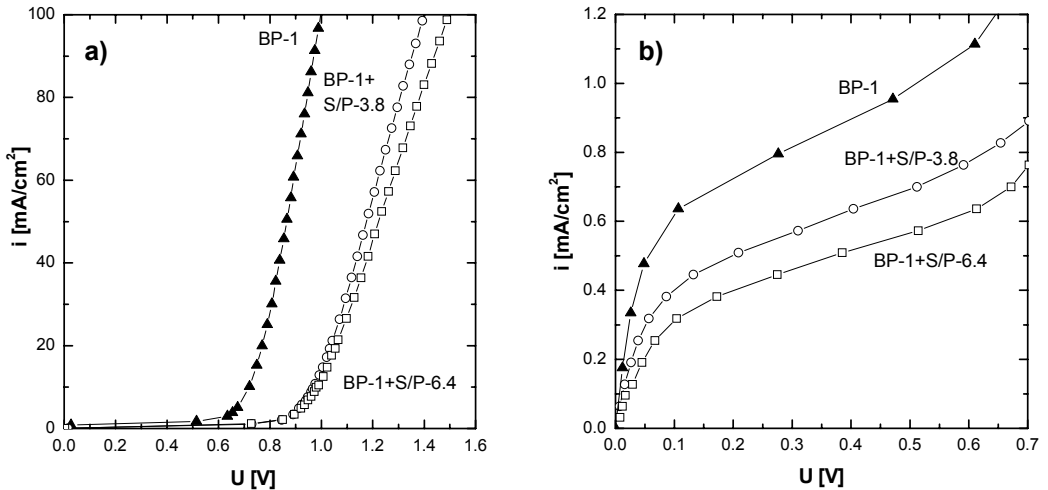


**Figure 12** *i-v* curves of a BP-1 and BP-1 + S/P laminates, measured in 2M NaCl. Influence of the layer composition. (a) Full curves, (b) focusing at low current density.

The S/P-6.4 swells less in water and has lower conductivity than the S/P-3.8 (see Table 3). As a result, its lamination to the BP-1 leads to a stronger decrease of  $i_{lim1}$  (48%, from 0.61 to 0.32 mA/cm<sup>2</sup>) higher resistance (22%, from 4.3 to 5.3 Ωcm<sup>2</sup>) and a lower  $i_{lim2}$  of about 38%.

Table 4 also presents the leakage of Cl<sup>-</sup> through the BP-1 and BP-1+S/P laminates. The Cl<sup>-</sup> flux through the BP-1 is 5.1 10<sup>-9</sup> mol/(cm<sup>2</sup>s). When the S/P-3.8 layer is added to the BP-1, the Cl<sup>-</sup> flux decreases to 3.5 10<sup>-9</sup> mol/(cm<sup>2</sup>s). It is important to note, that the Cl<sup>-</sup> flux through this membrane estimated by the change in  $i_{lim1}$  (0.61 mA/cm<sup>2</sup> for the BP-1 and 0.41 for the BP-1+S/P-3.8 laminate), using equation 3 (assuming a symmetrical decrease of the co-ion fluxes) is 3.4 10<sup>-9</sup> (mol/cm<sup>2</sup>s) and it is in excellent agreement with the measured value 3.5 10<sup>-9</sup> (mol/cm<sup>2</sup>s), indicating that the assumption of symmetrical flux decrease is valid in this case. When the S/P-6.4 layer is added to the BP-1, the  $i_{lim1}$  decreases further to 0.32 mA/cm<sup>2</sup>. The measurement of the Cl<sup>-</sup> for this laminate was not possible, because the values were below the detection limit of our method. However, using the  $i_{lim1}$  and the symmetrical flux decrease assumption like described above, we estimate that the Cl<sup>-</sup> flux is 2.7 10<sup>-9</sup> mol/(cm<sup>2</sup>s). It seems that the charge density of the S/P blend has a significant impact on the BPM selectivity. The BP-1+S/P-6.4 laminate has lower  $i_{lim1}$  and Cl<sup>-</sup> leakage due to the Donnan exclusion mechanism.

**Table 4:** Characteristics of the tailor made BPM arrangements.

Membrane	$i_{lim1}$	$i_{lim2}$	$U_{diss}$	$R_{diss}$	$R_{op}$	$\eta$ NaOH	$J_{Cl^-}$ 10 <sup>-9</sup> [mol/(cm <sup>2</sup> s)]		$t_{Cl^-}$
	[mA/cm <sup>2</sup> ]		[V]	[Ωcm <sup>2</sup> ]		[%]	measured	estimated	[%]
<b>BP-1</b>	0.61	298	0.90	4.3	8.1	90	5.1	-	0.49
<b>BP-1+S/P-3.8</b>	0.41	217	0.95	4.4	8.7	89	3.5	3.4	0.34
<b>BP-1+S/P-6.4</b>	0.32	184	0.96	5.3	10.4	89	-	2.7	0.26

It is important to note that the CMX and S/P-6.4 blend membrane have the same charge density ( $c_{char}$ =6.4 mol/L, Table 1 and 3) but the CMX membrane is thicker (163 μm in comparison to 65 μm of S/P-6.4). When laminated to the BP-1, they both cause nearly the same decrease of  $i_{lim1}$ . The thicker CMX membrane results in higher  $R_{op}$  and lower  $i_{lim2}$  in comparison to the S/P-6.4 (see Table 2 and 4). This



indicates that the achieved  $\text{Cl}^-$  leakage using the S/P-6.4 layer is probably close to the maximum achievable reduction through the cationic side of the BP-1. A further increase in the layer thickness of the cationic side of the BP-1 leads to water diffusion limitations.

In summary, the results of the modification of the BP-1 membrane show that the salt ion fluxes through the BP-1 can be reduced by the addition of extra layers. The reduction of the salt fluxes depends on the charge density and the thickness of the layers. The maximum reduction of  $\text{Cl}^-$  flux (47%) can be achieved with the BP-1+S/P-6.4 laminate. Because the cationic layer of the BP-1 contains more water than the anionic side, the increase in CEL thickness leads to a strong reduction of the co-ion flux, but also to a reduction in water flux into the BP-1 and therefore to water diffusion limitations. In order to achieve lower co-ion leakages through the cationic side of a BPM, tailor made BPMs have to be prepared with thinner anion exchange layers to avoid water diffusion limitations.

## 4.2 Tailor made asymmetric BPMs

### Effect of the AEL thickness

Tailor made BPMs were prepared as described in section 3.2. The cation exchange layer was always the same (S/P-3.8, 80  $\mu\text{m}$ ) while the thickness of the anion exchange layer (aminated Psf) was varied. The interface layer was always a thin film of S-PEEK SD80 and P4VP. Figure 13a shows the influence of the AEL thickness on the  $i_{\text{lim}1}$  and the shape of the plateau in the corresponding  $i$ - $v$  curves. The  $i_{\text{lim}1}$  decreases with increasing AEL thickness, as expected. Additionally, the shape of the plateau is better defined (more horizontal) at high AEL thickness. The membrane with the very thin layer (0.4  $\mu\text{m}$ ) does not have a well defined limiting current region. This is probably due to the high co-ion leakage through this layer [4]. With increasing the AEL thickness, the co-ion flux through the BPM and therefore the difference in co-ion depletion decreases, leading to a distinct plateau.

Figure 13b shows that both the  $i_{\text{lim}1}$  and the  $\eta_{\text{NaOH}}$  seem to reach a plateau for AEL thicker than 4 - 5  $\mu\text{m}$ . In order to avoid high co-ion leakage and having better efficiency, AEL thickness higher than 5  $\mu\text{m}$  should be used. To avoid water transport

limitations, the AEL should not be too thick. Therefore a BPM having the 10  $\mu\text{m}$  AEL is chosen for further investigations.

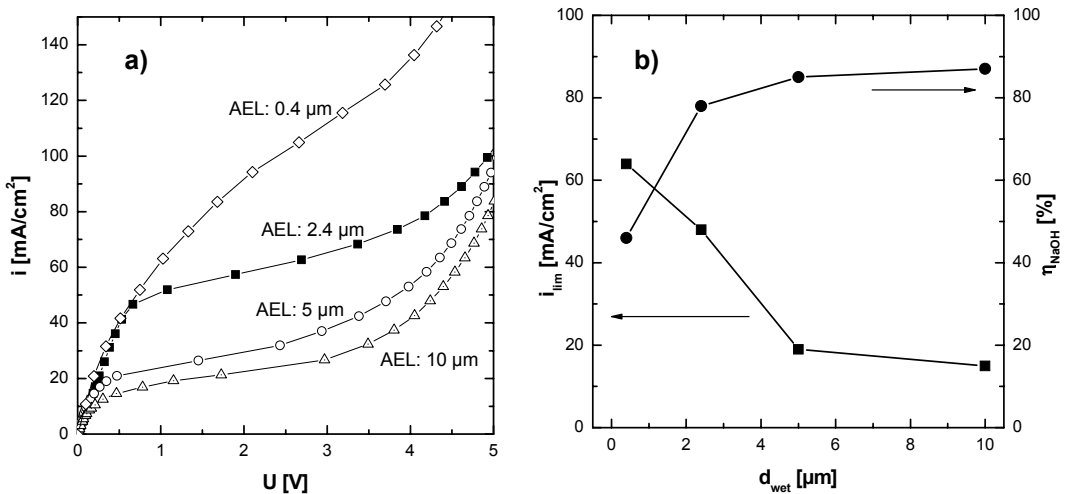


**Figure 13:** Effect of the AEL layer thickness on the properties of tailor made BPMs with constant CEL measured in 2M NaCl. (a)  $i$ - $v$  curves, (b) Dependence of  $i_{\text{lim}1}$  and current efficiency on the AEL thickness.

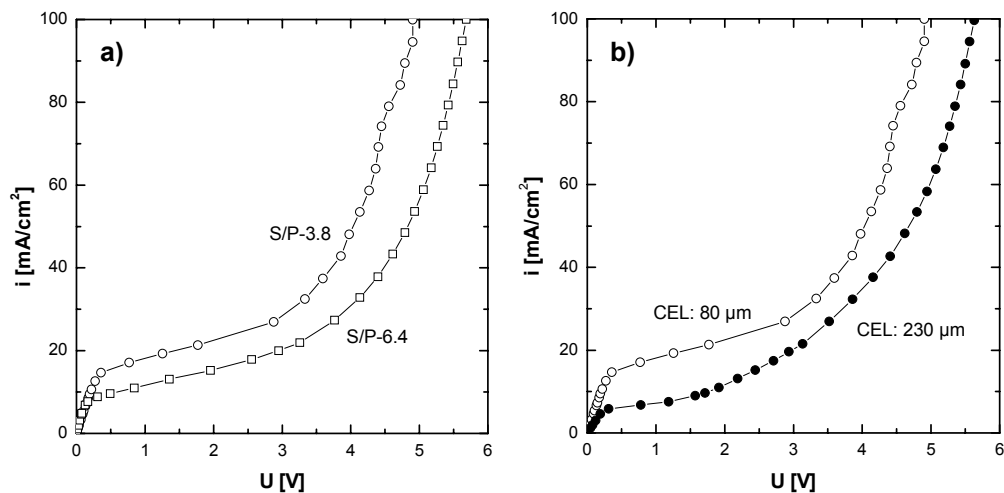
### Effect of the CEL composition and thickness

In these experiments, the anion exchange layer was always the same (aminated Psf, 10  $\mu\text{m}$ ) while the composition and the thickness of the CEL was varied. Figure 14a shows the  $i$ - $v$  curves and Table 5 shows the  $i_{\text{lim}1}$  and  $\text{Cl}^-$  fluxes of asymmetric BPMs prepared using S/P-3.8 and S/P-6.4 blends as CEL (see Table 3). The BPM with the S/P-6.4 CEL has a lower  $i_{\text{lim}1}$  and a lower  $\text{Cl}^-$  flux compared to the BPM with the S/P-3.8 CEL. The  $\text{Cl}^-$  flux through the BPM with the S/P-6.4 CEL is 31% lower than the flux through the BPM with the S/P-3.8 CEL.

**Table 5:** Influence of the cation exchange layer composition and thickness.

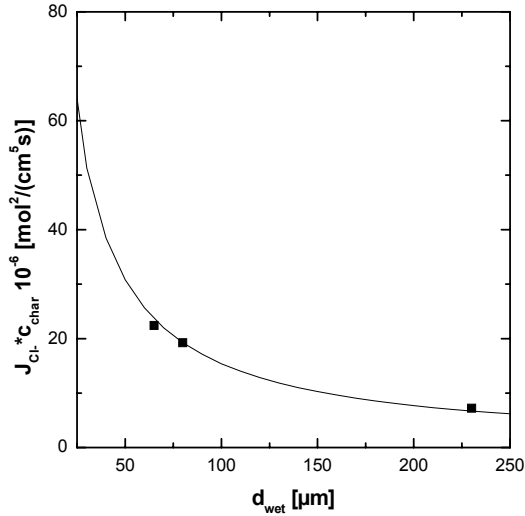
CEL	$d_{\text{CEL}}$ [ $\mu\text{m}$ ]	$i_{\text{lim}}$ [mA/cm <sup>2</sup> ]	$R_{\text{diss}}$	$R_{\text{op}}$	$J_{\text{Cl}^-}$ 10 <sup>-9</sup> [mol/(cm <sup>2</sup> s)]	
					[ $\Omega\text{cm}^2$ ]	
S/P-3.8	80	14.6	11.4	54.2	5.1	-
S/P-3.8	230	5.6	13.1	59.8	-	1.9
S/P-6.4	65	8.2	12.2	66.6	3.5	-

Figure 14b shows the  $i$ - $U$  curves of BPMs containing S/P-3.8 CELs of different thickness. The membrane with 230  $\mu\text{m}$  thickness has 62% lower  $i_{\text{lim}1}$  than the membrane with 80  $\mu\text{m}$  thickness (5.6 to 14.6  $\text{mA}/\text{cm}^2$ , respectively). For the 230  $\mu\text{m}$  S/P-3.8 membrane, the  $\text{Cl}^-$  flux was not detectable. However, if we use equation 3 (assuming symmetrical flux decrease), we estimate the  $\text{Cl}^-$  flux at 1.9  $\text{mol}/(\text{cm}^2\text{s})$ .



**Figure 14:** Effect of the S/P blend properties the  $i$ - $v$  curve of tailor made BPMs with constant AEL measured in 2M NaCl. (a) Influence of charge density, (b) Influence of layer thickness.

For the tailor made BPM, it is interesting to check the applicability of equation 14, which relates the  $\text{Cl}^-$  flux to the layer thickness and  $c_{\text{char}}$ , and the comparison between estimated and measured  $\text{Cl}^-$  fluxes. Using the measured properties for the S/P-3.8 layer, ( $J_{\text{Cl}^-}$ : 5.1  $10^{-9}$   $\text{mol}/(\text{cm}^2\text{s})$ ;  $d_{\text{wet}}$ : 80  $\mu\text{m}$ ;  $c_{\text{char}}$ : 3.8  $\text{mol}/\text{L}$ ), equation 14 gives  $\text{Cl}^-$  diffusion coefficient ( $D_{\text{Cl}^-, \text{S/P}}$ ) of 3.8  $10^{-14}$   $\text{cm}^2/\text{s}$ . Assuming that  $D_{\text{Cl}^-, \text{S/P}}$  is the same for the S/P layers (all layers contain the same materials: 60% S-PEEK and 40% PES), one can get a master curve showing the dependence of  $J_{\text{Cl}^-}$  normalised for the  $c_{\text{char}}$  versus the membrane thickness (see Figure 15). Our experimental (measured and estimated)  $J_{\text{Cl}^-}$  fluxes for the tailor made BPMs (see Table 5) follow nicely this master curve. This comparison shows that equation 14 is suitable to predict well the properties of the tailor made BPM and can be used as a tool to design a BPM with tailor made properties and selectivity.



**Figure 15:** Dependence of  $J_{Cl^-}$  normalised for  $c_{char}$  on  $d_{wet}$  of the S/P CEL. Comparison of the calculated (equation 14) and experimental fluxes.

In summary, the tailor made BPMs show a reduced  $Cl^-$  leakage compared to the commercial BP-1 membrane. The  $Cl^-$  leakage depends on the charge density and the thickness of the CEL and can be predicted by the master curve based on equation 14. Because of the thin AEL (10  $\mu\text{m}$ ) and therefore the high water flux through the anionic side of the BPM, the thickness of the CEL could be increased to 230  $\mu\text{m}$  without having water diffusion limitations. The principle of asymmetry can therefore be used to tailor BPMs to achieve high purity products at one side of the BPM process, while reducing the purity of the product at the other side.

## 5. Conclusions

In this work, we have shown that BPM asymmetry can be used to decrease the co-ion fluxes through the BPM. The thickness and charge density determine the co-ion leakage through the corresponding IEL.

Experiments with the commercial BP-1 membrane have shown that the cationic side of the membrane contains much more water and more co-ions than the anionic side. Therefore the limiting current density is more affected by the lamination of CELs. The addition of a thin S/P-6.4 CEL (65 $\mu\text{m}$ ) onto the cationic side of the BP-1

membrane (BP-1+S/P-6.4) produced the best BPM with a decrease in co-ion leakage of 47%.

Tailor made BPMs have been prepared showing a reduced  $\text{Cl}^-$  leakage compared to the commercial BP-1 membrane. The  $\text{Cl}^-$  leakage depends on the charge density and the thickness of the CEL. Because of the thin AEL (10  $\mu\text{m}$ ) and therefore the high water flux through the anionic side of the BPM, the thickness of the CEL (S/P-3.8) could be increased to 230  $\mu\text{m}$  leading to low  $\text{Cl}^-$  flux without water diffusion limitations.

The increase in bipolar membrane asymmetry decreases the co-ion leakage, but also causes an increase in membrane resistance leading to higher energy consumption for the production of acids and bases. However, the decrease in co-ion leakage and therefore the increase in product purity are higher than the corresponding increase in membrane resistance.

## 6. List of symbols

A	Membrane area [ $\text{m}^2$ ]
$c_{\text{char}}$	Charge density [mol/L]
c	Concentration [mol/L]
Cond	Conductivity [mS/cm]
$d_{\text{wet}}$	Thickness of the wet membrane layer [ $\mu\text{m}$ ]
D	Diffusion coefficient [ $\text{m}^2/\text{s}$ ]
F	Faraday constant (96485 A s/mol)
i	Applied current density [ $\text{A}/\text{m}^2$ ]
I	Applied current [A]
IEC	Ion exchange capacity [mol/kg <sub>dry</sub> ]
J	Flux [mol/( $\text{m}^2\text{s}$ )]
$\text{M}^+$	Salt or base cation (also as subscript)
N	Number of repeat units
P	Permselectivity [%]
R	Area resistance [ $\Omega \text{ cm}^2$ ]
SD	Sulphonation degree [%]

t	Time [s]
$t_{cr^-}$	Transport number of chloride [%]
T	Temperature [K]
U	Potential difference [V]
V	Circulated volume [L]
w	Water uptake [ $\text{kg}_{\text{water}}/\text{kg}_{\text{dry}}$ ]
x	Location normal to the membrane [m]
$X^-$	Salt or acid anion (also as subscript)
z	Valence
$\eta$	Current efficiency [%]
AEL	Anion exchange layer (also as subscript)
BPM	Bipolar membrane
CEL	Cation exchange layer (also as subscript)
ED-BPM	Bipolar membrane electrodialysis
IEL	Ion exchange layer
NMP	N-methyl-2-pyrrolidinone
PEEK	Poly(ether ether ketone)
PES	Poly(ether sulphone)
Psf	Polysulphone
P4VP	Poly-(4-vinyl pyridine)
S-PEEK	Sulphonated poly(ether ether ketone)
S/P	S-PEEK/PES blend, 60/40 (also as subscript)

**Superscripts / Subscripts**

0	At time zero
av	Arithmetic average
diss	Dissociation
i	Species i
lim	Limiting
m	Membrane phase
op	Operational
s	At the solution side
t	At given production time

## 7. References

- [1] J. Balster, D.F. Stamatialis, M. Wessling, "Electro-catalytic membrane reactors and the development of bipolar membrane technology", *Chemical Engineering and Processing* 43 (2004) 1115-1127.
- [2] F.G. Wilhelm, N.F.A. van der Vegt, M. Wessling, H. Strathmann, *Bipolar Membrane Preparation*, in A.J.B. Kemperman (ed.), *Bipolar membrane Handbook*, Twente University Press, Enschede, The Netherlands, 2000.
- [3] R. El Moussaoui, G. Pourcelly, M. Maeck, H.D. Hurwitz, C. Gavach, *Co-ion leakage through bipolar membranes, influence ion I-V responses and water-splitting efficiency*". *Journal of Membrane Science* 90 (1994) 283-292.
- [4] F. G. Wilhelm, I. Punt, N. F. A. van der Vegt, M. Wessling, H. Strathmann, *Optimisation strategies for the preparation of bipolar membranes with reduced salt ion leakage in acid-base electro dialysis*, *Journal of Membrane Science* 182 (2001) 13-28.
- [5] F. G. Wilhelm, I. Punt, N. F. A. van der Vegt, M. Wessling, H. Strathmann, *Asymmetric Bipolar Membranes in Acid-Base Electro dialysis*, *Industrial & Engineering Chemistry Research* 41 (2002) 579-586.
- [6] T. Aritomi, T. van der Boomgaard and H. Strathmann, *Current voltage curve of a bipolar membrane at high current density*, *Desalination* 104 (1996) 13-18.
- [7] J.J. Krol, M. Jansink, M. Wessling and H. Strathmann, *Behaviour of bipolar membranes at high current density: Water diffusion limitation*, *Separation and Purification Technology* 14 (1998) 41-52.
- [8] J. L. Gineste, G. Pourcelly, Y. Lorrain, F. Persin, C. Gavach, *Analysis of factors limiting the use of bipolar membranes: a simplified model to determine trends*, *Journal of Membrane Science* 112 (1996) 199-208.
- [9] D. Raucq, G. Pourcelly, C. Gavach, *Production of sulphuric acid and caustic soda from sodium sulphate by electromembrane processes. Comparison between electro-electrodialysis and electro dialysis on bipolar membrane*, *Desalination* 91 (1993) 163-175.

- [10] T.A. Davis, T. LaTerra, "On-site generation of acid and base with bipolar membranes: a new alternative to purchasing and storing regenerants", proceedings, 48<sup>th</sup> annual meeting, International Water Conference, 1987.
- [11] R. Simons, "Preparation of a high performance bipolar membrane", *Journal of Membrane Science* 78 (1993) 13-23.
- [12] J. Balster, O. Krupenko, I. Pünt, D.F. Stamatialis, M. Wessling, "Preparation and characterisation of monovalent ion selective cation exchange membranes based on sulphonated poly(ether ether ketone)", *Journal of Membrane Science* 263 (2005) 137-145.
- [13] F. G. Wilhelm, I. G. M. Punt, N. F. A. van der Vegt, H. Strathmann, M. Wessling, "Cation permeable membranes from blends of sulfonated poly(ether ether ketone) and poly(ether sulfone)", *Journal of Membrane Science* 199 (2002) 167-176.
- [14] B. Bauer, "Bipolare Mehrschichtmembranen (bipolar multilayer membranes)", Fraunhofer-Gesellschaft zur Förderung der Angewandten Forschung e.V (FhG) (Germany), DE Patent 4026154 (1992).
- [15] J. J. Krol, M. Wessling, H. Strathmann, "Concentration polarization with monopolar ion exchange membranes: current-voltage curves and water dissociation", *Journal of Membrane Science* 162 (1999) 145-154.
- [16] X. Tongwen and Y. Weihua, "Effect of cell configurations on the performance of citric acid production by a bipolar membrane electrodialysis", *Journal of Membrane Science* 203 (2002) 145-153.



## Chapter IV

### Multi-layer spacer geometries with improved mass transport

J. Balster, I. Pünt, D. F. Stamatialis, and M. Wessling

#### Abstract

In electro dialysis desalination processes, it is desirable to operate at the highest practicable current density in order to get the maximum ion flux per unit membrane area. The operating current density is limited by concentration polarisation. In this work the development of optimal spacer configurations to decrease concentration polarisation and improve the process performance is presented. Standard non-woven and multi-layer net spacers are tested and their performance in the light of mass transfer enhancement and cross flow power consumption is evaluated. We utilise multi-layer spacer configurations comprising a standard middle spacer with two thin outside net spacers which result in the highest mass transfer enhancement. When the diameter of the filament of the middle spacer is reduced the same mass transfer enhancement can be reached at 30 times lower cross-flow power consumption. Besides, at the same cross-flow power consumption the developed multi-layer spacer shows 20 percent higher mass transfer than a standard commercial non-woven net spacer.

Based on J. Balster et al., Journal of Membrane Science 282 (2006) 351-361.

## 1. Introduction

Many membrane processes are severely influenced by concentration polarisation. Electrodialysis used for desalination (Figure 1) suffers from it in particular.

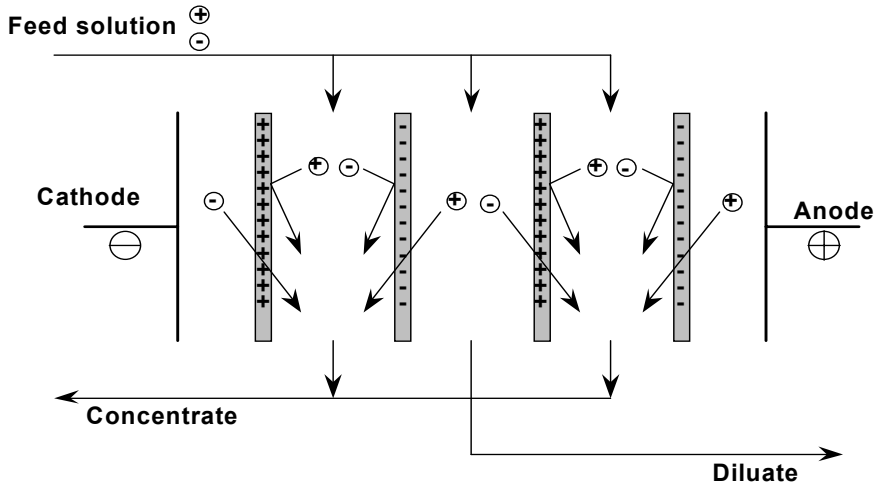


*Figure 1: Principle of the electro dialysis desalination process.*

Concentration polarisation in electro dialysis is caused by differences between ion transport number in the electrolyte solution and the ion-exchange membrane. Electro dialysis is a good technology to study methods to reduce concentration polarisation, since the phenomenon is well described and fully reversible. This in contrast to ultrafiltration for instance where concentration polarisation and fouling may occur simultaneously making thorough interpretation difficult. The consequences of concentration polarisation in electro dialysis are twofold. The difference in transport number leads to depletion of salt ions on the dilute side of the membrane, whereas at the same time the concentration near the membrane on the concentrate side increases (Figure 2) [1, 2].

Both effects impair the technical feasibility and the economics of the process. When, due to concentration polarisation, the salt concentration in the concentrate cell exceeds the solubility limits of the solution constituents, precipitation may occur, resulting in an additional electrical resistance and eventually in membrane damage.

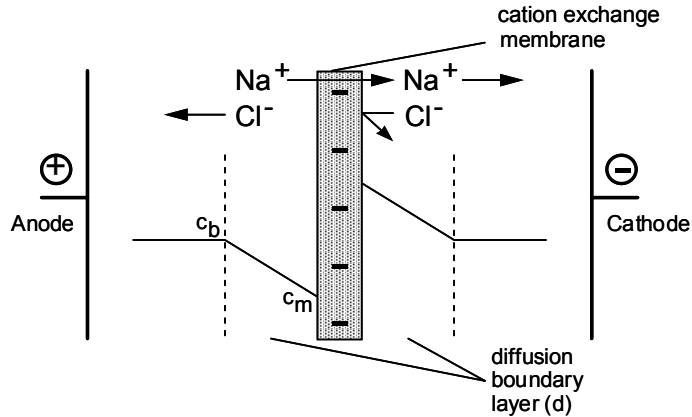


**Figure 2:** Schematic illustration of the concentration polarization in electrodialysis.

If in the dilute cell the salt concentration at the membrane surface is reduced to zero there are no more salt ions available to carry the electrical current and the limiting current density  $i_{lim}$  is reached (Figure 3).

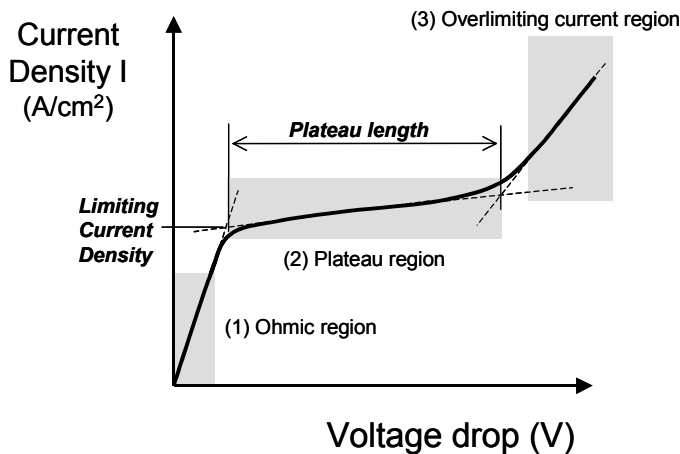


**Figure 3:** Typical current density – voltage drop curve for an ion exchange membrane showing the ohmic, the plateau and the overlimiting current region, taken from [5].

Further increase of the driving force ( $\Delta V$  across the membrane and boundary layer) does not increase the ionic flux. The plateau region of the current-voltage curve has been reached. At some critical voltage drop, transport occurs again: the overlimiting current sets in. Its nature has been disputed for some time and the reader is referred to [3-5] for details. A small percentage of the overlimiting current, in particular for

anion exchange membranes, is caused by enhanced water splitting. The remaining overlimiting flux is caused by electro-convection, a hydrodynamic effect that destabilises the laminar boundary layer [4]. Although small in magnitude, the implications of the water splitting are considerable. Water dissociation, leads to a loss of current utilisation and pH shifts on the membrane surface, which can lead to precipitation of multivalent ions on the membrane surface [6, 7]. Generally, every electro dialysis unit installed in the world is designed following a simple rule: the maximum current flowing through a stack must be 80% of the limiting current density at the lowest concentration in the dilute, resulting in high membrane areas for the removal of salt in very dilute solutions [8, 9].

In electro dialysis processes, the fluid flow mainly takes place in flat channels with rectangular cross-sections, where the membranes form the walls and the channels are filled with spacer material. The spacers act as mechanical stabilisers for the channel geometry and promote turbulence, which reduces the polarisation phenomena near the membranes, reducing the laminar boundary layer and increasing the mass transfer coefficient [10]. The spacer design itself has therefore a great effect on the process costs. A careful design may result in higher limiting current density and therefore in a reduction of the membrane surface area required for a given application [11]. Recently Li et al. [12, 13] developed novel spacers for mass transfer enhancement in membrane separations. These spacers have a multi layer structure (sandwich of spacers containing a bigger spacer in the middle with two thin outside spacers) and lead to 30% higher Sherwood numbers at the same cross flow power consumption in comparison to optimal non-woven net spacers [12]. The work primarily presents computational fluid dynamics simulations with an electrochemical characterisation of the limiting flux at an electrode in a flat flow channel. Li et al. [12] do not proof nor benchmark their spacers in a real membrane process.

In this work, the development and systematic evaluation of optimal spacer configurations to decrease concentration polarisation in electro dialysis and improve the process performance are discussed. Standard non-woven net spacers are compared with the spacers of Li et al. [12, 13] and our own tailor made multi-layer spacers in an electro dialysis desalination process in the light of mass transfer

enhancement and cross-flow power consumption. The main advantage of the application of our own multi-layer spacers is the lower resistance and power consumption due to the decrease of the channel height in the membrane stack.

## 2. Theory

### 2.1 Concentration polarisation and limiting current density

The current density  $i$  follows Faraday's law and is given by

$$i = \frac{zDF(c_b - c_m)}{\delta(t^m - t^{bl})} \quad (1),$$

where  $t^m$  and  $t^{bl}$  are the transport numbers of the ion in the membrane and in the boundary layer respectively,  $z$  is the valence of the ion,  $D$  is the diffusion coefficient of the ion,  $F$  is the Faraday constant,  $i$  is the electrical current density,  $c_b$  and  $c_m$  are the concentrations in the bulk and at the membrane surface, and  $\delta$  is the thickness of the boundary layer [14]. If the electrical potential difference is increased, the current density will increase, leading to an increased ion flux and consequently to a decreased ion concentration at the surface of the membrane (Figure 2). When the ion concentration at the membrane surface  $c_m$  approaches zero, a limiting current density  $i_{lim}$  is reached [6, 14]:

$$i_{lim} = \frac{zDFc_b}{\delta(t^m - t^{bl})} \quad (2).$$

A further increase in the driving force (electrical potential) at this point will not result in an increased ion flux (Figure 1c). In order to minimise the effect of polarisation, the thickness of the boundary layer must be reduced and hence the hydrodynamics and cell design must be improved [14].

The mass transfer coefficient in the boundary layer [6]

$$k_{bl} = \frac{D}{\delta} \quad (3),$$

is a function of the hydrodynamics of the feed solution (Schmidt and Reynolds number), i.e. the flow velocities, the cell geometry, the spacer design, and the salt diffusion coefficient. The  $k_{bl}$  can be directly related to the limiting current density using equation 2:

$$k_{bl} = \frac{i_{lim}(t^m - t^{bl})}{zFC_b} \quad (4).$$

## 2.2 Spacers - background

The geometric parameters of the spacers have a strong influence on mass transfer and flow resistance. A non-woven net spacer can be characterized by different parameters as shown in Figure 4: The distance between the spacer filaments  $l_1$  and  $l_2$  ( $l_1=l_2=l$ ), the angle between the spacer filaments  $\beta$ , the flow attack angle  $\alpha$ , the diameter of the filaments  $d_F$ , the height of the filaments  $h_F$ , and the height of the spacer  $h_{SP}$ .

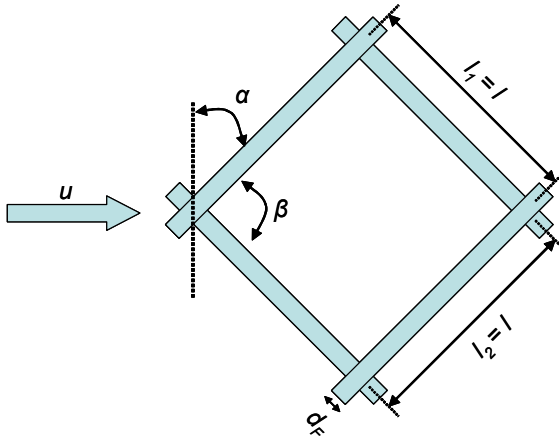


**Figure 4:** Geometric characteristics of a non-woven net spacer.

The porosity  $\varepsilon$  of a spacer is given by

$$\varepsilon = 1 - \frac{V_{Sp}}{V_{Ch}} \quad (5),$$

where  $V_{SP}$  and  $V_{Ch}$  are the volume of the spacer and of the channel per unit area, respectively. The porosity of the spacer can be calculated after determination of  $d_F$  and  $l$  [15, 16]:

$$\varepsilon = 1 - \frac{2\pi\left(\frac{d_F^2}{4}\right)l}{h_{Sp}l^2 \sin\beta} = 1 - \frac{\pi d_F^2}{2h_{Sp}l \sin\beta} \quad \text{for round filaments} \quad (6),$$

or

$$\varepsilon = 1 - \frac{2d_F h_F l}{h_{Sp}l^2 \sin\beta} \quad \text{for rectangular filaments} \quad (7).$$

The specific volume dependent surface of the spacer,  $S_{V,Sp}$ , was calculated as

$$S_{V,Sp} = \frac{A_{Sp}}{V_{Sp}} = \frac{\pi d_F l}{\pi\left(\frac{d_F^2}{4}\right)l} = \frac{4}{d_F} \quad \text{for round filaments} \quad (8),$$

or

$$S_{V,Sp} = \frac{A_{Sp}}{V_{Sp}} = \frac{2d_F l + 2h_F l}{d_F h_F l} = \frac{2}{d_F} + \frac{2}{h_F} \quad \text{for rectangular filaments} \quad (9).$$

The evaluation of spacer performance and optimisation of spacer geometry is based on two parameters [12]:

- the cross-flow pumping power consumption, and
- the mass transfer coefficient.

Mass transfer and cross-flow power consumption in geometrically similar spacers can be analysed by dimensional numbers [17, 18]. The mass transfer coefficient ( $\bar{k}$ ) taken as an average over the channel length ( $L$ ) is dependent on the density ( $\rho$ ), the dynamic viscosity ( $\mu$ ) and the diffusivity ( $D$ ) of the solution, the height of the channel ( $h_{Ch}$ ), the distance between the spacer filaments ( $l$ ), the flow attack angle ( $\alpha$ ), the angle between the spacer filaments ( $\beta$ ), and the liquid velocity ( $u$ ) [17].

Dimensionless analysis leads to the following relationship between dimensionless numbers [17-19]:

$$Sh = f(Re, Sc, \frac{l}{h_{Ch}}, \alpha, \beta) \quad (10),$$

where

$$Sh = \frac{\bar{k}h_{Ch}}{D}, \quad Sc = \frac{\mu}{\rho D}, \quad Re = \frac{\rho u h_{Ch}}{\mu} \quad (11-13).$$

The mechanical power consumption for the pumping per unit volume of spacer filled channel (SPC) is described by the physical relationship

$$SPC = \frac{\Delta P \phi_v}{Lwh_{Ch}} = \frac{\Delta P u w h_{Ch}}{Lwh_{Ch}} = \frac{\Delta P}{L} u \quad (14),$$

where  $\Delta P$  is the pressure drop over the channel,  $w$  is the width of the channel and  $\phi_v$  is the volumetric flow rate through the channel [19]. In equations 13 and 14, we use

$$u = \frac{V_{Ch}}{t}, \text{ for the empty channel} \quad (15),$$

and

$$u_{corr} = \frac{V_{Ch} - V_{Sp}}{t}, \text{ for the spacer filled channel} \quad (16),$$

where  $t$  is the residence time in the channel per unit area. After dimensional analysis the dimensionless Power number (Pn) can be obtained:

$$Pn = SPC \frac{\rho^2 h_{Ch}^4}{\mu^3} \quad (17).$$



Enhanced mass transfer in spacer-filled channels is mainly due to the following mechanisms [12]:

- Flow separation and boundary layer development,
- Flow acceleration and
- Swirling flows.

At low Reynolds numbers ( $10 < Re < 100$ ) flow separation and boundary layer development play a role in mass transfer enhancement. Flow acceleration occurs in the area restriction between a filament and the membrane. At higher Reynolds numbers ( $Re > 100$ ) a swirling flow exists, causing mass transfer enhancement due to mixing. Two types of swirling flows can be recognised: Transversal and longitudinal vortices. The axis of a transversal vortex is perpendicular to the mean flow direction (i.e. Karman vortex [20]), whereas the longitudinal vortices have their axis parallel to the mean flow direction [21]. Li et al [12] suggest that not only the coexistence of the longitudinal and transversal vortices is essential, but also the spatial distribution of the vortices is of great importance for the optimal spacer performance. They have shown that the vortices in non-woven net spacers mainly occur in the bulk of the flow, which can not be effective, since the resistance against mass transfer is situated in the immediate vicinity of the wall. Therefore the vortices should be generated close to the channel wall, i.e. the membrane.

In membrane processes, the performance of a spacer is often evaluated by its position in a Sh versus Pn plot. The Sh number represents the mean mass transfer coefficient averaged over the area of the channel walls (Equation 11). In electro dialysis, the limiting current density is directly related to the thickness of the diluted boundary layer (Equation 2). Therefore in this work, we evaluate the mass transfer coefficient in the boundary layer for each spacer based on the results of  $i_{lim}$  versus Re and Pn. Using this method, the effect of the spacer on the built up of vortices at the membrane walls can be easily evaluated (Equation 3 and 4).

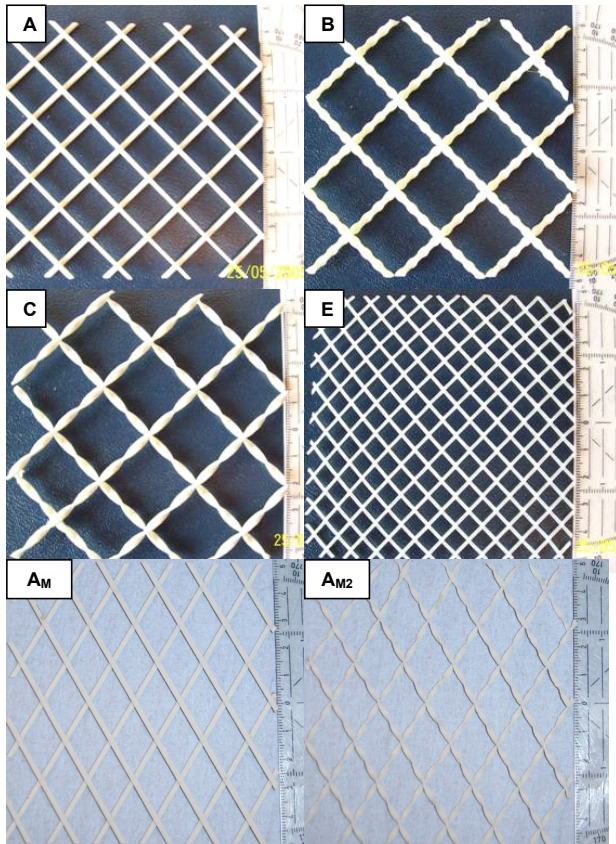
### 3. Experimental

Table 1 presents the specifications of all the spacers used in this work. The spacers A, A<sub>M1</sub>, A<sub>M2</sub>, B, C, I, and J of Li et al [12, 13] were kindly provided by the Separation Technology Group of the University of Twente, Enschede (manufactured by the Selective Laser Sintering (SLS) technology [22]). The filaments of the spacer A, I, and J are round, whereas the filaments of spacer B and C are modified. Spacer B has a round filament too, but with a twisted filament on top of it. Spacer C has a rectangular twisted filament.

**Table 1:** Geometric parameters of the tested spacers.

Spacer	Filament shape	$\alpha$ [°]	$\beta$ [°]	l [m m]	$d_F$ [mm]	$h_F$ [mm]	$h_{sp}$ [mm]	$\epsilon$	$S_{V,sp}$ [1/mm]	$V_{sp}$ $10^{-6}$ [m <sup>3</sup> ]
A	round	45	90	16	2.2	-	4.0	0.88	1.8	4.75
A <sub>M1</sub>	round	60	60	16	2.2	-	4.0	0.88	1.8	4.86
A <sub>M2</sub>	rectangular twisted	60	60	16	1.0	2.0	4.0	0.94	3.0	2.50
B	round twisted	45	90	25	2.0	3.3	6.0	0.93	1.5	4.41
C	rectangular twisted	45	90	25	1.0	3.0	6.1	0.96	2.7	2.40
D	rectangular	0	90	15	1.5	2.0	6.0	0.93	2.3	4.00
E	round	47.5	85	7	1.1	-	1.9	0.86	3.6	2.73
F	round	47.5	85	14.5	1.1	-	1.9	0.93	3.6	1.32
G	round	50	80	9	2.1	-	3.2	0.75	1.9	7.82
H	round	45	90	4	0.8	-	1.1	0.77	5.0	2.51
I	round	60	60	4	0.5	-	0.8	0.86	8.0	1.13
J	round	45	90	4	0.5	-	0.9	0.89	8.0	0.98
K	round	51	78	6	1.0	-	1.5	0.82	4.0	2.68

Additionally, two modified versions of spacer A were tested. The A<sub>M1</sub> spacer has a different flow attack and filament angle and the A<sub>M2</sub> spacer has twisted rectangular filaments. These spacers were prepared by rapid prototyping. The spacers D, E, F, G, and H are standard commercial non-woven net spacers with unmodified filaments as regularly used in state-of-the-art plate and frame membrane modules. Figure 5 shows photos of some of these spacers. The multi-layer spacers were prepared by stacking three spacers together (Figure 6).



**Figure 5:** Photos of the spacer A, B, C, E,  $A_{M1}$ , and  $A_{M2}$  showing the different filament shapes and geometries.

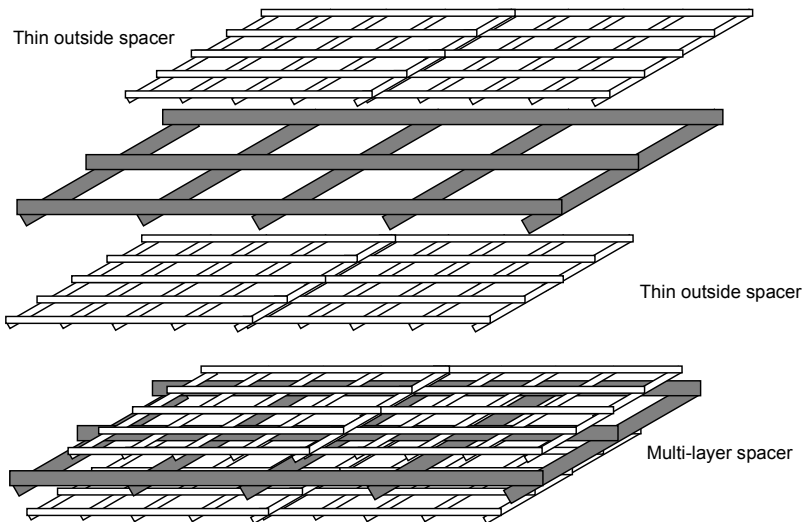


**Figure 6:** Schematic illustration of the multi-layer spacer.

The performance of the different spacer systems was evaluated by limiting current density measurements at different flow velocities in a simplified electro dialysis system, consisting of a single dilution and concentration channel pair. The electro dialysis system is a semi-automated lab scale system used in batch recycle mode. The electro dialysis membrane module (FuMATech, Germany) has a membrane area of  $100 \text{ cm}^2$  ( $10 \text{ cm} * 10 \text{ cm}$ ) for each membrane. More details about the setup and method can be found elsewhere [23]. For the tests, the commercial anion exchange membrane, AMX, and cation exchange membrane, CMX, (Tokuyama Soda, Japan) were used. The pressure drop of the investigated cell configuration was measured by pressure indicators placed at the inlet and the outlet of the cell.

Current-voltage curves were obtained under direct current with the stack configuration shown in Figure 7a. The hydrodynamics in compartment number 3 at the central CMX membrane are under investigation. The other membranes are auxiliary membranes preventing the transport of water dissociation products, formed at the two working electrodes, to the central compartments. During the experiment, the applied current density is increased stepwise and the system is allowed to reach a steady state. The voltage drop across the membrane module is measured, followed by the next increase in current density. First the current-voltage behaviour of the arrangement without the central membrane is measured to obtain a current voltage curve of the electrode and auxiliary compartments. Next, the central membrane is introduced and the current-voltage curve is measured again. The difference between the two curves for the same current density is the current-voltage behaviour of the central membrane in the module. The limiting current density of the membrane is determined by plotting the resistance of the membrane,  $R$ , versus the reciprocal current density [6]. This procedure is repeated with all different spacer configurations in compartment 3 and the limiting current densities of the different systems are compared. Figure 7b and 7c show typical experimental results for one spacer configuration.

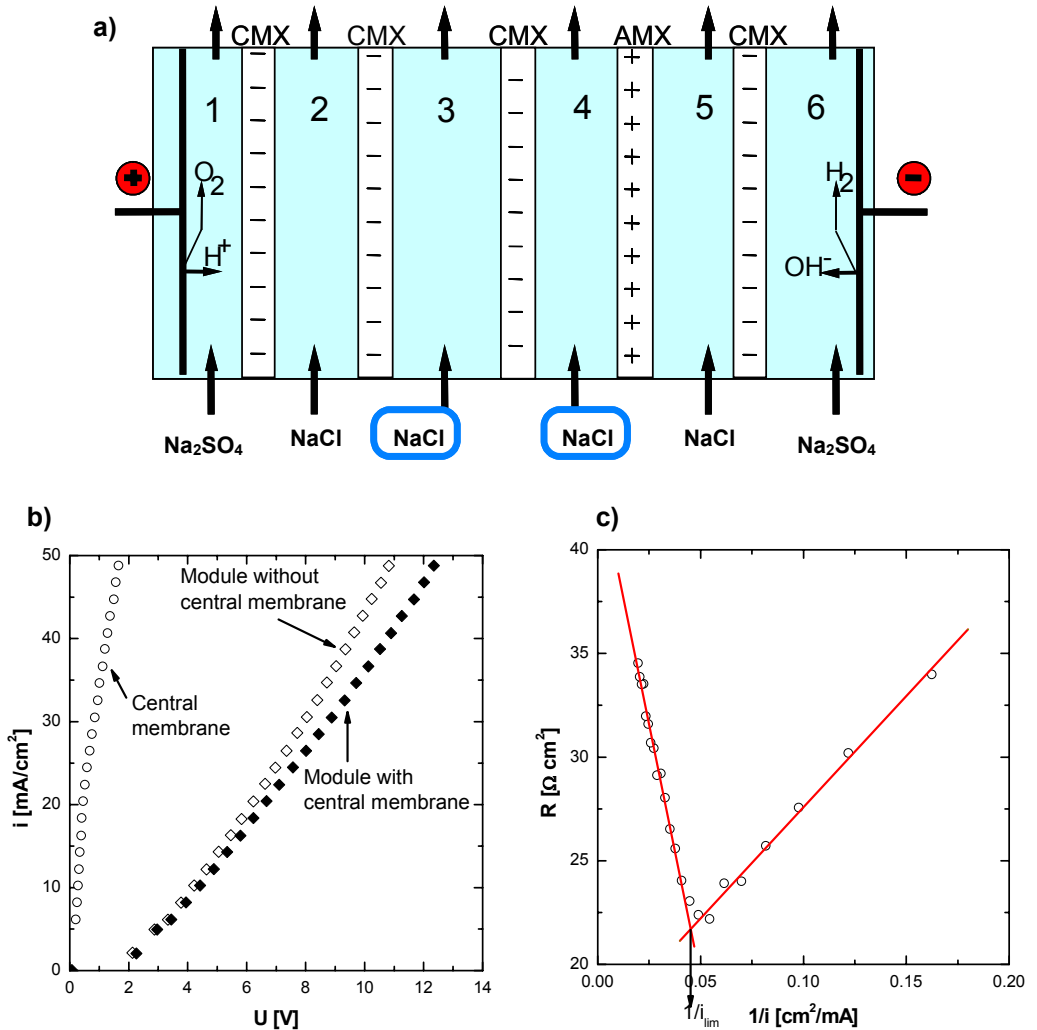


**Figure 7:** a) Schematic of the membrane arrangement in the electrodiagnosis stack. b) Current-voltage curves of the membrane module with and without the central membrane. The current-voltage curve of the central membrane is calculated by subtracting these results, c) Determination of the limiting current density of the central membrane.

In the compartments 1 and 6, a 0.5M  $\text{Na}_2\text{SO}_4$  solution was applied as electrolyte. In the compartments 2 and 5, 0.5M  $\text{NaCl}$  was applied as shielding solution and in the compartments 3 and 4, 0.1M  $\text{NaCl}$  was used as measurement solution. The physical properties of a 0.1M  $\text{NaCl}$  solution are:  $\rho = 1088 \text{ kg/m}^3$ ;  $\mu = 1 \text{ mPa s}$ ;

$$D_{\text{Na}^+} = 1.48 \cdot 10^{-9} \text{ m}^2/\text{s}; t_{\text{Na}^+}^{\text{bl}} = 0.39 [24].$$

## 4. Results and discussion

### 4.1 Single spacer

In this part the influence of the spacer geometry, filament shape and of the flow attack angle on the limiting current density is evaluated. The corresponding mass transfer coefficient (Equation 4) at different flow velocities (corrected for the spacer volume, see Equation 16) of single layer non-woven net spacers is estimated. Spacer A and D have unmodified filaments with a round and a squared shape respectively and differ in the flow attack angle. Both spacer B and C have the same flow attack angle as spacer A (see Table 1), but spacer B has filaments with regular variation of  $d_F$  (round twisted) and spacer C has twisted rectangular filaments (see Figure 5). Table 2 presents the limiting current density and mass transfer coefficient obtained for the single spacer configurations at two different volume flows measured in a 5.5mm channel.

**Table 2:** Limiting current density and mass transfer enhancement of different single spacers measured at two different volume flows (5.5mm channel).

Spacer	Filament shape	$\phi_V = 40 \text{ L/h}$			$\phi_V = 80 \text{ L/h}$		
		Re	$i_{lim}$ [mA/cm <sup>2</sup> ]	$k_{bl}$ $10^{-4}$ [cm/s]	Re	$i_{lim}$ [mA/cm <sup>2</sup> ]	$k_{bl}$ $10^{-4}$ [cm/s]
	<b>no spacer</b>	120.9	12.6 ± 0.1	5.4	241.8	18.0 ± 0.1	7.7
<b>A</b>	round	132.3	21.6 ± 0.5	9.2	264.6	25.9 ± 0.2	11.0
<b>A<sub>M1</sub></b>	round	132.6	17.8 ± 0.4	7.6	265.2	28.4 ± 0.6	12.1
<b>A<sub>M2</sub></b>	rectangular twisted	126.6	21.6 ± 0.3	9.2	253.3	31.7 ± 0.2	13.5
<b>B</b>	round twisted	130.5	17.8 ± 0.1	7.6	272.9	25.2 ± 0.1	10.7
<b>C</b>	rectangular twisted	125.9	19.1 ± 0.1	8.1	270.8	27.3 ± 1.0	11.6
<b>D</b>	rectangular	129.5	15.7 ± 0.1	6.7	259.9	24.8 ± 0.1	10.6

At low flow rates ( $120 < Re < 140$ ), spacer A shows the highest mass transfer in comparison to spacer B, C and D. Spacer B and C which contain the modified filaments show also an increased mass transfer compared to the spacer D and the configuration without spacer. Spacer D shows the lowest performance.

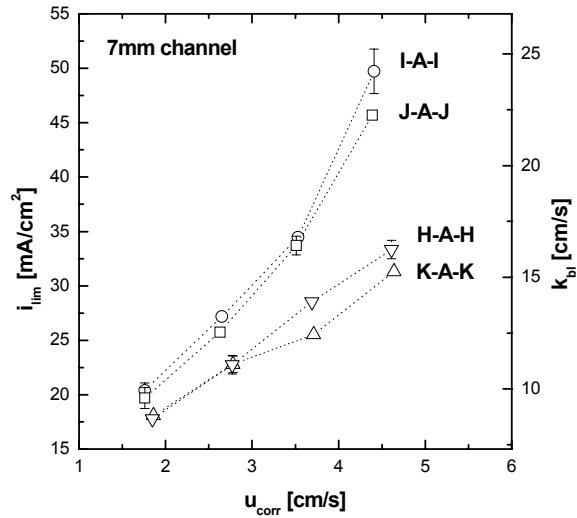
At higher flow rates ( $240 < Re < 280$ ) all spacers show similar performance. Nevertheless, the spacers B, C and D show a higher increase in mass transfer with rising flow velocity than spacer A. The modified filaments of spacer B (see Figure 5) are expected to create longitudinal vortices close to the membrane [12] which effectively enhance mass transfer, whereas the twisted tapes of spacer C (see Figure 5) can generate swirling flows [25-27], which have been extensively used in heat transfer enhancements [25]. However, both spacers B and C do not show a better performance than spacer A with the round filaments. Spacer D which shows the lowest performance at low flow rates performs better at high flow rates, but yet not better than the other spacers.

Finally the  $A_{M1}$  and  $A_{M2}$  spacers were studied in order to get a better insight into the influence of the flow attack angle and the filament shape on the performance of the spacer. Spacer  $A_{M1}$  has the same geometric parameters as spacer A, only the filament and flow attack angle are changed (see Table 1). Spacer  $A_{M2}$  has, besides these changes, rectangular twisted filaments too. At low flow rates ( $120 < Re < 140$ ), the performance of the  $A_{M1}$  spacer is lower than of the A and  $A_{M2}$  spacers (see Table 2). The changes in flow attack and filament angle do not improve the performance. At higher flow rates ( $240 < Re < 270$ ), both the  $A_{M1}$  and  $A_{M2}$  spacer show better performance than the A spacer. Especially the twisted filaments of spacer  $A_{M2}$  result in a high performance due to the creation of swirling flows. Based on above findings the spacer A,  $A_{M1}$  and  $A_{M2}$  are selected for the multi-layer spacer design.

## 4.2 Multi-layer spacer

The multi-layer spacers investigated in this work have three distinct layers (see Figure 6). They were created by using the spacer A,  $A_{M1}$ , or  $A_{M2}$  in the middle and the spacer H, I, J, or K on the outside. The thinner H, I, J, and K spacers close to the channel walls are expected to generate swirling flows, whereas the middle layer diverts the flow from the bulk to the channel walls [12]. The multi-layer spacers are used in a 7mm channel and indicated by the arrangement of the spacer layers, i.e. a multi-layer spacer with spacer A in the middle and spacer H on the outside is indicated as: H-A-H.

In order to find the outside spacers with the most promising geometric parameters, spacer A was first used in the middle and the spacers H, I, J, and K on the outside.



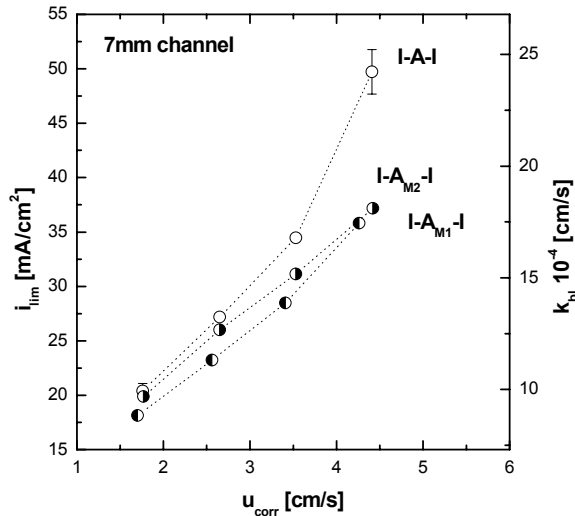
**Figure 8:** Dependence of the limiting current density and the corresponding mass transfer coefficient in the boundary layer on the corrected flow velocity for multi-layer spacer arrangements (7mm channel) with different outside layers.

Figure 8 shows the results of  $i_{lim}$  and  $k_{bl}$  (Equation 4) over the corrected mean flow velocity  $u_{corr}$  (Equation 16) inside the channel for the different multi-layer spacers. The multi-layers I-A-I and J-A-J show the best performance. At high flow velocities, the  $i_{lim}$  and  $k_{bl}$  increase dramatically. For the multi-layers H-A-H and K-A-K the increase in mass transfer is lower. Since the local Reynolds numbers for the thin spacers are lower than those of the thick ones, the coexistence of longitudinal and transversal vortices as the mass transfer enhancing mechanisms described by Li et al. [11] occur at higher flow velocities. However, even at low flow velocities (Reynolds numbers), the performance of the multi-layers I-A-I and J-A-J seems to be better compared to the single spacer A. In comparison to a channel without spacer, the enhancement of mass transfer for the I-A-I multi-layer is about 40% higher than the enhancement by the single spacer A.

Figure 9 compares the performance of multi-layer spacers with different middle spacers but with the same outside spacer. At low flow velocities, the performance of the multi-layer spacers I-A-I, I-A<sub>M1</sub>-I and I-A<sub>M2</sub>-I is comparable. At higher flow rates



the performance of the I-A-I spacer is better than of the other two multi-layer spacers. Both I-A<sub>M1</sub>-I and I-A<sub>M2</sub>-I have similar performance (see Figure 9).



**Figure 9:** Dependence of the limiting current density and the corresponding mass transfer coefficient in the boundary layer on the corrected flow velocity for multi-layer spacer arrangements (7mm channel) with different middle spacers.

It seems that in the multi-layer spacer the use of the modified spacers A<sub>M1</sub> (different flow attack angle) and A<sub>M2</sub> (twisted filaments) as middle spacers does not give any advantage. The effect of the modifications on mass transfer is less important than when they are applied as single layer spacers; especially at high flow rates (see Table 2). The creation of swirling flows by the twisted filaments of the middle spacer seems to reduce the effect of the outside net spacers. The diverting of the bulk flow to the outside walls through the middle spacer is most effective with the unmodified round filaments and the standard flow attack and filament angle (spacer A). They direct the flow from the bulk to the channel walls where the small outside spacers (spacer I) generate the swirling flows, creating the required mix of longitudinal and transversal vortices close to the membrane. This causes a decrease of the boundary layer thickness and an improvement of the mass transfer coefficient. Therefore no modified filament structures are needed for the middle spacer.

### 4.3 Down scale of the multi-layer spacers

The results of the previous section show that the multi-layer spacer I-A-I has the best performance. Nevertheless, this multi-layer is thick and requires the use of a thick channel configuration (7mm). In order to minimise the height of the channel and decrease the resistance and power consumption, thinner multi-layered spacers are required. In this section, the thin spacers E, F, and H are used in the middle and the thin I spacer on the outside. This allows the decrease of channel height from 7 to 3mm.

The multi-layer with the smallest filament length and height of the middle spacer, I-H-I, shows the highest mass transfer enhancement at low flow velocities, but the increase of  $i_{lim}$  and the corresponding  $k_{bl}$  is not as steep as from the multi-layer structures with longer filaments and bigger height of the middle spacers (I-E-I and I-F-I, Figure 10a).

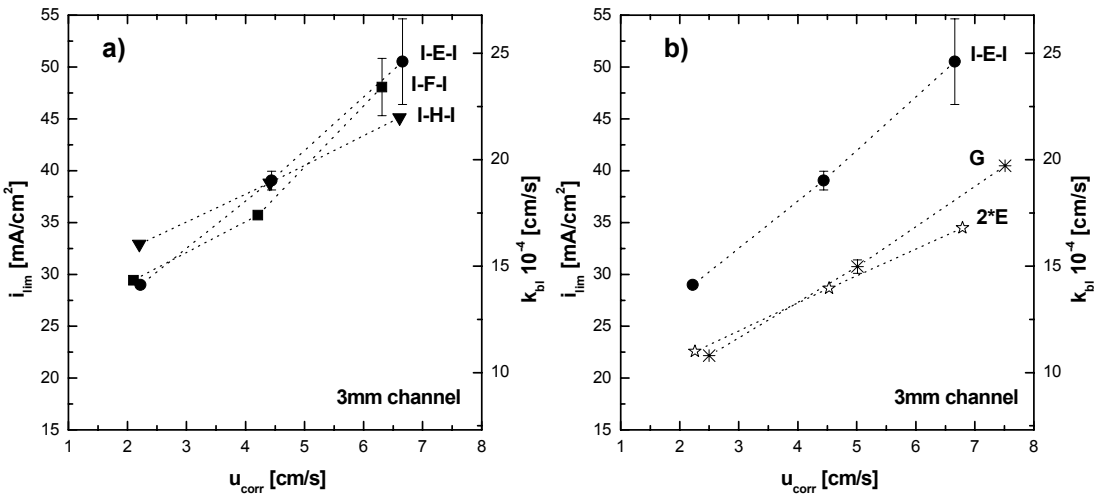


**Figure 10:** Dependence of the limiting current density and the corresponding mass transfer coefficient in the boundary layer on the corrected flow velocity for a) multi-layer spacer arrangements with different middle layers (3mm channel) b) a multi-layer spacer in comparison with a single spacer and a spacer package of two identical spacers (3mm channel).

Comparison of the I-E-I and I-F-I spacers shows that a change in filament length of the middle spacer, while keeping the spacer height constant, does not improve further the mass transfer. This indicates that the geometric parameters

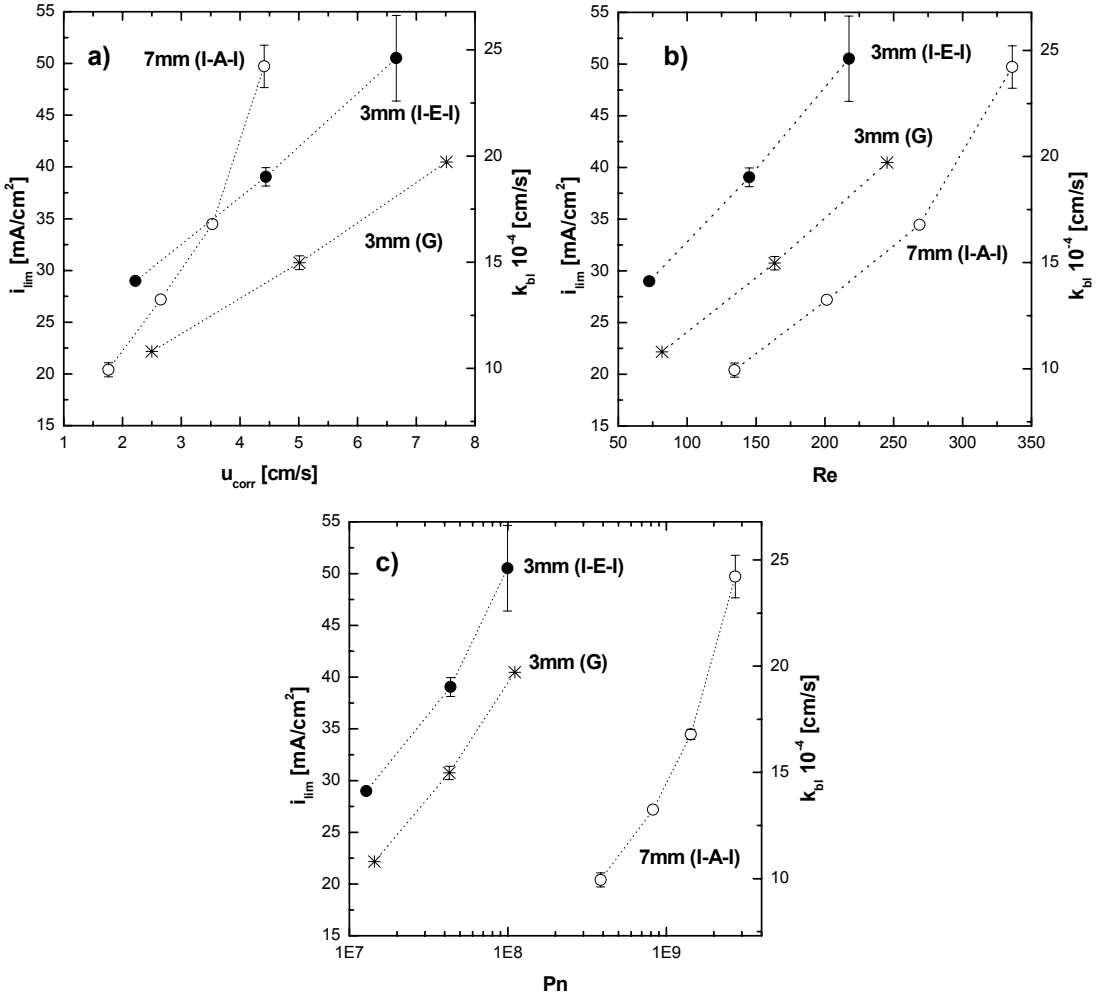
(filament length and height) of the middle spacer should be at least 2 times bigger than the ones of the outside spacers.

Figure 10b compares the performance of the I-E-I multi-layer spacer with standard non-woven net spacer G and a package of 2 spacers E (2\*E). The I-E-I spacer shows much higher mass transfer enhancement at low and high flow velocities than the other two spacers. When the flow velocity increases, the increase in mass transfer enhancement of the I-E-I spacer is steeper than of the other two spacers, probably indicating the creation of the additional mixing of longitudinal and transversal vortices close to the membrane surface. Therefore, one can conclude that downscaling of the multi-layer spacer configuration is possible by using a thinner middle spacer with smaller dimensions. This results in 20% higher limiting current density than the single layer non-woven standard net spacer G at the same flow velocities. However, for an industrial application of this multi-layer spacer, further reduction of the spacer thickness below 2mm would be necessary.

#### **4.4 Comparison of the optimal multi-layer spacers**

Figures 11 a, b and c compare the mass transfer enhancement and the limiting current density of the two optimal multi-layer spacers I-A-I (7mm channel) and I-E-I (3mm channel) with the standard spacer G (3mm channel). The mass transfer enhancement of the I-A-I spacer with increasing flow velocity is much steeper than for the single spacer G and the I-E-I spacer structure (Figure 11a). However, when taking the volume of the channels into account, by plotting  $i_{lim}$  and  $k_{bl}$  over the Reynolds numbers, then the mass transfer enhancement in the 7mm channel occurs at much higher Reynolds numbers (Figure 11b). In fact, the I-A-I spacer structure only shows a strong increase in mass transfer at Reynolds number greater than 300. At lower Reynolds numbers, even the standard spacer G shows a better performance than the I-A-I spacer. The I-E-I spacer shows the best performance probably due to the coexistence of the longitudinal and transversal vortices close to the membrane.

In order to make an economical evaluation, the limiting current density and the mass transfer coefficient is plotted over the cross-flow power consumption (Equation 17) (Figure 11c).



**Figure 11:** Dependence of the limiting current density and corresponding mass transfer coefficient of the most promising multi-layer spacers (I-A-I and I-E-I) with the single spacer G over a) the corrected flow velocity, b) the Reynolds number, c) the Power number.

The results show that in order to achieve a comparable increase in  $i_{lim}$  and  $k_{bl}$  for the I-A-I spacer structure in the 7mm channel as for the I-E-I spacer structure in the 3mm channel, a 30 times higher power input is required. This difference in power input is basically due to the height difference of the channels, as expected from Equation 17. Besides, the reduction of the cell volume will result in an additional energy saving resulting from the lower resistance of the dilute compartment. The mass transfer enhancement of the multi-layer structure I-E-I is in average 20%

higher than of the single spacer G at the same cross-flow power consumption. The I-E-I multi-layer spacer is therefore the most optimal spacer configuration developed in this work.

## 5. Conclusions

The mass transfer enhancement obtained by the application of single and multi-layer spacers was evaluated concerning the limiting current density at different flow velocities. The main results are:

- Single layer spacers with a flow attack angle and filament angle of  $60^\circ$  with rectangular twisted filaments resulted in the highest mass transfer due to the creation of swirling flows.
- The multi-layer I-A-I created by the combination of the middle spacer with round filaments and a flow attack angle of  $45^\circ$  with two thin net spacers on the outside showed the best performance. In the case of a multi-layer spacer, the middle spacer diverts the flow from the bulk to the channel walls, where the thin net spacers create a mix of longitudinal and transversal vortices close to the membrane, decreasing the boundary layer thickness. The creation of swirling flows by the middle spacer seems to reduce the effect of the outside net spacers. Therefore no modified filament structures are needed for the middle spacer.
- In order to reduce the energy consumption, thinner middle spacers were also studied. The best multi-layer, I-E-I, resulted in the same mass transfer enhancement as the I-A-I multi-layer at 30 times lower cross flow power consumption. This novel multi-layer spacer (I-E-I) showed a 20% higher mass transfer compared to a standard non-woven optimum net spacer (G) at the same cross flow power consumption. For an industrial application of this multi-layer spacer, a further reduction of the spacer thickness below 2mm would be necessary.

## 6. Acknowledgement

The authors would like to thank Prof. A. de Haan (Separation Technology Group of the University of Twente, Enschede, The Netherlands) for providing the spacers developed during the STW project TST.4473.

## 7. List of symbols

$A_{SP}$	spacer surface area [m <sup>2</sup> ]	
$c_b$	concentration in the bulk [mol/L]	
$c_m$	concentration at the membrane surface [mol/L]	
$d_F$	diameter of the spacer filament	
$D$	diffusion coefficient [m <sup>2</sup> /s]	
$D_{Na^+}$	diffusion coefficient of sodium [m <sup>2</sup> /s]	
$F$	Faraday constant (96485 A s/mol)	
$h_{Ch}$	height of the channel [m]	
$h_{Sp}$	height of the spacer [m]	
$i$	current density [A/m <sup>2</sup> ]	
$i_{lim}$	limiting current density [A/m <sup>2</sup> ]	
$\bar{k}$	average mass transfer coefficient [m/s]	
$k_{bl}$	mass transfer coefficient in the boundary layer [m/s]	
$l$	distance between the spacer filaments [m]	
$L$	length of the channel [m]	
$\Delta P$	pressure drop over the channel [Pa]	
$Pn$	Power number	$Pn = SPC \frac{\rho^2 h_{Ch}^4}{\mu^3}$
$R$	area resistance [ $\Omega$ cm <sup>2</sup> ]	
$Re$	Reynolds number	$Re = \frac{\rho u h_{Ch}}{\mu}$
$Sc$	Schmidt number	$Sc = \frac{\mu}{\rho D}$

Sh	Sherwood number	$Sh = \frac{\bar{k} h_{Ch}}{D}$	
SPC	specific power consumption in the channel		$SPC = \frac{\Delta P}{L} u$
t	time [s]		
$t^{bl}$	ion transport number in the boundary layer		
$t_{Na^+}^{bl}$	ion transport number of sodium in the boundary layer		
$t^m$	ion transport number in the membrane		
<b>u</b>	mean flow velocity [m/s]		
$u_{corr}$	mean flow velocity corrected for the spacer volume [m/s]		
$V_{Ch}$	Volume of the channel per unit area [m <sup>3</sup> ]		
$V_{Sp}$	Volume of the spacer per unit area [m <sup>3</sup> ]		
z	valence of the ion		

### Greek letters

$\alpha$	flow attack angle [°]
$\beta$	angle between crossing filaments [°]
$\delta$	thickness of the boundary layer [m]
$\varepsilon$	porosity of the spacer
$\phi_v$	volume flow [L/h]
$\mu$	dynamic viscosity of the solution [Pa s]
$\rho$	density of the solution [kg/m <sup>3</sup> ]

## 8. References

- [1] K.S. Spiegler, Polarization at ion exchange membrane-solution interfaces, *Desalination* 9 (1971) 367-385.
- [2] C. Forgacs, N. Ishibashi and J. Leibovitz, Polarization at ion exchange membranes in electrodialysis, *Desalination* 10 (1972) 181-214.

- [3] I. Rubinstein, B. Zaltzman, O. Kedem, Electric field in and around ion exchange membranes, *Journal of Membrane Science* 125 (1997) 17-21.
- [4] I. Rubinstein, B. Zaltzman, Electro-osmotically induced convection at a permselective membrane”, *Physical Review E*, 62 (2000) 2238-2251
- [5] R. Ibanez, D. F. Stamatialis, M. Wessling, Role of membrane surface in concentration polarization at cation exchange membranes, *Journal of Membrane Science* 239 (2004) 119-128.
- [6] H. Strathmann, *Ion-Exchange Membrane Separation Processes*, Elsevier (2004)
- [7] A. R. Da Costa, A. G. Fane, C. J. D. Fell, A. C. M. Franken, Optimal channel spacer design for ultrafiltration, *Journal of Membrane Science* 62 (1991) 275-291.
- [8] E. Korngold, L. Aronov, O. Kedem, Novel ion-exchange spacer for improving electrodialysis I. Reacted spacer, *Journal of Membrane Science* 138 (1998) 165-170.
- [9] V. K. Shahi, S. K. Thampy, R. Rangarajan, The effect of conducting spacers on transport properties of ion-exchange membranes in electrodriven separation, *Desalination* 133 (2001) 245-258.
- [10] S. Geissler, H. Heits, U. Werner, Description of Fluid Flow through Spacers in Flat-Channel Filtration Systems, *Filtration & Separation* 32 (1995) 538-544.
- [11] J.-M. Chiapello, M. Bernard, Improved spacer design and cost reduction in an electrodialysis system, *Journal of Membrane Science* 80 (1993) 251-256.
- [12] F. Li, W. Meindersma, A. B. de Haan, T. Reith, Novel spacers for mass transfer enhancement in membrane separations, *Journal of Membrane Science* 253 (2005) 1-12.
- [13] F. Li, W. Meindersma, A. B. de Haan, T. Reith, Spacer for use in a membrane separation device and a membrane separation device comprising such a spacer, International Patent, WO 2004/112945 A1.
- [14] M. Mulder, *Basic Principles of Membrane Technology* (2<sup>nd</sup> Ed.), Kluwer Academic Publishers (1996).



- [15] R. Habbe, Aufarbeitung krustenbildender Wässer durch Elektrodialyse mit Seeding-Technik und Luftblasenspülung – Verfahrensentwicklung und optimierung, Dissertation, Aachen 1993.
- [16] A. R. Da Costa, A. G. Fane, D. E. Wiley, Spacer characterization and pressure drop modelling in spacer-filled channels for ultrafiltration, *Journal of Membrane Science* 87 (1994) 79-98.
- [17] F. Li, W. Meindersma, A. B. de Haan, T. Reith, Optimization of commercial net spacers in spiral wound membrane modules, *Journal of Membrane Science* 208 (2002) 289-302.
- [18] G. Schock, A. Miquel, Mass transfer and pressure loss in spiral wound modules, *Desalination* 64 (1987) 339-352.
- [19] F. Li, W. Meindersma, A. B. de Haan, T. Reith, Experimental validation of CFD mass transfer simulations in flat channels with non-woven net spacers, *Journal of Membrane Science* 232 (2004) 19-30.
- [20] O. Inoue, T. Yamazaki and T. Bisaka, Numerical simulation of forced wakes around a cylinder, *International Journal of Heat and Fluid Flow*, 16(5) (1995) 327-332.
- [21] Y. Chen, M. Fiebig and N.K. Mitra, Conjugate heat transfer of a finned oval tube with a punched longitudinal vortex generator in form of a delta winglet-parametric investigations of the winglet, *International Journal of Heat and Mass Transfer*, 41(23) (1998) 3961-3978.
- [22] D.T. Pham, R.S. Gault, A comparison of rapid prototyping technologies, *Int. J. Mach. Tools Manuf.* 38 (1998) 1257-1287.
- [23] F. G. Wilhelm, I. Punt, N. F. A. van der Vegt, M. Wessling, H. Strathmann, Asymmetric Bipolar Membranes in Acid-Base Electrodialysis, *Industrial & Engineering Chemistry Research* 41 (2002) 579-586.
- [24] R.A. Robinson, R.H. Stokes, *Electrolyte solutions*, 2<sup>nd</sup> Edition, Butterworths, London (1954).
- [25] R.M. Manglik, A.E. Bergles, Swirl flow heat transfer and pressure drop with twisted-tape inserts, *Advances in Heat Transfer* 36 (2002) 283-266.

- [26] R.M. Manglik, A.E. Bergles, Heat transfer and pressure drop correlations for twisted-tape inserts in isothermal tubes, I. Laminar flows, *Journal of Heat Transfer* 115 (1993) 881-889.
- [27] R.M. Manglik, A.E. Bergles, Heat transfer and pressure drop correlations for twisted-tape inserts in isothermal tubes, II. Transition and turbulent flows, *Journal of Heat Transfer* 115 (1993) 890-896.

## Chapter V

### **Morphology and micro-topology of cation exchange polymers and the origin of the overlimiting current**

J. Balster, M.H. Yildirim, R. Ibanez, R.G.H. Lammertink,  
D.F. Stamatialis, V. Jordan, and M. Wessling

#### **Abstract**

In electro dialysis desalination processes, the operating current density is limited by concentration polarisation. In contrary to other membrane processes such as ultrafiltration, in electro dialysis current transport above the limiting current is possible. In this work the origin of the overlimiting current at cation exchange polymers is investigated. We show that under certain experimental conditions electro-convection is the origin of the overlimiting conductance. The theory concerning electro-convection predicts a shortening of the plateau length of membranes with increased conductive or geometrical heterogeneity. We investigate the influence of these two parameters and show that the creation of line undulations on the membrane surface normal to the flow direction, having distances ranging approximately 50% to 200% of the boundary layer thickness lead to an earlier onset of the overlimiting current. The plateau length of the undulated membranes is reduced up to 60% compared to a flat membrane.

## 1. Introduction

The optimisation of membrane based separation processes is severely influenced by concentration polarisation. Concentration gradients evolve in the feed at the membrane surface leading to an imbalance of membrane resistance and hydrodynamic boundary layer resistance. The boundary layer resistance approaches values equal to the membrane resistance or even higher. In membrane processes such as pervaporation, vapour permeation and ultrafiltration, concentration polarisation is observed by the fact that the transmembrane flux does not increase with increasing driving force (transmembrane pressure) and reaches a limiting flux ( $J_{lim}$ ) (see Figure 1a) [1]. In electro dialysis, the limiting flux is called the limiting current density ( $i_{lim}$ ). The voltage drop across the membrane is a measure of the driving force [2-4]. In contrary to the previous mentioned membrane processes, in electro dialysis current transport above the limiting current is possible. If the driving force is increased beyond a critical voltage drop the overlimiting current sets in and transport occurs again (see Figure 1b).

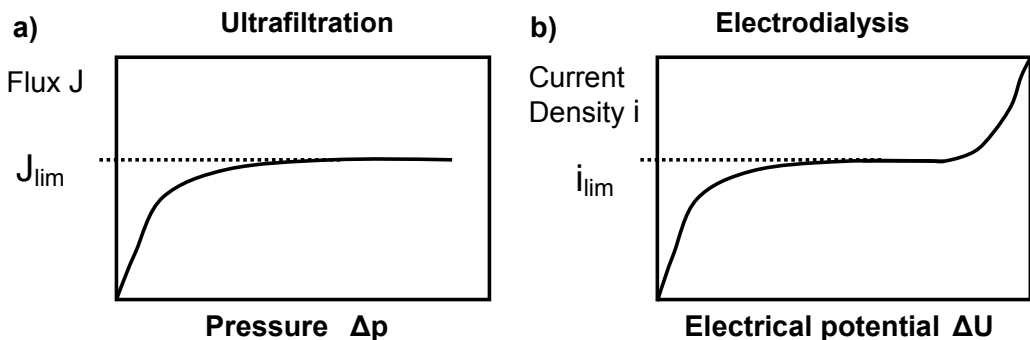


**Figure 1:** Comparison of the limiting flux in a) ultrafiltration and b) electro dialysis.

Concentration polarisation in electro dialysis is caused by differences between ion transport number in the electrolyte solution and the ion exchange membrane. The difference in transport number leads to depletion of salt ions on the dilute side of the membrane, whereas simultaneously the concentration near the membrane on the concentrate side increases [2, 5]. A typical current–voltage curve ( $i$ - $v$ ) of an ion exchange membrane can be divided into three regions (Figure 2). In region 1, the

Ohmic region, the current density increases linear with increasing voltage drop giving the ohmic resistance of the membrane. This part is followed by a plateau (region 2, the limiting current density), caused by ion-depletion in the hydrodynamic boundary layer. Inflection of the  $i$ - $v$  curve at the plateau is followed by region 3 where the slope of the  $i$ - $v$  curve increases again and ion transport sets in again (overlimiting current region) [3]. These values of the current density are normally averaged over time, because of fluctuations.

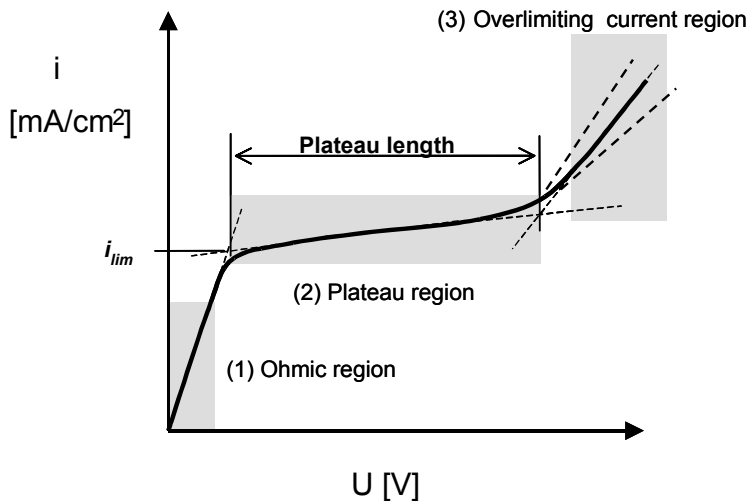


**Figure 2:** Schematic drawing of a typical  $i$ - $v$  curve of a monopolar ion-exchange membrane.

According to the theory of concentration polarisation, currents larger than the limiting current density may not be expected. For a long time, region 3 was attributed to the generation of acid or base by water splitting [6]. This hypothesis was based on experimental evidence of pH changes observed in desalination using anion exchange membranes. Later, however, the absence of water splitting at cation exchange membranes diluted this argument [7, 8]. The nature of the overlimiting flux has been disputed for some time and different hypothesis based on two different transport mechanisms have been made (see Figure 3) [9]:

1. The current is transported by protons and hydroxyl ions generated at the membrane-solution interface [6, 10].
2. The current is transported by salt ions through a secondary convective liquid flow called coupled convection [9].

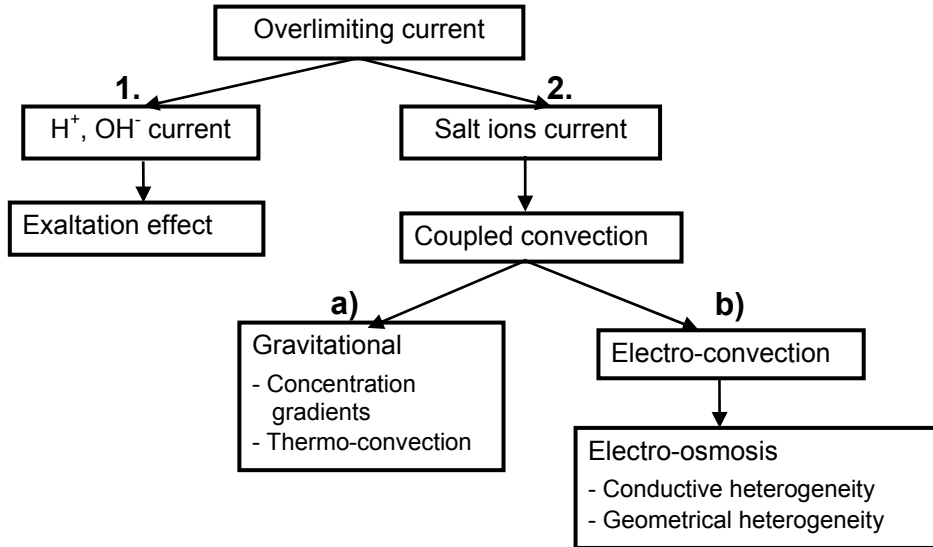


**Figure 3:** Possible secondary effects causing current growth above its limiting value adapted from [9].

The mechanism of the overlimiting current depends on the treated electrolyte and its concentration [11-13], the ion exchange membrane [1, 6-8, 13], and the construction of the electro dialysis cell [9, 13].

### 1.1 Current transport by protons and hydroxyl ions

As already mentioned before, the occurrence of the overlimiting current has been explained by water splitting, which was observed by pH changes in desalination using anion exchange membranes [6]. Protons and hydroxyl ions are generated and transported in a water dissociation layer formed between the ion exchange membrane and the boundary layer.

However, water splitting efficient enough to transport overlimiting currents can only be achieved if the membrane contains ionic groups which catalyse the water splitting reaction by protonation-deprotonation reactions [14, 15]. Using detailed mass balances for cation and anion exchange membranes (containing ionic groups which do not catalyse the water dissociation), Krol et al. [7, 8] verified that the majority of the ion transport occurs through a different mechanism. In fact, they also found no loss of membrane permselectivity which excludes the appearance of additional

charge carries. Choi et al. [11] and Tanaka [12] have also shown that the contribution of water dissociation to the overlimiting current was very low using cation exchange membranes. Only the presence of metal ions such as  $\text{Al}^{3+}$ ,  $\text{Co}^{2+}$ ,  $\text{Mg}^{2+}$  and  $\text{Mn}^{2+}$  on the surface of the cation exchange membrane which are able to form hydroxides, can lead to strong water dissociation. The magnitude of water splitting then also depends on the concentration of the metal ions.

From all the above it can be concluded, that water splitting is not the main cause of the overlimiting current and only contributes when groups are present which catalyse the water splitting reaction.

## 1.2 Current transport by salt ions

The fact that especially cation exchange membranes do not lose permselectivity in the overlimiting current region [7, 8, 11, 15, 16] suggests, that the current is transported by counter ions (Figure 3). Therefore several scientists suggested that the overlimiting behaviour of the ion exchange membranes may be based on a convective mixing mechanism that develops spontaneously in the ion depleted diffusion layer at the advanced state of concentration polarisation. This convective mixing is called coupled convection [17-19]. Two mechanisms responsible for coupled convection have been considered:

- gravitational convection caused by concentration or temperature gradients [17, 20], and
- electro-convection caused by electric space charge localised near the solution-membrane interface [21-30].

Both mechanisms are described in more detail in the following sections.

### Gravitational convection

The gravitational convection (Figure 3) is caused by the Archimedes force which appears in a membrane channel due to non-uniform distribution of the electrolyte concentration (concentration gradient) and/or non-uniform distribution of the electrolyte solution temperature (thermo-convection) [17, 20].

According to Zabolostsky et al. [20], gravitational convection may only play an important role in membrane systems with sufficiently large intermembrane distances and electrolyte solution concentrations and with small solution flow velocities. They calculated that in wide membrane channels (distance between the membranes of 3.5 cm) the gravitational force could be high enough to arise a considerable additional convective flux. However, their experiments in narrow channels (distance between the membranes of 1 mm) showed that the essential increase of salt ion fluxes in the overlimiting current region in the course of dilute solutions must be produced by mechanisms other than gravitational convection [9]. The orientation of the membrane system in the earth gravity field had no influence on the current transport.

Rubinstein et al. [24-26] neglected the influence of gravitational convection by a simple calculation. Gravitational instability of a laminar sublayer at a smooth solid / liquid interface in a well mixed bulk flow may only occur under certain hydrodynamic conditions. It will only destroy a horizontal diffusion layer with a positive upward density gradient if the respective Rayleigh number is larger than 1000. For a diffusion layer of a 0.001 or 0.1 M NaCl solution, with a thickness of 200  $\mu\text{m}$  or less, the Rayleigh number is 11.6 and 116, respectively. These values are at least one order of magnitude lower than the instability threshold.

Krol et al. [8] investigated the influence of the gravitational force by chronopotentiometric measurements of ion exchange membranes in different cell configurations (see Figure 4). They found that when the membrane was in the horizontal position (Figure 4b) gravitation can stabilise the concentration gradient in the laminar boundary layer. The occurrence of natural convection was minimised allowing the concentration profile to grow into the solution in time. Large fluctuations in voltage drop were found even if the membrane was in a horizontal position and no solution flow was applied (Figure 4b) and the depleted diffusion layer was stabilised by gravitation. Therefore, these fluctuations could not be a result of a forced convection but indicate hydrodynamic instabilities.



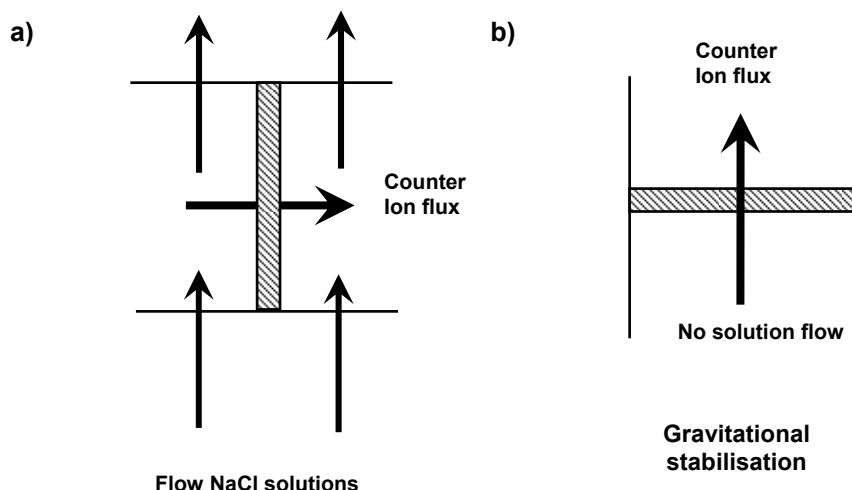


**Figure 4:** Schematic drawing of the membrane arrangements used in chronopotentiometry. a) The test membrane is in vertical position and solution flow through the cell is applied. b) The test membrane is in a horizontal position and no solution flow is applied.

All the discussion above indicate, that gravitational convection is most likely not the origin of the overlimiting current.

### Electro-convection

Rubinstein and co-workers [21, 24-30] explored the physical origin of enhanced transport in the overlimiting current region and elaborated the theory of electro-convection as a phenomenon that destabilises the hydrodynamic boundary layer (Figure 3). Electro-convection is defined as a non-gravitational free convection in macroscopic domains of the electrolyte solutions, caused by the interactions of a self-consistent electric field with the corresponding space charge. The following two modes of electroconvection in strong electrolytes may be distinguished. The first is the relatively recently invoked 'bulk' electroconvection, due to the volume electric forces acting on a macroscopic scale in a locally quasi-electroneutral electrolyte [31-38]. The second is the common electro-osmosis, either of the classical "first" kind or of the "second" kind, according to terminology of Dukhin [23, 39]. Electro-osmosis of the "first" kind [40-43] relates to the electrolyte slip resulting from the action of the tangential electric field upon the space charge of a quasi-equilibrium electric double

layer. (The notion of “induced-charge” electro-osmosis [42-44] refers to the dependence of the potential drop across quasi-equilibrium electric double layer, governing the electro-osmotic flow rate, on the applied electric field as opposed to the classical view in which this drop is regarded as a material constant). Electro-osmosis of the “second” kind invoked by Dukhin [45-48] pertains to the similar action of a tangential electric field upon the extended space charge of the non-equilibrium electric double layer.

At the developed stage of concentration polarisation at a homogeneous permselective solid liquid interface, such as that between an electrolyte solution and a homogeneous ion exchange membrane, electro-convection arises as a result of instability of quiescent conduction caused by electroosmosis of the secondary kind [23]. Electro-convection, developing from this instability, results in destruction of the diffusion layer, causing overlimiting conduction. Not far above the instability threshold, electro-convective vortices start oscillating in a periodic manner resulting in the appearance of a low frequency excess electric noise [25].

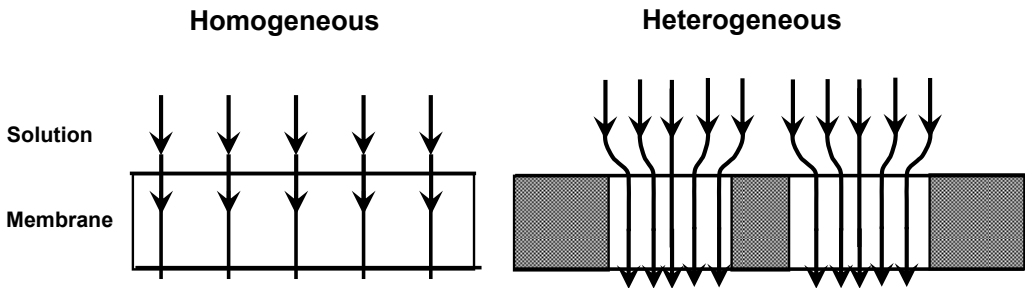


**Figure 5:** Scheme of the current line distribution close to a homogeneous and heterogeneous membrane surface.

The onset of electro-convection may be hastened by heterogeneity of the ion exchange membrane at a suitable length scale. Such heterogeneity is tantamount to inhomogeneous surface conductance and electric field lines concentration into spots of higher conductance (Figure 5). In this case, the equipotential surfaces are no longer parallel to the membrane and tangential forces appear. Flow vortices of the size typical of the surface heterogeneity result and precipitate the onset of instability, eventually, causing mixing of the diffusion layer [24]. According to this concept, elimination of the electro-osmotic slip along the membrane surface should preclude

the onset of electro-convection at a perfectly homogeneous membrane flat membrane, and, thus, no overlimiting conductance should occur through such a membrane (Figure 6). In fact, Rubinstein et al. [26] used a poly(vinyl alcohol) coating layer on the membrane surface (1-2  $\mu\text{m}$ ) to eliminate the lateral electro-osmotic slip and, thus, the overlimiting conductance.

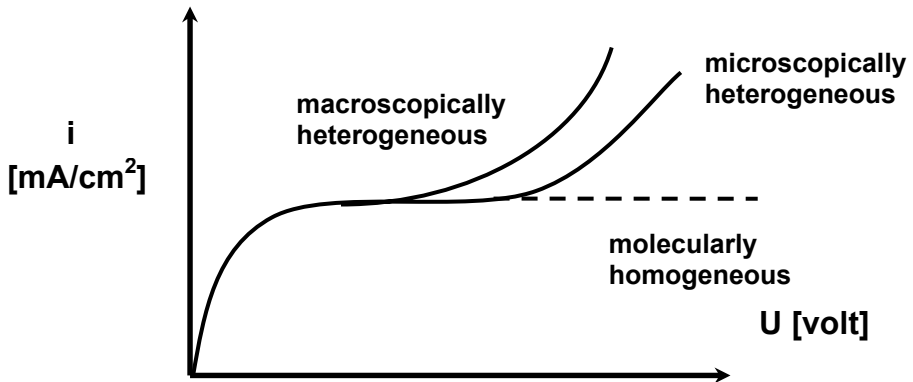


**Figure 6:** Dependence of the plateau length on the heterogeneity of the membrane.

Summarizing, to have an earlier onset of the over-limiting current, and reducing the plateau length of the membrane's polarization curve, a macroscopic heterogeneity of the membrane surface at the suitable length scale may be helpful (see Figure 6). The theoretical framework of Rubinstein et al. reveals that membrane conductive heterogeneity as well as a surface undulation (geometrical heterogeneity) may indeed affect the plateau length (Figure 6). According to their calculations, a decrease of the plateau length should be expected if one would be able to imprint surface undulations in the size range of the boundary layer thickness [21, 24-30]. Rubinstein et al. predicted that a 10 % increase in roughness of the flat surface would result in 30% decrease of the plateau length [25]. This prediction has not been proven experimentally yet.

### 1.3 Aim of this chapter

In this work our research aims to design conductive and surface architecture heterogeneity affecting the overlimiting current at cation exchange polymers. Therefore, we prepare membranes with designed inhomogeneity and try to answer experimentally the question posed by Rubinstein [24], “can one influence polarisation and local mixing of the boundary layer by designed inhomogeneity?”.

## 2. Experimental

### 2.1 Commercial membranes

Neosepta CMX and CMS (Tokuyama Soda Ltd., Japan), FT-CM (Fumatech, Germany) and Nafion (Dupont) membranes were used to investigate the influence of conductive heterogeneity on the current-voltage characteristics. Both Neosepta and Nafion are so called homogeneous ion exchange membranes (the polymer itself is conductive), while FT-CM is a so called heterogeneous ion exchange membrane (ion exchange resins in non-conductive polymer matrix).

The commercial CMX membrane was also coated with a poly-cation, poly(ethylenimine), PEI, to determine the differences in surface morphology and their effects on the onset of the overlimiting current. The PEI coating was made with the following protocol: The functional membrane groups were brought into the proton-form by immersing the CMX membrane in 1M HCl solution. The solution was replaced three times in 24 h for complete exchange of functional groups. The membrane was washed in ultra pure water until the rinse water was free of Cl<sup>-</sup>. Then, the membrane was immersed in 0.001 wt% aqueous PEI solution (solution 3 times replaced, in total 24 hours). Due to the strong electrostatic interaction between the cation exchange membrane and the PEI, the membrane surface was covered with a thin PEI layer. The membrane was then washed with ultra pure water to remove the excess of PEI and brought back into the sodium-form by immersion in 2M NaCl solution for 24 h. The NaCl solution was replaced three times for the complete exchange of functional groups. Excess NaCl was washed with ultra pure water for 24 h.

## 2.2 Tailor made membranes

All prepared membranes were based on sulphonated poly(ether ether ketone), S-PEEK, which was prepared by sulphonation of poly(ether ether ketone) (PEEK, 450PF, Victrex) as described in [49]. Different polymer solutions containing 10-20 wt% polymer in N-methyl-2-pyrrolidinone (NMP) were prepared, 3 solutions containing only S-PEEK with various sulphonation degree (SD) and 3 solutions containing S-PEEK blended with poly(ether sulphone), PES:

1. 100% S-PEEK (SD65%)
2. 100% S-PEEK (SD75%)
3. 60% S-PEEK (SD75%) with 40% PES
4. 100% S-PEEK (SD80%)
5. 80% S-PEEK (SD80%) with 20% PES,
6. 60% S-PEEK (SD80%) with 40% PES.

To prepare flat films of S-PEEK and S-PEEK/PES blends, the polymers were added in the desired amount to the solvent. After at least 24 h of stirring the polymer solution was filtered over a 25  $\mu\text{m}$  metal filter. The films were prepared by the evaporation technique [50, 51]. The solutions were cast on glass plates with a 0.5 mm casting knife. The films were dried for 1 week in  $\text{N}_2$  atmosphere at 40–80  $^\circ\text{C}$ , then immersed in water and subsequently dried under vacuum at 30 $^\circ\text{C}$  for 1 week. The membranes were stored in 0.1M NaCl.

Corrugated membranes were prepared by casting the polymer solution (10 and 20 wt% polymer) on a silicon machined master wafer having patterns etched into the surface by photolithography. The process comprises of three steps (Figure 7).

1. Preparation of a micro-structured master mould based on technologies derived from microelectronics and photolithography,
2. Casting the polymer solution onto the master,
3. Solidification into the micro-sized three-dimensional micro-architecture and release from the mould.

The films were dried for 1 week in  $\text{N}_2$  atmosphere at room temperature and removed from the mould by immersion in ultra pure water. Then the films were dried as described above.

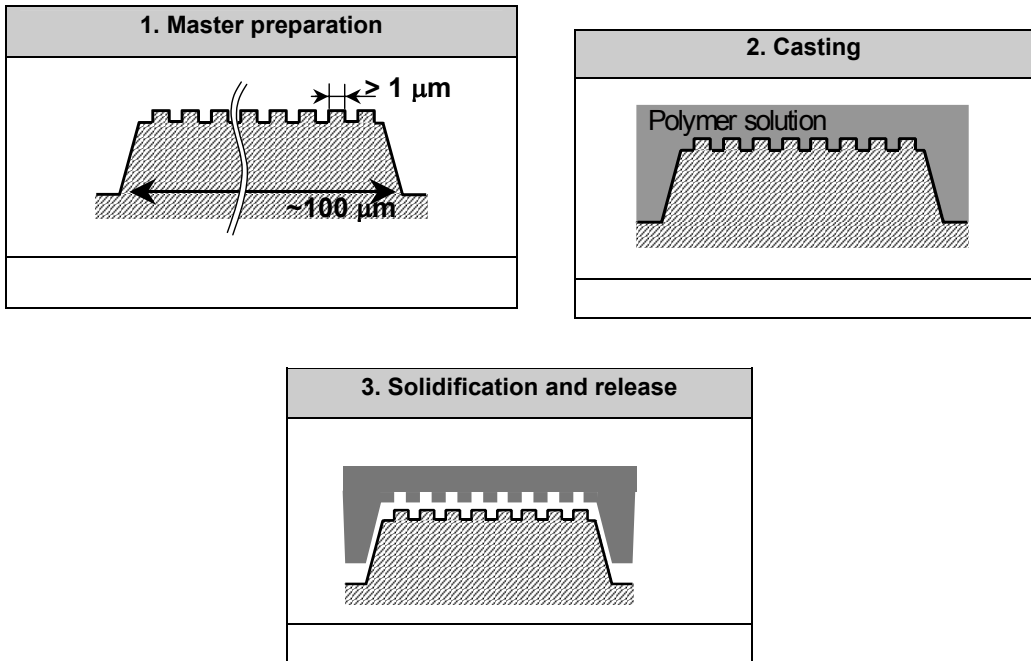


**Figure 7:** Preparation route of micro-patterning on ion exchange membranes. The resulting micro architecture carries the imprint profile of the mould.

Undulated membranes with two different line structures were prepared. The first structure contained dashed lines (Mould A, Figure 8a). In order to investigate the influence of the dimensions of the dashed lines on the overlimiting behaviour, the distance between the lines was varied (see Figure 8b).

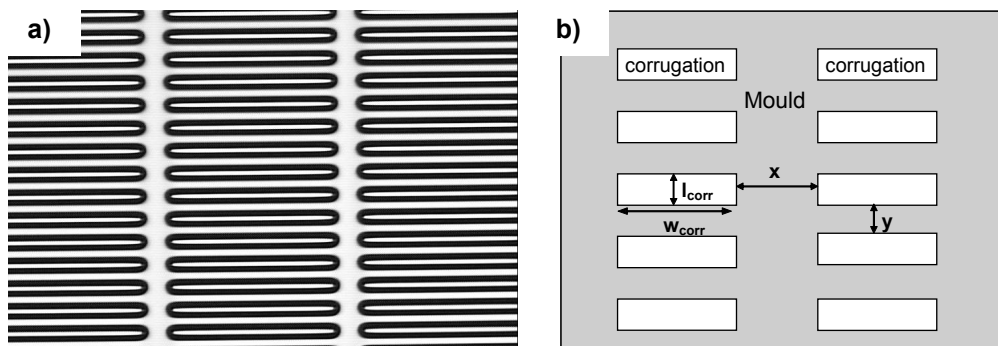


**Figure 8:** Schematic of Mould A with dashed line corrugation, a) optical microscope picture, b) scheme of the corrugations at the surface.

The corrugations were held constant with length of 360  $\mu\text{m}$  and width of 30  $\mu\text{m}$ . The distance in x position and in y position was varied (see Table 1).

**Table 1:** Geometrical parameters of the three A moulds.

Mould	x [ $\mu\text{m}$ ]	y [ $\mu\text{m}$ ]	$l_{\text{corr}}$ [ $\mu\text{m}$ ]	$w_{\text{corr}}$ [ $\mu\text{m}$ ]	Depth [ $\mu\text{m}$ ]
A1	25	50	30	360	35
A2	55	30	30	360	15 - 60
A3	75	50	30	360	40

The second structure (Mould B) contained continuous undulations with a width of 50  $\mu\text{m}$  and a depth of 20  $\mu\text{m}$ . The distance between the undulations was varied from 50 to 550  $\mu\text{m}$ . A scheme of the structure of Mould B is given in Figure 9.

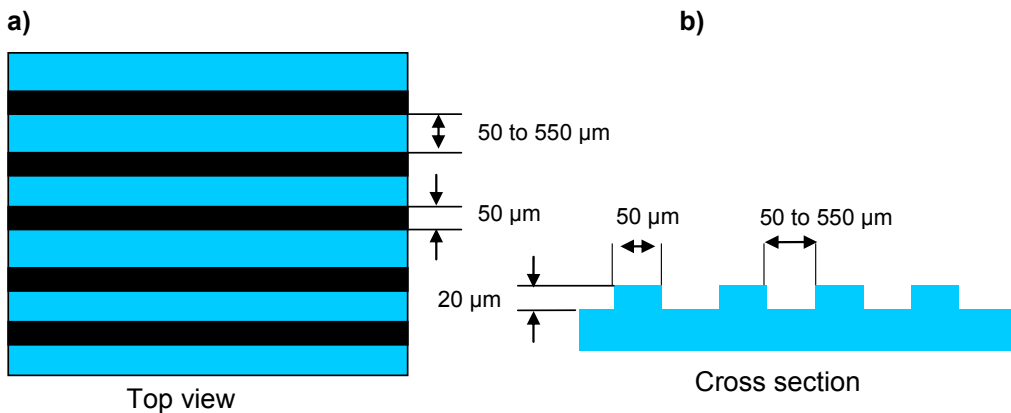


**Figure 9:** Scheme of the undulated Mould B, a) top view and b) cross-section.

### 2.3 Membrane characterisation

The commercial and tailor made CEMs were characterised by measurements of the ion exchange capacity (IEC), water uptake ( $w$ ) and electrical resistance ( $R$ ). These properties were used to calculate the degree of sulphonation (SD) and the specific conductivity (Cond) of the membrane [49, 50].

The geometrical characteristics of the moulds and prepared membranes were visualised by an Optical (Zeiss Axiovert 40 MAT) and a Scanning Electron Microscope (SEM, Jeol JSM-T220 and JSM 5600LV). The membrane samples used

for SEM were sputtered with a thin layer of gold (30 nm) using a Balzers Union SCD 040 sputtering device.

## 2.4 Current-voltage and chronopotentiometric measurements

The current density – voltage drop ( $i$ - $v$ ) and chronopotentiometric measurements were performed in a six compartment cell with a four electrode arrangement (Figure 10) under direct current using a 0.1M NaCl solution [7].

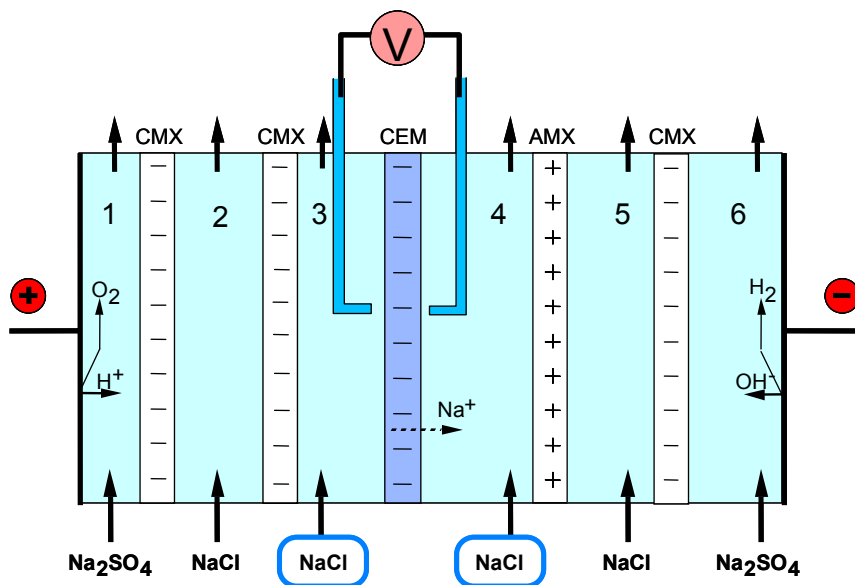


**Figure 10:** Six compartment cell configuration for the  $i$ - $v$  curve and chronopotentiometric measurements.

The membrane was first equilibrated in the measurement solution for more than 24 hours. The measurement solution was added in the compartments 3 and 4, next to the investigated membrane with the calomel reference electrodes. In the compartments 2 and 5, a 0.5M NaCl solution was used to reduce the influence of the electrode reactions at the working electrodes. The current was applied through the working electrodes in the compartments 1 and 6, whereas the electrical potential was measured close to the membrane surface in the compartments 3 and 4 with the calomel reference electrodes. The flow rate through the measurement compartments 3 and 4 was 300 ml/min.



The  $i$ - $v$  measurements are steady state measurements. They were determined by a stepwise increase of the current density through the cell and the corresponding steady state voltage drop values were recorded. The current density  $i$  follows Faraday's law and is given by:

$$i = \frac{zDF(c_b - c_m)}{\delta(t^m - t^{bl})} \quad (1),$$

where  $t^m$  and  $t^{bl}$  are the transport numbers of the ion in the membrane and in the boundary layer respectively,  $z$  is the valence of the ion,  $D$  is the diffusion coefficient of the ion,  $F$  is the Faraday constant,  $c_b$  and  $c_m$  are the concentrations in the bulk and at the membrane surface, and  $\delta$  is the thickness of the boundary layer [51]. When the ion concentration at the membrane surface  $c_m$  approaches zero, a limiting current density  $i_{lim}$  is reached [51]:

$$i_{lim} = \frac{zDFc_b}{\delta(t^m - t^{bl})} \quad (2).$$

The values of limiting current density and plateau length (p.l.) can be determined from the measured  $i$ - $v$  curves (see Figure 2).

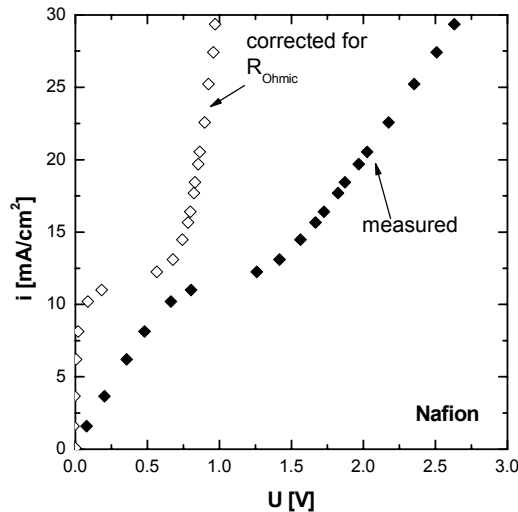


**Figure 11:** Measured and corrected  $i$ - $v$  curve of a commercial Nafion membrane.

In order to neglect the influence of the distance of the measurement capillaries to the membrane sample onto the *i-v* curves, a correction for the initial ohmic resistance ( $R_{\text{Ohmic}}$ ) was applied. In this case the ohmic voltage drop which equals the ohmic resistance was subtracted from the measured value ( $U$ ):

$$U_{\text{corr}} = U - iR_{\text{Ohmic}} \quad (3).$$

Figure 11 shows the *i-v* curves of a Nafion membrane with and without the correction for the ohmic resistance.

Chronopotentiometry is an electrochemical characterisation method that measures the electric potential response of a system to an imposed current. Investigation of kinetic effects, adsorption and transport phenomena near electrode surfaces can be performed with this technique [52-54]. Chronopotentiometric measurements are dynamic measurements. A constant current density is applied and the voltage drop between the electrode and a reference electrode is measured as a function of time. A typical example of a chronopotentiometric curve, measured with a commercial CMX membrane is fully explained in [8, 55]. When an electric current is applied to the ion exchange membrane system, concentration polarisation phenomena arise as a result of concentration gradients formed near to the membrane surface. The transient decrease of salt concentration occurring near the membrane until a steady state is reached can be studied by measuring the voltage drop across the membrane as a function of time [1, 56]. When the concentration reaches zero at the membrane surface, the voltage will rapidly increase. The time taken for voltage transition to occur after a constant current is applied is called the transition time ( $\tau$ ), and given by:

$$\tau = \frac{(c_b zF)^2 \pi D}{(i^m - i^{bl}) 4i^2} \quad \text{or} \quad (4),$$

$$i\tau^{1/2} = \frac{c_b zF (\pi D)^{1/2}}{(i^m - i^{bl}) 2} \quad (5).$$

Equation 4 is equivalent to the Sand equation (equation 5) [56] and shows that the transition time is proportional to the inverse of the current density squared [8]. The

transition time increases, when the membrane transport number decreases, in other words when the membrane is less selective [1]. In the overlimiting current region only a quasi steady state voltage drop is reached, characterised by large fluctuations [8]. These strong fluctuations are indications for the presence of hydrodynamic instabilities which occur in the depleted diffusion layer in this current region [57, 58]. The  $i_{lim}$  determined by the  $i$ - $v$  curve measurements and the membrane selectivity determined by chronopotentiometry were used in equation 2 to calculate the thickness of the hydrodynamic boundary layer for homogeneous membranes. The chronopotentiometric measurements were also used to evaluate the conductive heterogeneity of the membranes [8, 56, 59]. Therefore the experimentally determined transition times were compared with the transition times calculated for a 100% permselective membrane ( $t^m = 1$ ) [8].

## 2.5 Simulation of the solution stream line distribution

In order to simulate the flow stream lines of the liquid along the membrane surface, COMSOL, a multiphysics finite element analysis software was used to numerically model the coupled flow in two-dimensions at steady-state. The code solves the Navier-Stokes (NS) and continuity equations for incompressible flow. Velocity field lines for a 200  $\mu\text{m}$  layer along the membrane surface were calculated assuming a parabolic flow distribution, resulting in a linear flow profile at the membrane surface. The flow velocity was estimated to be 1 cm/s.

## 3. Results and discussion

### 3.1 Commercial membranes

Firstly, the effect of the conductive heterogeneity on the current-voltage behaviour of cation exchange membranes is investigated. Three homogeneous commercial cation exchange membranes were used (CMX, CMS and Nafion<sup>®</sup>). The conductive heterogeneity at both sides (indicated as a and b) towards the anode was investigated (see Table 2). The plateau length was identified from the intersection points depicted in Figure 2. The errors for the plateau length can be estimated from the linear regressions performed in regions 1 and 3 [1].

**Table 2:** Plateau lengths of commercial membranes.

Membrane	IEC [mol/kg <sub>dry</sub> ]	Plateau length [V]	
		a	b
CMX	1.65	0.74 ± 0.02	0.66 ± 0.02
CMS	2.09	1.14 ± 0.03	1.00 ± 0.03
Nafion <sup>®</sup>	0.89	0.78 ± 0.02	0.80 ± 0.02

The CMX and the Nafion membrane have lower plateau length than the CMS membrane. All three membranes are microscopically heterogeneous membranes containing functionalised polymers, but differ in their morphology (see Figure 12). The Nafion membrane contains  $\text{SO}_3^-$  and  $\text{COO}^-$  groups and a perfluorinated polymer backbone. It has the lowest IEC of the three membranes and seems to be more heterogeneous than CMX and CMS containing only  $\text{SO}_3^-$  groups. The even lower plateau length of the CMX membrane is probably due to the non-conductive reinforcement inside the membrane (Figure 12a). The CMS membrane contains a reinforcement too, but since it is a monovalent ion-selective membrane it contains a thin positively charged coating layer on both sides. This coating hides membrane surface heterogeneities and results in a longer plateau length compared to the other two membranes (Table 2). In contrary to the CMX and CMS membranes, the non-reinforced Nafion membrane does not show significant differences between the plateau lengths of the two membrane sides.

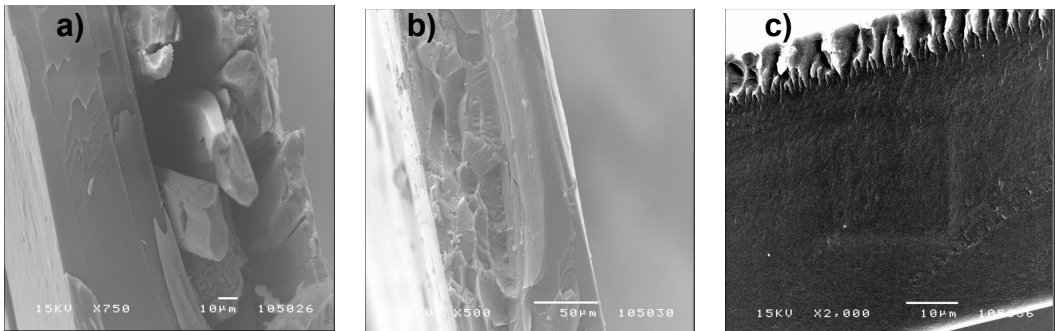


**Figure 12:** SEM pictures of the cross-sections of the a) CMX, b) CMS and c) Nafion membrane.

To have a better insight on how the surface morphology of a membrane influences the plateau length and the overlimiting current, the CMX membrane was coated with

a thin PEI coating (as described in section 2.1). A comparison of the  $i$ - $v$  curves (Figure 13a, corrected for the ohmic resistance) and the chronopotentiometric measurements (Figure 13b, not corrected) of a coated and an uncoated CMX shows the different behaviour of the membranes.

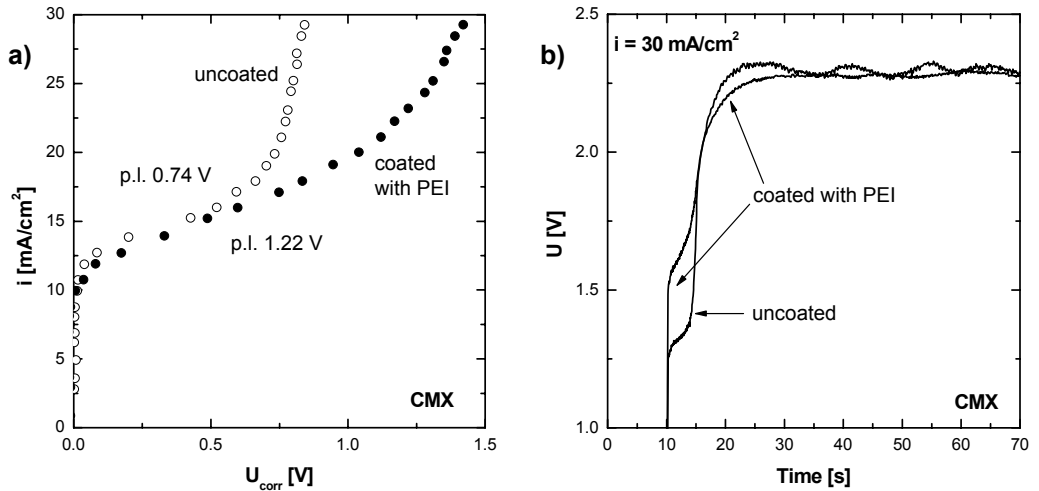


**Figure 13:** Comparison of a) the  $i$ - $v$  curve and b) the chronopotentiometric measurements of a CMX membrane before and after coating with PEI, measured in 0.1M NaCl.

The plateau length of the coated CMX is higher than of the uncoated one and it is the same for both membrane sides (Table 3). The overlimiting current appears at a higher potential. In addition, the slope of the current increase with voltage drop in the overlimiting current region is not as steep leading to higher resistance of the coated membrane (Figure 13a). The chronopotentiometric measurement shows that the voltage instabilities in the overlimiting region are lower for the coated membrane (Figure 13b). This indicates that the PEI coating on the CMX membrane leads to decreased hydrodynamic instabilities. The coating hides the surface heterogeneity and results in a later occurrence of the overlimiting current, but does not eliminate it. These experiments are consistent with the findings of Rubinstein et al [26], where they could shift and even eliminate the overlimiting conductance by poly(vinyl alcohol) coatings of 1-2  $\mu\text{m}$ .

**Table 3:** Plateau lengths of CMX membrane, before and after the PEI coating.

Membrane	Plateau length [V]			
	a		b	
	initial	coated	initial	coated
CMX	$0.74 \pm 0.02$	$1.22 \pm 0.02$	$0.66 \pm 0.02$	$1.18 \pm 0.02$

### 3.2 Heterogeneous vs. homogeneous commercial ion exchange membranes

After the investigation of the commercial homogeneous membranes (microscopically heterogeneous), here, we investigate the influence of the membrane surface heterogeneity of a reinforced heterogeneous cation exchange membrane (macroscopically heterogeneous), FT-CM (Figure 14) on the i-v curves.

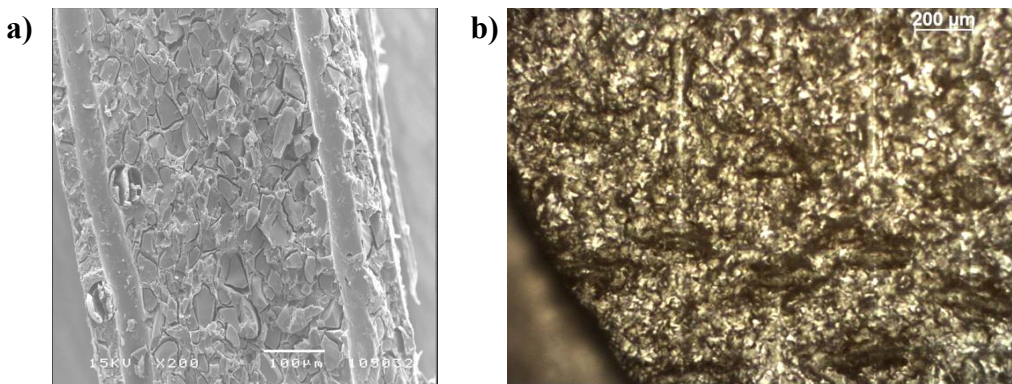


**Figure 14:** The heterogeneous FT-CM membrane, a) SEM photo of the cross-section and b) surface photo made with an optical microscope.

The images of the cross section (Figure 14a) and the surface (Figure 14b) show the heterogeneity of the FT-CM membrane, which contains ion exchange particles of different sizes and shapes glued together by a non-conductive polymer.

Chronopotentiometric and i-v curve measurements with the heterogeneous FT-CM were performed and the results are compared with the homogeneous CMX membrane (Figure 15). The comparison of the i-v curves (Figure 15a) corrected for the total ohmic resistance, shows significant differences between the two membranes. The resistance of the heterogeneous FT-CM membrane is higher in the

overlimiting region than the resistance from the homogeneous CMX membrane. The plateau length of the FT-CM membrane varies strongly and depends on the piece of the film that was investigated (plateau lengths from 0.70 until 1.21 V were measured). The chronopotentiometric measurements show, that the transition times of the FT-CM membrane are much lower than of the CMX membrane (Figure 15b). It is interesting to note, that the FT-CM membrane sample with the shortest plateau length (0.70 V) shows the strongest fluctuations in voltage drop in the overlimiting region indicating the presence of hydrodynamic instabilities in the boundary layer. In this case probably the overlimiting current sets in earlier due to electro-convection induced by the heterogeneity of the membrane sample.

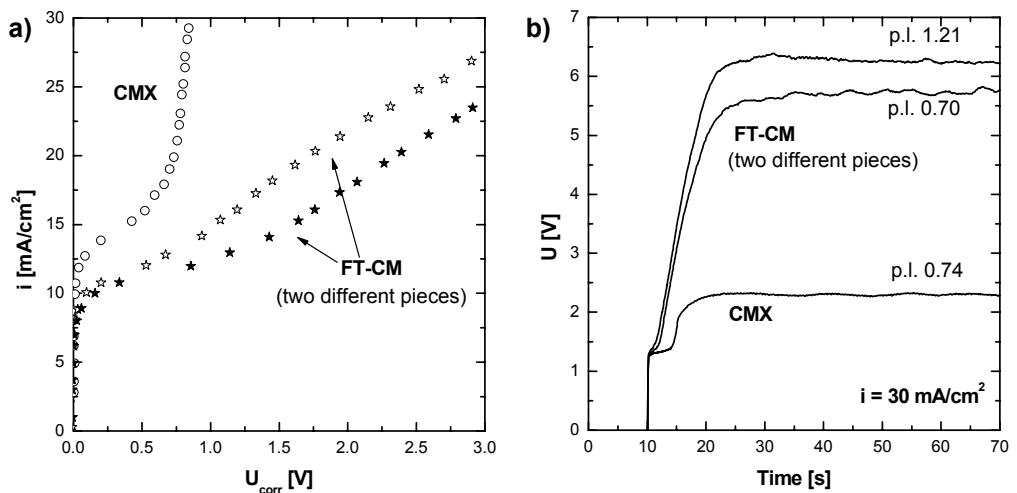


**Figure 15:** Comparison of the a)  $i$ - $v$  curve and b) chronopotentiometric measurements of the CMX and of two different pieces of the FT-CM membrane, measured in 0.1M NaCl.

A reason for the difference in plateau length between the FT-CM membrane samples might be due to the influence of the reinforcement of the membrane, which is not homogeneously distributed over the membrane surface (see Figure 16) and therefore changing the heterogeneity of the membrane surface. In some samples the distance between the non-conductive fibres of the FT-CM membrane is bigger than 200  $\mu\text{m}$ , which is in the range of the hydrodynamic boundary layer. According to Rubinstein et al. [21, 24-30], shortening of the plateau length occurs, if the

heterogeneities have a size of the magnitude of the boundary layer thickness. This could explain the earlier set in of the overlimiting current for these samples.

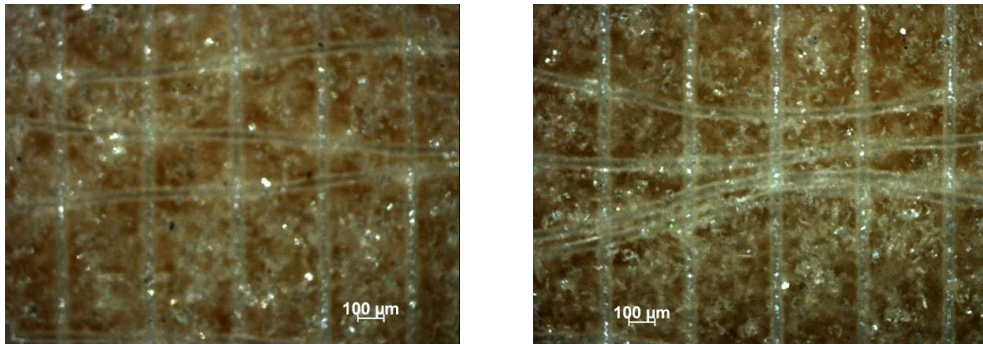


**Figure 16:** Pictures of the surface of the FT-CM membrane of different pieces of the membrane.

The heterogeneous nature of the FT-CM membrane can also be seen by plotting  $i\tau^{1/2}$  over the applied current density and comparing them with those calculated for membranes with different permselectivities (100% and 90%, see Figure 17).

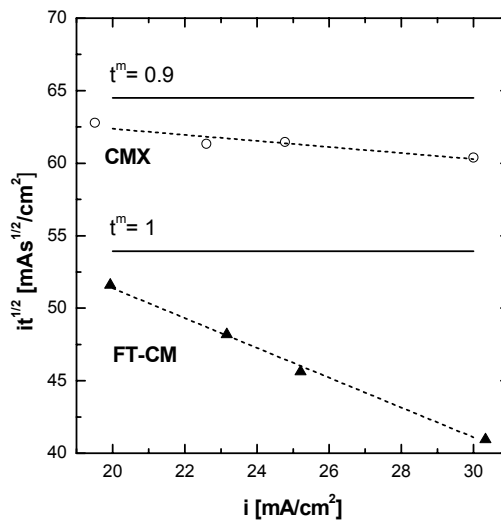


**Figure 17:** Comparison between experimental and calculated  $i\tau^{1/2}$  values for the CMX, the FT-CM, a 100% permselective membrane ( $t^m=1$ ) and 9% permselective membrane ( $t^m=0.9$ ).



The  $i\tau^{1/2}$  values were calculated according to equation 5, using a NaCl diffusion coefficient of  $1.48 \text{ m}^2/\text{s}$  and a  $\text{Na}^+$  solution transport number of 0.39 (values for a 0.1M NaCl solution [60]). The experimentally determined transition times of the CMX membrane are higher than of a 100% permselective membrane, showing homogeneous electrical field line distribution. Therefore the permselectivity of the CMX membrane can be calculated using the Sand equation.

The heterogeneous FT-CM membrane shows lower transition times than a 100% permselective membrane. This difference confirms that the membrane contains an inert, ion impermeable region. The reduced ion-permeable area of the FT-CM membrane corresponds to a locally higher current density at the points where the membrane is conductive (see Figure 5), causing a faster salt depletion near the membrane. Therefore lower transition times are observed because the entire membrane area is not available for ion conduction [56]. Since the current is normalised for the overall membrane area, impermeable areas have to be taken into account to avoid underestimation of current densities.

The results presented above show, that the surface heterogeneity of the membrane influences the plateau length and the overlimiting current. The results of the FT-CM membrane show that the conductive heterogeneity can shorten but also prolong the plateau length of the membrane, depending on the distance between the surface heterogeneities. Both cases have been reported by other researchers, too [1, 13, 56, 61].

### 3.3 Homogeneous blend membranes

In order to tailor the conductive heterogeneity of the membranes, tailor made cation exchange membranes using S-PEEK of various sulphonation degree and S-PEEK/PES blends were prepared and investigated. The errors of the initial measurements are estimated by linear regression performed in region 1 and 3 of the  $i$ - $v$  curve (Figure 2). The error for the equilibrated membranes is the standard deviation of the plateau lengths of the corresponding side measured over 6 weeks after the initial measurement.

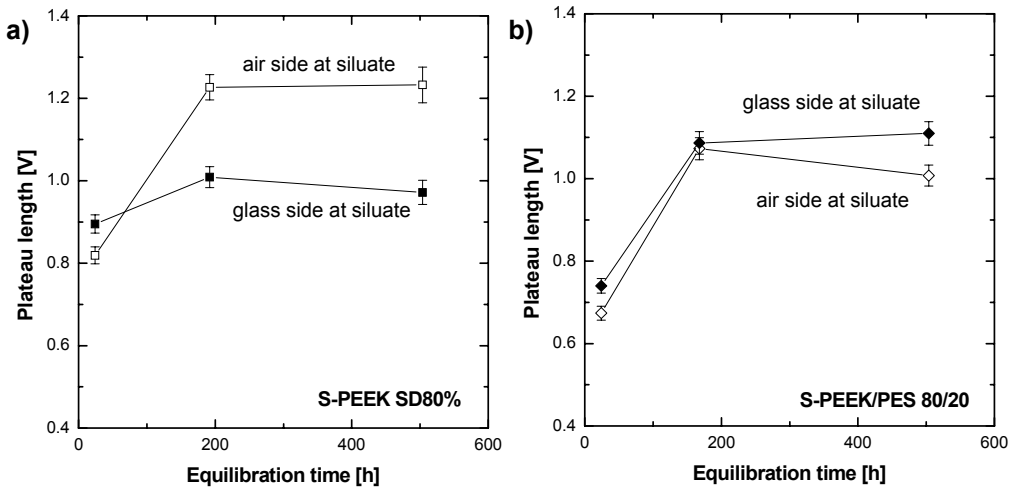


**Figure 18:** The effect of the equilibration time on the plateau length of a) S-PEEK membrane with a sulphonation degree of 80% and b) a S-PEEK/PES 80/20 blend (S-PEEK SD80%).

Figure 18 shows the measured plateau lengths of two tailor made membranes over time. For the pure S-PEEK membrane (SD80%) the plateau length of the air side increases significantly over time, whereas the plateau length of the glass side increases much less (see Figure 18a), in agreement with earlier studies [1]. The same effect can be seen with pure S-PEEK membranes of lower sulphonation degrees (see Table 4).

**Table 4:** Comparison of the initial plateau length and the average plateau length developed over time (6 weeks) of the tailor made membranes.

Membrane	Plateau length [V]			
	Air side		Glass side	
	initial	equilibrated	initial	equilibrated
100% S-PEEK (SD 65%)	0.71 ± 0.02	0.88 ± 0.13	0.93 ± 0.03	0.99 ± 0.09
100% S-PEEK (SD 75%)	0.73 ± 0.02	0.96 ± 0.06	0.89 ± 0.02	0.93 ± 0.05
100% S-PEEK (SD 80%)	0.82 ± 0.02	1.15 ± 0.13	0.90 ± 0.02	0.94 ± 0.07
80% S-PEEK (SD 80%)-20% PES	0.67 ± 0.02	1.05 ± 0.05	0.74 ± 0.02	1.08 ± 0.16
60% S-PEEK (SD 80%)-40% PES	0.58 ± 0.02	0.97 ± 0.15	0.75 ± 0.02	1.07 ± 0.05

With increasing membrane sulphonation degree the difference between the initial plateau lengths of the air side and the glass side, decreases. The plateau length of the air sides in the equilibrated state increases with increasing sulphonation degree,

while it stays constant for the glass sides, within the experimental error. The development of the plateau length of the S-PEEK/PES blends is different (Figure 18b). For both sides, it increases over time and reaches the same value at equilibrium (see Table 4).

It seems that the membrane sides obtain different surface heterogeneities during the drying process, as explained by Ibanez et al. [1]. These heterogeneities are not stable over time. The membranes are stored in solution, which allows the polymer matrix to swell. Because the membranes are in a hydrophilic environment, the polymer structures will relax to reduce the surface energy and entropy of the system. Therefore the hydrophilic groups of the polymer ( $\text{SO}_3^-$  groups) will orientate to the surface of the membrane and give a more homogeneous conductivity. An indication for this phenomenon is shown by the development of the transition times over time (see Table 5).

**Table 5:** Development of the  $i \tau^{1/2}$  values for the tailor made membranes over time. Initial vs. equilibrated values.

Membrane	$i \tau^{1/2}$ [ $\text{mAs}^{1/2}/\text{cm}^2$ ]			
	Air side		Glass side	
	initial	equilibrated	initial	equilibrated
100% S-PEEK (SD 65%)	$59.3 \pm 0.8$	$63.0 \pm 1.7$	$60.1 \pm 0.8$	$63.8 \pm 1.0$
100% S-PEEK (SD 75%)	$62.7 \pm 1.2$	$64.5 \pm 1.5$	$62.8 \pm 1.1$	$65.1 \pm 1.2$
100% S-PEEK (SD 80%)	$65.4 \pm 0.8$	$66.0 \pm 1.0$	$64.3 \pm 1.8$	$63.7 \pm 1.3$
80% S-PEEK (SD 80%)-20% PES	$61.8 \pm 1.1$	$63.3 \pm 1.0$	$61.4 \pm 1.0$	$62.7 \pm 1.1$
60% S-PEEK (SD 80%)-40% PES	$59.8 \pm 0.6$	$61.0 \pm 0.7$	$59.0 \pm 0.6$	$60.5 \pm 0.7$

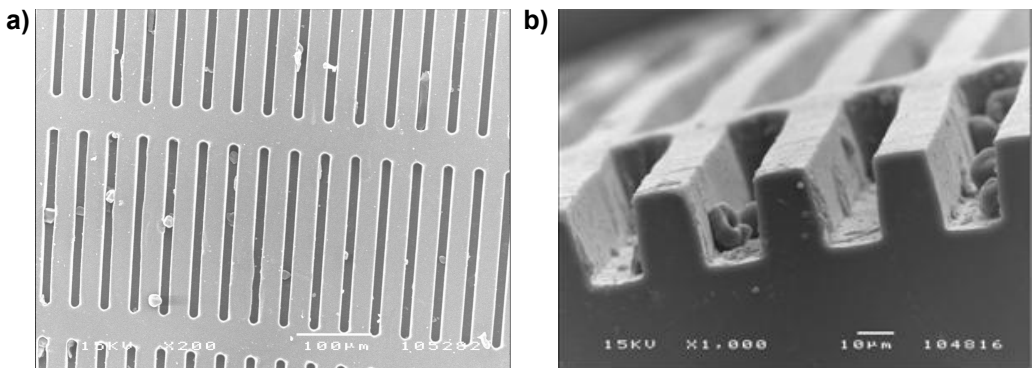
The  $i \tau^{1/2}$  values of the prepared membranes increase over time. Because no loss of permselectivity is found (the limiting current densities stay constant over time and are the same for both sides), these changes can only be due to a change in heterogeneity. The transition times are all higher than for a 100% permselective membrane, indicating a low amount of inert, ion impermeable regions and therefore a quite homogeneous electrical field line distribution. For the initial measurements a lower sulphonation degree and a higher amount of PES result in lower plateau length and lower transition times, especially for the air sides of the membranes. After equilibration, these differences are minimised. For the specific system

(S-PEEK/PES), it seems that the variation of sulphonation and blending cannot introduce sufficient conductive heterogeneity to induce electro-convection.

In conclusion, our results show that the conductive heterogeneity of the ion exchange membrane influences the occurrence of the overlimiting current density. An increased heterogeneity leads to smaller plateaus for the specific system. For the specific S-PEEK/PES polymer the required conductive heterogeneity can not be introduced by blending or the use of different sulphonation degrees. The investigation of the heterogeneous FT-CM has shown that this heterogeneity leads to a strong decrease of the transition times through the reduced ion-permeable area of the membrane. The plateau length can decrease, if the heterogeneities are in the range of the boundary layer thickness, indicating that a certain order in this heterogeneity is necessary to allow the build up of the electro-convective vortices in a quasi steady state.

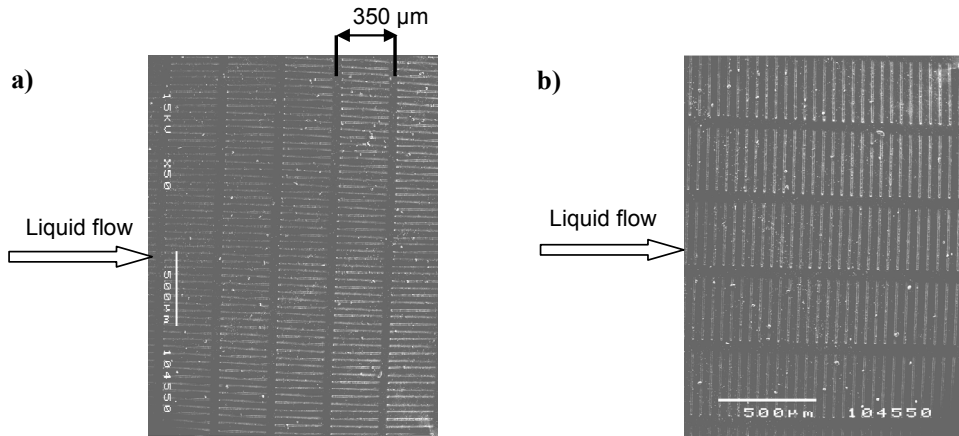
### 3.4 Effect of geometrical heterogeneity

To prove the prediction of Rubinstein et al. [21, 24-30] that a surface undulation shortens the plateau length, micro-engineered membranes were prepared using the Mould A (Figure 8). Pictures of a corresponding membrane structure are shown in Figure 19.



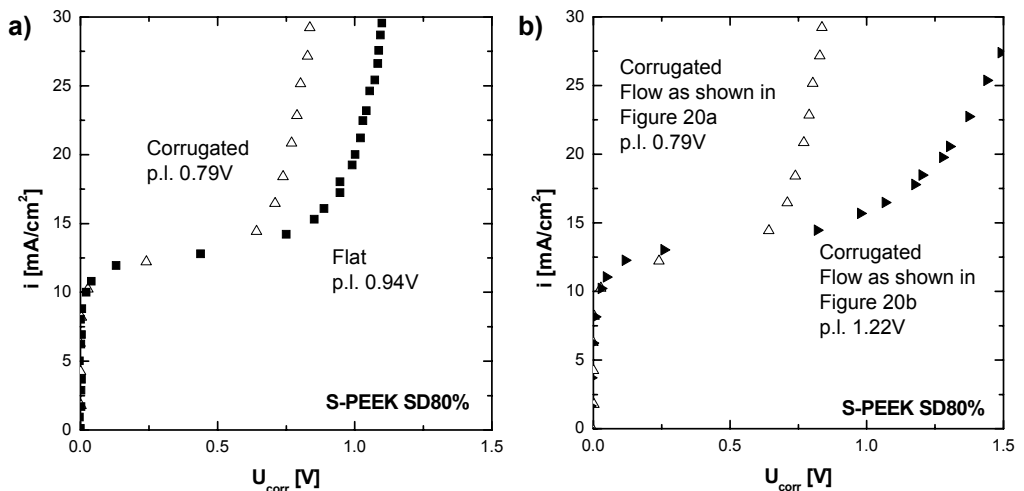
**Figure 19:** SEM pictures of a) the surface and b) the cross-section of one of the S-PEEK membranes.

First the Mould A1 with dimensions:  $x = 25\mu\text{m}$ ,  $y = 50\mu\text{m}$  and depth of  $35\mu\text{m}$  was used for the membrane preparation. The membrane was placed in the measurement cell in two different positions (see Figure 20). In the first position, the undulation was parallel to the flow direction (Figure 20a). In the second position, the undulation was perpendicular (turned  $90^\circ$ ) to the flow direction (Figure 20b).



**Figure 20:** Scheme of the different positions of the membrane corrugation towards the liquid flow.

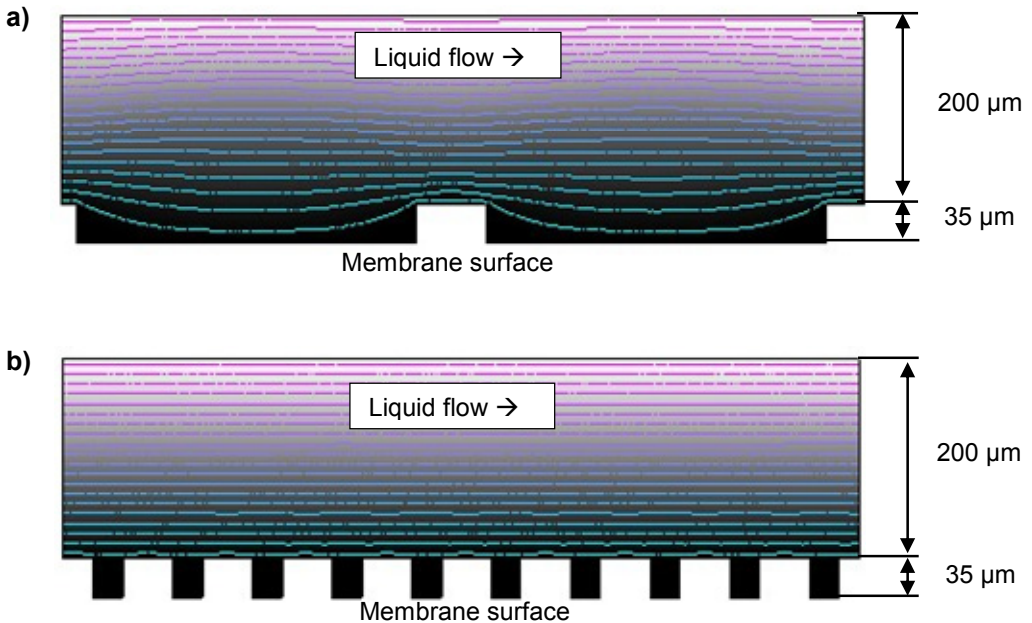
Figure 21 shows the plateau length of a pure S-PEEK SD80% membrane cast on Mould A1 (see Table 1).



**Figure 21:** Comparison of the  $i$ - $v$  curves of a) a flat and a corrugated membrane orientated to the flow as shown in Figure 20a, and b) the corrugated membranes with different orientation towards the liquid flow.

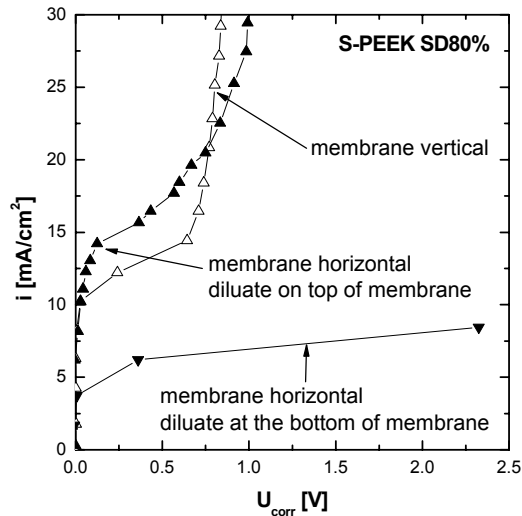
Compared to the glass side of a flat membrane, the corrugation of the membrane leads to a decrease of the plateau length of 16% if it is placed parallel towards the flow direction (as shown in Figure 20a). When the same membrane is turned by 90° (as shown in Figure 20b), the plateau length increases about 30% compared to the flat membrane, due to an increased boundary layer thickness.

Figure 22 shows the velocity field line distribution of the liquid flow over the membrane surface obtained by a COMSOL simulation using the geometrical parameters of the membrane surface assuming a parabolic flow distribution inside the cell. When the flow is parallel to the membrane undulation, as shown in Figure 20a, the flow goes inside the membrane undulations (Figure 22a). In contrast, a stagnant solution layer in the undulations is formed (Figure 22b), when the membrane undulations are placed perpendicular to the flow, as shown in Figure 20b. Then, the thickness of the desalinated boundary layer increases in comparison to the flow of Figure 20a and also in comparison to the flat membrane.



**Figure 22:** Velocity field lines of the liquid flow along the membrane surface simulated for a 200 μm layer on top of the membrane surface, a) surface corrugations parallel and b) surface corrugations perpendicular towards the liquid flow.

To study the influence of the gravitational force, the corrugated membrane described above (prepared by Mould A1) was placed into the measurement cell with the corrugations at the diluate side normal to the flow (Figure 20a), but in a horizontal position (see Figure 4b) and a solution flow was applied. Figure 23 shows the  $i$ - $v$  curves of two horizontal measurements in comparison with the measurement in vertical position (see Figure 4a).



**Figure 23:** Comparison of the  $i$ - $v$  curves of the undulated S-PEEK SD 80% membrane (Mould A1) measured in different positions.

The measurement of the undulated membrane in the horizontal position shows, that gravitation stabilises the boundary layer if the diluate is at the bottom side of the membrane. The diluted boundary layer grows into the solution over time, so that no overlimiting conductance is achieved (in agreement with Krol et al. [8]). If the diluate is on top of the membrane, a similar plateau length is found as when the membrane is placed in the vertical position. Therefore, the gravitational force is most likely not the origin of the overlimiting current, but gravitational forces contribute to the destabilisation as initiated by electro-convection.

In order to get a better insight in the influence of the geometrical parameters of the surface undulation of the membrane on the plateau length, a series of membranes was prepared using Mould A2. The geometrical parameters of these moulds were  $x = 55 \mu\text{m}$ ,  $y = 30 \mu\text{m}$  and the depth was varied from 15 to 60  $\mu\text{m}$  (see Table 1). The

membranes were prepared from two different materials: S-PEEK SD75% and S-PEEK/PES 60/40 using the same S-PEEK (SD75%). Figure 24 shows the plateau length determined by i-v curve measurements in 0.1M NaCl versus the depth of the moulds (measured by SEM).

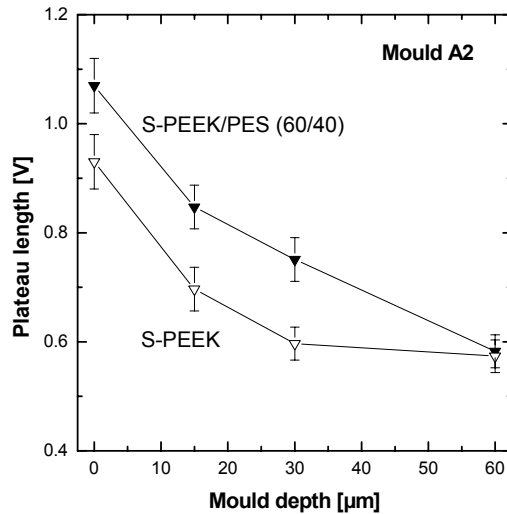


**Figure 24:** Plateau length of the S-PEEK and S-PEEK/PES blend membranes vs. the mould depth (Mould A2).

The plateau length of the membranes decreases significantly at higher depths. For the S-PEEK/PES blends the effect is stronger than for the pure S-PEEK membranes. The membranes containing only S-PEEK swell three times more in solution than the ones containing S-PEEK/PES [49]. The high swelling degree of the S-PEEK membrane might result in deformation and / or reduction of the depth of the membrane undulation in comparison to the less swollen S-PEEK/PES membrane, especially at higher mould depths.

Compared to the membrane prepared with Mould A1, the increase of the x distance from 25 to 55  $\mu\text{m}$  decreases the plateau length of the membrane, too. This indicates that in the case of Mould A, the small line structure parallel to the flow does not cause the earlier occurrence of electro-convection. It seems that the lines separating the small corrugations normal to the flow direction are responsible for the destabilisation of the hydrodynamic boundary layer. These lines are placed in



distance of  $350\mu\text{m}$ , which is the length of the small corrugations, and their thickness depends on the  $x$  value of the mould (see Figure 8b).

To have a better insight in the influence of the thickness of the lines normal to the flow a S-PEEK SD80% membrane was prepared with Mould A3 (with an increased  $x$  distance of  $75\mu\text{m}$ , see Table 1). Therefore the thickness of the lines normal to the flow is growing from  $55$  to  $75\mu\text{m}$  compared to the membrane prepared with Mould A2. The depth of the mould was  $40\mu\text{m}$ .

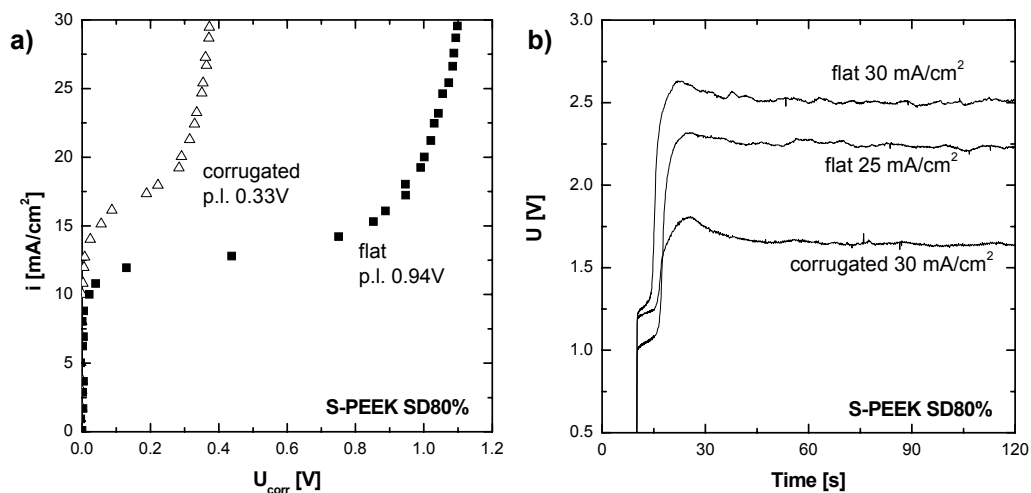


**Figure 25:** Comparison of the corrugated ( $x = 75\mu\text{m}$ ,  $y = 50\mu\text{m}$ , depth  $40\mu\text{m}$ , (Mould A3) and the flat S-PEEK SD80% membrane with a)  $i$ - $v$  curves and b) chronopotentiometric curves.

This increase of the thickness of the lines normal to the liquid flow leads to a tremendous decrease of the plateau length of the corrugated membrane (see Figure 25a). The resistance of the membrane in the overlimiting region is the same as in the ohmic region if the voltage drop caused by the plateau length is neglected. The limiting current density of the corrugated membrane is higher than of the flat one. This is probably due to a lower permselectivity and a higher surface area of this membrane compared to the flat one. The undulated membrane was cast with the same casting knife ( $0.5\text{ mm}$ ) as the flat membrane. Because of the  $40\mu\text{m}$  deep undulations, the selective layer is much thinner than from the flat membrane, which leads to a selectivity loss using this highly sulphonated polymer. In addition,

the undulated membrane has an increased surface area (ca. 7%, estimated by the difference of  $i_{lim}$  between air and mould side of the undulated membrane), for which the current density was not corrected.

The chronopotentiometric curves in Figure 25b present the voltage build up over time of the corrugated membrane compared to a flat one. The fluctuations in the overlimiting current region indicate the presence of electro-convection as cause for the overlimiting current for both membranes. The transition time of the corrugated membrane is higher than of the flat membrane due to the decreased permselectivity and increased membrane area. The transition times of the air and mould side of the undulated membrane are the same, taking the increased surface area of the mould side into account. Because the membranes are prepared by pure S-PEEK SD80%, the membrane material is completely homogeneous as seen before. The earlier onset of the overlimiting conductance of the undulated membrane compared to the flat membrane can therefore only be due to points of locally higher current density as a result of the geometrical undulation of the membrane surface. These points seem to appear after the build up of the diluted boundary layer. The distance between these points is in the right order to enhance the build-up of electro-convective vortices oscillating at the membrane surface, destroying the diffusional boundary layer.

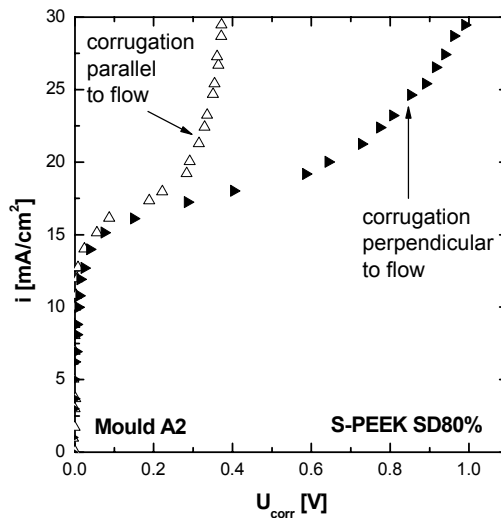


**Figure 26:** Comparison of the  $i$ - $v$  curves of the corrugated membrane (Mould A3) with different orientation of the undulations towards the liquid flow.

Turning this membrane by  $90^\circ$  (as shown in Figure 20b) destroys this effect and results in a longer plateau length (see Figure 26). It seems that the small geometrical undulations increase the boundary layer thickness due to a stagnant solution layer (see Figure 22).

According to Rubinstein et al. [25] a periodic distortion on the length scale of the diffusion layer thickness should lead to the earlier onset of overlimiting conductance through electro-convection. The boundary layer thickness of a S-PEEK SD 80% membrane in our system was determined between 230 and 250  $\mu\text{m}$ . The distance between the lines separating the small corrugations normal to the flow was 350  $\mu\text{m}$  (Mould A, Figure 8). Our measurements indicate therefore the validity of this theory. In order to investigate the influence of the distance between the lines, moulds like described in Figure 9 (Mould B) were used. Membranes with lines normal to the flow (50  $\mu\text{m}$  wide) were prepared varying the distance of the lines from 50 to 550  $\mu\text{m}$ . The depth of Mould B was 20  $\mu\text{m}$  and the membranes were prepared of pure S-PEEK SD80%. Figure 27 shows that a distance of 100  $\mu\text{m}$  between the lines is sufficient to reduce the plateau length of the membrane significantly. Further increase of the distance up to 550  $\mu\text{m}$  does not show further improvement.

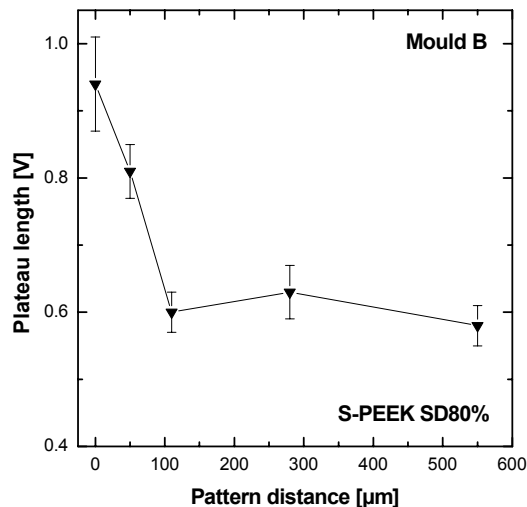


**Figure 27:** Comparison of the plateau length of a flat membrane and corrugated membranes with different distances between the lined corrugations (Mould B). The lines were placed perpendicular to the liquid flow.

In conclusion, it seems that the geometrical heterogeneity has a significant influence on the onset of the overlimiting current. Creating line undulations on the membrane surface having distances ranging from approximately 50% to 200% of the boundary layer thickness normal to the flow leads to an earlier onset of the overlimiting current. By an increase of the height of the undulations the effect can be enhanced. The theory of Rubinstein [21, 24-30] predicts a shortening of the plateau length if undulations in the size range of the boundary layer thickness are introduced into the membrane surface. Our measurements support the prediction of Rubinstein's theory and allows us to conclude that electro-convection is therefore the origin of the overlimiting current under the experimental conditions of this study.

#### **4. Conclusions**

The investigation of commercial cation exchange membranes has shown the influence of the surface heterogeneity on the plateau length. The coating of a commercial CMX membrane led to a strong increase of the plateau length and a later occurrence of the overlimiting current density. The investigation of a heterogeneous cation exchange membrane FT-CM showed, that the heterogeneity reduces the transition times of the membrane due to the concentration of the electrical field lines, but that this phenomenon is not directly result in an earlier onset of the overlimiting current. The surface heterogeneities have to be in a distance in the range of the boundary layer thickness to lead to an earlier onset of the overlimiting current.

The conductive heterogeneity using polymers of different sulphonation degrees or by blending with non-conducting polymer did not show any long term effect for the chosen S-PEEK/PES system.

However, the surface undulations had a big influence on the occurrence of the overlimiting current and the earlier onset of electro-convection. In fact, line undulations on the membrane surface normal to the flow direction, having distances ranging from approximately 50% to 200% of the boundary layer thickness, led to an earlier onset of the overlimiting current. By an increase of the height of the

undulations, the effect was enhanced. The plateau length of the undulated membranes could be reduced up to 60% compared to a flat membrane.

The theory of Rubinstein [21, 24-30] predicts a shortening of the plateau length if undulations are within the same range as the boundary layer thickness. Our measurements are consistent with this theory. Electro-convection is therefore most likely the origin of the overlimiting current, under the conditions used in this study.

## 5. Acknowledgements

The authors would like to thank Isaak Rubinstein for the fruitful discussions.

## 6. List of symbols

$c_b$	concentration in the bulk [mol/L]
$c_m$	concentration at the membrane surface [mol/L]
Cond	conductivity [mS/cm]
$D$	diffusion coefficient [ $m^2/s$ ]
$F$	Faraday constant (96485 A s/mol)
$i$	current density [ $A/m^2$ ]
IEC	ion exchange capacity [mol/kg <sub>dry</sub> ]
$i_{lim}$	limiting current density [ $A/m^2$ ]
$J_{lim}$	limiting flux [mol/( $m^2s$ )]
$l_{corr}$	length of the corrugation [ $\mu m$ ]
p.l.	plateau length [V]
$R$	area resistance [ $\Omega cm^2$ ]
$R_{Ohmic}$	Initial ohmic area resistance [ $\Omega cm^2$ ]
SD	sulphonation degree [%]
$t^{bl}$	ion transport number in the boundary layer
$t^m$	ion transport number in the membrane
$w$	water uptake [kg <sub>water</sub> /kg <sub>dry</sub> ]
$w_{corr}$	width of the corrugation [ $\mu m$ ]
$x$	distance between the rows containing small corrugations [ $\mu m$ ]

y	distance between the small corrugations [ $\mu\text{m}$ ]
z	valence of the ion
NMP	N-methyl-2-pyrrolidinone
PEEK	poly(ether ether ketone)
PES	poly(ether sulphone)
S-PEEK	sulphonated poly (ether ether ketone)

**Greek letters**

$\delta$	thickness of the boundary layer [m]
$\tau$	transition time [s]

**7. References**

- [1] R. Ibanez, D. F. Stamatialis, and M. Wessling, Role of membrane surface in concentration polarization at cation exchange membranes, *Journal of Membrane Science* 239 (2004) 119-128.
- [2] K.S. Spiegler, Polarization at ion exchange membrane-solution interfaces, *Desalination* 9 (1971) 367-385.
- [3] N.W. Rosberg, C.E. Tirell, Limiting currents in membrane cells, *Industrial & Engineering Chemistry Research* 49 (1957) 780-784.
- [4] V.K. Indusekhar, P. Meares, The effect of the diffusion layer on the ionic current from a solution into an ion-exchange membrane, in: D.B. Spalding (Ed.), *Physicochemical Hydrodynamics II*, Advance Publications, London, 1977, pp. 1031-1043.
- [5] C. Forgacs, N. Ishibashi and J. Leibovitz, Polarization at ion exchange membranes in electro dialysis, *Desalination* 10 (1972) 181-214.
- [6] R. Simons, The origin and elimination of water splitting in ion exchange membranes during water demineralisation by electro dialysis, *Desalination* 28 (1979) 41-42.
- [7] J.J. Krol, M. Wessling and H. Strathmann, Concentration polarization with monopolar ion exchange membranes: current-voltage curves and water dissociation, *Journal of Membrane Science* 162 (1999) 145-154.

- [8] J. J. Krol, M. Wessling and H. Strathmann Chronopotentiometry and overlimiting ion transport through monopolar ion exchange membranes, *Journal of Membrane Science* 162, (1999) 155-164.
- [9] V. I. Zabolotsky, V. V. Nikonenko, N. D. Pismenskaya, E. V. Laktionov, M. K. Urtenov, H. Strathmann, M. Wessling, and G. H. Koops, Coupled transport phenomena in overlimiting current electrodialysis, *Separation and Purification Technology* 14 (1998) 255-267.
- [10] V. I. Zabolotsky, N. D. Pismenskaya, and V. V. Nikonenko, Process of electrodialysis demineralization of a dilute electrolyte solution in membrane channels, *Elektrokhimiya* 26 (1990) 707-713.
- [11] J.-H. Choi, H.-J. Lee, and S.-H. Moon, Effects of Electrolytes on the Transport Phenomena in a Cation-Exchange Membrane, *Journal of Colloid and Interface Science* 238 (2001) 188-195.
- [12] Y. Tanaka, Water dissociation in ion-exchange membrane electrodialysis, *Journal of Membrane Science* 203 (2002) 227-244.
- [13] E. I. Belova, G. Y. Lopatkova, N. D. Pismenskaya, V. V. Nikonenko, C. Larchet, and G. Pourcelly, Effect of anion-exchange membrane surface properties on mechanisms of overlimiting mass transfer, *Journal of Physical Chemistry B* 110 (2006) 13458-13469.
- [14] R. Simons, Water splitting in ion exchange membranes, *Electrochimica Acta* 30 (1985) 275-282.
- [15] R. Simons, Strong electric field effects on proton transfer between membrane bound amines and water, *Nature* 280 (1979) 824-826.
- [16] I. Rubinstein, A. Warshawsky, L. Schechtman, and O. Kedem, Elimination of acid-base generation ('water-splitting') in electrodialysis, *Desalination* 51 (1984) 55-60.
- [17] M. Block, and J.A. Kitchener, Polarization phenomena in commercial ion-exchange membranes, *Journal of the Electrochemical Society* 113 (1966) 947-953.
- [18] S. Reich, B. Gavish, and S. Lifson, Visualization of hydrodynamic phenomena in the vicinity of a semipermeable membrane, *Desalination* 24 (1977) 295-296.

- [19] Q. Li, Y. Fang, and M. E. Green, Turbulent light scattering fluctuation spectra near a cation electro dialysis membrane, *Journal of Colloid and Interface Science* 91 (1983) 412-417.
- [20] V. I. Zabolotsky, V. V. Nikonenko, and N. D. Pismenskaya, On the role of gravitational convection in the transfer enhancement of salt ions in the course of dilute solution electro dialysis, *Journal of Membrane Science* 119 (1996) 171-181.
- [21] I. Rubinstein and F. Maletzki, Electroconvection at an electrically inhomogeneous permselective membrane surface, *Journal of the Chemical Society Faraday Transsition* 87 (1991) 2079-2087.
- [22] F. Maletzki, H.-W. Rosler, and E. Staude, Ion transfer across electro dialysis membranes in the overlimiting current range: stationary voltage current characteristics and current noise power spectra under different conditions of free convection, *Journal of Membrane Science* 71 (1992) 105-116.
- [23] S. S. Dukhin, and N. A. Mishchuk, Intensification of electro dialysis based on electroosmosis of the second kind, *Journal of Membrane Science* 79 (1993) 199-210.
- [24] I. Rubinstein, B. Zaltzman, and O. Kedem, Electric fields in and around ion-exchange membranes, *Journal of Membrane Science* 125 (1997) 17-21.
- [25] I. Rubinstein, B. Zaltzman, Electro-osmotically induced convection at a permselective membrane", *Physical Review E* 62 (2000) 2238-2251.
- [26] I. Rubinstein, B. Zaltzman, J. Pretz, and C. Linder, Experimental verification of the electro-osmotic mechanism of overlimiting conductance through a cation exchange electro dialysis membrane, *Russian Journal of Electrochemistry* 38 (2002) 956-967.
- [27] I. Rubinstein, B. Zaltzman, T. Pundik, Ion-exchange funneling in thin-film coating modification of heterogeneous electro dialysis membranes, *Physical Review E* 65 (2002), art. no. 041507.
- [28] I. Rubinstein, and B. Zaltzman, Electro-osmotic slip of the second kind and instability in concentration polarization at electro dialysis membranes, *Mathematical Models and Methods in Applied Sciences* 11 (2001) 263-300.



- 
- [29] I. Rubinstein, and B. Zaltzman, Wave number selection in a nonequilibrium electroosmotic instability, *Physical Review E* 68 (2003), art. no.032501.
- [30] I. Rubinstein, B Zaltzman, and I. Lerman, Electroconvective instability in concentration polarization and nonequilibrium electro-osmotic slip. *Physical Review E* 72 (2005), art. no. 011505.
- [31] R. S. Alexandrov, A. P. Grigin, and A. P. Davydov, Numerical study of electroconvective instability of binary electrolyte in a cell with plane parallel electrodes, *Russian Journal of Electrochemistry* 38 (2002) 1216-1222.
- [32] J. C. Baygents, and F. Baldessari, Electrohydrodynamic instability in a thin fluid layer with an electrical conductivity gradient, *Physics of Fluids* 10 (1998) 301-311.
- [33] R. Bruinsma, and S. Alexander, Theory of electrohydrodynamic instabilities in electrolytic cells, *Journal of Chemistry and Physics* 92 (1990) 3074-3085.
- [34] M. E. Buchanan, D. A. Saville, Electrohydrodynamic stability in Electrochemical systems, American Physic Society, Proceedings AIChE Annual Meeting 1999.
- [35] A. P. Grigin, The convective coulombic instability of binary electrolytes in cells with plane-parallel electrodes, *Soviet Electrochemistry* 21 (1985) 48-53.
- [36] A. P. Grigin, Coulomb convection in electrochemical systems, *Soviet Electrochemistry* 28 (1992) 247-269.
- [37] I. Lerman, I. Rubinstein, and B. Zaltzman, Absence of bulk electroconvective instability in concentration polarization, *Physical Review E* 71 (2005), art. no. 011506.
- [38] I. Rubinstein, T. Zaltzman, and B. Zaltzman, Electroconvection in a layer and in a loop, *Physics of Fluids* 7 (1995) 1467-1482.
- [39] S. S. Dukhin, Electrokinetic phenomena of the second kind and their applications, *Advanced Colloid Interface Science* 35 (1991) 173-196.
- [40] E. K. Zholkovskij, M. A. Vorotyntsev, and E. Staude, Electrokinetic Instability of Solution in a Plane-Parallel Electrochemical Cell, *Journal of Colloid and Interface Science* 181 (1996) 28-33.

- [41] S. S. Dukhin, and B. V. Derjaguin, *Electrophoresis*, 2nd edn. Nauka, Moscow 1976.
- [42] M. Z. Bazant, T.M. Squires, Induced-charge electro-osmosis, *Journal of Fluid Mechanics* 509 (2004) 217-252.
- [43] M.Z. Bazant, T.M. Squires, Induced-charge electrokinetic phenomena: theory and microfluidic applications, *Physical Review Letters* 92 (2004), art. no. 066101.
- [44] M. Z. Bazant, K. Thornton, and A. Ajdari, Diffuse-charge dynamics in electrochemical systems, *Physical Review E* 70 (2004), art. no. 021506.
- [45] Y. Ben, and H. C. Chang, Nonlinear Smoluchowski slip velocity and microvortex generation, *Journal of Fluid Mechanics* 461 (2002) 229-238.
- [46] S.S. Dukhin, and N. A. Mishchuk, Disappearance of limiting current phenomenon in the case of a granule of an ion-exchanger, *Colloid Journal of the USSR* 51 (1989) 570-581.
- [47] S. S. Dukhin, N. A. Mishchuk, and P. B. Takhistov, Electroosmosis of the second kind and unrestricted current increase in the mixed monolayer of an ion-exchanger, *Colloid Journal of the USSR* 51 (1989) 616-618.
- [48] N. Mishchuk, F. Gonzalez-Caballero, P. Takhistov, Electroosmosis of the second kind and current through curved interface, *Colloids and Surfaces A: Physical Engineering Aspects* 181 (2001) 131-144.
- [49] J. Balster, O. Krupenko, I. Pünt, D. F. Stamatialis, and M. Wessling, Preparation and characterisation of monovalent ion selective cation exchange membranes based on sulphonated poly(ether ether ketone), *Journal of Membrane Science* 263 (2005) 137-145.
- [50] F. G. Wilhelm, I. G. M. Punt, N. F. A. van der Vegt, H. Strathmann, M. Wessling, Cation permeable membranes from blends of sulfonated poly(ether ether ketone) and poly(ether sulfone), *Journal of Membrane Science* 199 (2002) 167-176.
- [51] M. Mulder, *Basic principles of membrane technology*, Chapter 3, 2<sup>nd</sup> Edition, Kluwer Academic Publishers, Dordrecht (1996).
- [52] A.J. Bard, *Electrochemical methods: fundamentals and applications*, John Wiley & Sons, New York (1980)

- 
- [53] P. Delahay, Chronoamperometry and chronopotentiometry, in Treatise on analytical chemistry, I.M. Kolthoff and P.J. Elving (Eds.), John Wiley & Sons, New York (1963) 2233-2265.
- [54] D.T. Sawyer, Experimental electrochemistry for chemists, John Wiley & Sons, New York (1974)
- [55] J.-H. Choi, and S.-H. Moon, Pore size characterization of cation-exchange membranes by chronopotentiometry using homologous amine ions, *Journal of Membrane Science* 191 (2001) 225-236.
- [56] J.-H. Choi, S.-H. Kim, and S.-H. Moon, Heterogeneity of Ion-Exchange Membranes: The Effects of Membrane Heterogeneity on Transport Properties, *Journal of Colloid and Interface Science* 241 (2001) 120-126.
- [57] I. Rubinstein, E. Staude, and O. Kedem, Role of the membrane surface in concentration polarization at ion-exchange membrane, *Desalination* 69 (1988) 101-114.
- [58] M. Taky, G. Pourcelly, F. Lebon, and C. Gavach, Polarization phenomena at the interfaces between an electrolyte solution and an ion exchange membrane : Part I. Ion transfer with a cation exchange membrane, *Journal of Electroanalytical Chemistry* 336 (1992) 171-194.
- [59] H.-W. Rosler, F. Maletzki, and E. Staude, Ion transfer across electro dialysis membranes in the overlimiting current range: chronopotentiometric studies, *Journal of Membrane Science* 72 (1992) 171-179.
- [60] R.A. Robinson and R.H. Stokes, *Electrolyte solutions*, 2<sup>nd</sup> Edition, Butterworths; London (1959).
- [61] E. Volodina, N. Pismenskaya, V. Nikonenko, C. Larchet, and G. Pourcelly, Ion transfer across ion-exchange membranes with homogeneous and heterogeneous surfaces, *Journal of Colloid and Interface Science* 285 (2005) 247-258.



## Chapter VI

### Preparation and characterisation of monovalent ion selective cation exchange membranes based on sulphonated poly(ether ether ketone)

J. Balster, O. Krupenko, I. Pünt, D. F. Stamatialis and M. Wessling

#### Abstract

This paper analyses the separation properties of various commercial cation exchange membranes (CEMs) and tailor made membranes based on sulphonated poly(ether ether ketone) and poly(ether sulphone) for binary electrolyte solutions containing protons and calcium ions. All membranes are thoroughly characterised and relations between their electrochemical properties and ion selectivity are drawn. The effect of current density and calcium ion concentration in the feed stream on the membrane selectivity is investigated. Our results show that the conductivity and the charge density of the membranes determine the calcium transport through the membranes. The calcium transport increases with increasing conductivity, however, it is lower for membranes with lower charge density. Therefore, the preparation of membranes with reasonable conductivities and low calcium transport is possible. Besides, the calcium flux increases with the increase of current density and / or calcium concentration for all membranes. For CEMs having a positively charged coating, the calcium flux is low at low current density but increases strongly at high current densities.

Based on Balster et al, Journal of Membrane Science 263 (2005) 137-145.

## 1. Introduction

Ion exchange membranes (IEM) carry fixed positive or negative charges (called anion exchange membranes, AEM or cation exchange membranes, CEM, respectively). They are generally used in the treatment of ionic aqueous solutions; e.g. electrodialytic concentration of seawater, desalination of saline water, demineralisation of whey, acid and alkali recovery and others [1-3].

The fouling of these permselective membranes is one of the major problems in electrodialysis and can be due to (i) build up of scale by hydroxide formation of divalent and trivalent ions, (ii) surface blocking by proteins or colloidal matter, or (iii) membrane poisoning by tensio-active agents [4]. Fouling increases the cell resistance, decreases permselectivity and could alter the membrane structure (reversible and irreversible fouling) [5-7].

A severe fouling due to scaling occurs, for instance, in the electroacidification of milk to produce high-purity bovine milk casein isolates by bipolar membrane electrodialysis. In this process, the property of bipolar membranes (membranes consisting of an anion and cation exchange membrane layer) to dissociate water into hydroxyl ions and protons is used for the protein precipitation. The direct acidification leads to removal of cations into the base compartment. The monovalent ions (basically  $\text{Na}^+$ ) form the base, whereas the bivalent ions (basically  $\text{Ca}^{2+}$ ) precipitate on the CEM induced by increased local concentration gradients at the membrane surface. Bazinet et al. [4, 8, 9] investigated this phenomenon extensively. Membrane scaling may be prevented when cation selective membranes are used allowing monovalent ions to pass but rejecting the calcium (Figure 1). These membranes, besides separating cations from anions could also separate ions with the same charge and different valences, improving the performances of existing processes without the addition of surface-active agents or polyelectrolytes in the solution to be treated [10-13].

The use of monovalent ion permselective membranes for electrodialysis has been applied mainly for edible-salt production purposes [14]. These membranes, while allowing concentration of  $\text{NaCl}$  from sea water, are capable of rejecting divalent ion salts ( $\text{CaSO}_4$ ,  $\text{MgSO}_4$ ), keeping them in the diluate with high efficiencies [15]. These salts if not retained could lead to rapid degradation of the membranes causing

scaling at the concentrate side [16]. A lot of research has already been performed to improve the permselectivity between cations in electrodialysis by Sata et al. [1, 17-19] resulting in various membrane modification methods. However, until now not much systematic research was performed on the investigation of the calcium transport through CEMs under varying conditions and in relation to the characteristics of the ion exchange membranes.

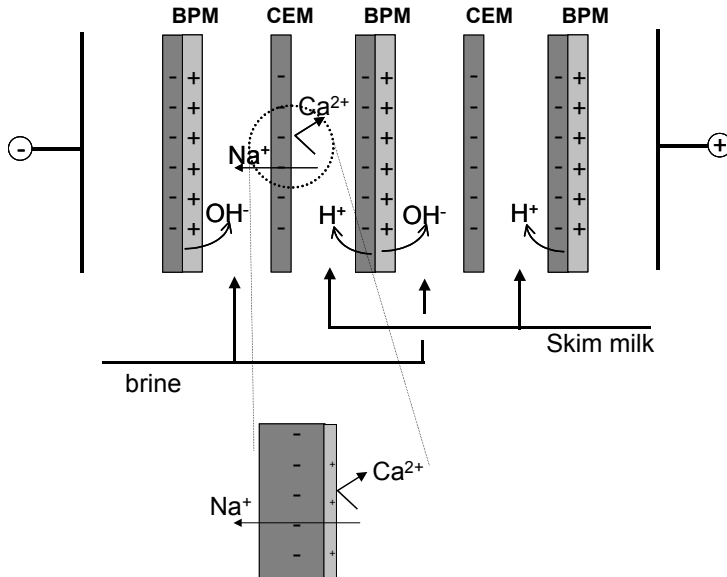


**Figure 1:** Bipolar membrane stack containing coated cation exchange Membranes with improved bivalent ion rejection behaviour due to repulsive properties of the coating.

In this work, our aim is to develop monovalent ion selective CEMs which, among others, could probably be used in skim milk electroacidification. We prepare cation exchange membranes with increased permselectivity for monovalent ions based on sulphonated poly(ether ether ketone), S-PEEK. Sulphonated aromatic polymers like S-PEEK can provide the ion exchange functionality and have been used to prepare homogeneous membranes [20]. To improve and modify the transport properties, these polymers are often blended with non-functional polymers or cross-linked by different means [21, 22]. In this study, S-PEEK was blended with poly(ether sulphone), PES, an amorphous polymer, which has stable properties over a wide temperature range [23]. The structures of S-PEEK and PES are shown by Wilhelm

et al. [24]. By blending S-PEEK with the non-functional polymer PES, we aim to tailor the conductivity and the swelling degree of the prepared membranes [24] and minimise the  $\text{Ca}^{2+}$  flux. The prepared membranes will be compared with commercial membranes under various conditions showing very promising results.

## 2. Experimental

### 2.1 Commercial membranes

Neosepta CMX, CM2 and CMS from Tokuyama Soda Ltd. (Tokyo, Japan), FT-FKB from Fumatech (Germany) and Selemion CMV from Asahi Glass (Japan) commercial CEMs were used (see Table 1). All these membranes were strongly acidic and delivered in the Na-form. The CMS membrane was claimed to be monovalent ion selective by the manufacturer.

**Table 1:** Properties of the commercial CEMs, given by the manufacturers.

Membrane	Properties	Electrical resistance [ $\Omega \text{ cm}^2$ ] <sup>(1)</sup>	Transport Number		
			Total Cation	$\text{Na}^+$	$\text{Ca}^{2+}$ , $\text{Mg}^{2+}$
CMX	High mechanical strength	2.5 – 3.5	0.98 <sup>&lt;(2)</sup>	0.70	0.28
CM-2	Low diffusion coefficient	2.0 – 3.0	0.98 <sup>&lt;(2)</sup>	0.70	0.28
CMV	NA	2.0 – 3.5	>0.91 <sup>(3)</sup>	NA	NA
CMS	Mono cation permselective	1.5 – 2.5	0.98 <sup>&lt;(2)</sup>	0.90 <sup>&lt;</sup>	0.1 <sup>&lt;</sup>
FT-FKB	NA	5 – 10	>0.98	NA	NA

<sup>(1)</sup> measured in 0.5M NaCl solution at 25°C

<sup>(2)</sup> measured by electrophoresis, 2 mA/cm<sup>2</sup>

<sup>(3)</sup> computed by the membrane potential measured across the membrane between 0.5M and 0.1M solutions

### 2.2 Tailor made membranes

As precursor polymer PEEK 450PF from Victrex was used. PEEK is an amorphous polymer, with low water absorption and high solvent resistance. The polymer was dried for more than 24 h in a vacuum oven, at 100 °C. One litre of concentrated sulphuric acid (95 - 98 wt% extra pure, as received) was placed in a reaction vessel



at 25 °C and 60 g polymer was added under stirring. The reaction mixture was stirred for several hours, at controlled temperature, to achieve the desired sulphonation [25, 26]. Then, the reaction vessel was immersed in an ice bath to stop the reaction. The sulphonated polymer (S-PEEK) was precipitated in demineralised water of max 5°C and washed until the pH was 7. The polymer was dried subsequently in air at room temperature and in a vacuum oven at 100 °C.

To prepare films of S-PEEK and S-PEEK/PES blends, the polymers were added in the desired amount to the solvent (NMP, 20 wt% polymer in solution). After a minimum of 24 h of stirring the polymer solution was filtered over a 25 µm metal filter. The films were prepared by the evaporation technique [24, 27]. The solutions were cast on glass plates with a 0.5 mm casting knife. The films were dried for 1 week in N<sub>2</sub> atmosphere at 40–80 °C. Since NMP was still present in the films after one week, the membranes were placed in a vacuum oven at 100 °C until a constant weight was reached. The dry membranes were stored in 0.5M NaCl solution and their thickness in wet state ( $d_{\text{wet}}$ ) was measured.

### **2.3 Membrane characterisation**

The commercial and tailor made CEMs were characterised by measurements of the ion exchange capacity (IEC), water uptake ( $w$ ) and electrical resistance ( $R$ ). These properties were used to calculate the degree of sulphonation (SD) and the specific conductivity (Cond) of the membrane.

The IEC of the membranes was determined by titration [28, 29]. For this, the CEM was first brought in the H<sup>+</sup> form by immersion into 1M HCl solution for 24 h (the solution was replaced in between for total ion exchange). To remove sorbed acid, the membrane was soaked in water and then was brought into the Na<sup>+</sup> form by immersing in 2M NaCl solution. To ensure complete exchange, the NaCl solution was renewed several times. The collected solutions were combined and titrated with NaOH to determine the proton content. The IEC was calculated as the ratio of total charge by the dry weight of the CEM. The degree of sulphonation was calculated according to [24]:

$$SD = \frac{M_{w,p}IEC}{1 - M_{w,f}IEC} \quad (1),$$

where  $M_{w,p}$  is the molecular weight of the non-functional polymer repeat unit and  $M_{w,f}$  is the molecular weight of the functional group including the counter ion ( $-\text{SO}_3\text{Na}$ ).

The water uptake of the CEMs was measured in different ionic forms following the weighing procedure [28]. The membrane was first brought into the desired ionic form ( $\text{H}^+$ ,  $\text{Na}^+$  or  $\text{Ca}^{2+}$ ) and the weight of the wet ( $m_{\text{wet}}$ ) and dry ( $m_{\text{dry}}$ ) sample was measured. The water uptake of the membrane is given by [24]:

$$w = \frac{m_{\text{wet}} - m_{\text{dry}}}{m_{\text{dry}}} \quad (2).$$

The charge density ( $c_{\text{char}}$ ) of the membrane can be calculated:

$$c_{\text{char}} = \frac{IEC}{w} \quad (3).$$

The electrical resistance of the membranes was measured in a six compartment cell with a four electrode arrangement (similar to Figure 2) under direct current using a 0.5M NaCl solution, as described by Krol et al. [30]. The membrane was first equilibrated in the measurement solution for more than 24 hours. The measurement solution was added in the compartments 3 and 4, next to the investigated membrane with the calomel reference electrodes. In the compartments 2 and 5, a NaCl solution with the same concentration was used as in the measurement compartments to reduce the influence of the electrode reactions at the working electrodes. The current was applied through the working electrodes in the compartments 1 and 6 whereas the electrical potential was measured close to the membrane surface in the compartments 3 and 4 with the calomel reference electrodes. The area resistance between the calomel reference electrodes was determined from the current-voltage curve (i-v curve) and was measured with and without the membrane. The difference of the two resistances was considered as the membrane area resistance (R). The dimensions, materials and typical operation

conditions of the test cell are described in [31]. The specific conductivity was then calculated using equation [24]:

$$\text{Cond} = \frac{d_{\text{wet}}}{R} \quad (4).$$

## 2.4 $\text{Ca}^{2+}$ flux measurements

The  $\text{Ca}^{2+}$  fluxes through the commercial and tailor made membranes were measured using a 2 and 6 compartment cell. In the 6 compartment cell (Figure 2), the central membrane was the one under investigation. In between the anode and the test membrane (between compartments 1/2 and 2/3) two CMX membranes were used. On the other side, an ACM membrane (Tokuyama) was placed to prevent transport of  $\text{Ca}^{2+}$  and  $\text{H}^+$  in compartment 5. A 0.5M  $\text{Na}_2\text{SO}_4$  solution was used in the electrode compartments (1, 6) and in the shield compartments (2, 5).

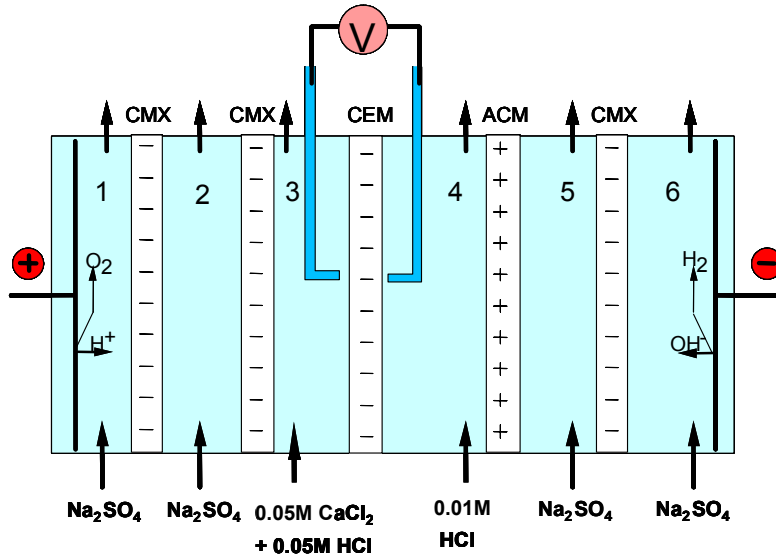


**Figure 2:** Six compartment cell configuration for the measurement of  $\text{Ca}^{2+}$  fluxes.

Like in the resistance measurements, the shield compartments were used to protect the measurement compartments from water dissociation products coming from the electrode reactions [30]:

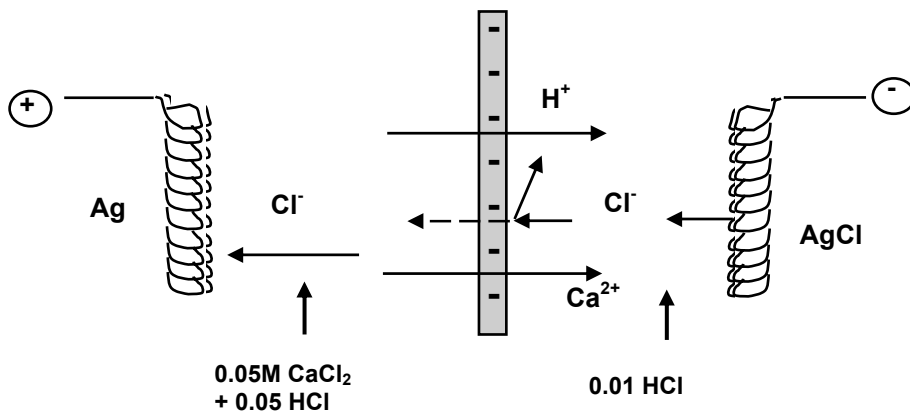
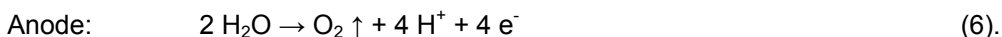
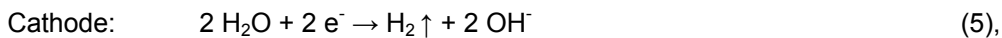


**Figure 3:** Two compartment configuration measurement of  $\text{Ca}^{2+}$  fluxes containing Ag/AgCl Electrodes.

In the 2 compartment cell, Ag/AgCl electrodes were used (Figure 3). The electrode reactions during an experiment are [30]:



The main advantage using this configuration is the absence of electrode reactions like water splitting. However, the experiment time is limited by the electrode deterioration.

All CEMs (commercial and tailor made S-PEEK/PES blends) were initially tested at the same conditions:

- 0.05M  $\text{CaCl}_2$  / 0.05M HCl solution in the anode compartment,
- 0.01M HCl solution in the cathode compartment,
- constant current density of 30  $\text{mA}/\text{cm}^2$ .

After the membrane screening, the commercial membranes were compared with the S-PEEK / PES blend membranes under various conditions, namely, at current

densities in the range 0-30 mA/cm<sup>2</sup> and using various anode compartment concentrations:

- 0.025M CaCl<sub>2</sub> / 0.075M HCl
- 0.05M CaCl<sub>2</sub> / 0.05M HCl
- 0.075M CaCl<sub>2</sub> / 0.025M HCl

(The calcium concentration in milk is in between 0.025M and 0.05M). All experiments were performed at 25 °C. The Ca<sup>2+</sup> concentrations were determined by elemental analysis (Atomic absorption spectroscopy) and the corresponding Ca<sup>2+</sup> flux ( $J(\text{Ca}^{2+})$ ) through the membrane was calculated from the concentration

change in time  $\left(\frac{dC_{\text{Ca}^{2+}}}{dt}\right)$  in the cathode compartment:

$$J(\text{Ca}^{2+}) = \frac{V * \frac{dC_{\text{Ca}^{2+}}}{dt}}{A} \quad (9),$$

where V is the volume of the circulated solution and A is the membrane area. Transport numbers of Ca<sup>2+</sup> ( $t_{\text{Ca}^{2+}}$ ) were calculated from the corresponding Ca<sup>2+</sup> fluxes:

$$t_{\text{Ca}^{2+}} = \frac{z_{\text{Ca}^{2+}} * J(\text{Ca}^{2+}) * F}{i} \quad (10),$$

where  $z_{\text{Ca}^{2+}}$  is the valence of calcium, F is the Faraday constant, and i is the applied current density. All the Ca<sup>2+</sup> fluxes through the membranes were normalised by the thickness of the wet membrane ( $d_{\text{wet}}$ ):

$$J_{\text{N}}(\text{Ca}^{2+}) = J(\text{Ca}^{2+}) * d_{\text{wet}} \quad (11).$$

This normalisation can be done, because all commercial membranes as well as the tailor made membranes have a homogeneous structure.

### 3. Results and discussion

#### 3.1 Characteristics of the commercial and tailor made CEMs

Tables 2 and 3 present the characteristics of the commercial and tailor made membranes. All commercial membranes besides FT-FKB, show similar properties (Table 2). Their IECs vary between 1.7 - 2.1 mol/kg<sub>dry</sub>, their water uptake between 0.15 - 0.33 kg<sub>water</sub>/kg<sub>dry</sub> and the conductivity between 1.7 - 4.8 mS/cm. Only the FT-FKB membrane has approximately 50% lower values.

The properties of the tailor made membranes are influenced by the sulphonation degree (SD) of the S-PEEK and the PES content of the blend (Table 3). A difference of 22% in the SD (from 61 to 83%) results in a water uptake increase of 85%. The conductivity increases even stronger from 3.4 to 8.6 mS/cm.

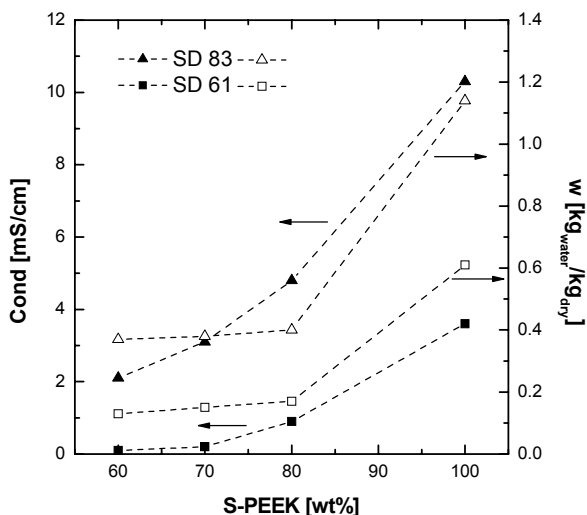


**Figure 4:** Dependence of conductivity and water uptake of the prepared S-PEEK/PES blends versus the S-PEEK content of the membrane.

Figure 4 presents the water uptake and the conductivity of the prepared membranes over the S-PEEK content of the blend. There, one can see that addition of 20 wt% PES reduces strongly the water uptake and therefore the membrane swelling. Wilhelm et al. [24] found that a PES content of 20–50% is the most suitable for blending. When the PES content is higher than 50% not all ion exchange groups are available for ion transport and the membrane has high resistance. When it is below 20% it cannot provide the physical crosslinking required for the reduction of the

water content. For the blends prepared with the lower sulphonated S-PEEK (SD 61%), the PES content should not exceed 30% because it results in membranes with very high resistance.

The charge densities of the commercial membranes and of the S-PEEK/PES blends prepared with the lower sulphonated S-PEEK (SD 61) are in the same range, from 5.4-7.0 mol/kg<sub>water</sub>. The blends prepared with the higher sulphonated S-PEEK (SD 83) and especially the membranes containing 100% S-PEEK have lower values, from 1.9 to 4.8 mol/kg<sub>water</sub>.

**Table 2: Characteristics and Ca<sup>2+</sup> fluxes of the commercial membranes.**

Membrane	d <sub>wet</sub> [μm]	Cond [mS/cm]	IEC [mol/kg <sub>dry</sub> ]	w [kg <sub>water</sub> /kg <sub>dry</sub> ]	c <sub>char</sub> [mol/kg <sub>water</sub> ]	J(Ca <sup>2+</sup> ) [10 <sup>-8</sup> mol/(cm <sup>2</sup> s)]	t <sub>Ca<sup>2+</sup></sub>	J <sub>N</sub> (Ca <sup>2+</sup> ) [10 <sup>-10</sup> mol/(cm s)]
<b>CMS</b>	138	3.5	2.09	0.30	6.97	2.2 ± 0.1	0.14	3.0
<b>FT-FKB</b>	105	1.7	0.81	0.15	5.40	4.1 ± 0.2	0.26	4.3
<b>CM-2</b>	126	3.3	2.05	0.31	6.61	5.0 ± 0.3	0.32	6.3
<b>CMV</b>	122	4.1	2.05	0.33	6.21	6.0 ± 0.1	0.38	7.3
<b>CMX</b>	163	4.8	1.65	0.26	6.35	4.9 ± 0.1	0.31	7.9

**Table 3: Characteristics and Ca<sup>2+</sup> fluxes of the tailor made membranes.**

Blend ratio S-PEEK / PES	d <sub>wet</sub> [μm]	Cond [mS/cm]	IEC mol/kg <sub>dry</sub>	w [kg <sub>water</sub> /kg <sub>dry</sub> ]	c <sub>char</sub> [mol/kg <sub>water</sub> ]	J(Ca <sup>2+</sup> ) [10 <sup>-8</sup> mol/(cm <sup>2</sup> s)]	t <sub>Ca<sup>2+</sup></sub>	J <sub>N</sub> (Ca <sup>2+</sup> ) [10 <sup>-10</sup> mol/(cm s)]
<b>83% sulphonated S-PEEK</b>								
<b>100 / 0</b>	105	8.6	2.21	1.14	1.94	3.4 ± 0.1	0.22	3.6
<b>80 / 20</b>	80	5.3	1.93	0.40	4.82	4.0 ± 0.1	0.25	3.2
<b>70 / 30</b>	55	3.1	1.65	0.38	4.33	3.6 ± 0.2	0.23	2.0
<b>60 / 40</b>	55	1.9	1.29	0.37	3.48	3.0 ± 0.3	0.19	1.6
<b>61% sulphonated S-PEEK</b>								
<b>100 / 0</b>	53	3.4	1.74	0.60	2.90	3.4 ± 0.3	0.22	1.8
<b>80 / 20</b>	50	1.0	1.14	0.17	6.68	3.2 ± 0.1	0.20	1.6
<b>70 / 30</b>	40	0.2	0.92	0.15	6.10	2.0 ± 0.2	0.13	0.8
<b>60 / 40</b>	50	0.1	0.86	0.13	6.35	1.3 ± 0.1	0.08	0.6



### 3.2 Ca<sup>2+</sup> transport through the commercial CEMs

The amount of Ca<sup>2+</sup> passing through the CMS membrane is the same when using the 2 or 6 compartment cell. The 2 compartment cell can be used only for limited time, but the Ca<sup>2+</sup> flux through the membrane reaches steady state quite fast, even for membranes with a low Ca<sup>2+</sup> permeability (such as CMS, see detailed results later). Therefore, the 2 compartment cell was selected to perform the measurements of the Ca<sup>2+</sup> fluxes for all membranes.

The CMS membrane seems to be the most selective commercial membrane (Table 2). The  $J(\text{Ca}^{2+})$  and the corresponding  $t_{\text{Ca}^{2+}}$  are at least 50% lower than for the other CEMs. The CMV membrane, however, has the highest apparent Ca<sup>2+</sup> flux of all commercial membranes. When the apparent  $J(\text{Ca}^{2+})$  is normalised for the geometrical thickness (see equation 11), the CMX has the highest Ca<sup>2+</sup> transport, followed by CMV and CM-2 membrane. For most of the CEMs the  $J_{\text{N}}(\text{Ca}^{2+})$  increases significantly with the membrane conductivity. The CMS membrane however deviates from this behaviour. Although it has similar electrical properties as the other membranes, it has lower  $J_{\text{N}}(\text{Ca}^{2+})$ . This might not only be result of material selectivity but it could also be due to the presence of a small positively charged layer on the membrane surface, indicated by Saracco [14] and Brown [32]. The positively charged coating probably rejects divalent ions, due to electrostatic repulsion, described by Chapotot et al. [10], Boucher et al. [33] and Sata et al. [34].

### 3.3 Ca<sup>2+</sup> transport through the tailor made CEMs

Figure 5 and Table 3 present the normalised Ca<sup>2+</sup> flux through the S-PEEK/PES blend membranes. Both S-PEEKs of SD 61 and 83% show similar behaviour. The  $J_{\text{N}}(\text{Ca}^{2+})$  through the membranes increases with increasing S-PEEK content in the blend (Figure 4). Having in mind that besides the low calcium flux, the blends should have acceptable conductivity (number on the symbols in Figure 4), four membranes actually have promising properties. These membranes (marked area in Figure 4) combine low  $J_{\text{N}}(\text{Ca}^{2+})$  with sufficient conductivities. The blends prepared with low sulphonated S-PEEK (SD 61) and high PES content (30-40%) have very low conductivities, but could potentially be used as coatings for CEMs.

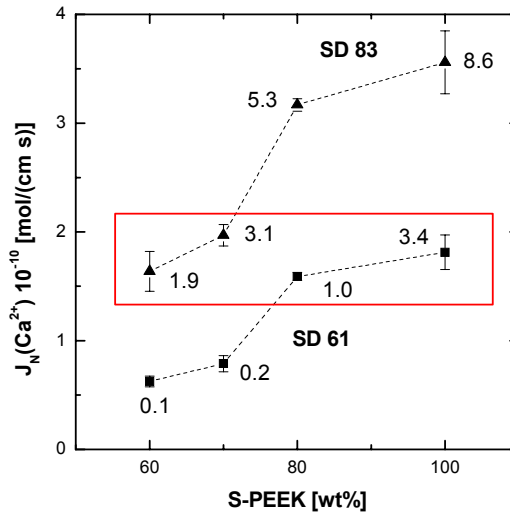


**Figure 5:** Dependence of the normalised  $\text{Ca}^{2+}$  flux on the SD and S-PEEK content of the blend membranes. The box identifies the membranes with reasonable conductivities (numbers next to the measurement points) and low  $\text{Ca}^{2+}$  transport.

For all blend membranes, the  $J_N(\text{Ca}^{2+})$  also increases significantly with the membrane conductivity. Only the membranes prepared by pure S-PEEK (100%) deviate from this behaviour. The flux does not increase as it would be expected based on their conductivity. The reason for this behaviour could be the high water uptake and therefore the low charge density of these membranes compared to the blends. This behaviour is discussed in more detail later.

### 3.4 Comparison between commercial and tailor made CEMs

The comparison of the  $\text{Ca}^{2+}$  fluxes through the commercial (Table 2) and the tailor made membranes (Table 3) shows that all tailor made membranes have generally higher  $\text{Ca}^{2+}$  selectivity. When plotting the  $J_N(\text{Ca}^{2+})$  over the conductivity of the commercial and S-PEEK/PES blends (Figure 6), a linear increase of the  $\text{Ca}^{2+}$  transport through the membranes with increasing conductivity is observed. A comparison of the slopes of  $J_N(\text{Ca}^{2+})$  over the conductivity for the different membranes shows that the membranes with the lower charge density (S-PEEK/PES SD 83 blends; 3.5-4.8 mol/kg<sub>water</sub>) have a less steep increase of  $J_N(\text{Ca}^{2+})$  (slope 0.48). The blends prepared by S-PEEK of SD 61 and the commercial membranes

have similar charge density (5.4-7.0 mol/kg<sub>water</sub>) and show steeper increase of  $J_N(\text{Ca}^{2+})$  (slope >1). Because the co-ion leakage of all commercial (Table 1) and all S-PEEK/PES blends [24] is approximately the same, the reduction of the  $\text{Ca}^{2+}$  transport through the membranes can not be explained by an increased co-ion leakage.

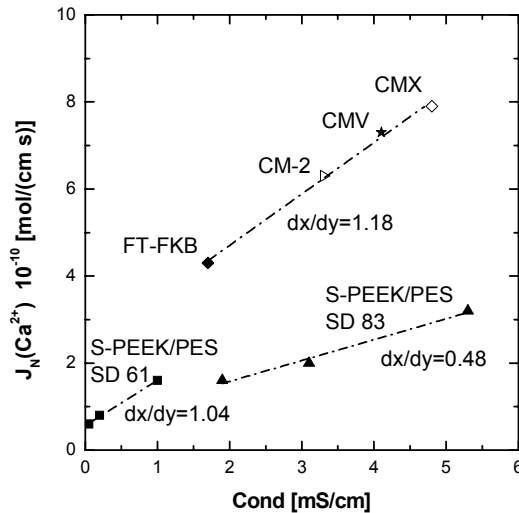


**Figure 6:** Dependence of the normalised  $\text{Ca}^{2+}$  transport and conductivity for the commercial and tailor made S-PEEK/PES blends containing 20-40% of PES.

It seems that membranes with lower charge density have increased selectivity for monovalent ions if the co-ion leakage is in the same range. A change of the membrane charge density has a stronger effect for multivalent ions than for monovalent ones. Chapotot et al. [10, 35] showed that divalent cations are preferred by CEMs because of their higher electrostatic attraction with the oppositely fixed charge sites, if no driving force was applied. This attraction, which increases with increasing charge density of the membrane, seems to have a strong influence on the  $\text{Ca}^{2+}$  transport through the membrane also when a driving force (electric current) is applied. It is important to add that the CMS membrane and the pure S-PEEK membranes were not considered in the discussion above. The CMS membrane probably contains a coating and a direct relation between the  $J_N(\text{Ca}^{2+})$  and the charge density can not be obtained. The pure S-PEEK membranes show high co-ion leakage due to substantial swelling, as shown by Wilhelm et al. [24].

The water uptake of the membranes depends on their ionic form (Table 4). For all commercial membranes and blends the differences in water uptake in various ionic forms are small. Only the membranes of pure S-PEEK behave differently. In our experiments, the feed solution is a mixture of HCl and CaCl<sub>2</sub> on one side and HCl on the other side of the membrane. Therefore, the water uptake under measurement conditions would probably be in between the water uptakes of the membrane in Ca- and H-form, and probably close to the water uptake in the Na-form. Therefore, the water uptake of the membranes in the Na-form was used for the calculation of the charge densities.

**Table 4:** Water uptake of two commercial and four S-PEEK/PES blend membranes, in different ionic forms.

Membrane	w [kg <sub>water</sub> / kg <sub>dry</sub> ]		
	H-form	Na-form	Ca-form
<b>CMX</b>	0.29	0.26	0.24
<b>CMS</b>	0.32	0.30	0.26
<b>S-PEEK SD 83 100%</b>	1.18	1.14	1.00
<b>S-PEEK SD 83 60%</b>	0.39	0.37	0.33
<b>S-PEEK SD 61 100%</b>	0.71	0.60	0.48
<b>S-PEEK SD 61 60%</b>	0.14	0.14	0.14

The CMX, CMS and two blends with S-PEEK contents of 60% were compared under various conditions in order to get a better insight on their performance. Figure 7 shows the  $J_N(\text{Ca}^{2+})$  of these membranes at various current densities. The  $J_N(\text{Ca}^{2+})$  increases linearly with increasing current for the CMX and the S-PEEK blend membranes like expected from the Nernst-Planck electrodiffusion equations [10, 35].

The behaviour of the CMS membrane seems to be different. At low current densities, the Ca<sup>2+</sup> transport is rather low. However, above current densities of 20 mA/cm<sup>2</sup> it increases significantly. It seems that the electrostatic repulsion from the positively charged coating layer of this membrane could be overcome at high current densities. This phenomenon, namely the decrease of selectivity of a membrane with a positive charged layer at higher current densities has also been reported by Chapotot et al. [10, 35].

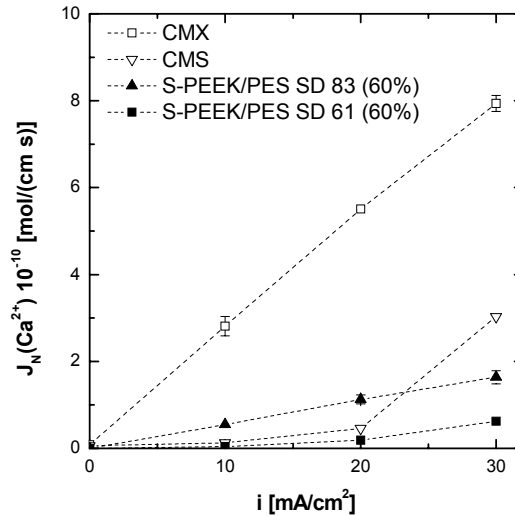


**Figure 7:** Dependence of the normalised  $Ca^{2+}$  flux on the applied current density.

At higher current densities, a depletion of  $H^+$  ions occurs next to the membrane, leading to an accumulation of  $Ca^{2+}$  ions. Because the electrostatic repulsion of the positively charged coating is based on the Donnan exclusion mechanism [5], an increase of  $Ca^{2+}$  ions leads to an increased  $Ca^{2+}$  transport and loss of selectivity of this layer.

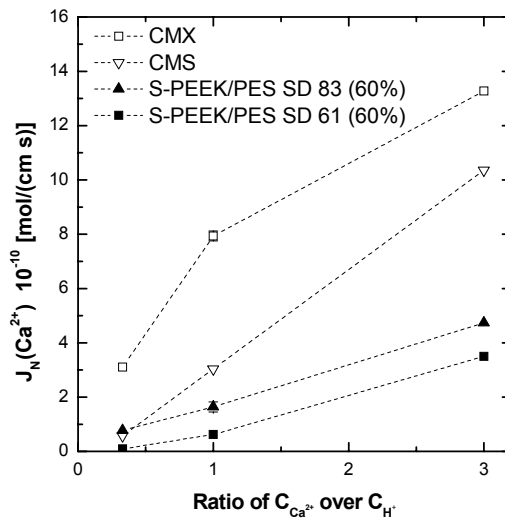


**Figure 8:** Dependence of the normalised  $Ca^{2+}$  flux on the concentration ratio of  $Ca^{2+} / H^+$  in the feed solution.

Figure 8 shows the normalised  $\text{Ca}^{2+}$  flux through the membranes, at various anode feed concentrations. All experiments were performed at constant current density  $i = 30 \text{ mA/cm}^2$ . The  $J_N(\text{Ca}^{2+})$  generally increases at higher  $\text{Ca}^{2+}$  concentrations. The transport of  $\text{Ca}^{2+}$  through most of the CEMs increases almost linear over the measured concentration range. The increase of  $\text{Ca}^{2+}$  transport through the CMS and CMX membranes is stronger than for the S-PEEK/PES blends. At high  $\text{Ca}^{2+}$  concentrations, the  $\text{Ca}^{2+}$  transport through the CMX decreases. This is probably due to the difference of mobility of the  $\text{Ca}^{2+}$  and  $\text{H}^+$  ions at high current densities. Chapotot et al. [10, 35] calculated the ratio of the apparent rate constants of the penetration of  $\text{H}^+$  and  $\text{Ca}^{2+}$  ions. They reported that with increasing concentration ratio of  $\text{Ca}^{2+}$  over  $\text{H}^+$  the apparent rate constants ratio of  $\text{H}^+$  over  $\text{Ca}^+$  increases, resulting in a higher proton transport. This phenomenon which was only observed at high current densities ( $30 \text{ mA/cm}^2$ ) [35], results in higher contribution of  $\text{H}^+$  in the current transport and therefore in a decrease of  $\text{Ca}^{2+}$  flux.

#### 4. Conclusions

In this work various commercial CEMs and tailor made S-PEEK/PES blend membranes were characterised and compared. The S-PEEK/PES blends showed good selectivities between monovalent ( $\text{H}^+$ ) and bivalent ( $\text{Ca}^{2+}$ ) ions and reasonable conductivities. It was shown that the conductivity, the IEC and the water uptake of the membrane determine the  $\text{Ca}^{2+}$  transport. Membranes with high conductivity and high charge density have higher  $\text{Ca}^{2+}$  transport. When decreasing the charge density while keeping the conductivity constant, the electrostatic attraction of  $\text{Ca}^{2+}$  to the charge sites of the membrane decreases, resulting in lower  $\text{Ca}^{2+}$  transport. It seems that membranes with positively charged coating (CMS) have good selectivities, as long as the current density is not too high. Besides, for the blend and the CMS membrane the  $J_N(\text{Ca}^{2+})$  increases linearly with the increase of  $\text{Ca}^{2+}$  concentration. However, at high current density, the  $\text{Ca}^{2+}$  selectivity of the CMX membrane increases at higher  $\text{Ca}^{2+}$  concentrations probably due to differences in transport rate between  $\text{H}^+$  and  $\text{Ca}^{2+}$ .

## 5. Acknowledgements

The authors would like to thank Gérald Pourcelly for the fruitful discussion.

## 6. List of symbols

A	membrane area [ $\text{cm}^2$ ]
$C_{\text{Ca}^{2+}}$	concentration of calcium [mol/L]
$c_{\text{char}}$	charge density [mol/kg <sub>water</sub> ]
Cond	conductivity [mS/cm]
$d_{\text{wet}}$	thickness of the wet membrane [ $\mu\text{m}$ ]
F	Faraday constant (96485 As/mol)
i	current density [ $\text{A}/\text{cm}^2$ ]
IEC	ion exchange capacity [mol/kg <sub>dry</sub> ]
J	ion flux through the membrane
$J_{\text{N}}$	ion flux through the membrane normalised for the wet thickness of the membrane [mol/(cm s)]
$m_{\text{wet}}$	mass of the sample in wet state [kg]
$m_{\text{dry}}$	mass of the sample in the dry state [kg]
$M_{\text{w,p}}$	molecular weight of the polymer repeat unit [kg]
$M_{\text{w,f}}$	molecular weight of the functional group [kg]
R	membrane area resistance [ $\Omega \text{ cm}^2$ ]
SD	sulphonation degree [%]
t	time [s]
$t_{\text{Ca}^{2+}}$	transport number of calcium [-]
V	circulated volume [L]
w	water uptake [kg <sub>water</sub> /kg <sub>dry</sub> ]
$z_{\text{Ca}^{2+}}$	valence of the calcium ion [-]
CEM	cation exchange membrane
S-PEEK	sulphonated poly(ether ether ketone)
PES	poly(ether sulphone)
AEM	anion exchange membrane
NMP	N-methyl-2-pyrrolidinone

## 7. References

- [1] T. Sata, T. Sata, W. Yang, Studies on cation-exchange membranes having permselectivity between cations in electrodialysis, *Journal of Membrane Science* 206 (2002) 31-60.
- [2] Y. Kubuchi, H. Motomura, Y. Noma, F. Hanada, Application of ion-exchange membranes to the recovery of acids by diffusion dialysis, *Journal of Membrane Science* 27 (1986) 173.
- [3] T. Sata, New application of ion-exchange membranes, in: J. Kohovec (Ed.), *Macromolecules*, VSP, Utrecht, The Netherlands (1992) p. 451.
- [4] L. Bazinet, F. Lamarche, D. Ippersiel, D. Montpetit, J. Amiot, Identification of Skim Milk Electroacidification Fouling: A Microscopic Approach, *Journal of Colloid and Interface Science* 237 (2001) 62-69.
- [5] F.G. Donnan, The theory of membrane equilibrium in presence of a non-dialysable electrolyte, *Z. Elektrochem.* 17 (1911) 572.
- [6] E. Korngold, in: G. Bedford (Ed.), *Synthetic Membrane Process*, Academic Press, New York (1984) 191-220.
- [7] C. Gavach, Symposium sur les applications alimentaires de l'électrodialyse, *Foundation des Gouverneurs, Saint-Hyacinthe, Québec, 23 et 24 Mars 1999.*
- [8] L. Bazinet, F. Lamarche, D. Ippersiel, J. Amiot, Bipolar Membrane Electroacidification To Produce Bovine Milk Casein Isolate, *J. Agric. Food Chem* 47 (1999) 5291-5296.
- [9] L. Bazinet, D. Ippersiel, D. Montpetit, B. Mahdavi, J. Amiot, F. Lamarche, Effect of membrane permselectivity on the fouling of cationic membranes during skim milk electroacidification, *Journal of Membrane Science* 174 (2000) 97-110.
- [10] A. Chapotot, G. Pourcelly, C. Gavach, F. Lebon, Electrotransport of proton and divalent cations through modified cation-exchange membranes, *Journal of Electroanalytical Chemistry* 286 (1995) 25-37.
- [11] T. Sata, R. Izuo, Y. Mizutani and R. Yamane, Transport properties of ion-exchange membranes in the presence of surface active agents, *Journal of Colloid and Interface Science* 40 (1972) 317-328.



- [12] Y. Tanaka, M. Seno, Treatment of ion exchange membranes to decrease divalent ion permeability, *Journal of Membrane Science* 8 (1981) 115-127.
- [13] T. Sata, Modification of properties of ion exchange membranes. II. Transport properties of cation exchange membranes in the presence of water-soluble polymers, *Journal of Colloid and Interface Science* 44 (3) (1973) 393.
- [14] G. Saracco, Transport properties of monovalent-ion-permselective membranes, *Chemical engineering Science*, 52 (17) (1997) 3019-3031.
- [15] G. Saracco, M.C. Zanetti, Ion transport through monovalent-anion-permselective membranes, *Industrial & Engineering Chemistry Research* 33 (1994) 96-101.
- [16] T. Nishiwaki, Concentration of electrolytes prior to evaporation with an electromembrane process, in: R.E. Lacey, S.Loch (Ed.), *Industrial Processes with Membranes*, Chapter VI, Wiley-Interscience, New York.
- [17] T. Sata, Change of transport properties of cation exchange membranes, *Journal of Polymer Science* 16 (1978) 1063 –1080.
- [18] T. Sata, Properties of ion – exchange membranes combined anisotropically with conducting polymers. 2. Relationship of electrical potential generation to preparations of composite membranes, *Chemistry of Materials* 3 (1991) 838 –843.
- [19] T. Sata, K. Kawamura, M Higa, K. Matsusaki Electrolytic transport properties of cation exchange membranes in the presence of cyclodextrins, *Journal of Membrane Science* 183 (2) (2001) 201 –212.
- [20] V.L. Rao, Polyether Sulfones, *Journal of Macromolecular Science – Reviews in Macromolecular Chemistry and Physics*, C39 (1999) 655-711.
- [21] W. Chui, J. Kerres, G. Eigenberger, Development and characterisation of ion-exchange polymer blend membranes, *Separation and Purification Technology*, 14 (1998) 145-154.
- [22] A.J. van Zyl, J.A. Kerres, W. Chui, M. Junginger, Application of new sulfonated ionomer membranes in the separation of pentene and bentane by facilitated transport, *Journal of Membrane Science* 137 (1997) 173-185.
- [23] J.E. Mark (Ed.), *Polymer Data Handbook*, University of Cincinnati, Oxford University Press, USA

- [24] F. G. Wilhelm, I. G. M. Punt, N. F. A. van der Vegt, H. Strathmann, M. Wessling, Cation permeable membranes from blends of sulfonated poly(ether ether ketone) and poly(ether sulfone), *Journal of Membrane Science* 199 (2002) 167-176.
- [25] C. Bailly, D.J. Williams, F.E. Karasz, W.J. Mac Knight, The sodium salts of sulphonated poly(aryl ether ether ketone) (PEEK): Preparation and characterisation, *Polymer* 28 (1987) 1009-1016.
- [26] N. Shibuya, R.S. Porter, Kinetics of PEEK Sulfonation in concentrated sulphuric acid, *Macromolecules* 25 (1992) 6495-6499.
- [27] M. Mulder, Basic principles of membrane technology, Chapter 3, 2<sup>nd</sup> Edition, Kluwer Academic Publishers, Dordrecht (1996).
- [28] H. Strathmann, Electrodialysis, in: W.S. Winston Ho, K.K. Sirkar (Ed.), *Membrane Handbook*, Van Nostrand Reinhold, New York (1992) p. 218-262.
- [29] F. Helfferich, Ion exchange, McGraw Hill, New York 1962.
- [30] J.J. Krol, M. Wessling, H. Strathmann, Concentration polarization with monopolar ion exchange membranes: current-voltage curves and water dissociation, *Journal of Membrane Science* 162 (1999) 145-154.
- [31] F. G. Wilhelm, N. F. A. van der Vegt, M. Wessling, H. Strathmann, Chronopotentiometry for the advanced current-voltage characterisation of bipolar membranes, *Journal of Electroanalytical Chemistry* 502 (2001) 152-166.
- [32] C.J. Brown, Acid and metal recovery by Recoflo sorption, 23<sup>rd</sup> CIM Annual Conference of Metallurgist, Quebec City, Canada 1984.
- [33] M. Boucher, N. Turcotte, V. Guillemette, G. Lantagne, A. Chapotot, G. Pourcelly, R. Sandeaux, C. Gavach, Recovery of spent acid by electrodialysis in zinc hydrometallurgy industry: performance study of different cation-exchange membrane, *Hydrometallurgy* 45 (1997) 137-160.
- [34] T. Sata, R. Izuo, K. Takata, Modification of the transport properties of ion exchange membranes. IX. Layer formation on a cation exchange membrane by acid-amid bonding, and transport properties of the resulting membrane, *Journal of Membrane Science* 45 (1989) 197-208.

- [35] A. Chapotot, G. Pourcelly, C. Gavach, Transport competition between monovalent and divalent cations through cation-exchange membranes. Exchange isotherms and kinetic concepts, *Journal of Membrane Science* 96 (1994) 167-181.



## **Appendix Chapter VI**

### **Improvement of the monovalent ion selectivity of commercial membranes**

J. Balster, O. Krupenko, I. Pünt, D.F. Stamatialis and M. Wessling

## 1. Introduction

In chapter VI monovalent ion selective membranes are prepared based on sulphonated poly(ether ether ketone). In this work, we investigate the  $\text{Ca}^{2+}$  transport through a commercial CMX membrane modified with different coatings. The influence of the coating on the  $\text{Ca}^{2+}$  flux and the coating stability are investigated.

## 2. Experimental

Three different coatings were prepared and tested: Polyethylenimine (PEI), aminated polysulphone (A-Psf), and a blend of sulphonated poly(ether ether ketone) and poly(ether sulphone), S-PEEK/PES. The S-PEEK had a sulphonation degree (SD) of 61%. The S-PEEK/PES and A-Psf solutions were simply casted with a 50  $\mu\text{m}$  casting knife on the membrane surface, resulting in coating thicknesses of approximately 5  $\mu\text{m}$  for the 10 wt% solution and 2.5  $\mu\text{m}$  for the 5 wt% solution. The PEI coating was applied by immersion [1, 2]. A detailed description of the immersion process can be found in chapter V.

For all membranes the electrical properties and the ion fluxes were measured using a two compartment cell configuration (see chapter VI) containing Ag / AgCl electrodes (30  $\text{mA}/\text{cm}^2$ , 0.05M  $\text{CaCl}_2$  / 0.05M HCl in the anode and 0.01M HCl in the cathode compartment).

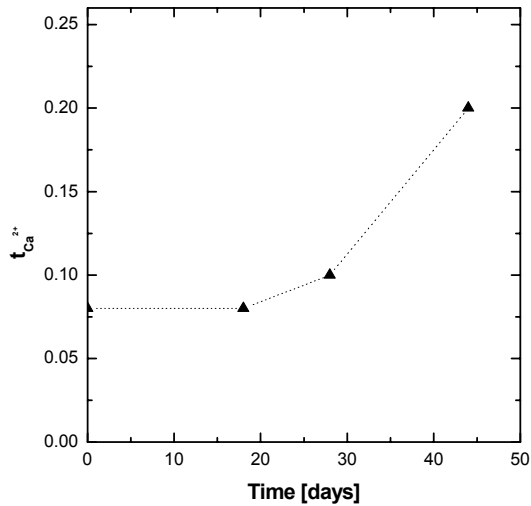
## 3. Results and discussion

Table 1 presents the  $\text{Ca}^{2+}$  flux through the various membranes, showing the strongest decrease for those having the positively charged PEI and A-Psf coatings. For the membrane modified with PEI, the  $\text{Ca}^{2+}$  flux is significantly lower at higher molecular weight (MW) of the PEI. The negatively charged S-PEEK/PES coating is not as effective as the positively charged ones.

**Table 1:**  $\text{Ca}^{2+}$  transport properties of the coated and initial CMX membrane.

Membrane	$J(\text{Ca}^{2+})$ $10^{-8} [\text{mol}/(\text{cm}^2\text{s})]$	$t_{\text{Ca}^{2+}}$
CMX	$4.9 \pm 0.1$	0.31
CMX – PEI (immersed, MW 25000)	$3.2 \pm 0.1$	0.20
CMX – PEI (immersed, MW 50000)	$1.2 \pm 0.1$	0.08
CMX – A-Psf (5 wt%)	$2.9 \pm 0.2$	0.19
CMX – A-Psf (10 wt%)	$1.6 \pm 0.1$	0.10
CMX – S-PEEK/PES (60/40) (SD 61%) (10 wt%)	$3.7 \pm 0.1$	0.24

For all coated membranes, besides the PEI, the  $\text{Ca}^{2+}$  flux is constant over time. The PEI coating disappears after 20 days and the  $\text{Ca}^{2+}$  transport increases significantly (Figure 3).

**Figure 3:** Transport number of  $\text{Ca}^{2+}$  versus time through CMX coated with PEI (MW 50000).

#### 4. Conclusions and outlook

The use of a positively charged coating strongly decreases the  $\text{Ca}^{2+}$  flux through the membrane. Coatings with PEI are not stable in time, however, the A-Psf coatings seem to be stable.

Chapter II has shown that casting A-Psf on S-PEEK/PES membranes results in stable coating layer because of the penetration of the polymers. The combination of

a monovalent ion selective S-PEEK/PES membrane with an A-Psf coating should improve the selectivity of these membranes even further. This can be a subject of a future work.

## 5. List of symbols

J	Ion flux through the membrane [mol/(cm <sup>2</sup> s)]
SD	Sulphonation degree [%]
$t_{Ca^{2+}}$	Transport number of calcium
MW	Molecular weight [g/mol]
A-Psf	Aminated polysulphone
PEI	Polyethylenimine
PES	Poly(ether sulphone)
S-PEEK	Sulphonated poly(ether ether ketone)

## 6. References

- [1] T. Sata, W. Yang, "Studies on cation-exchange membranes having permselectivity between cations in electrodialysis", *Journal of Membrane Science* 206 (2002) 31-60.
- [2] T. Sata, "Studies on ion exchange membranes with permselectivity for specific ions in electrodialysis", *Journal of Membrane Science* 93 (1994) 117-135.



## Chapter VII

### Electrochemical acidification of milk by whey desalination

J. Balster, I. Pünt, D.F. Stamatialis, and M. Wessling

#### **Abstract**

In this chapter a process configuration for the electrochemical acidification of milk by bipolar membrane electroacidification is proposed. In this process, the casein whey produced by the chemical acidification of milk is first demineralised. Combining the demineralisation with bipolar membrane electro dialysis, the used acid can be recovered and the whey can be neutralised by the produced base.

In this research we focus on the scaling and fouling behaviour of different CEMs to be used in this process, showing that monovalent ion selective membranes show a low scaling behaviour. The possibility of desalinating milk to produce the needed acid and base is investigated. This configuration has higher resistance and power consumption compared to the desalination of casein whey and is rather unstable due to the precipitation of casein inside the stack caused by local pH changes in the desalination compartment. The influence of different membrane configurations on the process efficiencies and the power consumption is tested. Using a part of the casein whey to buffer the acid compartment process current efficiencies of 0.86 for the production of acid and 0.87 for the production of base can be achieved.

## 1. Introduction

Whey proteins have excellent functional properties and high nutritional value. Casein is extensively used as an ingredient in food products because of these properties. It can be produced by isoelectric precipitation from milk using chemical acidification. Chemical acidification however, produces too large amounts of salts, which have to be separated from the whey resulting in waste streams.

Bazinet et al [1-6] developed a procedure to produce acid casein via bipolar membrane (BPM) electroacidification (BPMEA). BPMEA uses the property of bipolar membranes to split water and the selectivity of cation exchange membranes (CEMs) for demineralisation for the protein precipitation (see Figure 1) [1].

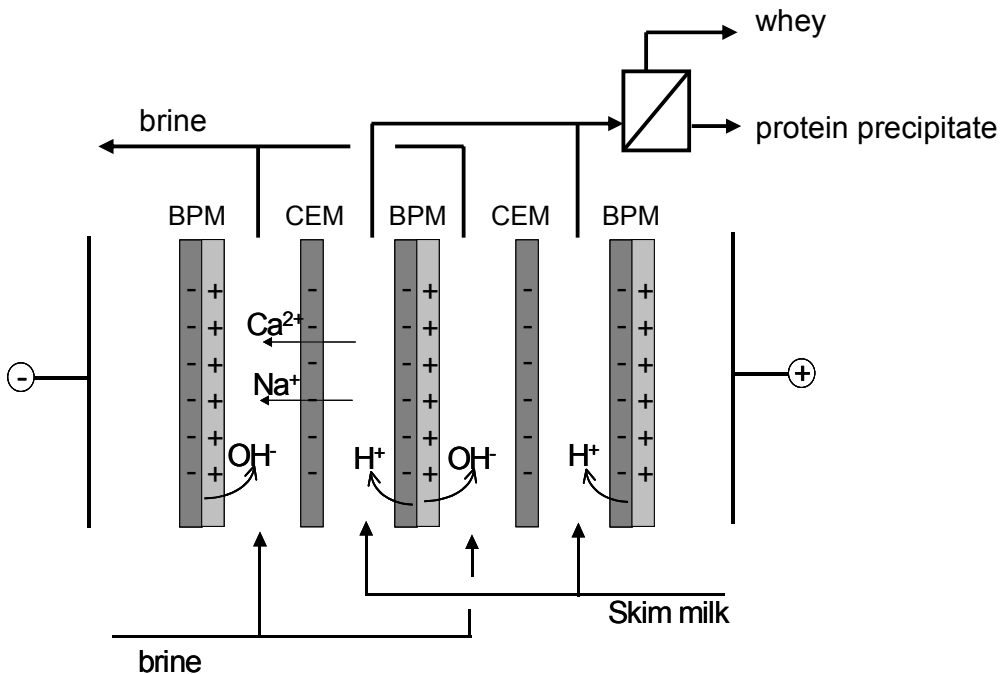


**Figure 1:** Electroacidification of milk via bipolar membrane electro dialysis.

The direct acidification leads to removal of cations into the base compartment. The monovalent ions form the base. The protons cause the proteins to precipitate, in the best case outside the stack. The following problems exist in this process:

1. The bivalent cations precipitate on the CEM in the base compartment causing scaling. The scaling of the membranes can be prevented using cation selective membranes allowing monovalent ions to pass but rejecting the bivalent ones. Lots of research has been performed on the improvement of permselectivity between cations in electrodialysis and the development of monovalent ion selective membranes [7-11].
2. The direct acidification of concentrated milk inside the electrodialysis membrane stack leads frequently to uncontrolled protein precipitation on the membrane surface and on the spacers separating them. In particular, the acidification of milk inside the stack can lead to clogging of the stack or burning of the membranes by short-circuits introduced through local deposits.

In this chapter, we propose an alternative process. The whey produced by the chemical acidification of milk is demineralised before further use. By combining this demineralisation with bipolar membrane electrodialysis (ED-BPM), the acid could be recovered and the whey could be neutralised by the produced base. Figure 2 shows the suggested process scheme of the described solution.

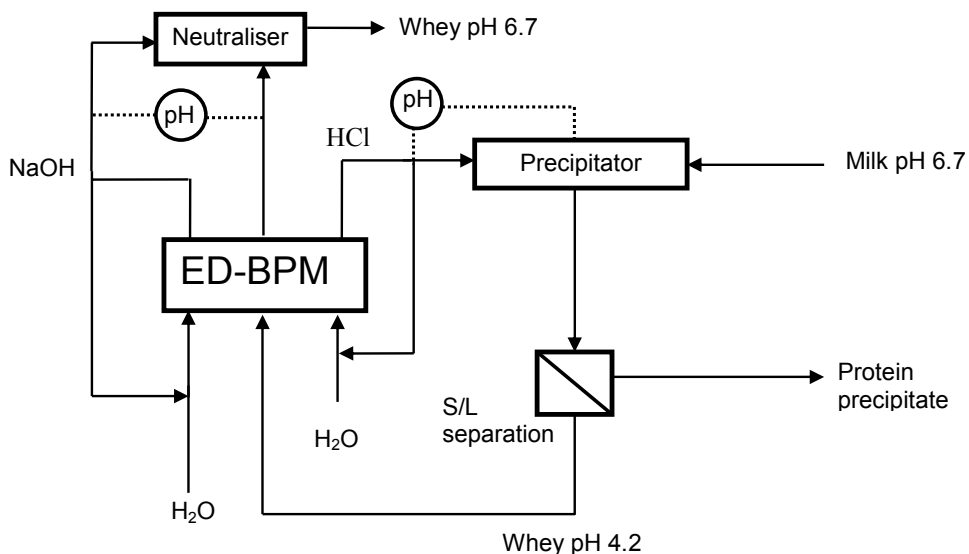


**Figure 2:** Process scheme for the recovery of acid and base from the acidic whey. The recovered streams are reused in the acidification and neutralisation process.

In this process, the acidic whey is desalinated in the membrane stack (see Figure 3). The anions migrate through the anion exchange membrane (AEM) and form acid. This acid is used to acidify milk in the precipitator. The cations migrate through the cation exchange membrane and form a base, which is used to neutralise the whey after demineralisation.

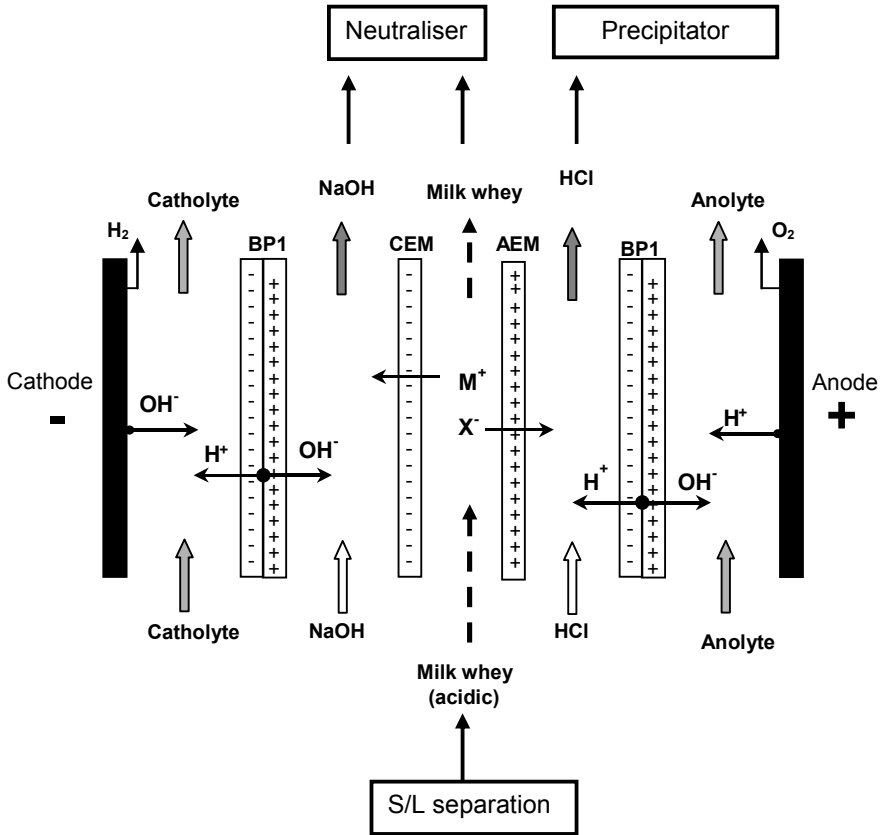


**Figure 3:** Membrane stack configuration for the recovery of acid and base from the acidic whey stream.

The aim of this study is to investigate the feasibility of this process. We will report lab scale tests with the membrane configuration shown in Figure 3 with casein whey and investigate the scaling and fouling behaviour using various CEMs. Besides, the desalination of milk will be investigated, too. Subsequently, this membrane configuration will be tested in a pilot module and the efficiencies of the process will be estimated.

## 2. Experimental

### 2.1 Membranes

Neosepta AFN; AMX, CMX, CMX-S, CMS as monopolar ion exchange membranes and the BP-1 as BPM from Tokuyama Soda Ltd. (Japan) were used. In addition tailor made membranes based on a blend of 60 wt% sulphonated poly(ether ether ketone), S-PEEK, with a sulphonation degree of 80% and 40 wt% poly(ether sulphone), PES, were used [11]. The S-PEEK/PES blend membrane is denoted as S/P in the text.

### 2.2 Membrane characterisation

The membranes were characterised by measurements of the ion exchange capacity (IEC), the degree of sulphonation, the water uptake ( $w$ ), the electrical resistance ( $R$ ) and the permselectivity ( $P$ ). The resistance was determined in 0.5M NaCl solution and the permselectivity by placing the membrane between 0.5M and 0.1M NaCl solutions [11, 12]. The properties of all membranes are given in Table 1.

**Table 1:** Properties of the monopolar ion exchange membranes.

Membrane	Properties	R [ $\Omega\text{cm}^2$ ]	IEC [mol/kg <sub>dry</sub> ]	w [kg <sub>water</sub> /kg <sub>dry</sub> ]
CMX	high mechanical strength	3.4	1.7	0.3
CMX-S	high mechanical strength monovalent ion selective	9.3	1.7	0.3
CMS	monovalent ion selective	4.1	2.1	0.3
S/P 60/40	monovalent ion selective	5.2	1.3	0.3
AMX	high mechanical strength	2.7	1.4	0.3
AFN	low organic fouling	1.0	2.5	0.4

### 2.3 Lab scale tests

The lab scale tests were performed in batch mode using a five compartment membrane stack (Figure 3). The membrane area per membrane was 23.76 cm<sup>2</sup>. The voltage drop over the CEM was measured with calomel reference electrodes [13]. The experiments were performed at 25°C at a volume flow of 18 L/h. The applied current density was 10 mA/cm<sup>2</sup>.

As starting solution for the experiments, 2L of 0.5M Na<sub>2</sub>SO<sub>4</sub> was used as electrolyte, 2L of 0.1M HCl as acid and 2L of 0.1M NaOH as base. In the desalination compartment (middle compartment, Figure 3) milk or casein whey (delivered from DMV-International, The Netherlands) was used.

## 2.4 Pilot scale tests

The pilot scale tests were performed with the same membrane configuration and solutions as described above. The electro dialysis pilot system was a semi-automated setup used in batch recycle mode. The electro dialysis membrane module (Fumatech, Germany) had an area of 100 cm<sup>2</sup> (10cm \* 10cm) for each membrane [14]. The distance between the membranes was 3 mm. In the electrolyte and in the acid and base compartments a standard non-woven net spacer was used (the spacer G in chapter IV and/or [15]). In the desalination compartment the multi-layer spacer indicated as I-E-I (chapter IV) was used. The experiments were performed at 25°C at volume flows of 40 L/h. The applied current density was 10 mA/cm<sup>2</sup>. The current efficiency for the acid and base was calculated by [16]:

$$\eta = \frac{(c_0 - c_t)VF}{It} \quad (1),$$

where  $c_0$  and  $c_t$  are the equivalent concentration of the produced acid and base at time 0 and  $t$  respectively,  $V$  is the circulated volume of solution per compartment, and  $I$  the applied current.

## 2.5 Ion analysis

The composition of the acids and bases before and after the experiments was analysed by the analytical laboratory of DMV-International using standardised methods on ion analysis.

The concentration of acid and base was analysed by titration with Titrino 716 DMS from Methrom (Switzerland).

### 3. Results and discussion

#### 3.1 Scaling and fouling of CEMs

In order to get an insight in the scaling and fouling behaviour of different CEMs the commercial CMX, the monovalent ion selective CMX-S and CMS, and the tailor made S/P 60/40 blend were investigated. As AEM the Neosepta AFN was used in all experiments. The initial resistance and permselectivity of the CEMs were determined. The membranes were used in the ED-BPM process (Figure 3) for whey desalination for 60 min at current density of 10 mA/cm<sup>2</sup>. Afterwards the membranes were rinsed with water to remove protein residue from the membrane surface and their resistances and permselectivities were measured again (indicated as “used”). The membranes were subsequently rinsed with a 0.1M HCl solution and their properties were determined again (indicated as “cleaned”). The results are shown in Table 2.

**Table 2:** Properties of the CEMs before and after the whey desalination for 60 min.

Membrane	R [ $\Omega\text{cm}^2$ ]			P [%]		
	initial	used	cleaned	initial	used	cleaned
<b>CMX</b>	3.4	5.4	3.4	98	98	98
<b>CMX-S</b>	9.3	9.8	9.3	98	98	98
<b>CMS</b>	4.1	5.2	4.1	98	98	98
<b>S/P 60/40</b>	5.2	5.3	5.2	97	97	97

For all membranes, a white deposit (scaling) was observed (see examples in Figure 4). This caused an increase of the membrane resistance. The CMX membrane shows the strongest increase followed by the monovalent ion selective CMS and CMX-S membrane. For the CMX membrane a layer of precipitated calcium was found, especially at the cathode side directed to the base compartment. Also the CMS membrane shows such a layer, but much less developed. The resistance of the S/P 60/40 membrane increased only slightly. The permselectivities of all membranes stayed constant indicating that no functional groups were “lost” during the process. After rinsing with 0.1M HCl the resistances of the membranes

reached the initial values again, showing that the scaling was completely reversible (see Table 2).

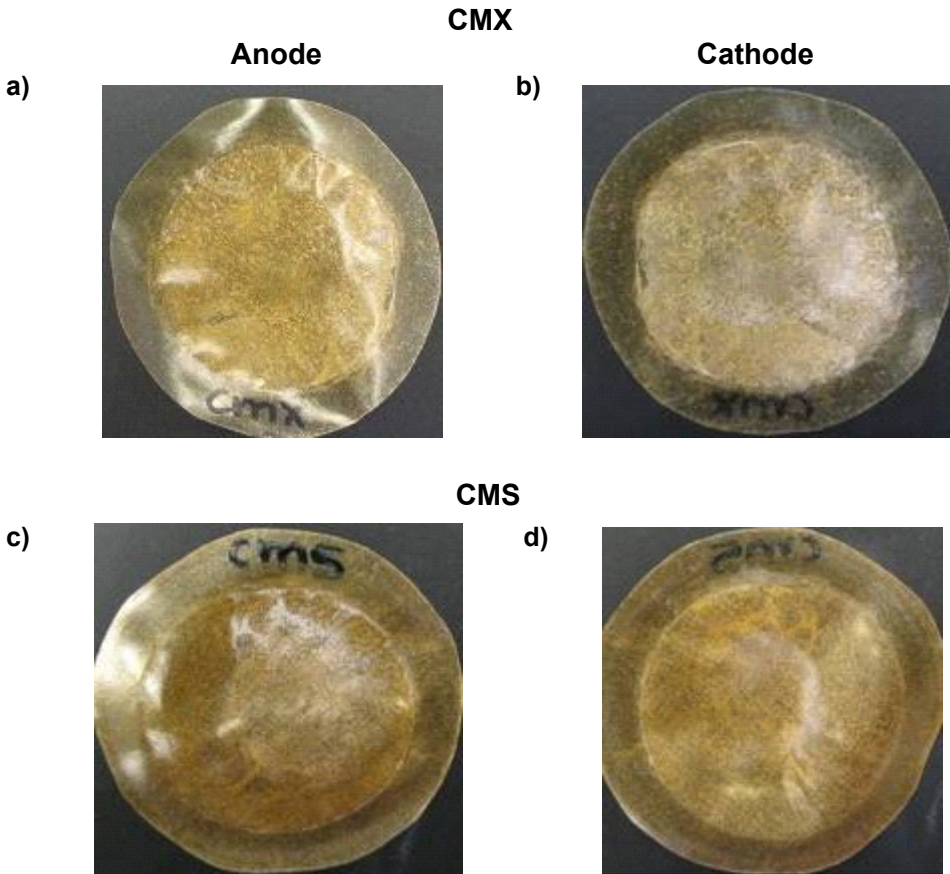


**Figure 4:** Pictures of the used CMX, (a, b) and CMS membrane, (c, d), after 60 min of whey desalination. The membranes were rinsed with water after the process to remove protein fouling.

Afterwards, to increase the impact of the scaling on the membranes, three subsequent runs were made, changing only the whey in the desalting compartment. For all membranes, the resistances increased due to scaling. The CMX membrane showed the highest resistance and slight decrease of permselectivity. The CMX-S, CMS and especially the S/P 60/40 showed better performance (see Table 3). The initial properties of the membranes could be recovered by rinsing with 0.1M HCl.



**Table 3:** Properties of the CEMs before and after the whey desalination for 3 times 60 min.

Membrane	R [ $\Omega\text{cm}^2$ ]			P [%]		
	initial	used	cleaned	initial	used	cleaned
CMX	3.4	7.1	3.4	98	95	98
CMX-S	9.3	10.2	9.3	98	98	
CMS	4.1	5.5	4.1	98	97	98
S/P 60/40	5.2	5.6	5.2	97	97	97

Besides the effects of scaling on the properties of the CEM, it is important to stress the differences in voltage drop over the membrane ( $U_{\text{mem}}$ ). Figure 5 presents the development of the membrane resistance during the whey desalination. The voltage drop over the CEMs ( $U_{\text{mem}}$ ) measured during the desalination process is much higher than expected from the increase of the membrane resistance introduced by scaling (Table 2 and 3). One part of the increased  $U_{\text{mem}}$  can be due to the increase of the solution resistance in the desalination compartment. However, this resistance increase should be comparable for all measurements, hence another mechanism depending on the used membranes has to be considered.

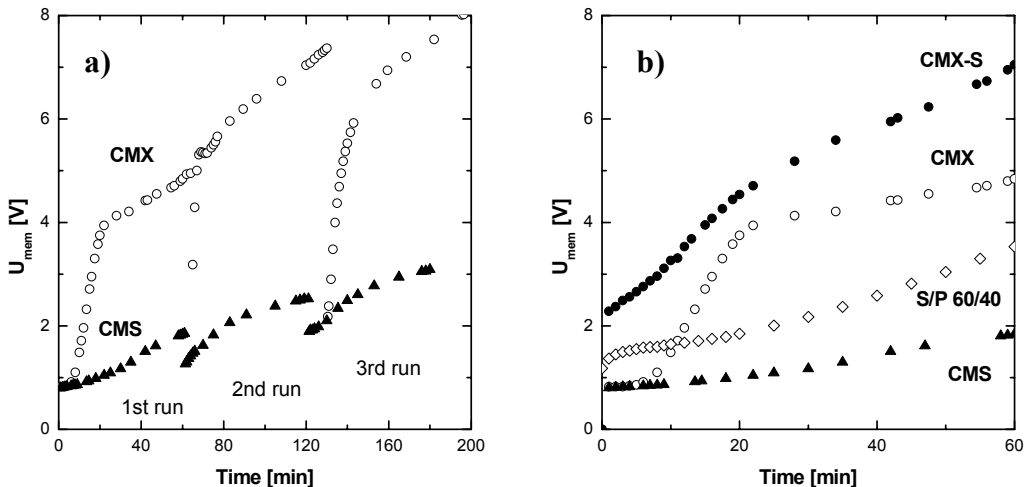
**Figure 5:** Development of  $U_{\text{mem}}$  measured during the desalination of whey for a) 3 times 60 min and b) 60 min.

Figure 5a shows the development of  $U_{\text{mem}}$  of the CMX and CMS membrane for 180 min (3 runs a 60 min). It is obvious that the increase of  $U_{\text{mem}}$  is much stronger for the CMX than of the CMS membrane. When the whey solution is changed after 60 min,  $U_{\text{diss}}$  drops significantly. Because the scaling layer is not affected by the change of the whey solution (acidic rinsing is needed to recover the membrane properties), the additional membrane resistance is probably due to protein fouling. The proteins present in the casein whey stick to the surface of the CEMs and increase the resistance of the membranes during the process. When the solution is changed parts of the deposited protein layer are removed, resulting in a decrease of the membrane resistance. When the new whey solution is applied, the deposited layer is built up again within a few minutes, increasing the  $U_{\text{mem}}$  again. The fouling tendency of the membranes can therefore be evaluated by comparing  $U_{\text{mem}}$  during the whey desalination during the first 60 min (Figure 5b).

The CMS membrane shows the lowest increase in  $U_{\text{mem}}$  over time followed by the S/P 60/40 membrane and the CMX membrane. The CMS membrane has therefore not only a low scaling tendency but also a low fouling behaviour for the applied feed stream. The CMX membrane shows a strong increase in the first 20 min of the process, indicating the high scaling but also high fouling tendency. The CMX-S membrane has already initially a very high resistance, which increases strongly during the process. Because the membrane has a low scaling tendency one can conclude that this membrane shows a high fouling tendency. The S/P 60/40 membrane shows a rather low resistance increase in the first 20 min. After this, however the resistance increases steeper than of the CMX membrane, indicating a stronger fouling tendency of this membrane over time. The high concentration of PES in the S/P blend leads probably to higher protein fouling because of its hydrophobic nature.

In conclusion, the CMS membrane shows the most promising properties for the whey desalination process. The membrane has a low initial resistance, a low scaling behaviour and seems to be more fouling resistant than the other tested membranes.

### 3.2 Comparison of the desalination of whey and milk

Another possibility to produce the acid and base needed for the casein precipitation from milk is the desalination of milk instead of the casein whey. The advantage of this process is that the  $\text{Ca}^{2+}$  present in the milk is bound to protein complexes, resulting in a lower scaling and protein fouling of the CEMs. For the desalination of milk, the configuration described before (Figure 3) is used. The Neosepta AFN was used as AEM and the Neosepta CMS membrane was used as CEM. Figure 6 shows the development of the voltage drop measured of the cell ( $U_{\text{cell}}$ ) and over the CMS membrane ( $U_{\text{mem}}$ ) during the process.

The  $U_{\text{mem}}$  of the CMS membrane for the desalination of whey is lower at the beginning of the process, due to the higher conductivity of the whey in comparison to the milk. During the process the increase of  $U_{\text{mem}}$  desalinating whey is steeper than during the desalination of milk, probably due to the higher fouling and scaling tendency of the membrane in contact with whey as described above. The development of the  $U_{\text{cell}}$  shows a significant difference. Because of the lower salt content and conductivity of the milk compared to the whey,  $U_{\text{cell}}$  is much higher.

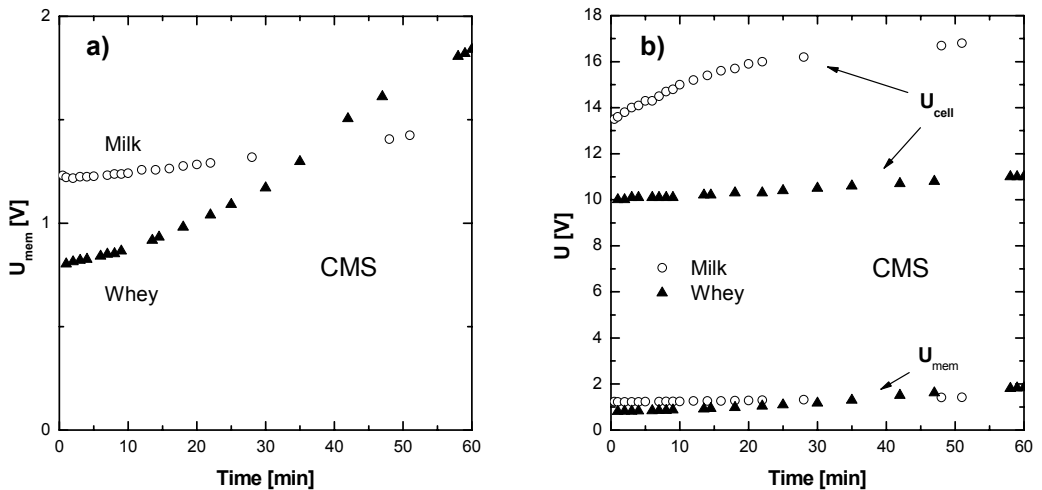


**Figure 6:** Comparison of the development of the voltage drops measured, a) over the membrane and, b) the cell for the desalination of milk and whey.

Besides, another effect was discovered during these experiments which leads to an increase in resistance. The proton leakage of the AFN membrane seemed to be

high enough to cause precipitation of casein in the desalination compartment (Figure 7). This shows that already small pH changes in the milk compartment can lead to local precipitation of casein proteins onto the AEM.



**Figure 7:** Picture of the casein proteins precipitated on the AFN membrane in the desalination cell during the desalination of milk.

We can conclude therefore that the desalination of whey as source for the production of acid and base is the preferred configuration.

### **3.3 Efficiencies and power consumption of different membrane configurations during pilot scale experiments**

In this part of the research the influence of the membrane configuration on the efficiency and power consumption of the whey desalination pilot process is investigated (see section 2.4).

In the first series of experiments the influence of the AEM was investigated. Therefore two different runs using AFN or AMX membranes together with the CMX membrane were performed. The efficiencies for acid-base production using the AMX membrane are higher than those of the AFN membrane (Table 4). Especially the efficiency of the acid production by the AMX / CMX configuration is much higher, indicating the high proton leakage through the AFN membrane, which was already indicated earlier.

**Table 4:** Comparison of the current efficiencies using different AEMs.

Membrane configuration	Current efficiency	
	acid	base
AFN / CMX	0.37	0.72
AMX / CMX	0.59	0.81

Due to the higher efficiency, the AMX membrane was used further in experiments with various CEMs. The influence of the different membrane on the ion transport and the efficiencies is shown in Table 5.

**Table 5:** Ion fluxes and current efficiencies of the process using different membrane configurations.

Membrane configuration	$J_i$ $10^{-9}$ [mol/(cm <sup>2</sup> s)]					Current efficiency	
	Na <sup>+</sup>	K <sup>+</sup>	Ca <sup>2+</sup>	SO <sub>4</sub> <sup>2-</sup>	Cl <sup>-</sup>	acid	base
AMX / CMX	39.15	45.39	13.26	12.03	45.13	0.59	0.81
AMX / CMX-S	21.75	56.72	0.52	9.12	59.85	0.65	0.83
AMX / CMS	43.13	65.58	0.60	17.46	39.96	0.68	0.89

The use of the monovalent ion-selective CMS membranes leads to high efficiencies for the base production. The Ca<sup>2+</sup> fluxes through the CMS and CMX-S membranes are much lower than through the CMX membrane, leading to a lower scaling rate. These measurements are in agreement with the scaling behaviour measured in section 3.1. The CMX-S membrane shows not only a lower transport of Ca<sup>2+</sup>, but also of Na<sup>+</sup> and K<sup>+</sup>. Due to this effect, the transport of the very mobile H<sup>+</sup> ion is preferred, reducing the efficiency of the base production.

The CMX-S has a high resistance. The development of the  $U_{\text{cell}}$  and the corresponding power consumption  $P$  of the different membrane configurations is shown in Figure 8.

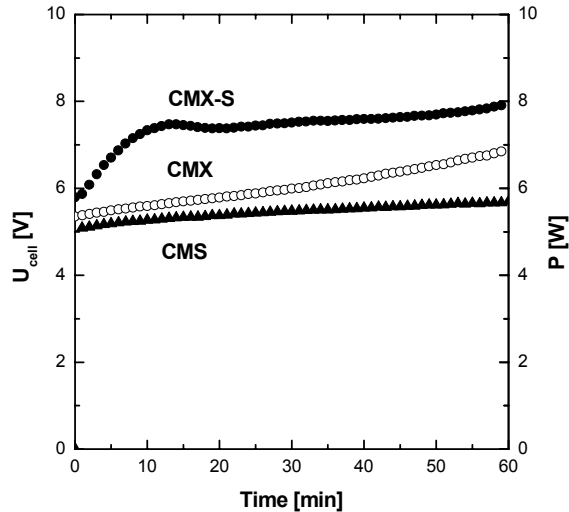


**Figure 8:** Comparison of the voltage drop and the corresponding power consumption of the different membrane configurations over time.

The resistance of the configuration containing the CMX-S membrane increases strongly in the first 10 min compared to the other configurations. Then, the voltage drop increases less sharp. This result is in good agreement with the scaling experiments in section 3.1, showing the higher fouling tendency of the CMX-S membrane also at pilot scale, where the hydrodynamic conditions are better. The CMX membrane did not show this strong increase in resistance at the beginning of the process. It seems that the fouling under the hydrodynamic conditions in the pilot stack (using the multi-layer spacer configuration developed in chapter IV) is not so strong. The higher flow velocities and the enhanced mixing using the multi-layer spacers reduce the protein fouling. The stronger increase in resistance of the CMX during the process can therefore be explained by the increased scaling rate due to the higher  $\text{Ca}^{2+}$  fluxes compared to the other CEMs (see Table 5).

The CMS membrane shows the lowest increase in resistance over time and the highest efficiency for the base generation. Therefore this membrane can be considered as the most suitable for the considered ED-BPM process for casein whey desalination.

Generally, the efficiencies for the acid production indicate that the proton leakage through the AMX membrane is still rather high. To improve the efficiency we mix a

part of the whey with 0.1M HCl solution in the ratio 1/1 in the acid compartment of the ED-BPM stack. This results in higher efficiency of the acid production (see Table 6).

**Table 6:** Comparison of the ion fluxes using different liquors in the acid compartment.

Membrane configuration	Acid	$J_i$ $10^{-9}$ [mol/(cm <sup>2</sup> s)]					Current efficiency	
		Na <sup>+</sup>	K <sup>+</sup>	Ca <sup>2+</sup>	SO <sub>4</sub> <sup>2-</sup>	Cl <sup>-</sup>	acid	base
AMX-CMS	HCl	43.13	65.58	0.60	17.46	39.96	0.68	0.89
AMX-CMS	HCl + whey	28.76	59.06	1.89	14.76	53.29	0.86	0.87

The buffering effect of the applied casein whey increases the pH in the acidic compartment and lowers the proton leakage through the AMX membrane.

We can conclude therefore, that the ED-BPM process using casein whey as source of the recovered acids and bases seems to be feasible. When using the monovalent ion selective CMS membrane, the scaling seems to be low and reversible. In addition, the protein fouling tendency is very low. Together with the buffering of the acid with a part of the casein whey, the process has very promising current efficiencies.

## 4. Conclusions

In this chapter we proposed a process configuration for the electrochemical acidification of milk by ED-BPM. The casein whey produced by the chemical acidification of milk is first demineralised. Combining the demineralisation with bipolar membrane electrodialysis (ED-BPM), the used acid could be recovered and the whey could be neutralised by the produced base.

In the first part of our research we focussed on the scaling and fouling behaviour of different CEMs used in this process. The commercial available Neosepta CMS membranes showed low scaling and the lowest fouling behaviour of the tested membrane. The scaling occurred during the process was fully reversible by rinsing with 0.1 HCl.

In the second part, the possibility of desalinating milk to produce the needed acid and base was investigated. This configuration has higher resistance and power consumption compared to the desalination of casein whey. In addition this process is rather unstable due to the precipitation of casein inside the stack caused by local pH changes in the desalination compartment.

In the third part, we investigated the influence of the different membrane configurations on the efficiencies and the power consumption of the process. Using AMX / CMS membrane configuration showed the most promising results. When part of the casein whey is mixed with the acid the process current efficiencies reaches 0.86 for the production of acid and 0.87 for the production of base.

## 5. Acknowledgement

The authors would like to thank Albert Verver from DMV International for the fruitful discussions, the supply of whey and milk and the ion analyses performed at DMV International.

## 6. List of symbols

$C_0$	Concentration at time 0 [mol/L]
$C_t$	Concentration at time t [mol/L]
F	Faraday constant (96485 As/mol)
i	Current density [A/cm <sup>2</sup> ]
IEC	Ion exchange capacity [mol/kg <sub>dry</sub> ]
$J_i$	Ion flux through the membrane
P	Permselectivity [%]
R	Membrane area resistance [ $\Omega$ cm <sup>2</sup> ]
SD	Sulphonation degree [%]
t	Time [s]
V	Circulated volume [L]
w	Water uptake [kg <sub>water</sub> /kg <sub>dry</sub> ]
AEM	Anion exchange membrane
BPM	Bipolar membrane



BPMEA	Bipolar membrane electroacidification
CEM	Cation exchange membrane
ED-BPM	Bipolar membrane electrodialysis
S-PEEK	Sulphonated poly(ether ether ketone)
S/P	Blend of sulphonated poly(ether ether ketone) and poly(ether sulphone)
PES	Poly(ether sulphone)

## 7. References

- [1] L. Bazinet, F. Lamarche, D. Ippersiel, and J. Amiot, Bipolar Membrane Electroacidification To Produce Bovine Milk Casein Isolate, *J. Agric. Food Chem* 47 (1999) 5291-5296.
- [2] L. Bazinet, D. Ippersiel, C. Gendron, C. Tetreault, J. Rene-Paradis, J. Beaudry, M. Britten, B. Mahdavi, J. Amiot, and F. Lamarche, Comparison between reconstituted and fresh skim milk chemical and electrochemical acidifications, *Journal of the Science of Food and Agriculture* 82 (2002) 1356-1364.
- [3] L. Bazinet, D. Ippersiel, C. Gendron, J. Beaudry, B. Mahdavi, J. Amiot, and F. Lamarche, Cationic balance in skim milk during bipolar membrane electroacidification, *Journal of Membrane Science* 173 (2000) 201-209.
- [4] L. Bazinet, D. Ippersiel, D. Montpetit, B. Mahdavi, J. Amiot, and F. Lamarche, Effect of membrane permselectivity on the fouling of cationic membranes during skim milk electroacidification, *Journal of Membrane Science* 174 (2000) 97-110.
- [5] L. Bazinet, F. Lamarche, D. Ippersiel, D. Montpetit, and J. Amiot, Identification of Skim Milk Electroacidification Fouling: A Microscopic Approach, *Journal of Colloid and Interface Science* 237 (2001) 62-69.
- [6] L. Bazinet, D. Montpetit, D. Ippersiel, B. Mahdavi, J. Amiot, and F. Lamarche, Neutralization of hydroxide generated during skim milk electroacidification and its effect on bipolar and cationic membrane integrity, *Journal of Membrane Science* 216 (2003) 229-239.

- [7] T. Sata, T. Sata, W. Yang, Studies on cation-exchange membranes having permselectivity between cations in electrodialysis, *Journal of Membrane Science* 206 (2002) 31-60.
- [8] T. Sata, Change of transport properties of cation exchange membranes, *Journal of Polymer Science* 16 (1978) 1063 –1080.
- [9] T. Sata, Properties of ion – exchange membranes combined anisotropically with conducting polymers. 2. Relationship of electrical potential generation to preparations of composite membranes, *Chemistry of Materials* 3 (1991) 838 –843.
- [10] T. Sata, K. Kawamura, M Higa, K. Matsusaki Electrolytic transport properties of cation exchange membranes in the presence of cyclodextrins, *Journal of Membrane Science* 183 (2) (2001) 201 –212.
- [11] J. Balster, O. Krupenko, I. Pünt, D. F. Stamatialis, and M. Wessling, Preparation and characterisation of monovalent ion selective cation exchange membranes based on sulphonated poly(ether ether ketone), *Journal of Membrane Science* 263 (2005) 137-145.
- [12] F. G. Wilhelm, I. G. M. Pünt, N. F. A. van der Vegt, H. Strathmann, and M. Wessling, Cation permeable membranes from blends of sulfonated poly(ether ether ketone) and poly(ether sulfone), *Journal of Membrane Science* 199 (2002) 167-176.
- [13] J.J. Krol, M. Wessling and H. Strathmann, Concentration polarization with monopolar ion exchange membranes: current-voltage curves and water dissociation, *Journal of Membrane Science* 162 (1999) 145-154.
- [14] F. G. Wilhelm, I. Punt, N. F. A. van der Vegt, M. Wessling, H. Strathmann, Asymmetric Bipolar Membranes in Acid-Base Electrodialysis, *Ind. Eng. Chem. Res* 41 (2002) 579-586.
- [15] J. Balster, I. Punt, D. F. Stamatialis, and M. Wessling, Multi-layer spacer geometries with improved mass transport, *Journal of Membrane Science* 282 (2006) 351-361.
- [16] X. Tongwen, and Y. Weihua, Effect of cell configurations on the performance of citric acid production by a bipolar membrane electrodialysis, *Journal of Membrane Science* 203 (2002) 145-153.

## Summary

This thesis aims to develop more efficient monopolar and bipolar membrane electro dialysis processes. Three main topics have been investigated:

1. Membrane selectivity
2. Concentration polarisation
3. Membrane scaling and fouling

### A. Membrane selectivity

All three parts are responsible for lowering of the process efficiencies and feasibilities. The membrane selectivity, especially for bipolar membranes, lowers the product purities and the current efficiency of the process. In addition a good water splitting activity is necessary to lower the energy input.

**Chapter I** gives an overview on electrochemical membrane reactors, in particular the bipolar membrane.

**Chapter II** reports the effects of various parameters affecting the water splitting of a bipolar membrane. The amount of functional groups and the water content of the interface layer have a significant influence on the resistance. The use of an anion exchange layer containing different groups showed that the membrane resistance was strongly reduced using layers with ionic groups catalysing the water splitting reaction. In addition, two different types of catalysts were tested, based on iron and pyridine. The pyridine based interface layer proved to be a good tool to prepare tailor made bipolar membranes containing anion exchange layers with high base stability without having water splitting catalytic functional groups. Therefore this interface layer was used in the following chapter for the development of tailor made bipolar membranes.

To improve selectivity and current efficiency of the bipolar membranes new asymmetric membranes with reduced salt leakages were prepared in **Chapter III**. The flux of salt ions across a bipolar membrane was determined by the co-ion transport across the respective membrane layer. Asymmetry is used to decrease the co-ion fluxes through the membrane and shows that the change of the layer

thickness and charge density of the corresponding ion exchange layer determines the co-ion flux. The modification of a commercial BP-1 membrane with an additional thin cation exchange layer on the cationic side resulted in a 47% lower salt leakage. Thicker layers resulted in water diffusion limitations into the bipolar interface. In order to avoid water diffusion limitations, tailor made bipolar membranes with thin anion exchange layers were prepared, to increase the water flux into the membrane. As a result a bipolar membrane could be prepared with a thick cation exchange layer showing a 62% decreased salt ion leakage through the cationic side of the membrane.

### **B. Concentration polarisation**

The reduction of concentration polarisation, which restricts the operating current densities, was achieved in two different ways. In **Chapter IV** optimal spacer configurations were developed to decrease concentration polarisation and improve the process performance. Standard non-woven and multi-layer net spacers were tested and their performance in the light of mass transfer enhancement and cross flow power consumption was evaluated. Multi-layer spacer configurations comprising a standard middle spacer with two thin outside net spacers resulted in the highest mass transfer enhancement. When the diameter of the filament of the middle spacer was reduced the same mass transfer enhancement can be reached at 30 times lower cross-flow power consumption. Besides, at the same cross-flow power consumption the developed multi-layer spacer shows 20 percent higher mass transfer than a standard commercial non-woven net spacer.

In **Chapter V** the origin of the overlimiting current density was investigated. The theory concerning electro-convection, a convective mixing mechanism strong enough to destroy the diluted boundary layer, predicts a shortening of the plateau length of membranes with increased conductive or geometrical heterogeneity. The investigation of commercial cation exchange membranes has shown the influence of the surface heterogeneity on the plateau length. The investigation of a heterogeneous cation exchange membrane FT-CM showed, that the heterogeneity reduces the transition times during chronopotentiometry due to the concentration of the electrical field lines. However, this phenomenon was not enough to result in an

earlier onset of the overlimiting current. The surface heterogeneities have to be in a certain distance to lead to an earlier onset of the overlimiting current. The creation of membranes with surface undulations showed a significant influence on the occurrence of the overlimiting current and the earlier onset of electro-convection. The creation of line undulations on the membrane surface perpendicular to the flow direction, having distances ranging from approximately 50% to 200% of the boundary layer thickness, lead to an earlier onset of the overlimiting current. By an increase of the height of these undulations the effect was enhanced. The plateau length of the undulated membranes could be reduced by 60% compared to a flat membrane. Under the used experimental conditions electro-convection is most likely the origin of the overlimiting current.

### **C. Membrane scaling and fouling**

In the next two chapters, the scaling and fouling behaviour of membranes was investigated. In order to avoid scaling monovalent ion selective membranes had to be prepared. In **Chapter VI** the separation properties of various commercial cation exchange membranes and tailor made membranes based on sulphonated poly(ether ether ketone) and poly(ether sulphone) for binary electrolyte solutions containing protons and calcium ions were analysed. All membranes were thoroughly characterised and relations between their electrochemical properties and ion selectivity were drawn. The results showed that the conductivity and the charge density of the membranes determine the calcium transport through the membranes. The calcium transport increases with increasing conductivity, however, it is lower for membranes with lower charge density. Therefore, the preparation of membranes with reasonable conductivities and low calcium transport was possible. Besides, the calcium flux increased with the increase of current density and / or calcium concentration. For cation exchange membranes having a positively charged coating, the calcium flux was low at low current density but increased strongly at high current densities. In the **Appendix** different coatings were applied to a commercial CMX membrane and their selectivities and stabilities were evaluated. Using a thin coating layer of aminated polysulphone resulted in a selective and stable coating.

In **Chapter VII** a process configuration for the electrochemical acidification of milk by bipolar membrane electrodialysis was proposed. The demineralisation of casein whey combined with bipolar membrane electrodialysis was used to recover acid and base which could be reused for acidification and neutralisation. The research focussed on the scaling and fouling behaviour of different cation exchange membranes. The commercial Neosepta CMS membranes showed low scaling and the lowest fouling behaviour of the tested membranes. The scaling occurred during the process was fully reversible by rinsing with 0.1M HCl. In addition, the influence of the different membrane configurations on the efficiencies and the power consumption of the process was investigated. The AMX / CMS membrane configuration showed the most promising results. When part of the casein whey is mixed with the acid the process current efficiencies reach 0.86 for the acid and 0.87 for the base production.

## Samenvatting

Dit proefschrift beoogt om efficiëntere monopolaire en bipolaire elektrolyse processen te ontwikkelen. Drie hoofdonderwerpen zijn onderzocht:

- A. Membraan selectiviteit
- B. Concentratie polarisatie
- C. Membrane scaling en vervuiling

### A. Membraan selectiviteit

Alle drie delen zijn verantwoordelijk voor een verlaging van de proces efficiëntie en mogelijkheden. De membraanselectiviteit, met name voor bipolaire membranen, verlaagt de zuiverheid van het product en de stroomefficiëntie van het proces. Daarnaast is een goede watersplitsingsactiviteit nodig om een het energieverbruik te verlagen.

**Hoofdstuk I** geeft een overzicht van elektrochemische membraanreactoren, in het bijzonder van de bipolaire membranen.

**Hoofdstuk II** rapporteert de effecten van verschillende parameters die de watersplitsing van een bipolair membraan beïnvloeden. Het aantal functionele groepen and het watergehalte van de tussenlaag dragen voor een aanzienlijk deel bij aan de weerstand. Het gebruik van een anion uitwisselende laag met verschillende groepen liet zien dat de membraan weerstand sterk gereduceerd werd door het gebruik van ionische groepen die de watersplitsing katalyseerden. Daarbij werden twee verschillende katalysatoren getest, gebaseerd op ijzer en pyridine. The tussenlaag die gebaseerd was op pyridine bleek goed te voldoen om op maat gemaakte bipolaire membranen te maken met hoge loogbestendigheid zonder watersplitsende katalytische functionele groepen. Daarom werd deze tussenlaag gebruikt in het volgende hoofdstuk over de ontwikkeling van op maat gemaakte bipolaire membranen.

Om de selectiviteit en stroomefficiëntie te verhogen van de bipolaire membranen werden nieuwe membranen met gereduceerde zoutlekage gemaakt in **Hoofdstuk III**. De flux van zoutionen door een bipolair membraan werd bepaald aan

de hand van het co-ion transport over een respectievelijke membraanlaag. Asymmetrie is gebruikt om de co-ion flux door het membraan te verminderen en liet zien dat een verandering in de laagdikte en ladingsdichtheid van de corresponderende ionuitwisselende laag de flux van co-ionen bepaalt. De verandering van een commercieel BP-1 membraan met additioneel een dunne kationuitwisselende laag op de kationzijde resulteerde in een 47% lagere zoutlekkage. Dikkere lagen resulteerden in waterdiffusielimiteringen naar de bipolaire tussenlaag. Om de waterdiffusielimiteringen tegen te gaan werden op maat gemaakte bipolaire membranen ontwikkeld met dunne anion uitwisselende lagen om zodoende de waterflux in het membraan te verhogen. Als resultaat werd een bipolair membraan gemaakt met een dikke kation laag die een 62% lagere zoutlekkage door de kationzijde van het membraan liet zien.

### **B. Concentratie polarisatie**

De vermindering van concentratie polarisatie, die de werkbare stroomdichtheid beperkt, werd bereikt op twee verschillende manieren. In **Hoofdstuk IV** werden optimale spacerconfiguraties ontwikkeld om de concentratiepolarisatie te verminderen en het proces te verbeteren. Standaard non-woven en multi-laags net spacers werden getest en hun prestaties werden geëvalueerd aan de hand van de verhoging van de massa transport overdracht en het cross-flow energie verbruik. Multi-laags spacer configuraties bestaande uit een middelste spacer met twee dunne net spacers aan de buitenzijde resulteerden in de sterkste massaoverdracht verhoging. Wanneer de diameter van de vezel in het middelste spacer werd gereduceerd, kon dezelfde massaoverdracht verhoging gehaald worden met een 30 keer lagere cross-flow energie verbruik. Bovendien, bij hetzelfde cross-flow energieverbruik lieten de ontwikkelde multi-laags spacers een 20 procent hogere massaoverdracht zien dan een standaard commerciële non-woven net spacer.

In **Hoofdstuk V** werd de oorsprong van de overlimerende stroomdichtheid onderzocht. De theorie aangaande elektroconvectie, een convectief mengmechanisme dat sterk genoeg is voor het verstoren van de grenslaag, voorspelt een verkorting van de plateaulengte van membranen met een verhoogde conductieve of geometrische heterogeniteit. Het onderzoek van commerciële kation



uitwisselende membranen liet de invloed van oppervlakte heterogeniteit op de plateaulengte zien. Het onderzoek aan een heterogeen kationuitwisselend membraan, FT-CM, liet zien dat de heterogeniteit de overgangstijden tijdens chronopotentiometrie door een concentratie van de veldlijnen vermindert. Desalniettemin was dit fenomeen niet genoeg om een eerder begin van de overlimiterende stroomdichtheid in gang te zetten. De oppervlakte heterogeniteiten moeten een bepaalde afstand hebben om tot een eerder begin van de overlimiterende stroomdichtheden te leiden. De verwezenlijking van membranen met oppervlakte ribbels lieten een significante invloed op het optreden van de overlimiterende stroomdichtheid en een eerder begin van de electro-convectie zien. Het maken van ribbels op het oppervlak loodrecht op de richting van de stroming, met afstanden in de range van 50% tot 200% van de grenslaagdikte, leiden tot een eerder begin van de overlimiterende stroomdichtheid. Door een vergroting van de hoogte van de ribbels werd het effect versterkt. De plateaulengte van de geribbelde membranen kon 60% gereduceerd worden ten opzichte van vlakke membranen. Onder de experimentele condities is elektro-convectie hoogstwaarschijnlijk de oorzaak van de overlimiterende stroomdichtheden.

### **C. Membraan scaling en vervuiling**

In de volgende twee hoofdstukken werd de scaling en vervuiling van membranen onderzocht. Om de scaling te vermijden moesten monovalent ion selectieve membranen ontwikkeld worden. In **Hoofdstuk VI** worden de scheidingseigenschappen van verscheidene commerciële kation uitwisselende membranen en op maat gemaakte membranen gebaseerd op poly(ether ether keton) en poly(ether sulfon) voor binaire elektrolyt oplossingen met protonen en calcium ionen geanalyseerd. Alle membranen werden grondig gekarakteriseerd en relaties tussen hun elektrochemische eigenschappen en ion selectiviteit werden gelegd. The resultaten lieten zien dat de geleidbaarheid en de ladingsdichtheid van de membranen het calcium transport door de membranen bepaald. Het calcium transport wordt groter met toenemende geleidbaarheid en is daarentegen lager voor membranen met een lagere ladingsdichtheid. Daardoor was de vervaardiging van een membraan met een redelijke geleidbaarheid en een laag calcium transport mogelijk. Daarnaast bleek de calciumflux te vergroten met toenemende

stroomdichtheid en/of calcium concentratie. Voor kationen met een positief geladen coating, was de calciumflux laag bij lage stroomdichtheden maar nam deze sterk toe bij hogere stroomdichtheden. In de **Appendix** werden verschillende coatings toegepast op een commercieel CMX membraan en werden de selectiviteiten en stabiliteiten geëvalueerd. Het gebruik van een dunne coatingslaag van geamineerd polysulfon resulteerde in een selectieve en stabiele coating.

In **Hoofdstuk VII** wordt een procesconfiguratie voor de elektrochemische acidificatie van melk met behulp van bipolaire membranen voorgesteld. De ontzouting van caseïne wei gecombineerd met bipolaire membraan elektrolyse werd gebruikt voor de herwinning van zuur en base die gebruikt kan worden voor acidificatie en neutralisatie. Het onderzoek spitte zich toe op de scaling en het vervuilinggedrag van verscheidene kationuitwisselende membranen. De commerciële Neosepta CMS membranen lieten de minste scaling en vervuilinggedrag van de geteste membranen zien. De scaling die tijdens het proces optrad, was volledig reversibel door spoelen met 0.1M HCl. Daarnaast werd de invloed van verscheidene membraan configuraties op de efficiëntie en het energieverbruik onderzocht. De AMX/CMS membraanconfiguratie liet de meest belovende resultaten zien. Wanneer een deel van de caseïne wei wordt gemengd met het zuur bereikt de proces stroomefficiëntie 0.86 voor het zuur en 0.87 voor de loog productie.

# CURRICULUM VITAE

## PERSONAL DETAILS

### BALSTER, Jörg Henning

Date and place of birth: 28-07-1975 Nordhorn, Germany

German Nationality, Male, Married.

## EMPLOYMENT RECORD & INVOLVMENT IN RESEARCH PROJECTS

- 05.2006 – 05.2007 *Researcher at the European Membrane Institute (EMI), University of Twente, Enschede, The Netherlands.*
- 05.2002 – 05.2006 *PhD student in the Membrane Technology Group, University of Twente, Enschede, The Netherlands. Topic: "Membrane module and process development for monopolar and bipolar membrane electrodialysis".*
- 10.2001 – 05.2002 *Master thesis at the Membrane Technology Group, University of Twente, The Netherlands. Topic: "Functionalised Carbon Molecular Sieve membranes for gas separation processes".*
- 10.2000 – 02.2001 *Project work at the University of Applied Sciences Münster, Steinfurt, Germany. Topic: "Modellierung und Simulation von Membranreaktoren".*
- 04.2000 – 08.2000 *Diplom-work at the Cognis Deutschland GmbH, Düsseldorf, Germany. Topic: "Heterogen katalysierte Umesterung von Triglyceriden zu Fettsäuremethylestern am Beispiel von festen Ionenaustauschern und anderen neuartigen Katalysatoren".*
- 10.1998 – 02.1999 *Practical Internship, Fraunhofer Institute of Environmental, Safety and Energy Technology, UMSICHT, Oberhausen, Germany Topic: "Marktrecherche zur Verfestigung von Abfällen mit hydraulischen Bindemitteln"*
- 06.1996 - 09.1996 *Practical training at the Ewabo Chemikalien GmbH in Wietmarschen, Germany.*
- 06.1995 – 06.1996 *Civil service at the Bürgerhilfe e.V. in Nordhorn, Germany.*

## **EDUCATION**

- 2000 - 2002     Master of Chemical Engineering, University of Applied Sciences  
Münster, Germany
- 1996 - 2000     Chemical Engineering, University of Applied Sciences Münster,  
Germany
- 1992 – 1995     Fachgymnasium Technik Nordhorn, Germany
- 1988 – 1992     Realschule Uelsen, Germany
- 1986 – 1988     Orientierungsstufe Uelsen, Germany
- 1982 – 1986     Grundschule Wilsum, Germany

## List of publications

1. J.N. Barsema, J. Balster, N.F.A. van der Vegt, G.H. Koops, V. Jordan, M. Wessling, Ag Functionalized Carbon Molecular Sieve Membranes for separating O<sub>2</sub> and N<sub>2</sub>, *Mat. Res. Soc. Symp. Proc.* (2003) 752.
2. J.N. Barsema, J. Balster, V. Jordan, N.F.A. van der Vegt, M. Wessling, Functionalized Carbon Molecular Sieve membranes containing Ag-nanoclusters, *Journal of Membrane Science* 219 (2003) 47-57.
3. J.N. Barsema, S.D. Klijnstra, J.H. Balster, N.F.A. van der Vegt, G.H. Koops, M. Wessling, Intermediate polymer to carbon gas separation membranes based on Matrimid PI, *Journal of Membrane Science* 238 (2004) 93-102.
4. J. Balster, D.F. Stamatialis, M. Wessling, Electro-catalytic membrane reactors and the development of bipolar membrane technology, *Chemical Engineering and Processing* 43 (2004) 1115-1127.
5. D.F. Stamatialis, H.H.M. Rolevink, J. Balster, G.H. Koops, Controlled drug delivery through tailor-made blend polymeric membranes, *Journal of Controlled Release* 101 (2005) 302-304.
6. J. Balster, O. Krupenko, I. Pünt, D.F. Stamatialis, M. Wessling, Preparation and characterisation of monovalent ion selective cation exchange membranes based on sulphonated poly(ether ether ketone), *Journal of Membrane Science* 263 (2005) 137-145.
7. M. Girones, A. Peters, D.M. Sterescu, J. Balster (ed.), *Network Young Membranes 7<sup>th</sup> Meeting*, Conference booklet, Enschede, The Netherlands, 2005.
8. J. Balster, I. Pünt, D.F. Stamatialis, M. Wessling, Multi-layer spacer geometries with improved mass transport, *Journal of Membrane Science* 282 (2006) 351-361.
9. J. Balster, R. Sumbharaju, S. Srikantharajah, I. Pünt, D.F. Stamatialis, V. Jordan, M. Wessling, Asymmetric bipolar membrane: A tool to improve product purity, *Journal of Membrane Science*, Accepted for publication October 2006.